# CATIONIC AND DICATIONIC PHOSPHINE COMPLEXES OF TIN AND GERMANIUM

by

Elizabeth MacDonald

Submitted in partial fulfilment of the requirements
for the degree of Doctor of Philosophy

at

Dalhousie University
Halifax, Nova Scotia
August 2013

© Copyright by Elizabeth MacDonald, 2013

## DEDICATION PAGE

This thesis is dedicated to my grandparents: Rita Penny, Theresa MacDonald, and Bertram MacDonald.

# TABLE OF CONTENTS

**LIST OF TABLES** ..... **vii**

**LIST OF FIGURES** ..... **x**

**LIST OF SCHEMES** ..... **xv**

**ABSTRACT** ..... **xvi**

**LIST OF ABBREVIATIONS AND SYMBOLS USED** ..... **xvii**

**ACKNOWLEDGEMENTS** ..... **xix**

**CHAPTER 1 INTRODUCTION** ..... **1**

**1.1 Complexes of a Cationic Acceptor and a Pnictogen Donor** ..... **3**

1.1.1 Complexes of a Phosphenium Acceptor and a Phosphine Donor ..... 3

1.1.2 Complexes of a Pnictenium Acceptor and a Pnictogen Donor ... 7

**1.2 Complexes Involving Germanium Acceptors with Pnictogen, Carbon, and Oxygen Donors** ..... **13**

1.2.1 Neutral Complexes of Germanium Acceptors with Nitrogen, Phosphorus, and Arsenic Donors ..... 13

1.2.2 Cationic Complexes of Germanium Acceptors with Carbon, Oxygen, Nitrogen, and Arsenic Donors ..... 17

**1.3 Complexes involving Tin Acceptors with Pnictogen and Oxygen Donors** ..... **21**

1.3.1 Neutral Complexes of Tin Acceptors with Nitrogen, Pnictogen, and Arsenic Donors ..... 22

1.3.2 Cationic Complexes of Tin Acceptors with Oxygen, Nitrogen, and Phosphorus Donors ..... 25

**1.4 Summary** ..... **30**

**CHAPTER 2 INTERACTIONS BETWEEN CHLOROSTANNANES AND ALUMINUM TRICHLORIDE** ..... **32**

**2.1 Background** ..... **32**

**2.2 Synthesis, Isolation, and Characterization** ..... **32**

**2.3 Molecular Structures** ..... **34**

**2.4 Summary and Conclusion** ..... **38**

**CHAPTER 3 PHOSPHINE STABILIZED GERMYLIUM AND GERMYLDIYLIUM CATIONS AND DICATIONS** ..... **39**

**3.1 Background** ..... **39**

**3.2 Synthesis, Isolation, and Characterization ..... 39**
**3.3 Molecular Structures ..... 43**
**3.4 Summary and Conclusion ..... 47**
**CHAPTER 4 A PHOSPHINE STABILIZED CHLOROSTANNYLIUM CATION AND A CHLOROSTANNYLDIYLIUM DICATION ..... 48**
**4.1 Background ..... 48**
**4.2 Synthesis, Isolation, and Characterization ..... 50**
**4.3 Molecular Structures ..... 54**
**4.4 Summary and Conclusion ..... 57**
**CHAPTER 5 PHOSPHINE STABILIZED ALKYLSTANNYLIUM CATIONS AND ALKYLSTANNYLDIYLIUM DICATIONS ..... 58**
**5.1 Background ..... 58**
**5.2 Phosphine Complexes of Stannylium Cations ..... 59**
5.2.1 Synthesis, Isolation, and Characterization ..... 59
5.2.2 Molecular Structures ..... 60
**5.3 Diphosphine Complexes of Stannylium Cations and Distannylium Dications ..... 64**
5.3.1 Synthesis, Isolation, and Characterization ..... 64
5.3.2 Molecular Structures ..... 66
**5.4 Cyclic Diphosphine Complexes of Stannyldiylium Dications ..... 70**
5.4.1 Synthesis, Isolation, and Characterization ..... 70
5.4.2 Molecular Structures ..... 72
**5.5 Summary and Conclusion ..... 75**
**CHAPTER 6 PHOSPHINE AND DIPHOSPHINE STABILIZED DIALKYLCHLOROSTANNYLIUM CATIONS ..... 76**
**6.1 Background ..... 76**
**6.2 Synthesis, Isolation, and Characterization ..... 76**
**6.3 Molecular Structures ..... 79**
**6.4 Summary and Conclusion ..... 83**
**CHAPTER 7 CONCLUSIONS AND FUTURE WORK ..... 85**
**7.1 Thesis Summary ..... 85**
**7.2 Future Work ..... 85**
7.2.1 Phosphine-Stannane Complexes and Phosphine Stabilized Stannylium Cations ..... 85

7.2.2 Arsine Stabilized Stannylium Cations ..... 91
7.2.3 Phosphine Stabilized Germylium Cations and Germyldiylium Dications ..... 91
7.2.4 Phosphine Stabilized Germyliumylidene Cation and Germyliumdiylidene Dication ..... 92
7.2.5 Diphosphines, Triphosphines and Cyclophosphines as Ligands for Stannylium and Germylium Cations ..... 94
**CHAPTER 8 EXPERIMENTAL ..... 98**
**8.1 General ..... 98**
**8.2 Preparation and Characterization of Compounds in Chapter 2 ..... 100**
8.2.1 $Me_3SnClAlCl_3$ ..... 100
8.2.2 $Me_2SnCl_2AlCl_3$ ..... 101
8.2.3 $Bu_2SnCl_2AlCl_3$ ..... 102
8.2.4 General Preparation of $R_3SnClAlCl_3$ for NMR Studies ..... 103
8.2.5 General Preparation of $R_2SnCl_2AlCl_3$ for NMR Studies ..... 103
8.2.6 General Preparation of $R_2SnCl_2(AlCl_3)_2$ for NMR Studies ..... 104
**8.3 Preparation and Characterization of Compounds in Chapter 3 ..... 104**
8.3.1 $[Me_3PMe_2GeCl][AlCl_4]$ ..... 104
8.3.2 $[Cy_3PEt_3Ge][AlCl_4]$ ..... 105
8.3.3 $[Me_3PEt_3Ge][AlCl_4]$ ..... 106
8.3.4 $[iPr_3PMe_2GeCl][OTf]$ ..... 107
8.3.5 $[Me_3PPh_3Ge][OTf]$ ..... 108
8.3.6 $[dmpe(Et_3Ge)_2][OTf]_2$ ..... 110
8.3.7 $[dmpe(Ph_3Ge)_2][OTf]_2$ ..... 111
8.3.8 $[(dmpe)Me_2Ge][OTf]_2$ ..... 113
**8.4 Preparation and Characterization of Compounds in Chapter 4 ..... 114**
8.4.1 $(PMe_3)_2SnCl_4$ ..... 114
8.4.2 $[(PMe_3)_2SnCl_3][AlCl_4]$ ..... 116
8.4.3 $[(PMe_3)_2SnCl_2][AlCl_4]_2$ ..... 117
**8.5 Preparation and Characterization of Compounds in Chapter 5 ..... 119**
8.5.1 $[Me_3PMe_3Sn][AlCl_4]$ ..... 119
8.5.2 $[Me_3PMe_3Sn][OTf]$ ..... 121
8.4.3 $[iPr_3PMe_3Sn][AlCl_4]$ ..... 122

8.5.4 $[Cy_3PMe_3Sn][AlCl_4]$ ..... 123
8.5.5 $[tBu_3PMe_3Sn][AlCl_4]$ ..... 125
8.5.6 $[(dmpe)SnMe_3][AlCl_4]$ ..... 125
8.5.7 $[(dmpm)SnMe_3][AlCl_4]$ ..... 127
8.5.8 $[dmpe(SnMe_3)_2][OTf]_2$ ..... 128
8.5.9 $[dmpm(SnMe_3)_2][AlCl_4]_2$ ..... 130
8.5.10 $[(dmpe)Bu_2Sn][AlCl_4]_2$ ..... 132
8.5.11 $[(dmpe)Bu_2Sn][OTf]_2$ ..... 133
8.5.12 $[(dmpm)Bu_2Sn][AlCl_4]_2$ ..... 135
8.5.13 $[(dmpm)Me_2Sn][OTf]_2$ ..... 137
**8.6 Preparation and Characterization of Compounds in Chapter 6 ..... 138**
8.6.1 $dmpe(SnMe_2Cl_2)_2$ ..... 138
8.6.2 $[Me_3PMe_2SnCl][AlCl_4]$ ..... 139
8.6.3 $[(dmpe)Bu_2SnCl][AlCl_4]$ ..... 140
8.6.4 $[(dmpm)Me_2SnCl][AlCl_4]$ ..... 142
**8.7 Preparation and Characterization of Compounds in Chapter 7 ..... 143**
8.7.1 $dmpe(iPr_3SnOTf)_2$ ..... 144
8.7.2 $[SnCl_4][CoCp_2]$ ..... 145
8.7.3 $Me_3P(Me_3SnCl)_2$ ..... 145
8.7.4 $[Et_3AsMe_3Sn][AlCl_4]$ ..... 146
8.7.5 $[(Me_3P)_2Ge][OTf]_2$ ..... 147
8.7.6 $[(dmpe)GeCl][OTf]$ ..... 147
8.7.7 $[Me_3PCl][GeCl_3]$ ..... 148
8.7.8 $[(tBu_3P_3)Me_2GeCl][AlCl_4]$ ..... 149
**8.8 Preparation and Characterization of a byproduct from the reaction of dmpe with $AlCl_3$ ..... 149**
8.8.1 $[(dmpe)_2AlCl_2][AlCl_4]$ ..... 149
**8.9 Crystallographic Experimental Details ..... 151**
**APPENDIX A1. NOMENCLATURE ..... 171**
**REFERENCES ..... 172**

## LIST OF TABLES


Table 1.1.2.1 Possible coordinate bonds between pnictogen elements P, As, Sb, and Bi. ..... 9

Table 2.2.1 $^{119}Sn\{^{1}H\}$ NMR data for mixtures of $R_3SnCl$ (R = Me, iPr, Ph) or $R_2SnCl_2$ (R = Me, Bu, Ph) with $AlCl_3$. ..... 34

Table 2.3.1 Selected interatomic distances (Å) for $Me_3SnClAlCl_3$, $Me_2SnCl_2AlCl_3$, and $Bu_2SnCl_2AlCl_3$. ..... 37

Table 2.3.2 Selected interatomic angles (°) for $Me_3SnClAlCl_3$, $Me_2SnCl_2AlCl_3$, and $Bu_2SnCl_2AlCl_3$. ..... 38

Table 3.2.1 $^{31}P\{^{1}H\}$NMR chemical shifts for phosphine stabilized cations and dications of germanium. ..... 43

Table 3.3.1 Selected structural parameters for $[Cy_3PEt_3Ge][AlCl_4]$, $[dmpe(Et_3Ge)_2][OTf]_2$, and $[Me_3PPh_3Ge][OTf]$ ..... 47

Table 4.2.1 Selected NMR data for $SnCl_4(PMe_3)_2$, $[SnCl_3(PMe_3)_2][AlCl_4]$ and $[SnCl_2(PMe_3)_2][AlCl_4]_2$ ..... 54

Table 4.3.1 Selected structural parameters for $SnCl_4(PMe_3)_2$, $[SnCl_3(PMe_3)_2][AlCl_4]$ and $[SnCl_2(PMe_3)_2][AlCl_4]_2$ ..... 57

Table 5.2.1.1 $^{31}P\{^{1}H\}$ and $^{119}Sn\{^{1}H\}$ NMR data for $[R_3PMe_3Sn][AlCl_4]$ (where R = Me, iPr, Cy and tBu) and $[Me_3PMe_3Sn][OTf]$ ..... 60

Table 5.2.2.1 Selected interatomic distances (Å) for $[R_3PMe_3Sn][AlCl_4]$ (where R = Me, iPr, Cy and tBu) and $[Me_3PMe_3Sn][OTf]$ ..... 63

Table 5.2.2.2 Selected interatomic and torsion angles (°) for $[R_3PMe_3Sn][AlCl_4]$ (where R = Me, iPr, Cy and tBu) and $[Me_3PMe_3Sn][OTf]$ ..... 64

Table 5.3.1.1 $^{31}P\{^{1}H\}$ and $^{119}Sn\{^{1}H\}$ NMR data for $[(dmpe)Me_3Sn][AlCl_4]$, $[(dmpm)Me_3Sn][AlCl_4]$, $[dmpe(Me_3Sn)_2][OTf]_2$, and $[dmpm(Me_3Sn)_2][AlCl_4]_2$. ..... 66

Table 5.3.2.1 Selected interatomic distances (Å) for $[(dmpe)Me_3Sn][AlCl_4]$, $[(dmpm)Me_3Sn][AlCl_4]$, $[dmpe(Me_3Sn)_2][OTf]_2$, and $[dmpm(Me_3Sn)_2][AlCl_4]_2$. ..... 69

Table 5.3.2.2 Selected interatomic angles (°) for $[(dmpe)Me_3Sn][AlCl_4]$, $[(dmpm)Me_3Sn][AlCl_4]$, $[dmpe(Me_3Sn)_2][OTf]_2$, and $[dmpm(Me_3Sn)_2][AlCl_4]_2$. ..... 70

Table 5.4.1.1 $^{31}P\{^{1}H\}$ and $^{119}Sn\{^{1}H\}$ NMR data for $[(dmpe)Bu_2Sn][AlCl_4]_2$, $[(dmpe)Bu_2Sn][OTf]_2$, $[(dmpm)Bu_2Sn][AlCl_4]_2$,and $[(dmpm)Me_2Sn][OTf]_2$ ..... 72

Table 5.4.2.1 Selected interatomic distances (Å) for $[(dmpe)Bu_2Sn][AlCl_4]_2$ and $[(dmpm)Bu_2Sn][AlCl_4]_2$. ..... 74

Table 5.4.2.2 Selected interatomic angles (°) for $[(dmpe)Bu_2Sn][AlCl_4]_2$ and $[(dmpm)Bu_2Sn][AlCl_4]_2$. ..... 74

Table 6.2.1 $^{31}P\{^{1}H\}$NMR data for $dmpe(Me_2SnCl_2)_2$, $[Me_3PMe_2SnCl][AlCl_4]$, $[(dmpe)Bu_2SnCl][AlCl_4]$, and $[(dmpm)Me_2SnCl][AlCl_4]$ ..... 78

Table 6.3.1 Selected interatomic distances (Å) for $[Me_3PMe_2SnCl][AlCl_4]$, $[(dmpe)Bu_2SnCl][AlCl_4]$, $[(dmpm)Me_2SnCl][AlCl_4]$, and $dmpe(Me_2SnCl_2)_2$. ..... 82

Table 6.3.2 Selected interatomic angles (°) for $[Me_3PMe_2SnCl][AlCl_4]$, $[(dmpe)Bu_2SnCl][AlCl_4]$, $[(dmpm)Me_2SnCl][AlCl_4]$, and $dmpe(Me_2SnCl_2)_2$. ..... 83

Table 7.2.1.1 Selected interatomic distances (Å) for $dmpe(iPr_3SnOTf)_2$, $[Me_3PMe_3Sn][OTf]$, and $[dmpe(Me_3Sn)_2][OTf]_2$. ..... 86

Table 7.2.1.3 Selected structural parameters for $Me_3P(Me_3SnCl)_2$. ..... 90

Table 7.2.4.1 Selected interatomic distances (Å) and angles (°) for $[(Me_3P)_2Ge][OTf]_2$ and $[(dmpe)GeCl][OTf]$ ..... 94

Table 8.9.1 Selected crystallographic data and collection parameters for compounds in chapter 2. ..... 151

Table 8.9.2 Selected crystallographic data and collection parameters for compounds in chapter 3. ..... 152

Table 8.9.3 Selected crystallographic data and collection parameters for compounds in chapter 3. ..... 153

Table 8.9.4 Selected crystallographic data and collection parameters for compounds in chapter 3. ..... 154

Table 8.9.5 Selected crystallographic data and collection parameters for compounds in chapter 3. ..... 155

Table 8.9.6 Selected crystallographic data and collection parameters for compounds in chapter 4. ..... 156

Table 8.9.7 Selected crystallographic data and collection parameters for compounds in chapter 4. ..... 157

Table 8.9.8 Selected crystallographic data and collection parameters for compounds in chapter 5. ..... 158

Table 8.9.9 Selected crystallographic data and collection parameters for compounds in chapter 5. ..... 159

Table 8.9.10 Selected crystallographic data and collection parameters for compounds in chapter 5. ..... 160

Table 8.9.11 Selected crystallographic data and collection parameters for compounds in chapter 5. ..... 161

Table 8.9.12 Selected crystallographic data and collection parameters for compounds in chapter 5. ..... 162

Table 8.9.13 Selected crystallographic data and collection parameters for compounds in chapter 5. ..... 163

Table 8.9.14 Selected crystallographic data and collection parameters for compounds in chapter 5. ..... 164

Table 8.9.15 Selected crystallographic data and collection parameters for compounds in chapter 6. ..... 165

Table 8.9.16 Selected crystallographic data and collection parameters for compounds in chapter 6. ..... 166

Table 8.9.17 Selected crystallographic data and collection parameters for compounds in chapter 7. ..... 167

Table 8.9.18 Selected crystallographic data and collection parameters for compounds in chapter 7. ..... 168

Table 8.9.19 Selected crystallographic data and collection parameters for compounds in chapter 7. ..... 169

Table 8.9.20 Selected crystallographic data and collection darameters for $[(dmpe)_2AlCl_2][AlCl_4]$, a byproduct from reactions involving dmpe and $AlCl_3$. ..... 170

## LIST OF FIGURES


Figure 1.1 (**a**) An example of a C-O bond-forming reaction (Fischer Esterification), (**b**) a C-C bond-forming reaction (Grignard) and (**c**) a C-N bond-forming reaction (substitution by a nucleophilic nitrogen). ..... 1

Figure 1.2 (**a**) Poly(phenylene vinylene) (PPV) is an organic photovoltaic material, (**b**) carbon nano-tubes are investigated for use as supercapacitors, and (**c**) the natural product taxol is used as an anti-cancer agent. ..... 2

Figure 1.1.1.1 A phosphine stabilized phosphenium cation can be represented by a Lewis (**1**) or dative (**2**) model. Illustration adapted from reference . ..... 5

Figure 1.1.1.2 Diphosphines with various hydrocarbon tethers to make a variety of monocations (**5**) and dications (**6**). ..... 6

Figure 1.1.1.3 Frameworks **8-12** can be generated by the use of various diphosphine ligands however structures such as **13** and **14** (dashed box) have not been observed. Illustration adapted from reference 1. ..... 7

Figure 1.1.2.1 Targeted branched tricationic frameworks featuring a phosphorus trication stabilized by three arsines (left) and a phosphorus trication stabilized by three phosphines (right) ..... 10

Figure 1.1.2.2 A series of bipy complexes containing $[SbF_2]^+$, $[SbF]^{2+}$ and $[Sb]^{3+}$ acceptors. Illustration adapted from reference 15. ..... 11

Figure 1.2.1.1 A schematic representation of the salt $[GeF_3(Me_3\text{-tacn})][Cl]$. ..... 14

Figure 1.2.2.1 An example of a $[RGe]^+$ cation (**A**), and examples of $[ClGe]^+$ cations (**B** and **C**). ..... 17

Figure 1.2.2.2 Examples of N-heterocyclic cations **D** and **E**. Illustration adapted from reference 34. ..... 18

Figure 1.2.2.3 Schematic drawing (dashed box) and selected examples of Sn, Ge based bis-ylenes, which can potentially act as Janus-head ligands. Illustration adapted from reference 35. ..... 19

Figure 1.2.2.4 Examples of germanium(II) cations stabilized by azamacrocycles, crown ethers, and cryptand ligands. ..... 20

Figure 1.2.2.5 A schematic representation of the solid state structure of $[GeCl\{o\text{-}C_6H_4(AsMe_2)_2\}][GeCl_3]$ showing the $A^-C^+$ interactions. The inset shows the cationic moiety, $[GeCl\{o\text{-}C_6H_4(AsMe_2)_2\}]^+$. ..... 21

Figure 1.3.1.1 Examples of compounds containing intermolecular dative P–Sn interactions. ..... 24

Figure 1.3.1.2 Schematic Structure of $[SnCl_4(AsPh_3)_2]$ (left) and $[SnBr_4AsPh_3 \cdot AsPh_3]$ (right). ..... 25

Figure 1.3.2.1 Generic structures of frameworks for stannylium cations with 0, 1, or 2 donor groups where cations like **M** remain elusive. ..... 26

Figure 1.3.2.2 A schematic of [bis(4-phenylimidazole)trimethyltin]chloride. ..... 27

Figure 1.3.2.3 Single examples of frameworks **O**, **P**, and **Q**. ..... 28

Figure 2.3.1 POV-Ray ball and stick representation of the asymmetric unit in the molecular structure of $Me_3SnClAlCl_3$(bottom). Two-units of $Me_3SnClAlCl_3$ are expanded for clarity (top) with the thermal ellipsoid plots drawn at the 50% probability level. Hydrogen atoms omitted for clarity..... 35

Figure 2.3.2 POV-Ray representation of the asymmetric unit (top) in the molecular structure of $Me_2SnCl_2AlCl_3$ along with a POV-Ray image of the unit cell (bottom). Thermal ellipsoid plots are at the 50% probability level with hydrogen atoms omitted for clarity. ..... 36

Figure 2.3.3 POV-Ray representation of unit cell of $Bu_2SnCl_2AlCl_3$ (left) along with a POV-Ray representation of one of the tin centers in found in the dimer. Thermal ellipsoid plots are at the 50% probability level with hydrogen atoms omitted for clarity. ..... 36

Figure 3.3.1 POV-Ray representation of $[Me_3PMe_2GeCl][AlCl_4]$ (left), $[Cy_3PEt_3Ge][AlCl_4]$ (middle), and $[iPr_3PMe_2GeCl][OTf]$ (right). Thermal ellipsoids are at the 50% probability level, hydrogen atoms are omitted for clarity..... 44

Figure 3.3.2 POV-Ray representation of $[(dmpe)Me_2Ge][OTf]_2$ (top) and $[dmpe(Et_3Ge)_2][OTf]_2$ (bottom), thermal ellipsoids are at the 50% probability level, hydrogen atoms are omitted for clarity. ..... 45

Figure 3.3.3 POV-Ray view of $[dmpe(Ph_3Ge)_2][OTf]_2$ (left) and $[Me_3PPh_3Ge][OTf]$ (right). Thermal ellipsoids are at the 50% probability level, hydrogen atoms are omitted for clarity. ..... 46

Figure 4.1.1 Examples of tin(IV) halides forming coordination complexes with ethers (**A**), sulfides (**B**), pyridines (**C**), diphosphines (**D**), phosphines (**E**) and phosphine oxides (**F**). Coordination complexes in the dashed box (**G** and **H**) are not observed. ..... 49

Figure 4.2.1 Dichloromethane-$d_2$ solution $^{31}P\{^1H\}$ NMR spectrum (top) and solid state $^{31}P$ CP/MAS NMR spectrum (bottom) of $(PMe_3)_2SnCl_4$. ..... 51

Figure 4.2.2 Dichloromethane-$d_2$ solution $^{31}P\{^1H\}$ NMR spectrum (top) and solid state $^{31}P$ CP/MAS NMR spectrum (bottom) of $[SnCl_3(PMe_3)_2][AlCl_4]$. Asterisk indicates a small $[Me_3PH]^+$ impurity present in the top spectrum. ..... 52

Figure 4.2.3 Dichloromethane-$d_2$ solution $^{31}P\{^1H\}$ NMR spectrum (top) and solid state $^{31}P$ CP/MAS NMR spectrum (bottom) of $[SnCl_2(PMe_3)_2][AlCl_4]_2$. ..... 53

Figure 4.3.1 Evacuated two bulb vessel setup for large scale crystallizations toward the isolation of chlorostannylphosphine complexes. The dark areas represent Teflon connections and stars represent crystals of the product of interest. ..... 55

Figure 4.3.2 POV-Ray views of $SnCl_4(PMe_3)_2$, the cation in $[SnCl_3(PMe_3)_2][AlCl_4]$ and the dication in $[SnCl_2(PMe_3)_2][AlCl_4]_2$ including the anion contacts between tin and chlorine atoms of the aluminates. Thermal ellipsoids are at the 50% probability level, hydrogen atoms and anions are omitted for clarity. ..... 56

Figure 5.1.1 An example of an intermolecular $[Me_3Sn]^+$ stabilized by $(Me_3Sn)_3P$ which has a Sn-P interatomic distance of 2.547(1) Å. ..... 59

Figure 5.2.2.1 POV-Ray representation of the molecular structures containing a $[Me_3Sn]^+$ unit base stabilized by phosphines of varying steric bulk. Thermal ellipsoid plots are at the 50% probability level with hydrogen atoms omitted for clarity. ..... 62

Figure 5.2.2.2 POV-Ray representation of the two unique salts located in the unit cell of $[Me_3PMe_3Sn][OTf]$. Thermal ellipsoids are at the 50% probability level with hydrogen atoms omitted for clarity. ..... 62

Figure 5.3.2.1 POV-Ray representation of the molecular structures of $[(dmpe)Me_3Sn][AlCl_4]$ (top, with 2-units showing) and $[(dmpm)Me_3Sn][AlCl_4]$ (bottom). Thermal ellipsoid plots are at the 50% probability level with hydrogen atoms omitted for clarity. ..... 67

Figure 5.3.2.2 POV-Ray representation of the molecular structures of $[dmpe(Me_3Sn)_2][OTf]_2$ (top) and $[dmpm(Me_3Sn)_2][AlCl_4]_2$ (bottom). Thermal ellipsoid plots are at the 50% probability level with hydrogen atoms omitted for clarity. ..... 68

Figure 5.4.2.1 POV-Ray representation of the molecular structures of $[(dmpe)Bu_2Sn][AlCl_4]_2$ (top left), $[(dmpe)Bu_2Sn][OTf]_2$ (top right), $[(dmpm)Bu_2Sn][AlCl_4]_2$ (bottom left), and $[(dmpm)Me_2Sn][OTf]_2$ (bottom right). Thermal ellipsoid plots are at the 50% probability level with hydrogen atoms omitted for clarity. ..... 73

Figure 6.1.1 Representative examples of neutral compounds involving Sn-P dative bonds where there are one or more chlorine atoms present on tin. ..... 76

Figure 6.3.1 POV-Ray representation of $dmpe(Me_2SnCl_2)_2$ (bottom) and $[Me_3PMe_2SnCl][AlCl_4]$ (Top). Thermal ellipsoids are at the 50% probability level, hydrogen atoms are omitted for clarity. ..... 80

Figure 6.3.2 POV-Ray representation of $[(dmpe)Bu_2SnCl][AlCl_4]$ (left) and $[(dmpm)Me_2SnCl][AlCl_4]$ (right), thermal ellipsoids are at the 50% probability level, hydrogen atoms are omitted for clarity. ..... 81

Figure 7.2.1.1 POV-Ray view of the molecular structure of $dmpe(iPr_3SnOTf)_2$. Thermal ellipsoids are drawn at the 50% probability level and hydrogen atoms were omitted for clarity. ..... 87

Figure 7.2.1.2 POV-Ray view of the molecular structure of $[CoCp_2]_2[SnCl_4]\cdot CH_2Cl_2$. Thermal ellipsoids are drawn at the 50% probability level and hydrogen atoms on everything but $CH_2Cl_2$ were omitted for clarity. ..... 89

Table 7.2.1.2 Selected structural parameters for $[CoCp_2]_2[SnCl_4]$. ..... 89

Figure 7.2.1.3 POV-Ray view of the molecular structure of $Me_3P(Me_3SnCl)_2$. Thermal ellipsoids are drawn at the 50% probability level and hydrogen atoms were omitted for clarity. ..... 91

Figure 7.2.4.1 POV-Ray view of the molecular structure of $[(Me_3P)_2Ge][OTf]_2$ (left) and [(dmpe)GeCl][OTf] (right). Thermal ellipsoids are drawn at the 50% probability level and hydrogen atoms were omitted for clarity. ..... 93

Figure 7.2.5.1 Tethering phosphines as a way to generate unique trications, dications with a coordination number of 5 and cations with a coordination number of 6. ..... 96

Figure 7.2.5.2 $^{31}P\{^{1}H\}$ NMR (202.5 MHz) of a reaction mixture containing $tBu_3P_3$, $Me_2GeCl_2$ and $AlCl_3$. ..... 97

## LIST OF SCHEMES


Scheme 1.1.1.1 General synthetic approach to phosphine stabilized phosphenium cations. (**a**) Cations like **3** can be made by using 2 equivalents of $PR_2Cl$ in the presence of $GaCl_3$. (**b**) Cations like **4** can be made by adding $GaCl_3$ to $R_2PCl$ followed by the addition of $PR'_3$. (**c**) An alternate route to making **4** is by taking **3** and conducting a phosphine exchange reaction using $PR'_3$**.** Illustration adapted from reference . ..... 5

Scheme 1.1.2.1 Coordinative approach toward the synthesis of phosphine stabilized pnictenium (top), pnictine stabilized phosphenium (middle), and pnictine stabilized pnictenium (bottom) cations. ..... 8

Scheme 1.1.2.2 Synthesis of pnictine stabilized phosphenium cation (**a**), dipnictine stabilized phosphorus dication (**b**), diphosphine stabilized $[P]^+$ fragment (**c**), and a diarsonium dication (**d**). ..... 10

Scheme 1.1.2.3 Contrasting reactivity between in situ formed phosphenium, arsenium and stibenium cations. Scheme adapted from reference 14. ..... 12

Scheme 1.2.1.1 Reactions of $GeCl_4$ with $R_3P$ (top), $HPR_2$ (middle) and $H_2PR$ (bottom). ..... 15

Scheme 1.2.1.2 The preparation of $[[\{(Me_3Si)_2CH\}(Ph)P]_2Ge]_2$ complex via salt elimination reaction..... 16

Scheme 1.2.2.1 Protonation of a N-heterocyclic germylene to the germylium ion (**a**) or to give the germanium(II) cation **F** (**b**). Illustration adapted from reference 34. ..... 18

Scheme 1.2.2.2 The synthesis of a monocationic germanium cage compound by the reaction of **G** with HOTf to give **H**. Illustration adapted from reference 35..... 19

Scheme 1.3.2.1 Synthesis of tetrakis(trimethylstannyl)ammonium and –phosphonium cations. ..... 29

Scheme 1.3.2.2 **R** can be prepared by reacting 1,2,4-diazaphospholide with $Sn[N(SiMe_3)_2)]_2$. **R** in the presence of $[Sm(3,5\text{-}tBu_2dp)_3]$ gives **S**. ..... 30

Scheme 7.2.5.1 Potential products from a reaction mixture containing $R_2PR_2P$, $R_3ECl$, and TMSOTf. ..... 95

## ABSTRACT

This dissertation explores the synthesis and characterization of phosphine stabilized tetrel (group 14) cations. Tetrel cations are readily generated by reacting a halogermane or halostannane with a Lewis acid to generate an in situ germylium, stannylium cation or an in situ germyldiylium, stannyldiylium dication. A Lewis base such as a phosphine is added to the mixture to produce the corresponding salt with dative P-Sn or P-Ge connectivity. Tin and germanium salts represent new as well as unique cationic structures for phosphorus containing species. The preparation of these salts is proven to be generalizable, reproducible, and can be isolated as pure materials in moderate to high yields.

## LIST OF ABBREVIATIONS AND SYMBOLS USED

| | |
|---|---|
| 3,5-$^{t}Bu_2$dp | 3,5-di-*tert*-butyl-1,2,4-diazaphosphole |
| δ | chemical shift |
| A | anion |
| $A^-C^+$ | anion-cation |
| Abs. | halide abstracting agent |
| ANCl | 10-chloro-5-hydrophenarsazine |
| Ar | aryl |
| bipy | 2,2′-bipyridine |
| br | broad resonance |
| *c.a.* | calculated average |
| CP | cross polarization |
| *d* | doublet |
| depe | bis(diethylphosphino)ethane |
| dipp | 2,6-di-*iso*-propylphenyl |
| dmpe | bis(dimethylphosphino)ethane |
| dmpm | bis(dimethylphosphino)methane |
| dppe | bis(diphenylphosphino)ethane |
| d.p. | decomposition point |
| $\{^1H\}$ | proton decoupled |
| *I* | nuclear spin |
| in situ | in the reaction mixture |
| in vacuo | under dynamic vacuum |
| $^nJ_{AB}$ | n-bond coupling constant between nuclei A and B |
| *m* | multiplet |
| MAS | magic angle spinning |
| $Me_3$-tacn | 1,4,7-trimethyl-1,4,7-triazacyclononane |
| m.p. | melting point |
| NMR | nuclear magnetic resonance |
| ORTEP | Oak Ridge thermal-ellipsoid plot |

| | |
|---|---|
| OTf | $CF_3SO_3$ (triflate) |
| Pn | pnictogen (a group 15 element) |
| POV-Ray | Persistence of Vision Raytracer |
| *q* | quartet |
| *s* | singlet |
| T | tether |
| *t* | triplet |
| tbp | trigonal bipyramidal |
| TMS | trimethylsilyl |
| VSEPR | valence shell electron pair repulsion |

## ACKNOWLEDGEMENTS

I would like to recognize my family and friends for their support through the years of study at Dalhousie University, especially during the thesis writing process. I would like to express gratitude towards Prof. Neil Burford, without his continued support and dedication; without Neil's effort I would not have been successful in my studies… thank you for not giving up on me. There are many other individuals within the Burford group (both past and present) who have helped me along my way with my studies: Dr. Yuen-ying Carpenter, Saurabh Chitnis, Dr. Eamonn Conrad, Lauren Doyle, Paul Gray, Dr. Michael Holthausen, Dane Knackstedt, Stewart Lucas, Janet 'Rampage' Pickup, Dr. Alasdair Robertson, Dr. Marc Whalen, and Meehan Yogendra. I would also like to thank Prof. Jan Weigand and his group for allowing me to have the opportunity to travel to Germany to participate in research as well as learn some new lab skills.

Thank you to Dr. Ulli Werner-Zwanziger for all of her help with solid state NMR and Dr. Mike Lumsden for all of his help with the solution NMR. Credit should be given to Lauren Doyle for her contribution to this work, Lauren was very helpful during the initial (discovery) process for this project – she was also one of the best summer students anyone could have asked for. I am grateful to Dr. Andreas Decken who has run X-Ray analysis on all crystals I send in his direction at the University of New Brunswick. Andreas is the person to 'blame' for encouraging me to pursue graduate studies and I'm grateful he did.

My gratitude is extended to the department office staff consisting of Deanna Wentzell, Giselle Andrews, Cheryl Stanton, Cheryl Coolen and Sean Hartwell who made my last two years here easier with all of their help with anything administrative. Thank you to Mike Boutilier and Rick Conrad for fixing broken down pumps and other equipment and thank you to Jürgen Muller and Todd Carter for fixing broken glass as well as creating new glassware. Thank you to my committee over the years consisting of: Prof. Russell Boyd, Prof. Kevin Grundy, Prof. Norman Schepp, and Prof. Mark Stradiotto. I am greatly indebted to Stephen Beaton for his support, advice and friendship.

I want to extend a very special thank you to Kathy MacDonald and Dr. Wayne MacDonald (Mom and Dad) for all of their support over my lifetime and encouraging me to continue to do my best at whatever I do, I consider myself lucky to have parents like them. Additionally, a thank you is in order for my grandparents whom all have passed during the course of my studies and the primary reason I chose to stay at Dalhousie University. I am very happy with the decision I made and as a result I have no regrets about my choice.

I am grateful to have such a wonderful group of friends which includes: Stephen Beaton, Dr. Claire Kanasewich, Andrew Robertson, Jenna Flogeras, Serena Sanford, Robbie Silliker, and Robin Slipp. I am very fortunate that Neil allowed me to participate in activities outside of chemistry and because of that I gained some valuable experience dealing with stress, pressure, disappointment and success. I have enjoyed my time throwing hammers which was a nice method to relieve stress from chemistry related work, doing so enabled me to train with so many excellent athletes from a variety of disciplines. I am grateful to have trained under the guidance of Jonathan Doucette who dramatically improved my physical strength and technical execution of the hammer throw event. This brings me to the last person who needs acknowledgement and possibly a gold star, Jonathan Moulins. Without my best friend, this four year journey would have been even more challenging than it already has been and thank you for helping me keep it together.

## CHAPTER 1 INTRODUCTION

Modern applications of synthetic chemistry have evolved to demonstrate a diverse scope of reactions ranging from natural product synthesis to new materials. The majority of these compounds are structures based on the ability to generate bonds between carbon and elements such as sulfur, oxygen, phosphorus, nitrogen and carbon itself to create complicated functional scaffolds. Organic chemistry is a well evolved and understood synthetic area relative to the development of the chemistry of the transition metals or main group elements; the evolution can be viewed as starting with reactions involving small and simple C-O, C-C, and C-N bond-forming processes (Figure 1.1) to build more elaborate and synthetically useful compounds for applications in materials, solar cells, and natural products (Figure 1.2).

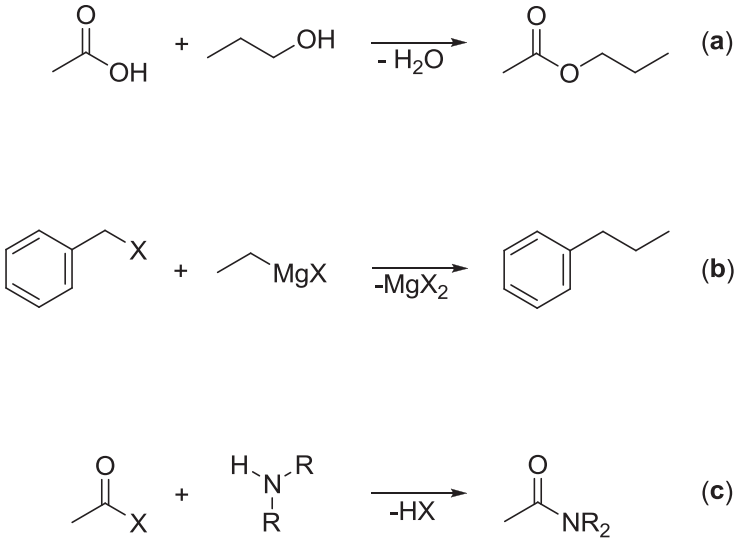


Figure 1.1 (**a**) An example of a C-O bond-forming reaction (Fischer Esterification), (**b**) a C-C bond-forming reaction (Grignard) and (**c**) a C-N bond-forming reaction (substitution by a nucleophilic nitrogen).

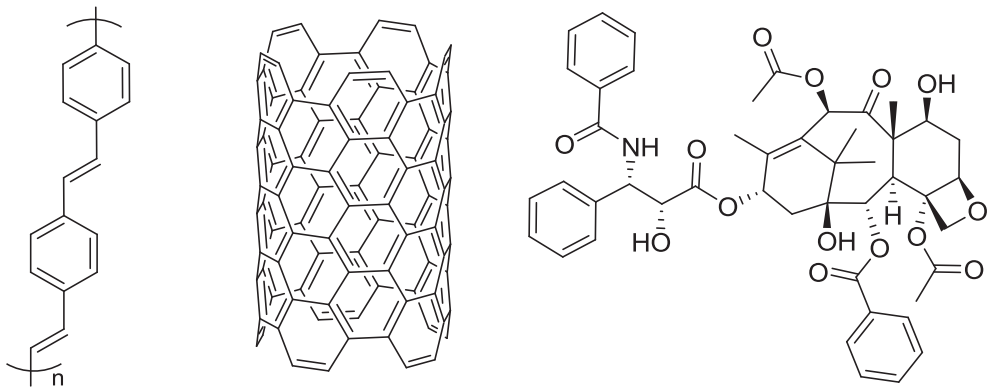


(**a**) (**b**) (**c**)

Figure 1.2 (**a**) Poly(phenylene vinylene) (PPV) is an organic photovoltaic material, (**b**) carbon nano-tubes are investigated for use as supercapacitors, and (**c**) the natural product taxol is used as an anti-cancer agent.

One could envisage a similar progression in synthetic processes occurring for the main group complexes with the potential to make new materials with different properties in comparison to the organic analogues. However, a fundamental understanding of the heavier p-block chemistry is underdeveloped compared to carbon chemistry. The underlying research needs to investigate and understand covalent and dative interactions between the elements as well as advance bond-forming reactions. Progression in this area would then utilize the library of bond-forming reactions toward the synthesis of more complex frameworks. Once a comprehensive understanding of the reaction mechanism is acquired in areas such as knowledge of the reaction stereoselectivity and the effects of substituents (electronic or steric), the synthesis of complex macromolecular architectures would be attainable.

Throughout the literature there are many examples of E-N and E-P (E = Ge, Sn) bonds (dative and covalent) that have been synthesized and investigated. However there are few reports of $P\rightarrow E^+$ salts which warrant the investigations of cationic phosphine stabilized frameworks of tin and germanium to better understand their bonding interactions. By using the $ER_3^+$ moiety, the Lewis acidity (electrophilicity) at the group 14 center is enhanced thus increasing the acceptor strength of the tetrel.

The scope of this dissertation is to investigate the fundamental dative interactions of phosphorus with germanium and tin. This will encompass expanding the library of $P\rightarrow Ge^+$ and $P\rightarrow Sn^+$ compounds by utilizing a variety of frameworks containing monophosphines and diphosphines along with a variety of $R_nEX_{4-n}$ (n= 0, 2, or 3) compounds. The introduction will look at phosphine stabilized phosphenium cations and pnictine stabilized pnictenium cations. The synthesis toward the $Pn\rightarrow Pn^+$ frameworks uses halide abstraction to strengthen the Pn-Pn interaction. The $P\rightarrow E^+$ interactions are made by the same halide abstraction method and discussion of this aspect of the project will provide useful background information. The remainder of the introduction thereafter aims to give the reader a general idea of the tetrel acceptors (neutral or cationic) with pnictogen and selected p-block donors.

## 1.1 Complexes of a Cationic Acceptor and a Pnictogen Donor

### 1.1.1 Complexes of a Phosphenium Acceptor and a Phosphine Donor

Phosphine stabilized phosphenium cations (Figure 1.1.1.1), which contain a single P–P dative bond were first proposed as products of the reaction of a diphosphine with alkyl or

aryl halides.[1] Additionally, chlorophosphines in the presence of halide abstracting agents such as $AlCl_3$ can similarly synthesize these salts.[2] Inter- and intramolecular phosphine-phosphenium compounds represent examples of complexes involving homoatomic coordinate bonding between phosphorus. This is not unique to phosphorus as there are examples of homoatomic As-As and Sb-Sb examples in the literature along with mixed pnictogen species (Pn–Pn′, where Pn ≠ Pn′).[3,4,5,6,7,8,9,10,11,12,13,14,15,16] Although the geometry of each phosphorus center in derivatives of **1** are consistent with a phosphinophosphonium nomenclature, the bonding interaction is better described by **2** where facile ligand exchange reactions implicate the Lewis acid-base definition.[5] The reactions throughout are relatively high yielding synthetic processes as a result of the influence of the molecular cationic charge. The P-P connectivity has been verified by use of techniques such as single-crystal X-Ray crystallography, solid-state NMR spectroscopy, and solution NMR spectroscopy along with FT-Raman spectroscopy to identify the P-P stretching frequency. Various derivatives were synthesized which have been characterized by the aforementioned techniques.[1] Chlorophosphine derivatives such as **3** are prepared from a chlorophosphine and 0.5 equivalents of an appropriate halide-abstracting agent ($GaCl_3$ or TMSOTf; Scheme 1.1.1.1). Phosphine stabilized phosphenium derivatives of type **4** can be prepared directly from combinations of a chlorophosphine, a phosphine, and a halide abstractor (Scheme 1.1.1.1).[1]

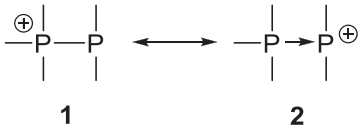

**1** **2**

Figure 1.1.1.1 A phosphine stabilized phosphenium cation can be represented by a Lewis (**1**) or dative (**2**) model. Illustration adapted from reference 1.

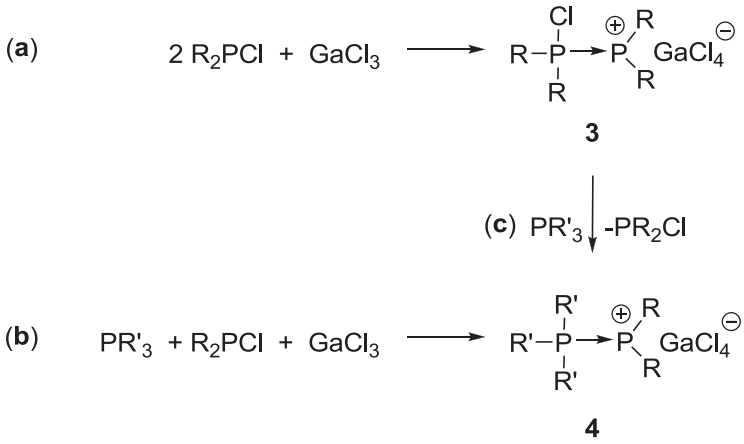

**3** **4**

Scheme 1.1.1.1 General synthetic approach to phosphine stabilized phosphenium cations. (**a**) Cations like **3** can be made by using 2 equivalents of $PR_2Cl$ in the presence of $GaCl_3$. (**b**) Cations like **4** can be made by adding $GaCl_3$ to $R_2PCl$ followed by the addition of $PR'_3$. (**c**) An alternate route to making **4** is by taking **3** and conducting a phosphine exchange reaction using $PR'_3$**.** Illustration adapted from reference 1.

The bonding angles around each phosphorus center in conjunction with the P–P bond lengths in these species indicate the presence of a stereochemically active lone pair of electrons on the tricoordinate phosphine and imply that no significant π-bonding is involved.[1] Ligand exchange at the phosphenium center can be effected by any neutral molecule that is a stronger donor than the stabilizing phosphine in the P-P salt (**1**), as illustrated in Scheme 1.1.1.1 by the replacement of $R_2PCl$ in **3** for $R'_3P$.[1] This is a versatile and convenient method for the formation of various element–phosphorus

bonds.[2-4] For example, exchange reactions with diphosphines bearing a hydrocarbon tether (T) can lead to polyphosphorus cations **5** and dications **6** (Figure 1.1.1.2).[5]

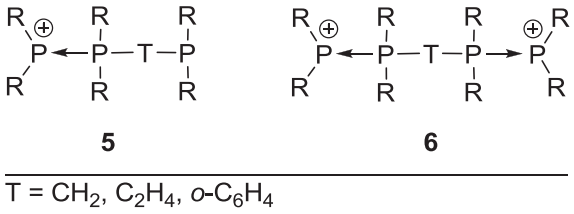


Figure 1.1.1.2 Diphosphines with various hydrocarbon tethers to make a variety of monocations (**5**) and dications (**6**).

Bidentate ligands offer a means of diversification for the coordination chemistry of acceptor sites that are restricted to a single ligand.[5] Figure 1.1.1.3 demonstrates the application of this approach to diphosphine-phosphenium systems. The first examples of triphosphorus monocations are defined by complexes of phosphenium cations interacting with diphosphinomethane ligand **8**, and tetraphosphorus dications are defined by complexes of two phosphenium units tethered by a diphosphinomethane **9**, diphosphinoethane **10**, diphosphinohexane **11**, or diphosphinobenzene **12** ligands.[5] The observations demonstrate the preference for pendant **8** and tethered **9**, **10**, **11**, and **12** arrangements over the corresponding chelate complexes **13** and **14** which have not be observed.[5]

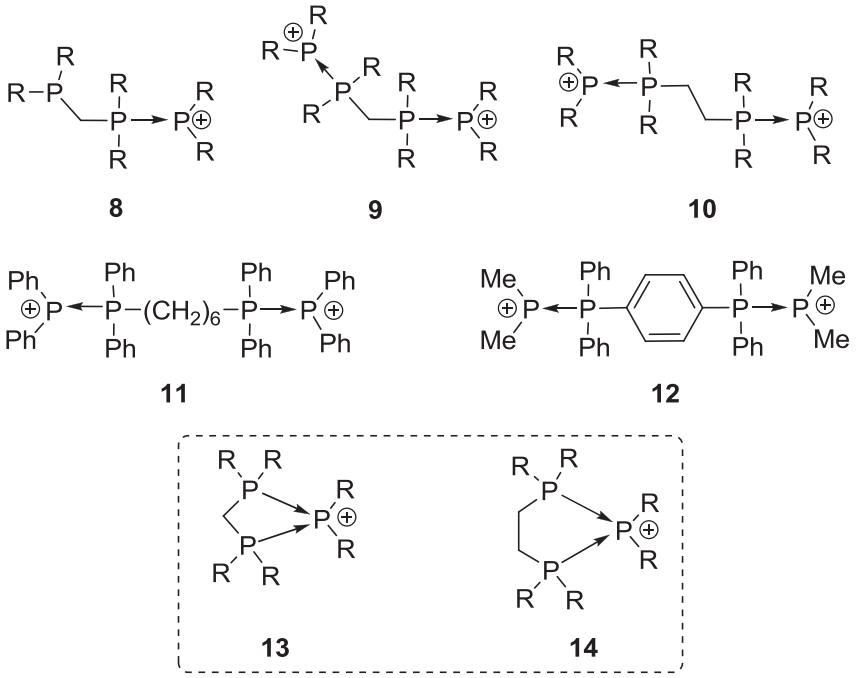


Figure 1.1.1.3 Frameworks **8-12** can be generated by the use of various diphosphine ligands however structures such as **13** and **14** (dashed box) have not been observed. Illustration adapted from reference 1.

## 1.1.2 Complexes of a Pnictenium Acceptor and a Pnictogen Donor

Reports of P, As, Sb, Bi containing cations, denoted inter-pnictogen (Pn) cations, have seen an increase in recent years. Synthesis of $Pn \rightarrow Pn^+$ frameworks has been carried out by abstracting a halide one pnictogen center to then induce pnictogen-pnictogen coupling.[11-16] Arsenium ($R_2As^+$), stibenium ($R_2Sb^+$), and bismuthenium ($R_2Bi^+$) cations have been stabilized by a variety of tertiary phosphines (alkyl and aryl functionality on phosphorus).[11-14] Additionally, arsenium, stibenium and bismuthenium cations can be base stabilized by alkyl or aryl arsines and stibines.[12,13] Attempts to generate bismuthine stabilized pnictenium cations has been investigated; however the lone pair of electrons on bismuth are seemingly too inert to form dative bonds or the bismuth center itself is not

Lewis basic enough to form the dative interaction. Future studies in this area could lead to the isolation and characterization of bismuthine stabilized pnictenium cations by means of a well-designed ligand such as a tris(dialkylamino)amine[17] to increase the basicity of the 6*s* electron on the bismuth atom. One could envisage there are many structural possibilities that contain phosphine stabilized pnictenium ($P\rightarrow Pn^{+}$), pnictine stabilized phosphenium ($Pn\rightarrow P^{+}$) or pnictine stabilized pnictenium ($Pn\rightarrow Pn^{+}$) cations with various examples of each framework type reported in the literature (Scheme 1.1.2.1).[11] The results of the pnictogen stabilized pnictenium cations are best summarized in Table 1.1.2.1 where the inherent inertness of Bi 6*s* lone pair is further exemplified.[11]

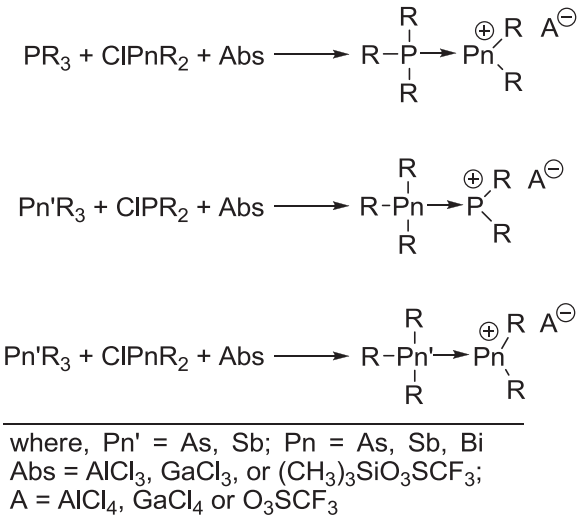


Scheme 1.1.2.1 Coordinative approach toward the synthesis of phosphine stabilized pnictenium (top), pnictine stabilized phosphenium (middle), and pnictine stabilized pnictenium (bottom) cations.

Table 1.1.2.1 Possible coordinate bonds between pnictogen elements P, As, Sb, and Bi.

| | | | |
|---|---|---|---|
| P→P[1,8] | As→P[11,12,23] | Sb→P[12] | **Bi→P*** |
| P→As[2,18] | As→As[11,18,19] | **Sb→As*** | **Bi→As*** |
| P→Sb[14,19-21] | As→Sb[8,20,21] | Sb→Sb[10,22] | **Bi→Sb*** |
| P→Bi[19] | As→Bi[13,21,14] | Sb→Bi[14] | **Bi→Bi*** |

* Examples that have not been isolated to date/published.

Throughout the pnictogen coordination chemistry research there has been some contrasting reactivity in the arsine stabilized phosphenium frameworks in comparison to the phosphine stabilized phosphenium analogues. This is prominent when comparing a series of reactions of $PMe_3$, $AsMe_3$ with $Me_nPCl_{3-n}$ (n = 0,1,2) and $AlCl_3$ as illustrated in Scheme 1.1.2.2.[11] The phosphine and arsine frameworks are analogous for the pnictine stabilized phosphenium cations (Scheme 1.1.2.2, **a**) and bis-pnictine stabilized phosphorus(III) dications (Scheme 1.1.2.2, **b**); all reactions proceed as expected with the exception of the one that uses $PCl_3$.[11] When an attempt is made to generate a branched trication (Figure 1.1.2.1) using $PCl_3$ with three equivalents of $PMe_3$ and halide abstracting agent, a linear cation is isolated. This linear salt contains a $P(I)^+$ center flanked by two phosphine segments; there was no noted formation of the trication (Scheme 1.1.2.2, **c**).[23] When a similar reaction was carried out using $AsMe_3$, the salt $[Me_3AsMe_3As][OTf]_2$ is observed and isolated instead of a branched arsenic trication (Scheme 1.1.2.2, **d**).[11,24]

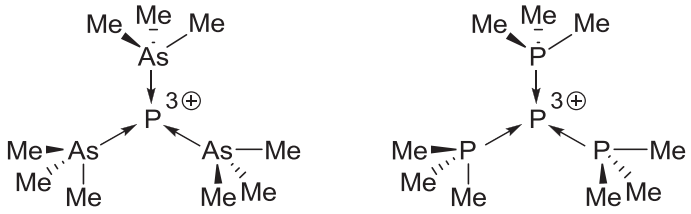

Figure 1.1.2.1 Targeted branched tricationic frameworks featuring a phosphorus trication stabilized by three arsines (left) and a phosphorus trication stabilized by three phosphines (right).

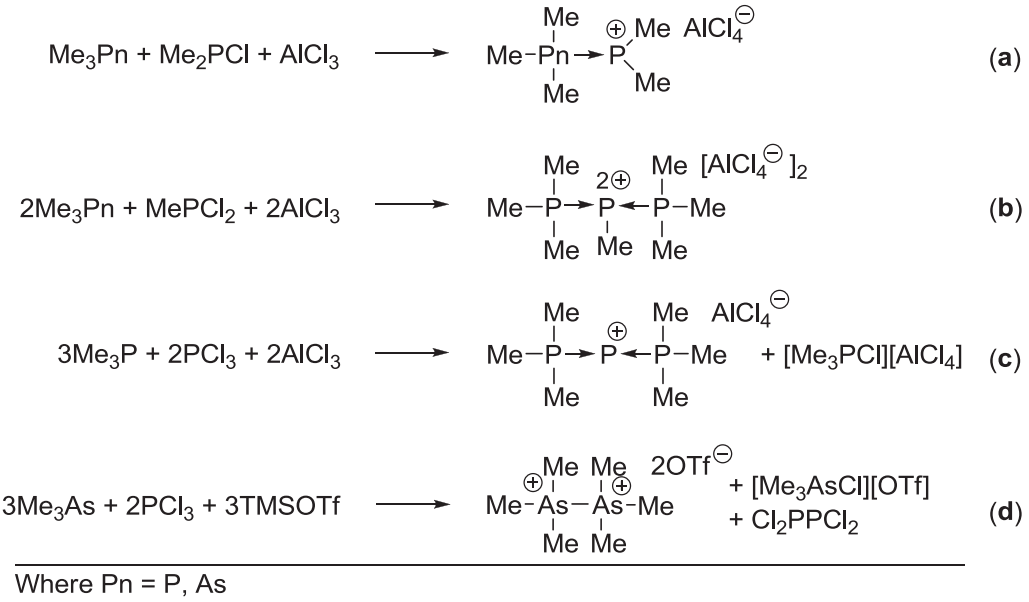


Scheme 1.1.2.2 Synthesis of pnictine stabilized phosphenium cation (**a**), dipnictine stabilized phosphorus dication (**b**), diphosphine stabilized $[P]^+$ fragment (**c**), and a diarsonium dication (**d**).

When fluorine functionality is present on a pnictogen center instead of bromine or chlorine groups, a pnictogen trication can be readily synthesized. For example, $SbF_3$ can undergo sequential fluoride abstraction, in the presence of TMSOTf and bipy, where the mono-, di- and trications have been identified depending on the reaction stiochiometry (Figure 1.1.2.2).[15] The reaction exploits the fluoride affinity of $[Me_3Si]^+$ toward the removal of three fluorides from the antimony center, gaseous TMSF provided an additional driving force during the reaction.

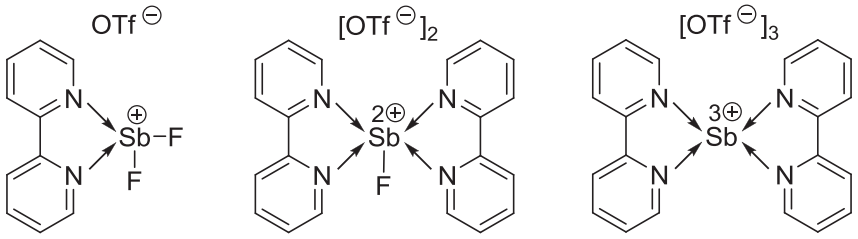


Figure 1.1.2.2 A series of bipy complexes containing $[SbF_2]^+$, $[SbF]^{2+}$ and $[Sb]^{3+}$ acceptors. Illustration adapted from reference 15.

Organocyclophosphines as a Lewis base behave differently for phosphenium cations compared to the heavier pnictenium analogues (As, Sb, Bi). The phosphenium ion inserts into the P–P bond resulting in a ring expansion reaction as illustrated in Scheme 1.1.2.3 **a**.[14] However, in the case of As, Sb and presumably Bi, the organocyclophosphine behaves as a Lewis base (Scheme 1.1.2.3 **b**, **c**, and **d**).[14] In the presence of excess $AlCl_3$ and $SbCl_3$, two $P_4Cy_4$ stabilizes a redox coupled $[ClSb–SbCl]^{2+}$ core. Scheme 1.1.2.3 **b** can viewed as the intermediate process to generating the caged complex seen in Scheme 1.1.2.3 **d** by means of using the excess $SbCl_3$ to couple two $[P_4Cy_4SnCl_2][AlCl_4]$ units together.

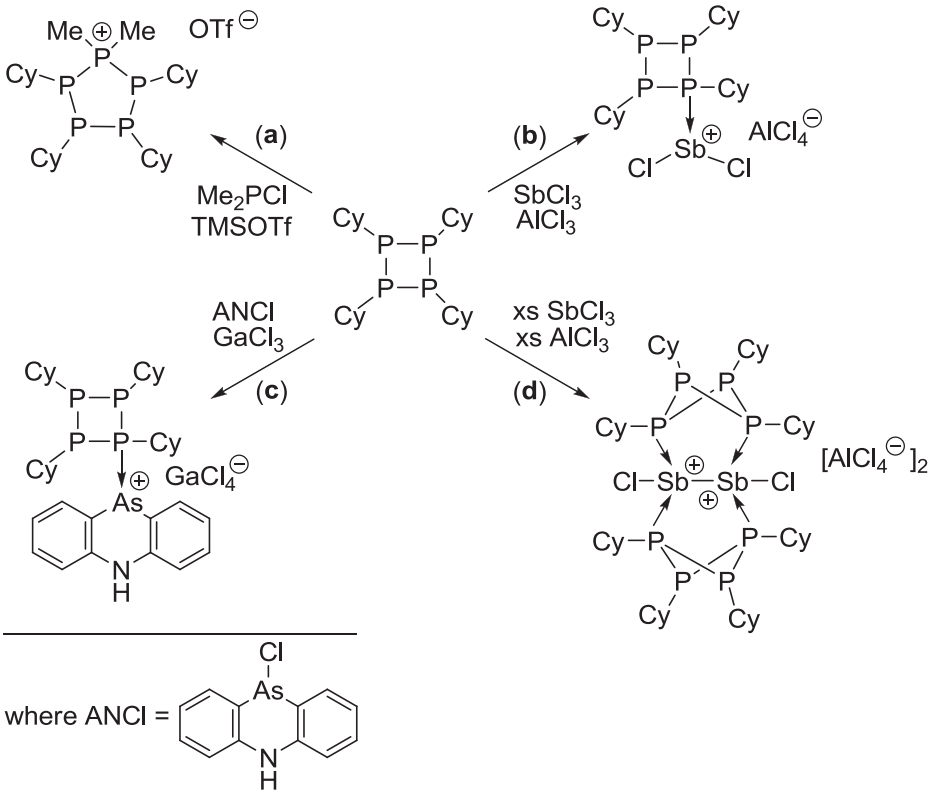


Scheme 1.1.2.3 Contrasting reactivity between in situ formed phosphenium, arsenium and stibenium cations. Scheme adapted from reference 14.

The application of coordination chemistry forming reactions has proven to work well for base stabilizing the heavier pnictenium cations with either hetero- or homopnictines.[11-16] This has been successfully implemented in the formation of pnictine stabilized pnictenium cations (Pn→$Pn^+$) along with the formation of pnictine stabilized phosphenium (Pn→$P^+$) and phosphine stabilized pnictenium (P→$Pn^+$) cations. The halide abstraction and coordinative bond approach is an effective way to tailor the interactions of ambiphilic species to be either Lewis basic or acidic. The following section will begin to look at a variety of frameworks that contain tetrel acceptors with pnictogen donors that are either cationic or neutral. The breadth of this will look at the synthetic approach used

to make these interactions all the while revealing what gaps need to investigated in this area.

## 1.2 Complexes Involving Germanium Acceptors with Pnictogen, Carbon, and Oxygen Donors

Exploratory studies involving germanes with the pnictines to form donor-acceptor complexes were carried out in the 1960's using IR and Raman techniques as a primary method to characterize the compounds.[25] The studies investigated how pnictines (as well as many other donor types) interacted with halo germanes to make 5 or 6 coordinate complexes and to determine the relative geometry of the substituents on germanium (i.e. *cis* or *trans*). The section below gives a brief overview some of the neutral and cationic Pn-Ge (Pn = N, P, As) complexes, in which the pnictogen center behaves as the Lewis base.

### 1.2.1 Neutral Complexes of Germanium Acceptors with Nitrogen, Phosphorus, and Arsenic Donors

Infrared studies have been used to identify derivatives of the type $[GeF_4L]$ (where L = $NH_3$, $NMe_3$, $NMeH_2$ or MeCN) which are five coordinate complexes.[26,27,28] These complexes were assigned to have a trigonal bipyramidal (tbp) geometry with the ligand residing in the axial position and the covalent groups located in the remaining positions. Tridentate nitrogen adducts of $GeF_4$ have been found to be air stable and solution stable in dry $CH_2Cl_2$ or MeCN. Displacement of $F^-$ from $GeF_4$ by a neutral ligand is rare, but this can be achieved by using 1,4,7-trimethyl-1,4,7-triazacyclononane ($Me_3$-tacn), which forms $[GeF_3(Me_3\text{-tacn})]_2[GeF_6]$ upon reaction with $[GeF_4(MeCN)_2]$ in $CH_2Cl_2$.[29] The

$[GeF_3(Me_3\text{-tacn})]_2[GeF_6]$ salt (Figure 1.2.1.1) is insoluble in most common solvents, however the minor product, $[GeF_3(Me_3\text{-tacn})][F]$, was isolated and structurally characterized.[29] This minor product showed a facially coordinated aza-macrocycle with the germanium center to produce a 6 coordinate complex.[29]

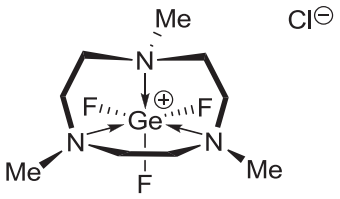


Figure 1.2.1.1 A schematic representation of the salt $[GeF_3(Me_3\text{-tacn})][Cl]$.

Acceptor-donor complexes involving $GeX_4$ (X= Cl, Br, I) in the presence of amines and phosphines produce less stable products in comparison to $GeF_4$.[29] Nitrogen donor complexes of $GeCl_4$ or $GeBr_4$ hydrolyze easy as solids and in solution; complexes of $GeI_4$ are less clearly understood with only a few X-Ray studies on coordination complexes with $GeI_4$.[29] The first phosphine complex of $GeF_4$ was only published in 2008 to the best of my knowledge.[30] The colorless $[GeF_4(PR_3)_2]$ (R=Me or Ph) and $[GeF_4(L\text{-}L)]$ (L-L = $R_2P(CH_2)_2PR_2$, R = Me, Et, Ph) are synthesized by reacting $[GeF_4(MeCN)_2]$ with a ligand to make the corresponding complex.[30] The aforementioned complexes have been characterized by $^{19}F$ and $^{31}P$ NMR spectroscopy and the chelating complexes have been additionally characterized by X-Ray crystallography.[30] Notably, bidentate ligands chelate *cis* and most commonly in the equatorial plane as opposed to an equatorial-axial manner. In contrast, when alkyl phosphines such as $PMe_3$ were reacted with $GeCl_4$, the product isolated was $[Me_3PCl][GeCl_3]$ and not the predicted *trans*-$[GeCl_4(PMe_3)_2]$ (Scheme 1.2.1.1).[30,31,32] Similar trichlorogermanate products are formed by reaction of $GeCl_4$ with

various alkyl phosphines at room temperature, and the steric bulk at phosphorus seems to have no influence on the redox chemistry.[30] If aryl phosphines are employed, no reaction was observed; this was attributed to the poor Lewis basicity of the aryl phosphines.[30] Primary ($PRH_2$) and secondary ($PR_2H$) phosphines also reduce $GeCl_4$ to Ge(II) species, resulting in the loss of HCl to form neutral trichlorophosphines ($RHPGeCl_3$ or $R_2PGeCl_3$) (Scheme 1.2.1.1).[31,32]

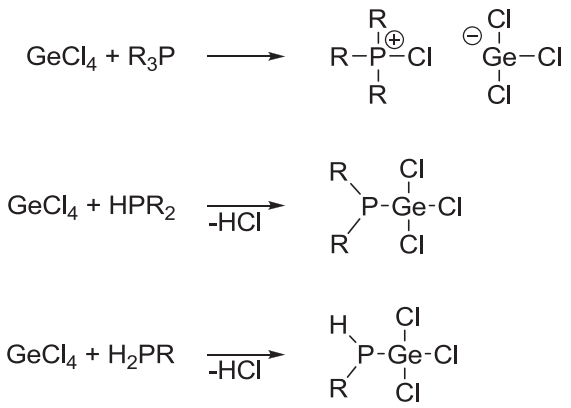


Scheme 1.2.1.1 Reactions of $GeCl_4$ with $R_3P$ (top), $HPR_2$ (middle) and $H_2PR$ (bottom).

A recent review outlined alternate approaches to generate germanium phosphorus compounds by exploiting anionic phosphorus containing ligands for the stabilization of cationic germanium centers to create charged separated complexes.[33] This approach eliminates the need for anions with the added benefit of a more Lewis basic phosphorus atom by virtue of utilizing a phosphide ($R_2P^-$).[33] Phosphides are excellent examples of anionic donors making them readily able to complex with germanium centers, an example is the salt elimination reaction of [K][{$(Me_3Si)_2CH$}(Ph)P] with $GeCl_2$(1,4-dioxane) to generate the dimer [[{$(Me_3Si)_2CH$}(Ph)P]$_2$Ge]$_2$ (Scheme 1.2.1.2).[33] Through

variable temperature and multinuclear NMR studies, the dimeric structure is maintained in solution.[33] The chemistry of salt elimination reactions involving anionic ligands with germanium in general has a broad scope especially when considering the possibilities for diverse ligand designs.[33] Additionally, salt elimination reactions provide an excellent driving force for converting the reactants to the products. Furthermore, this type of chemistry has been expanded to the other tetrel elements silicon, tin and lead.

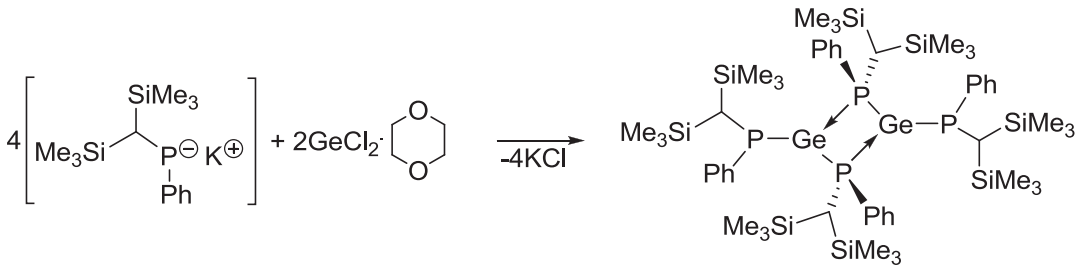


Scheme 1.2.1.2 The preparation of $[[\{(Me_3Si)_2CH\}(Ph)P]_2Ge]_2$ complex via salt elimination reaction.

Neutral arsenic-germanium complexes can be generated by the direct combination of $GeCl_4$ with $AsR_3$ (R = Me, Et) to readily form *trans*-$[GeCl_4(AsR_3)_2]$.[30] Both the methyl and ethyl derivatives have been structurally characterized by X-Ray crystallography. These complexes were found to decompose in solution over the course of a few days to produce arsenic(V) containing species (such as $Et_3AsCl_2$).[30] No complexation was observed when reactions were conducted with $AsPh_3$ and *o*-$C_6H_4(AsMe_2)_2$ as possible donors.[30]

Many donor-acceptor complexes containing germanium as an acceptor have been documented since the 1960's with particular focus on halogermanes. Notably, progressing from the lighter halogens to the heavier halogens results in decreased

stability of the adducts formed; similarly, coordination complexes with the heavy pnictogens have the same effect.

### 1.2.2 Cationic Complexes of Germanium Acceptors with Carbon, Oxygen, Nitrogen, and Arsenic Donors

Organosubstituted cations of the type $[R_3Ge]^+$ are Lewis acidic moieties which are fundamental to the study of group 14 elements.[34] Only a few germanium cations have been isolated and structurally characterized by single crystal X-Ray diffraction studies.[35] Figure 1.2.2.1 shows selected examples of cationic germanium compounds in the form $[RGe]^+$ (**A**) and $[ClGe]^+$ (**B**, **C**).[34,36,37] There have been reports on the synthesis of series of salts containing *nido*-cluster type cations of the composition $[(C_5Me_5)E]^+$ (**A**) which can be viewed as a $[Ge]^{2+}$ species stabilized by an $\eta^5$ interaction from $[C_5Me_5]^-$. [36,38,39] A germanium(II) cation **B** has been isolated where the germanium center is stabilized by three $\eta^6$ interactions and the triflate salt of **C** shows a $[ClGe]^+$ core stabilized by two carbenes. **C** was initially isolated as the by-product from the synthesis of the cryptand encapsulated germanium dication.[37,40] The germanium center in **C** is stabilized by two strong σ-donor carbenes.

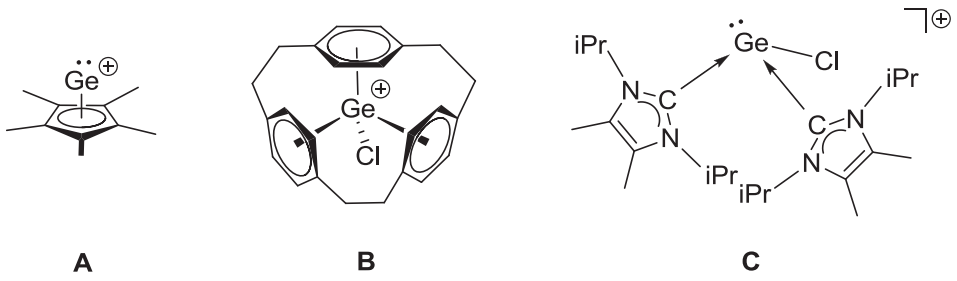


Figure 1.2.2.1 An example of a $[RGe]^+$ cation (**A**), and examples of $[ClGe]^+$ cations (**B** and **C**).

N-heterocyclic cations like **D** and **E** (Figure 1.2.2.2) are of particular interest since they are examples of $Ge^{2+}$ cations in the +2 oxidation state and are due to the electron delocalization across the heterocyclic ring where both Ge–N bonds are identical.[34] Protonation of a germylene can result in two possible reaction pathways resulting in the formation of a nonplanar germylium ion (Scheme 1.2.1.1 **a**).[34] Protonation of the carbon backbone reveals a germylium cation with one dative Ge-N and one covalent Ge-N bond (Scheme 1.2.1.1 **b**).[34]

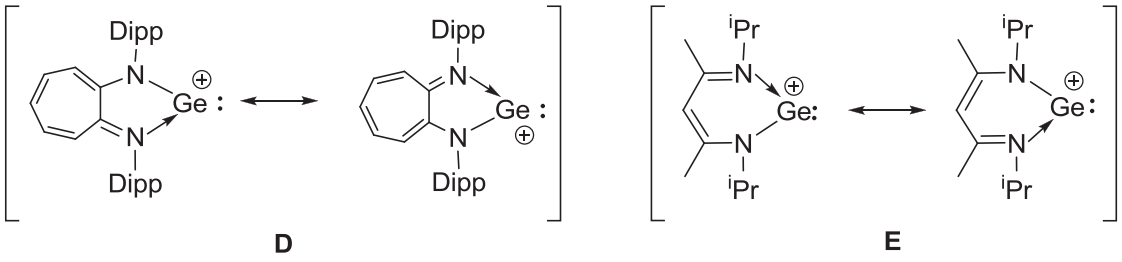


Figure 1.2.2.2 Examples of N-heterocyclic cations **D** and **E**. Illustration adapted from reference 34.

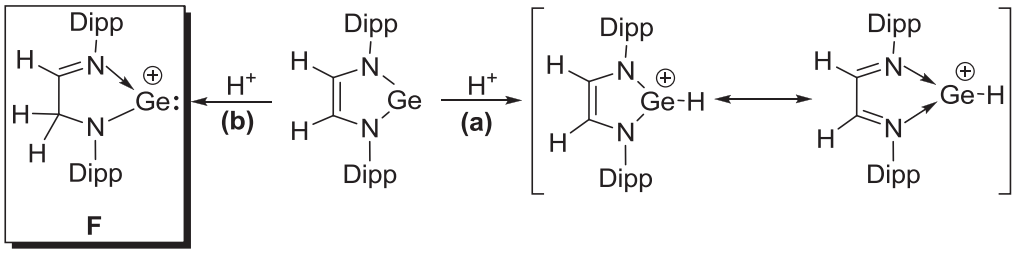


Scheme 1.2.2.1 Protonation of a N-heterocyclic germylene to the germylium ion (**a**) or to give the germanium(II) cation **F** (**b**). Illustration adapted from reference 34.

Another approach to synthesize germanium cations is to use multidentate ligands to form cationic cage compounds of various shapes, sizes and charges (Figure 1.2.2.3)[35] As an example, a ligand from a neutral homoleptic germanium(II) pyrazolyl compound can be removed by treatment with triflic acid (HOTf) to generate a Janus head bis-germylene

cation as illustrated in Scheme 1.2.2.2.[35] The pyrazole by-product is easily separated by vacuum sublimation and products **G** and **H** can be obtained as analytically pure material after recrystallization.[35]

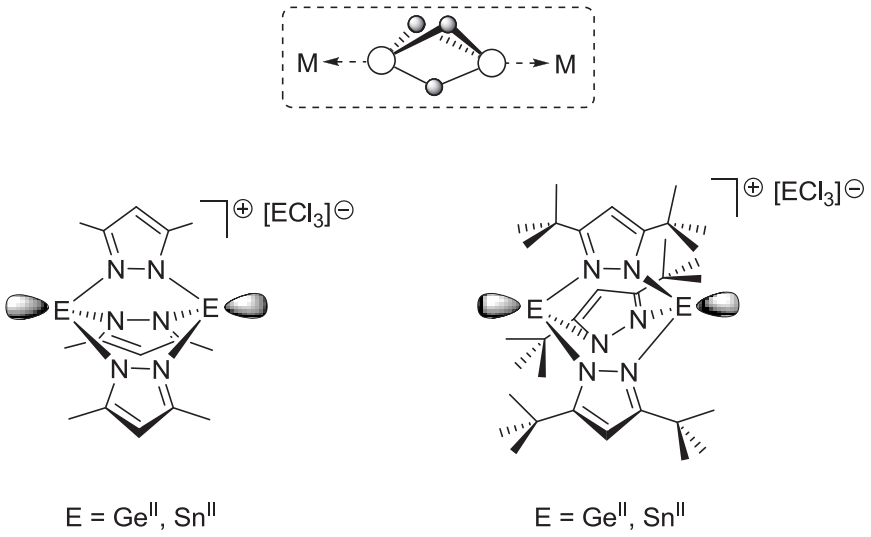


Figure 1.2.2.3 Schematic drawing (dashed box) and selected examples of Sn, Ge based bis–ylenes, which can potentially act as Janus-head ligands. Illustration adapted from reference 35.

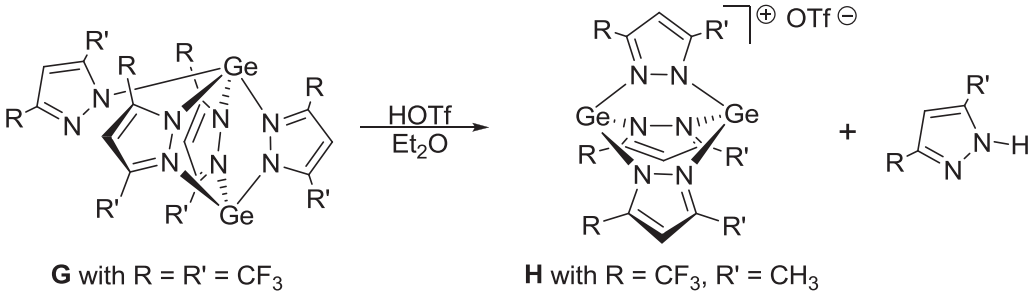


Scheme 1.2.2.2 The synthesis of a monocationic germanium cage compound by the reaction of **G** with HOTf to give **H**. Illustration adapted from reference 35.

The molecular structure of **G** and **H** contained two germanium atoms that were $\mu_2$-bridged by three pyrazolyl ligands with the triflate counter ion in close spatial proximity to the cationic moieties (Ge···O contact of 2.633 Å in **G** and 2.825 Å in **H**).[35] The Ge···O

distances suggest only a weak interaction between germanium and the triflate anion, significantly shorter contacts have been observed for related cationic germanium(II) species.[35,41] An interesting feature of the otherwise asymmetrical substituted cage complex **H** is that the $CH_3$ groups are located on one side with the $CF_3$ groups on the other side; in addition, the triflate anion is located near the $CH_3$ (positive) region of the cage.[35] Isolation of germanium(II) dications has been advanced by the use of crown and cryptand ligands with a few examples illustrated in Figure 1.2.2.4.[37,42,43] The macrocyclic ligands function by first encapsulating the cation, second by way of protecting the germanium center from participating in side reactions and preventing significant interactions from the anions.

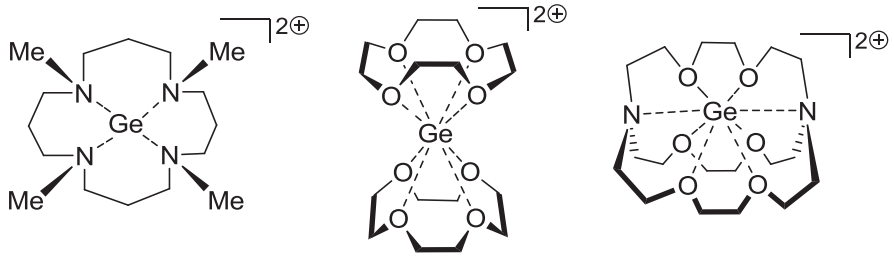


Figure 1.2.2.4 Examples of germanium(II) cations stabilized by azamacrocycles, crown ethers, and cryptand ligands.

Examples of arsine stabilized germanium cations are rare and the only crystallographically authenticated complex has been synthesized by reacting 1,2 bis(dimethylarsino)-benzene with [$GeCl_2$(1,4 dioxane)] in dichloromethane.[44] The structure of [GeCl{*o*-$C_6H_4(AsMe_2)_2$}][$GeCl_3$] reveals a pyramidal geometry at germanium and with the diarsine symmetrically chelating (Figure 1.2.2.5, inset).[44] The chlorine atoms on the $[GeCl_3]^-$ anion is weakly associated with $[Ge\text{-}Cl]^+$. In the solid state

of $[GeCl\{o\text{-}C_6H_4(AsMe_2)_2\}][GeCl_3]$ the $A^-C^+$ interactions create a polymeric species as illustrated in Figure 1.2.2.5.[44]

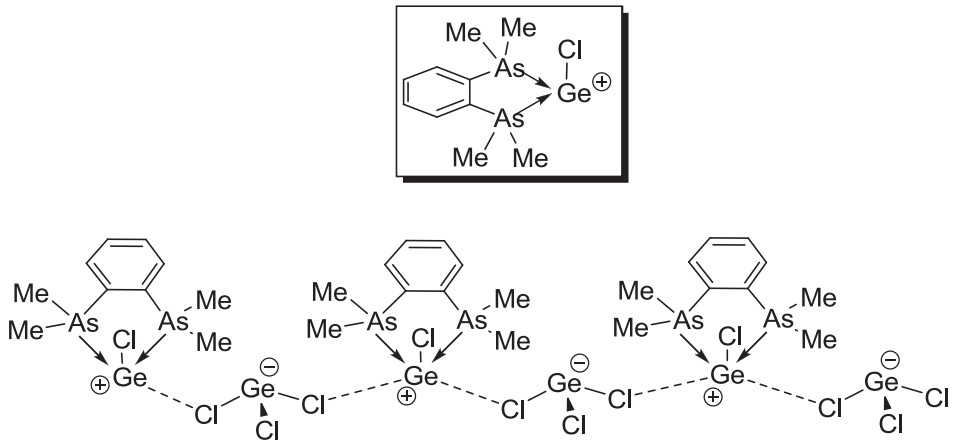


Figure 1.2.2.5 A schematic representation of the solid state structure of $[GeCl\{o\text{-}C_6H_4(AsMe_2)_2\}][GeCl_3]$ showing the $A^-C^+$ interactions. The inset shows the cationic moiety, $[GeCl\{o\text{-}C_6H_4(AsMe_2)_2\}]^+$.

## 1.3 Complexes involving Tin Acceptors with Pnictogen and Oxygen Donors

Coordination chemistry involving tin with nitrogen and oxygen donors has been explored and extensively reported between 1950 and 1975, particularly research involving tetrel acceptors.[45,46,47] The hypervalent derivatives of tin have attracted interest as models for the intermediate structures of nucleophilic substitutions at tetracoodinate group 14 centers.[48] Most of the known neutral tin adducts reported involve hard nitrogen or oxygen donors while less is known about tin interactions with phosphine or arsenic donors. This section will give an overview of Sn–N and Sn-P adducts along with information covering selected examples of some of the tin cations.

### 1.3.1 Neutral Complexes of Tin Acceptors with Nitrogen, Pnictogen, and Arsenic Donors

Initially in the 1970's there were only a few reported single crystal X-Ray structures for neutral nitrogen tin complexes that were either five or six coordinate.[45] Since then considerable efforts have been made to further study N→Sn coordination complexes. The difficulty of isolation was a result of compounds reactivity toward moisture and air and partly due to the fact that the structural question of *cis-trans* isomerization could be settled by IR, Raman, or NMR techniques.[45] When $SnX_4$ is reacted with a neutral nitrogen donor ligand, a corresponding six coordinate tin complex, *trans*-$[SnX_4(NR_3)_2]$, is formed. If a bidentate nitrogen donor is employed, the *cis* product is exclusively observed.[45] As the Lewis acidity decreases from $SnF_4$ to $SnI_4$, isolation of the heavier halide derivatives was more difficult as a result of a weak Sn–N interaction.[44] Much of the reported research has been conducted using $SnCl_4$ and $SnBr_4$ while only a few $SnF_4$ adducts with neutral ligands have been examined, often as a part of a larger survey with the heavier $SnX_4$ analogues.[45] In a $SnX_4$ series using bipy as the ligand, the longest Sn-N bonds were found in $SnI_4$ (2.28(2) Å) and the shortest Sn–N bond length with $SnF_4$ (2.157(7) Å).[45] Complexes involving $SnX_4$ (X= F, Cl, Br, I) with hard nitrogen donors form the stable adducts in the order of $SnF_4 > SnCl_4 > SnBr_4 > SnI_4$ which follows the trend of increasing Lewis acidity. The $SnF_4(NR_3)_2$ complexes are hydrolytically stable adducts; however, nitrogen donor complexes of $SnCl_4$ or $SnBr_4$ hydrolyze easily both as solids and in solution.[45] Complexes of $SnI_4(NR_3)_2$ are more labile in solution and few X-Ray studies have been conducted on structures containing $SnI_4$.[45]

The first single X-Ray structure of a hypervalent complex with a phosphine donor was reported in 1973 and was consistent with all of the spectroscopic studies conducted on *trans*-$SnX_4L_2$ (where L = monophosphine ligand) complexes.[49] A *trans* configuration was previously inferred from vibrational spectroscopy[31] and confirmed by a solid state structure.[45] In the molecular structure of $[SnCl_4(PEt_3)_2]$, the X-Ray diffraction data complemented the Mössbauer data on a series of phosphine complexes of tin(IV) chloride.[45] With the isolation of $[SnCl_4(PEt_3)_2]$, much of the work focused on the isolation of more $SnX_4$ (X = Cl, Br, I) complexes with many other phosphine donors; in addition, chemists began to investigate how bidentate phosphines interact with tin(IV) halides.[45]

In 2006 the molecular structure of $SnF_4$ with $PCy_3$ was reported, the structure was the centrosymmertic *trans*-$[SnF_4(PCy_3)_2]$ with a P–Sn bond length of 2.654(1) Å.[50] In addition to forming a complex with a monodentate ligand to make a six coordinate tin environment, $SnF_4$ can form coordination complexes with bidentate ligands such as 1,2-bis(diethylphosphino)ethane (depe).[50] The structure of $[SnF_4\{Et_2P(CH_2)_2Et_2P\}]$ confirms the *cis* (chelated) geometry deduced from previously conducted NMR studies. The P–Sn distance of 2.606 Å in $[SnF_4\{Et_2P(CH_2)_2Et_2P\}]$ is shorter than the bond length in $[SnF_4(PCy_3)_2]$; this is possibly due to the steric effects caused by the bulky cyclohexyl substituents compared to the ethyl substituents of the bidentate phosphine.[50] With any of the phosphine $SnX_4$ compounds, the trend in bond length is similar to the Sn–N complexes; the shortest bond lengths are found in $[SnF_4(PR_3)_2]$ while the longest bond lengths are in the structures of the type $[SnI_4(PR_3)_2]$. In general, $[SnX_4(PR_3)_2]$ species have more reactive/labile bonds in comparison to their $[SnX_4(NR_3)_2]$ counterparts.[50,45]

A small number of phosphine adducts with $SnX_4$ or $RSnX_3$ have been structurally authenticated, but only a few adducts with the less Lewis acidic $R_3SnX$ moieties have been isolated.[48,49,51] Figure 1.3.1.1 shows examples of $R_3SnX$ compounds which contain an intramolecular P–Sn bond, including some of the longer P–Sn distances reported in literature.[48,51] The long P–Sn interatomic distances are not surprising since the phosphine donors used are weak Lewis bases and the tin moieties used are less Lewis acidic than the $SnX_4$ counterparts. Donor-acceptor complexes with intra- or intermolecular P–Sn interactions using $SnR_4$ moieties have not been reported to date.[48]

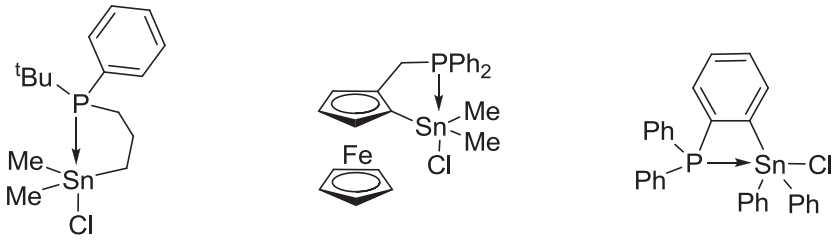


Figure 1.3.1.1 Examples of compounds containing intermolecular dative P–Sn interactions.

Reactions involving arsines with $SnF_4$ have been carried out where a few of the coordination adducts have been characterized by single crystal X-Ray crystallography, and most of the success has been accomplished by using $AsPh_3$ in combination with $SnX_4$ (X = Cl, Br).[52] A 2:1 adduct is formed between $AsPh_3$ and $SnCl_4$ (Figure 1.3.1.2, left) but $SnBr_4$ forms the coordination complex shown in Figure 1.3.1.2 (right) which has the same 2:1 empirical formula but with one $AsPh_3$ group coordinating to tin and the second $AsPh_3$ interacts with a bromine.[52] Notably, in $[SnBr_4AsPh_3 \cdot AsPh_3]$ the equatorial Sn–Br bonds are shorter in comparison to the unique axial Sn–Br bond. The Sn-As bond in $[SnBr_4AsPh_3 \cdot AsPh_3]$ is longer than in $[SnCl_4(AsPh_3)_2]$ as expected considering the lower

Lewis acidity of $SnBr_4$.[51] Compounds such as $[SnX_4AsR_3 \cdot AsR_3]$ are thought to be a precursor for a decomposition route to salts with a general formula $[SnX_3][AsR_3X]$.[51]

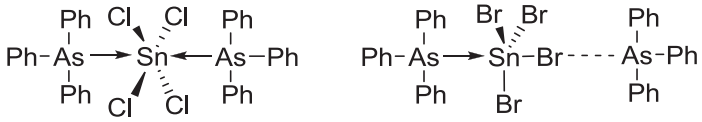


Figure 1.3.1.2 Schematic Structure of $[SnCl_4(AsPh_3)_2]$ (left) and $[SnBr_4AsPh_3 \cdot AsPh_3]$ (right).

### 1.3.2 Cationic Complexes of Tin Acceptors with Oxygen, Nitrogen, and Phosphorus Donors

The search for stable examples of tin(IV) cations was initiated about half a century ago; however, only a few examples have been reported and isolated.[53] Free tricoordinate stannylium (**I**), and tetra- and pentacoordinate stannylium cations (**J**-**N**) are a prominent topic of recent research in the field of organotin chemistry (Figure 1.3.2.1).[54] These species are heavy analogs of carbocations ($[R_3C]^+$) and there is fundamental interest associated with their stability, bonding, and reactivity.[54] In addition, cations of tin have had an increase in interest toward applied research for the polymerization of alkenes, acylation of alcohols, and Diels-Alder reactions.[54,55,56,57,58,59,60]

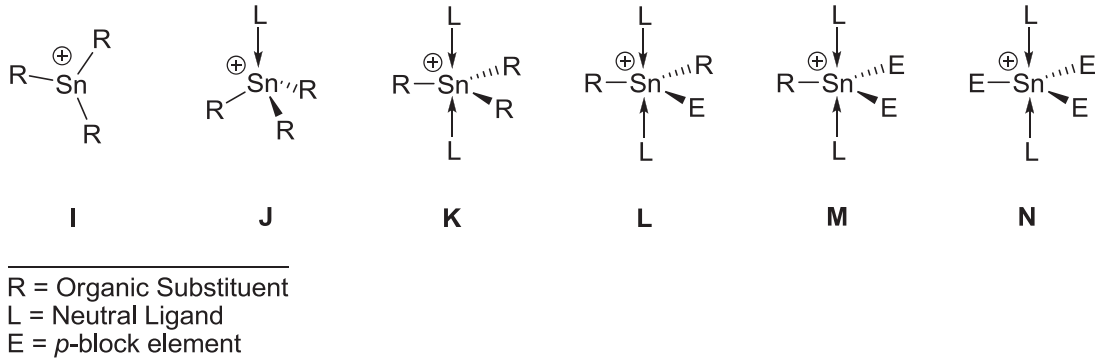


Figure 1.3.2.1 Generic structures of frameworks for stannylium cations with 0, 1, or 2 donor groups where cations like **M** remain elusive.

Several stannylium ions (**I**) have been isolated and characterized by X-Ray crystallography where the triorgano derivatives stabilized by a combination of bulky substituents in conjunction with weakly coordinating anions to generate free cations.[54,54,61] $[E_3Sn]^+$ and $[RSnE_2]^+$ frameworks have been isolated where the tin centers are stabilized by one or two donor groups.[54] The most common framework is five coordinate triorgano tin derivatives (**K**).[54] The use of $[NCN]^-$ tridentate ligands enables stabilization of stannylium cations even in the presence of anions, such as halogenides.[54] A triorgano tin structure of type **K** (Figure 1.3.2.1) was isolated and crystallographically characterized by using two equivalents 4-phenylimidazole with trimethyltin chloride to produce the corresponding cation shown in Figure 1.3.2.2.[62] Cations like the one shown in Figure 1.3.2.2 are of interest because of reports that organotin compounds could potentially display antitumor activity.[62]

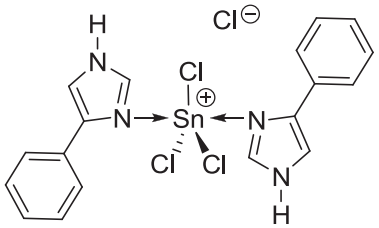


Figure 1.3.2.2 A schematic of [bis(4-phenylimidazole)trimethyltin]chloride.

There are only single examples of the types: **J** ($[R_3Sn]^+$), **L** ($[(L)_2(R_2SnE)]^+$), and even fully inorganic **N** ($[(L)_2(SnE_3)]^+$) as illustrated in Figure 1.3.2.3.[53,63,64] Stannylium cations of the type $[(L)_2(RSnE_2)]^+$ (**M**) are still elusive, although several attempts have been made at their isolation.[53] In the structure of $[L^{CN}(Bu)_2Sn]^+$ [$L^{CN}$ = (2-(N,N-dimethylaminomethyl)phenyl], **O**, three carbon atoms are localized at the base of the square pyramid which is capped by the nitrogen donor atom.[53] The Sn(1)–N(1) distance was found to be 2.258(4) Å. In addition this is the first four-coordinate triorganotin(IV) ionic compound.[63] The reaction of $(2,6\text{-}[P(O)(OEt)_2]_2\text{-}4\text{-}^tBuC_6H_2)SnCl$ with $[Ph_3C][PF_6]$ gave the tin(IV) cation **P** in high yield.[63] This reaction was unprecedented in tin chemistry and can formally be interpreted as a Lewis base-acid complex or as oxidative addition of the trityl cation to the stannylene.[63] The synthesis of **Q** was accomplished by the addition of $Sn(NMe_2)_4$ to a solution of $[Ph_2MeNH][B(C_6F_5)_4]$ in $CH_2Cl_2$, the crude product was described as a viscous yellow oil.[63] Nevertheless, crystals were grown from a concentrated $CH_2Cl_2$ solution, and crystallographic studies revealed the structure $[Sn(NMe_2)_3(HNMe_2)_2]^+$, with two molecules of dimethylamine coordinated to the metal center in the axial positions.[63]

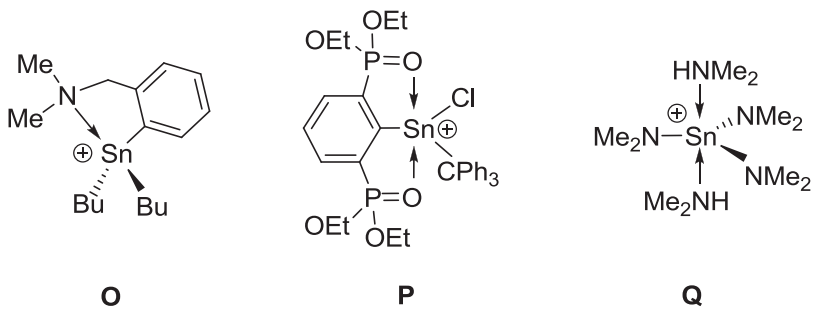


**O** **P** **Q**

Figure 1.3.2.3 Single examples of frameworks **O**, **P**, and **Q**.

One of the more interesting cations found in literature is the tetrakis(stannyl)-phosphonium and ammonium cations which can be alternatively viewed as tris(stannyl)phosphine stabilized stannylium cations.[65,66,67] There are only a few discrete tetra-metal ammonium, phosphonium, and arsonium ions of the form $[PnL_4]^+$ (L = metal or metalloid; Pn = N, P, As) that have been reported.[65] In contrast, frameworks where all groups surrounding the pnictonium cations with main group element substituents like $[(R_3M)_4Pn]$ (R = H, alkyl, aryl; M = Si, Ge, Sn; Pn = N, P ) were previously unknown.[65] This is due to the labile nature of these cations as they are in equilibrium with $[(R_3M)_4Pn]^+$ and the anion on one side and $[R_3M]^+$ with $(R_3M)_3Pn$ on the other.[65] However, the presence of weakly coordinating anions favors the formation of the desired $[(R_3M)_4Pn][A]$ salt.[65] Both the phosphonium and ammonium ions can be made as triflate salts (Scheme 1.3.2.1 **a**); however, the phosphonium cation can be made with $BPh_4^-$ (Scheme 1.3.2.1 **b**) and $SiF_5^-$ (Scheme 1.3.2.1 **c**) anions.[65,66] It is important to mention that these reactions are high yielding and the products are made in high purity.

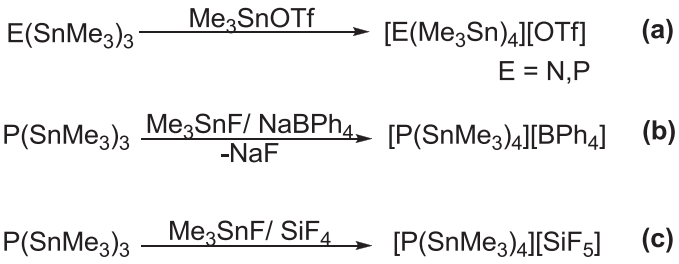


Scheme 1.3.2.1 Synthesis of tetrakis(trimethylstannyl)ammonium and –phosphonium cations.

Only two single crystal X-Ray structures have been reported of the perstannylated cations, both structures are of the triflate anion with ammonium and phosphonium cations.[65] The triflate counter ions have a weak interaction with the tin atoms that is within the sum of the van der Waals radii and outside the sum of the covalent radii for a typical Sn–O bond.[65] The Sn–O interaction (3.07 Å) in $[(Me_3Sn)_4N]^+$ results in a strongly distorted trigonal bipyramidal coordination at the tin center, whereas the tin atom normally has an ideal tetrahedral geometry. The N atom has an almost perfect tetrahedral coordination sphere; however the Sn–N bond length (2.178(5) Å) is about 7% longer than the Sn–N bond in $(Me_3Sn)_3N$ (2.038 Å). The Sn–P bond length in the cation $[(Me_3Sn)_4P]^+$ (2.547(1) Å) is slightly elongated compared to the Sn–P bond length in stannylphosphines (2.52 Å).[65] The tin atoms had a distorted tbp coordination (Sn···O 3.12 Å) while the tetrahedral $Sn_4P$ core was not distorted.[65]

An alternate method to obtain stannylammonium frameworks is accomplished through using $Sn[N(SiMe_3)_2)]_2$ ($Sn^{II}$ starting material) and reacting it with 1,2,4-diazaphospholide to produce a stannylated ammonium ion, **S** (Scheme 1.3.2.2).[67] The X-Ray structure analysis of **S** revealed the ammonium cation stabilized by a samarium tetradiazaphospholido anion.[67] The cationic moiety adopts a slightly distorted tetrahedron

with four tin atoms, four [3,5-$^{t}$Bu$_2$dp]$^-$ ligands, and one tetra-metal-coordinate nitrido ion ($N^{3-}$).[67] The arrangement of the atoms and the average of the Sn-N bond length within the core is 2.150(1) Å similar to those found in **R** despite the removal of a ligand.[67]

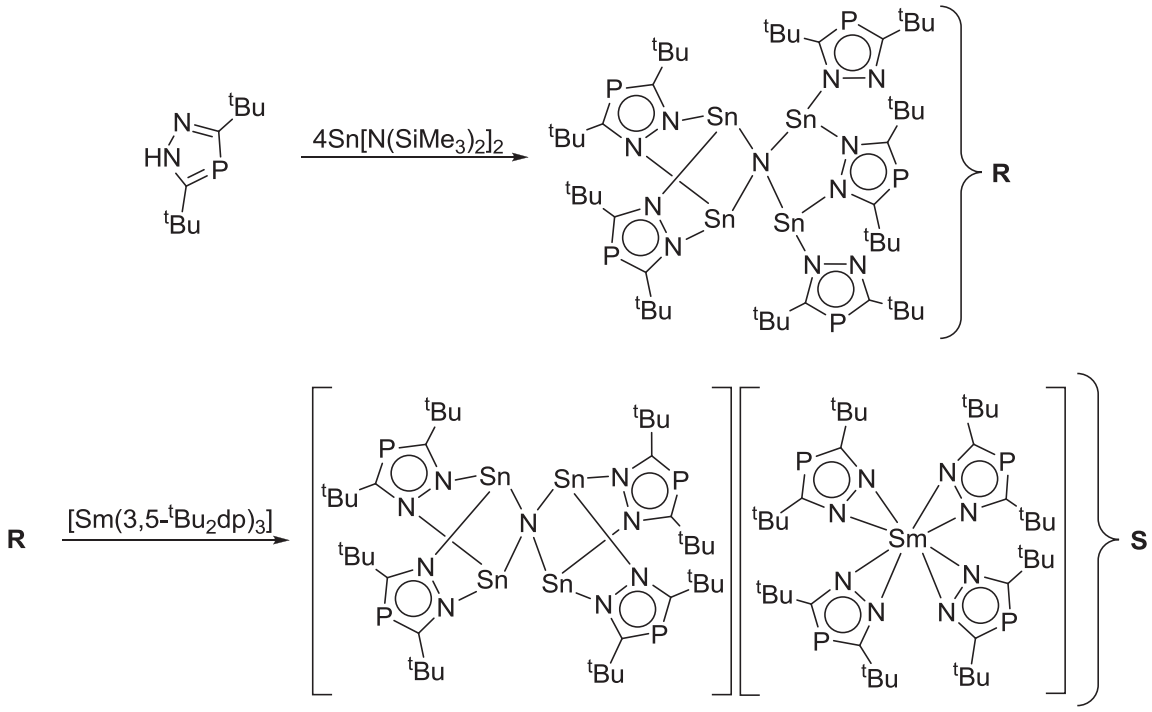


Scheme 1.3.2.2 **R** can be prepared by reacting 1,2,4-diazaphospholide with $Sn[N(SiMe_3)_2)]_2$. **R** in the presence of $[Sm(3,5\text{-}^{t}Bu_2dp)_3]$ gives **S**.

## 1.4 Summary

The formation of ($Pn\rightarrow Pn^+$) frameworks provides precedent toward the isolation of ($Pn\rightarrow E^+$) (where E = Sn, Ge) interactions where this dissertation discusses the formation of phosphorus dative complexes with germanium or tin cations. However, before the document discusses the results of [$P\rightarrow E^+$] interactions, chapter 2 starts by looking at reactions between stannanes and $AlCl_3$ as insight for the reaction mechanism and addition

order. The next section will mark the importance of mixing the stannanes (or germanes) with $AlCl_3$ as there is NMR and X-Ray evidence of in situ formation of aluminate ($AlCl_4^-$) centers along with trapped stannylium ($R_3Sn^+$) cations. Stannanes were selected for this study as tin is NMR active and $^{119}Sn\{^1H\}$ NMR spectroscopy is a diagnostic probe to monitor these reactions as $^1H$ and $^{13}C$ NMR spectroscopy typically do not reveal meaningful information. In addition, $^{27}Al$ ($I = 5/2$), $^{35}Cl$ ($I = 3/2$) and $^{73}Ge$ ( $I = 9/2$) would not be able to reveal much information as a result of the quadrapolar nuclei relaxing rapidly with signal broadening rendering the nuclei not easily observable. Tin has proven effective as a sensitive reaction probe for this process owing to the nuclei being the center of the reaction process. The complexes of $R_nSn_{4-n}AlCl_3$ (where n = 2, 3) were characterized by single crystal X-Ray diffraction which has provided conclusive evidence for significant Sn-Cl-Al interactions.

Chapter 3 will look at the phosphine stabilized germanium cationic and dicationic frameworks complemented by solid state structures and multinuclear NMR data. This includes using different alkylphosphines along with a variety of alkyl- and arylgermanes. The salts are made by first mixing the selected germane with either TMSOTf or $AlCl_3$ followed by the addition of phosphine to generate the corresponding salts. Chapters 4-6 will look at a large variety of phosphine stabilized tin cationic and dicationic salts with alkylchloro functional groups accompanied by discussion of the new phosphorus tin salts.

# CHAPTER 2 INTERACTIONS BETWEEN CHLOROSTANNANES AND ALUMINUM TRICHLORIDE

## 2.1 Background

The first confirmed example of a stannylium salt was $[Bu_3Sn][CB_{11}Me_{12}]$.[68] Notably, the sum of the angles around tin was 353.1° imposed by a weak anion interaction in the axial position. This was reflected in the $^{119}Sn\{^1H\}$ NMR chemical shift of 453 ppm for $[Bu_3Sn][CB_{11}Me_{12}]$ which is well below the expected *c.a.* 1500 ppm for a free cation.[69] It was in 2003 when the first true stannylium cation, $[Tip_3Sn][B(C_6F_5)_4]$, was isolated supported by $^{119}Sn\{^1H\}$ NMR, solid state NMR, X-Ray crystallography, and calculations.[69] For stannylium cations, the anion-cation ($A^-C^+$) interactions generally result from the long Sn-C bond exposing the electrophilic tin center in comparison to its lighter analogues germanium and silicon.[70]

This chapter investigates the reactions between $R_3SnCl$ or $R_2SnCl_2$ with $AlCl_3$ to better understand the activation of the Sn-Cl bond. To the best of my knowledge there is only one report discussing reactions of alkyltinchlorides with $AlCl_3$ to generate Sn-Cl-Al complexes.[71] The report only described the synthesis, isolation and characterization by melting point for these complexes.

## 2.2 Synthesis, Isolation, and Characterization

Equimolar amounts of $Me_3SnCl$ and $AlCl_3$ produce a pale yellow clear reaction mixture with a $^{119}Sn\{^1H\}$ resonance at 255 ppm, confirmed to be the adduct $Me_3SnClAlCl_3$. A similar synthesis was repeated for $iPr_3SnCl/AlCl_3$ ($^{119}Sn\{^1H\}$ = 321 ppm ) and $Ph_3SnCl/AlCl_3$ ($^{119}Sn\{^1H\}$ = -150 ppm). The $^{119}Sn\{^1H\}$ NMR spectrum of

$iPr_3SnCl/AlCl_3$ revealed the tin nucleus shifted downfield in comparison to the $iPr_3SnCl$, starting material in the absence of $AlCl_3$. This could be due the aluminum interacting with the tin chlorine which would place a partial positive charge on tin and a partial negative charge on aluminum. The bridging chlorine between tin and aluminum is confirmed by X-Ray crystallography and it is plausible that a similar process could occur in solution. However, in the case of the $Ph_3SnCl$ the tin environment is more shielded in the presence of $AlCl_3$ and furthermore, $Ph_3SnCl$ has seemingly undergone a transmetallation/solvent activation reaction with $AlCl_3$ and dichloromethane as the reaction mixture produced a deep red-brown oil. By $^{119}Sn\{^1H\}$ NMR spectroscopy, there is a single resonance present at -150 ppm which is consistent with $SnCl_4$ with no evidence of $Ph_3SnCl$ remaining. Additionally, the mixture transformed to a red-brown slurry within 20 mins of adding the reactants together.

Reactions of $R_2SnCl_2$ in the presence of $AlCl_3$ show an upfield shift in comparison to the respective starting material in the absence of $AlCl_3$. This is evident when looking at mixtures of $Bu_2SnCl_2/AlCl_3$ ($^{119}Sn\{^1H\}$ = 107 ppm) and $Bu_2SnCl_2/2AlCl_3$ ($^{119}Sn\{^1H\}$ = -40 ppm) (Table 2.2.1). The tin nuclei for reactions of $Me_2SnCl_2$ in the presence of one and two equivalents of $AlCl_3$ showed a similar upfield trend. When $Ph_2SnCl_2$ is reacted with any stoichiometry of $AlCl_3$, there is a tin $^{119}Sn\{^1H\}$ resonance at -150 ppm which is characteristic of $SnCl_4$ and analogous to the $Ph_3SnCl$ reaction with $AlCl_3$. Mixtures of $SnCl_4$ with a large excess of $AlCl_3$ only show a resonance at -150 ppm indicating there is no interaction between the two reactants.

Table 2.2.1 $^{119}Sn\{^{1}H\}$ NMR data for mixtures of $R_3SnCl$ (R = Me, iPr, Ph) or $R_2SnCl_2$ (R = Me, Bu, Ph) with $AlCl_3$.

| Compound | $CH_2Cl_2$ | $AlCl_3$ | $2AlCl_3$ |
|---|---|---|---|
| $Me_3SnCl$ | 171 | 255 | 255 |
| $iPr_3SnCl$ | 111 | 321 | 321 |
| $Ph_3SnCl$ | -46 | -150 | -150 |
| $Me_2SnCl_2$ | 137 | 107 | 56 |
| $Bu_2SnCl_2$ | 127 | 100 | -40 |
| $Ph_2SnCl_2$ | 29 | -150 | -150 |
| $SnCl_4$ | -150 | -150 | -150 |

## 2.3 Molecular Structures

Single crystal X-Ray diffraction studies have been completed on the tin-aluminum trichloride complexes of $Me_3SnClAlCl_3$ (Figure 2.3.1), $Me_2SnCl_2AlCl_3$ (Figure 2.3.2), and $Bu_2SnCl_2AlCl_3$ (Figure 2.3.3). Selected interatomic distances and angles are summarized in Table 2.3.1 and Table 2.3.2. The tin atoms in $Me_3SnClAlCl_3$ and $Me_2SnCl_2AlCl_3$ are consistent with VSEPR and have a tbp geometry; the aluminate anions are tetrahedral. $Bu_2SnCl_2AlCl_3$ on the other hand crystallizes as a dimeric species with each of the tin atoms exhibiting an octahedral geometry. $^{119}Sn\{^{1}H\}$ NMR spectroscopy does not provide evidence for a dimeric $(Bu_2SnCl_2AlCl_3)_2$ species in solution as $^{119}Sn$-$^{119}Sn$ or $^{119}Sn$-$^{117}Sn$ coupling is absent.

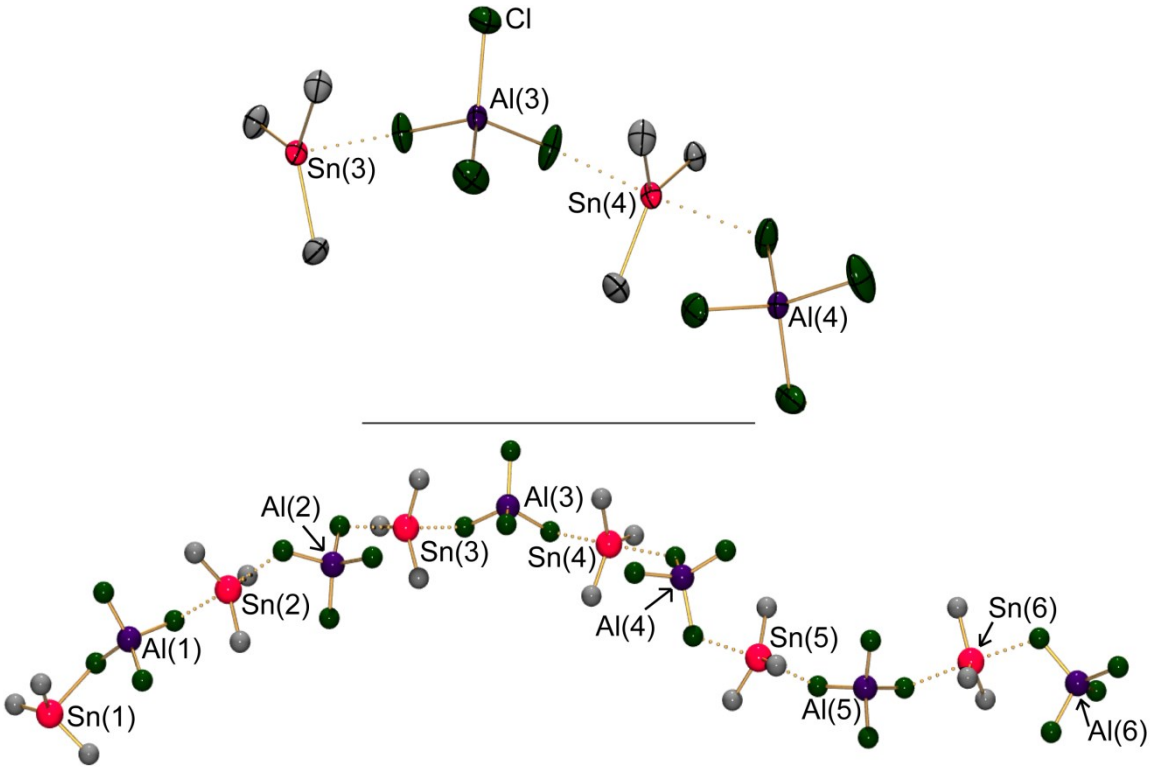


Figure 2.3.1 POV-Ray ball and stick representation of the asymmetric unit in the molecular structure of $Me_3SnClAlCl_3$(bottom). Two-units of $Me_3SnClAlCl_3$ are expanded for clarity (top) with the thermal ellipsoid plots drawn at the 50% probability level. Hydrogen atoms omitted for clarity.

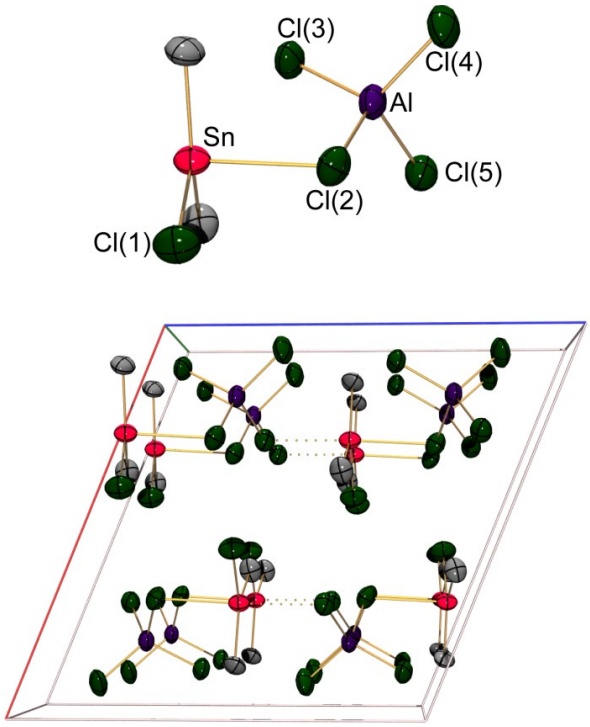


Figure 2.3.2 POV-Ray representation of the asymmetric unit (top) in the molecular structure of $Me_2SnCl_2AlCl_3$ along with a POV-Ray image of the unit cell (bottom). Thermal ellipsoid plots are at the 50% probability level with hydrogen atoms omitted for clarity.

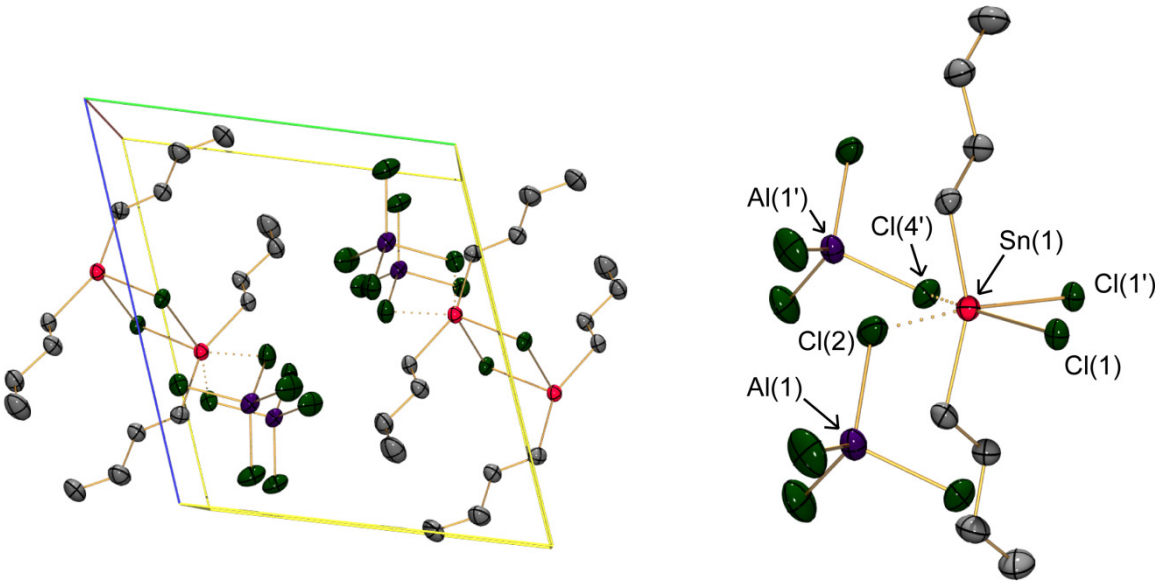


Figure 2.3.3 POV-Ray representation of unit cell of $Bu_2SnCl_2AlCl_3$ (left) along with a POV-Ray representation of one of the tin centers in found in the dimer. Thermal ellipsoid plots are at the 50% probability level with hydrogen atoms omitted for clarity.

The Sn···Cl interatomic distances in $Me_3SnClAlCl_3$ exhibit the range 2.7287(13) Å-2.8626(13) Å. In $Me_2SnCl_2AlCl_3$ the Sn···Cl distances are 2.757(2) Å and 2.795(2) Å while $Bu_2SnCl_2AlCl_3$ has a Sn···Cl interaction of 2.7856(7) Å. In $Me_2SnCl_2AlCl_3$ and $Bu_2SnCl_2AlCl_3$ the covalent Sn-Cl distances are 2.331(2) Å and 2.4862(6) Å, 2.6743(6) Å respectively. The Sn-Cl interatomic distances in $Bu_2SnCl_2AlCl_3$ are slightly outside the sum of the covalent radii (2.40 Å); this longer than average chorine bond is a result of the dimeric structure which is observed for many examples of halide bridged dimers (eg: $Al_2Cl_6$). In general, the Al-Cl bonds are slightly elongated if the chlorines also interact with tin.

Table 2.3.1 Selected interatomic distances (Å) for $Me_3SnClAlCl_3$, $Me_2SnCl_2AlCl_3$, and $Bu_2SnCl_2AlCl_3$.

| **Compound** | **Atom** | **Sn-Cl** | **Sn···Cl[$AlCl_3$]** |
|---|---|---|---|
| $Me_3SnClAlCl_3$ | Sn(1) | - | 2.7387(13) |
| | Sn(2) | - | 2.7906(12), 2.7959(13) |
| | Sn(3) | - | 2.7823(13), 2.8626(13) |
| | Sn(4) | - | 2.8076(14), 2.8163(14) |
| | Sn(5) | - | 2.7942(15), 2.8201(14) |
| | Sn(6) | - | 2.7808(13), 2.8244(16) |
| $Me_2SnCl_2AlCl_3$ | Sn(1) | 2.331(2) | 2.757(2), 2.795(2) |
| $Bu_2SnCl_2AlCl_3$ | Sn(1) | 2.4862(6), 2.6743(6) | 2.7856(7), 3.197 |

Table 2.3.2 Selected interatomic angles (°) for $Me_3SnClAlCl_3$, $Me_2SnCl_2AlCl_3$, and $Bu_2SnCl_2AlCl_3$.

| Compound | Atom | C-Sn-C | Cl···Sn···Cl[a,b] |
|---|---|---|---|
| $Me_3SnClAlCl_3$ | Sn(1) | 119.3(2), 123.0(2), 117.6(2) | - |
| | Sn(2) | 121.2(3), 121.2(2), 117.6(3) | 172.96(5) |
| | Sn(3) | 121.9(3), 121.2(3), 116.9(3) | 172.50(4) |
| | Sn(4) | 122.9(2), 119.4(3), 117.8(2) | 168.25(4) |
| | Sn(5) | 119.4(4), 120.0(3), 120.6(4) | 172.47(6) |
| | Sn(6) | 120.6(3), 117.9(3), 121.5(3) | 173.18(5) |
| $Me_2SnCl_2AlCl_3$ | Sn(1) | 147.0(4) | 176.14(6) |
| $Bu_2SnCl_2AlCl_3$ | Sn(1) | 154.17(8) | 79.008(18), 157.760(16) |

[a] The chlorine interactions are specific to the ones that have also have an interaction with an aluminum center.
[b] Cl-Sn-Cl covalent angle in $Bu_2SnCl_2AlCl_3$ is 79.659(19)° whereas the Cl···Sn···Cl interaction from the aluminate-like structures in $Bu_2SnCl_2AlCl_3$ is 126.10°.

## 2.4 Summary and Conclusion

A variety of reactions of alkyltin chlorides with $AlCl_3$ were investigated and the products characterized by $^{119}Sn\{^1H\}$ NMR spectroscopy and single crystal X-Ray diffraction. Interactions involving $AlCl_3$ with dialkyltin dichloride and trialkyltin chloride were explored leading to the characterization and isolation of compounds containing Sn–Cl–Al linkages which are aluminate chlorine atoms effectively stabilizing $[R_3Sn]^+$ or $[R_2SnCl]^+$ moiety. The synthesis was carried out where the reactions could effectively be done at room temperature and in a solvent which avoids the need for melt conditions. However, the crystalline yields of the complexes tend to be low with the material being sensitive to moisture. It is advisable to do the $E/AlCl_3$ (E = Stannane, germane) step *in situ* in the amount required to generate cationic phosphine complexes of tin and germanium.

# CHAPTER 3 PHOSPHINE STABILIZED GERMYLIUM AND GERMYLDIYLIUM CATIONS AND DICATIONS

## 3.1 Background

Coordination compounds involving phosphine ligands on germanium are rare and examples of salts have not been reported. Neutral germanium phosphorus coordination chemistry is limited to a few examples. A 1995 article reported that there were only two Ge-P coordination complexes crystallographically characterized.[72] The molecular structures were of $GeI_2PPh_3$ and $GeCl_2PPh_3$.[73] Since then there has been an increased amount of published examples of Ge-P coordination complexes with germanium(II) halides.[30,44] In a 2012 review[33] there were more examples of Ge-P coordination complexes by means of multidentate anionic ligands with phosphine donors. This chapter focuses on the synthesis and characterization of the first phosphine complexes of germanium cations.

## 3.2 Synthesis, Isolation, and Characterization

Equimolar amounts of $Me_3P$, $Me_2GeCl_2$ and $AlCl_3$ were combined together which produced a colorless clear reaction mixture. This solution showed a $^{31}P\{^1H\}$ NMR resonance at -15.3 ppm, this resonance was assigned to$[Me_3PMe_2GeCl][AlCl_4]$ (equation 3.1). Colorless parallelepiped crystals were grown by layering the reaction mixture with $Et_2O$ over the course of two days at -25°C. The material was confirmed to be $[Me_3PMe_2GeCl][AlCl_4]$. Equimolar amounts of $Me_3P$, $Et_3GeCl$ and $AlCl_3$ produced $[Me_3PEt_3Ge][AlCl_4]$ (equation 3.2) with a $^{31}P\{^1H\}$ NMR signal at -21.7 ppm. Crystals of $[Me_3PEt_3Ge][AlCl_4]$ were obtained by layering the colorless, clear reaction mixture with

$Et_2O$ to give a colorless, translucent solid over the course of two days; however the material isolated diffracted poorly.

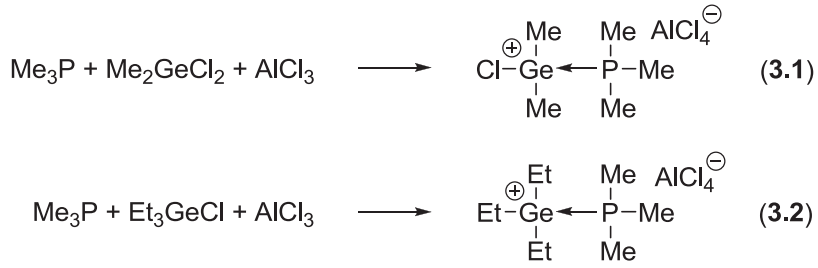


In the presence of equimolar amounts of $iPr_3P$, $Me_2GeCl_2$ and TMSOTf, the salt $[iPr_3PMe_2GeCl][OTf]$ (equation 3.3) is readily synthesized confirmed to have a $^{31}P\{^1H\}$ NMR resonance at 26.5 ppm. Colorless parallelepiped crystals of $[iPr_3PMe_2GeCl][OTf]$ were grown by layering the reaction mixture with $Et_2O$ which slowly diffused over the course of two days at -25°C. Equimolar amounts of $Cy_3P$, $Et_3GeCl$ and $AlCl_3$ were combined together which produced a pale yellow clear mixture confirmed to be $[Cy_3PEt_3Ge][AlCl_4]$ (equation 3.4) with a $^{31}P\{^1H\}$ NMR resonance at 13.6 ppm. Solvent was removed by vacuum to reveal pale yellow oil. The oil can be dissolved in $CH_2Cl_2$ and layered with hexane to grow a few X-Ray quality crystals over the course of 2 days at -25°C. The colorless block crystals of $[Cy_3PEt_3Ge][AlCl_4]$ were isolated with a small amount of pale yellow oil. After many attempts the oil could not be separated from the crystals.

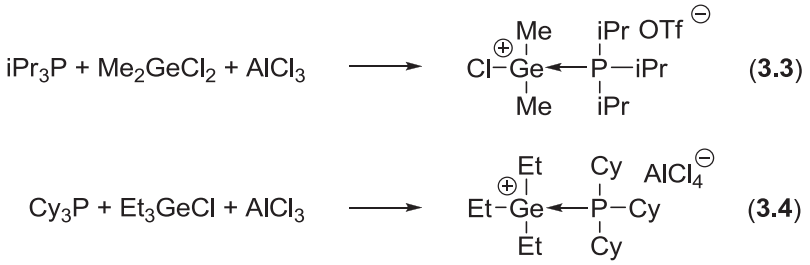


One equivalent of dmpe in the presence of two equivalents of $Et_3GeCl$ and TMSOTf gives $[dmpe(Et_3Ge)_2][OTf]_2$ (equation 3.5) which produced a colorless clear reaction mixture with a $^{31}P\{^1H\}$ NMR resonance at -12.3 ppm. Colorless parallelepiped crystals of $[dmpe(Et_3Ge)_2][OTf]_2$ were grown by layering the reaction mixture with $Et_2O$ and over the course of two days at -25°C. One equivalent of dmpe and $Me_2GeCl_2$ in the presence of two equivalents of TMSOTf produce a colorless clear reaction mixture to give $[(dmpe)Me_2Ge][OTf]_2$ (equation 3.6) with a $^{31}P\{^1H\}$ NMR resonance at 2.60 ppm. Colorless plate crystals of $[(dmpe)Me_2Ge][OTf]_2$ were grown by slow evaporation of $CH_3CN$ over the course of 6 days at room temperature, $CH_3CN$ was used as it allowed all of the material to dissolve and did not displace the diphosphine in $[(dmpe)Me_2Ge][OTf]_2$, additionally, $CH_2Cl_2$ was not able to dissolve all material which made crystallization more challenging.

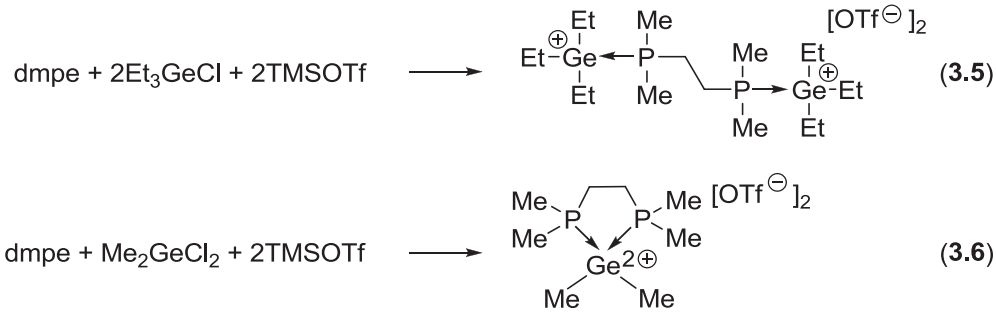

Phosphine stabilized triphenylgermylium salts were synthesized and characterized. $Ph_3GeCl$ was used in conjunction with TMSOTf to avoid transmetallation/solvent activation reactions that were found to occur when $Ph_3GeCl$ was in a $CH_2Cl_2$ solution with $AlCl_3$. Equimolar mixtures of $Me_3P$, $Ph_3GeCl$ and TMSOTf produce a colorless clear solution containing $[Me_3PPh_3Ge][OTf]$ (equation 3.7) with a $^{31}P\{^1H\}$ NMR broad resonance at -19.0 ppm. Colorless plate-like crystals of $[Me_3PPh_3Ge][OTf]$ were grown by layering the reaction mixture with hexane and cooling the mixture to -25°C over the course of two days. One equivalent of dmpe in the presence of two equivalents of $Ph_3GeCl$ and TMSOTf produced a colorless clear reaction mixture containing $[dmpe(Ph_3Ge)_2][OTf]_2$ (equation 3.8) with a $^{31}P\{^1H\}$ resonance at -11.2 ppm. Colorless rod-shaped crystals of $[dmpe(Ph_3Ge)_2][OTf]_2$ were grown by layering the reaction mixture with hexane and cooling the mixture to -25°C for two days.

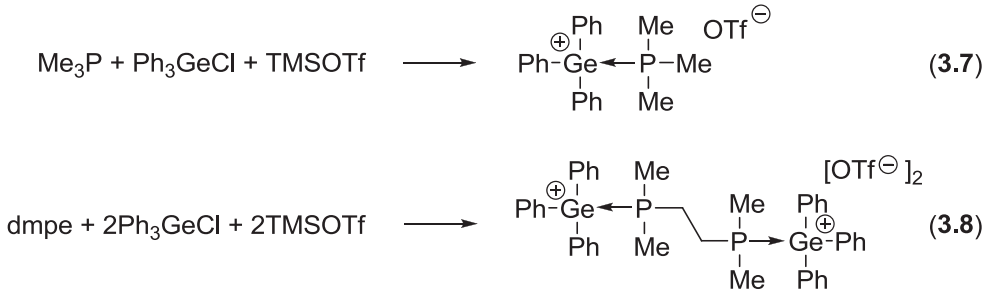

Table 3.2.1 $^{31}P\{^{1}H\}$NMR chemical shifts for phosphine stabilized cations and dications of germanium.

| Compound | $^{31}P\{^{1}H\}$ NMR: δ, ppm |
|---|---|
| $[Me_3PEt_3Ge][AlCl_4]$ | -21.7 |
| $[Me_3PMe_2GeCl][AlCl_4]$ | -15.3 |
| $[iPr_3PMe_2GeCl][OTf]$ | 26.5 |
| $[Cy_3PEt_3Ge][AlCl_4]$ | 13.6 |
| $[dmpe(Et_3Ge)_2][OTf]_2$ | 2.6 |
| $[(dmpe)Me_2Ge][OTf]_2$ | -12.3 |
| $[Me_3PPh_3Ge][OTf]$ | -19.0 |
| $[dmpe(Ph_3Ge)_2][OTf]_2$ | -11.2 |

## 3.3 Molecular Structures

Single crystal X-Ray diffraction studies were carried out on the phosphine complexes of germanium cations shown in Figures 3.3.1-3.3.3 with selected bond lengths and angles summarized in Table 3.3.1. The molecular structures of $[iPr_3PMe_2GeCl][OTf]$ and $[Me_3PMe_2GeCl][AlCl_4]$ were disordered precluding discussion of the interatomic parameters; however, connectivity between phosphorus and germanium is confirmed. Additionally, the compositions of compounds were verified by elemental analysis. The geometry at germanium in $[Cy_3PEt_3Ge][AlCl_4]$ (Figure 3.3.1 middle) is close to an ideal tetrahedral geometry (tetrahedral three angle sum = 328.5°) where the sum of the C-Ge-C angles are 331.5(2)° and 337.6(2)°.

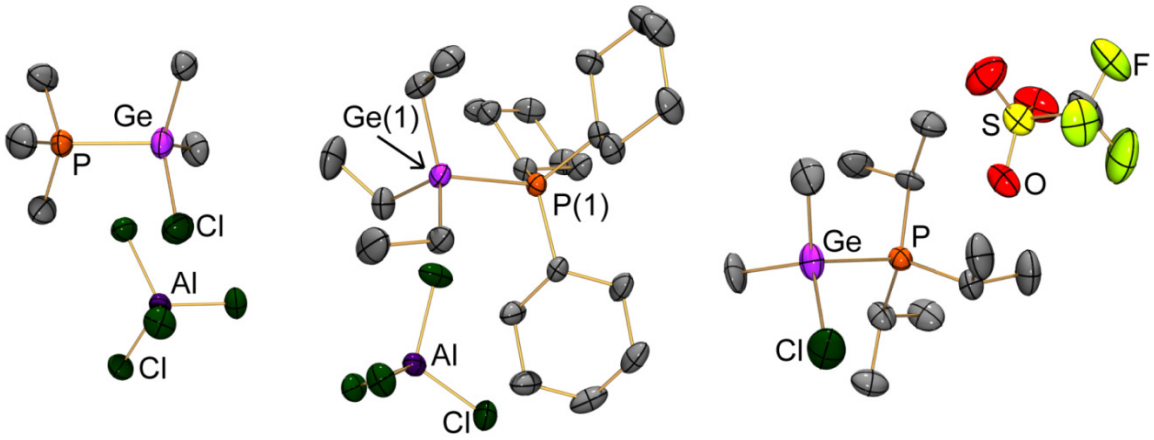


Figure 3.3.1 POV-Ray representation of $[Me_3PMe_2GeCl][AlCl_4]$ (left), $[Cy_3PEt_3Ge][AlCl_4]$ (middle), and $[iPr_3PMe_2GeCl][OTf]$ (right). Thermal ellipsoids are at the 50% probability level, hydrogen atoms are omitted for clarity.

The molecular structures of $[(dmpe)Me_2Ge][OTf]_2$ and $[dmpe(Ph_3Ge)_2][OTf]_2$ are preliminary which precludes discussion until better quality data are collected. Nevertheless, the data confirm Ge-P connectivity which is consistent with that for the other salts discussed in this section. In the structure of $[(dmpe)Me_2Ge][OTf]_2$ there is a disordered triflate anion, the data were used to confirm Ge-P connectivity. The geometry at germanium in $[dmpe(Et_3Ge)_2][OTf]_2$ is distorted tetrahedral (ideal three angle sum = 328.5°)with a C-Ge-C angle sum of 339.9(5)° for Ge(1) and 335.5(2)° for Ge(2). Consistently, the geometry for germanium in $[Me_3PPh_3Ge][OTf]$ is distorted tetrahedral with a C-Ge-C angle sum of 336.10(13)°.

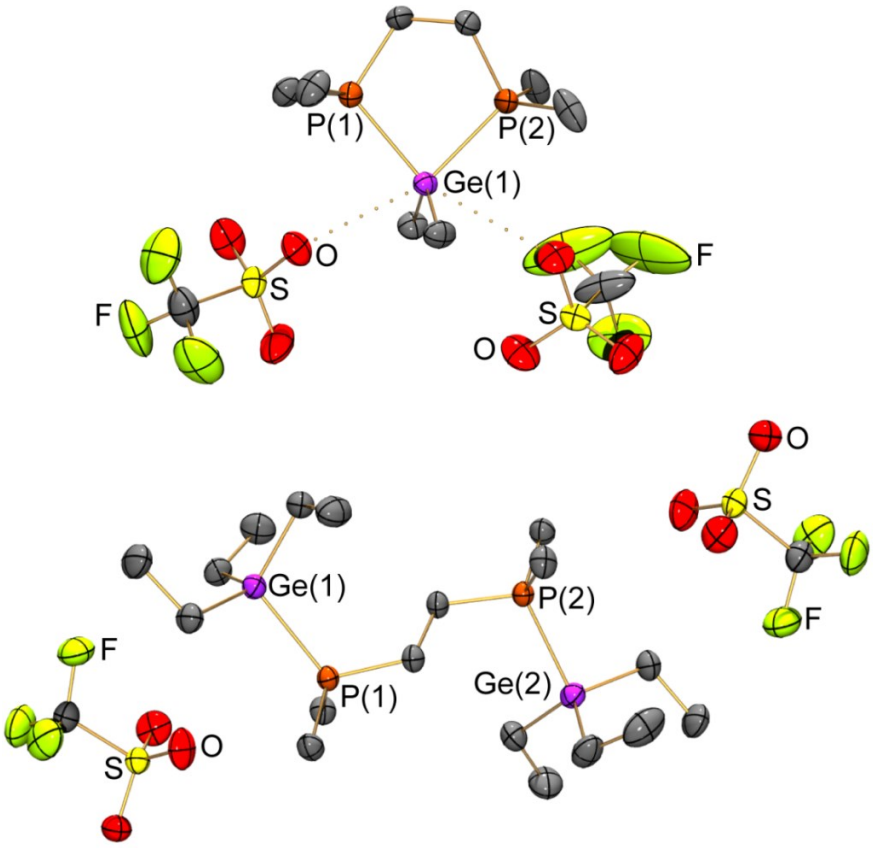


Figure 3.3.2 POV-Ray representation of $[(dmpe)Me_2Ge][OTf]_2$ (top) and $[dmpe(Et_3Ge)_2][OTf]_2$ (bottom), thermal ellipsoids are at the 50% probability level, hydrogen atoms are omitted for clarity.

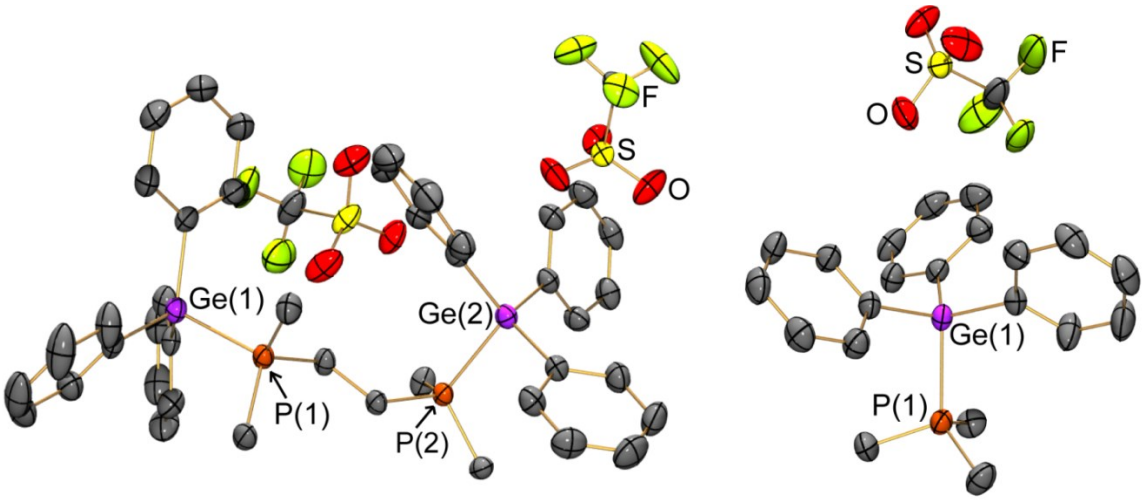


Figure 3.3.3 POV-Ray view of $[dmpe(Ph_3Ge)_2][OTf]_2$ (left) and $[Me_3PPh_3Ge][OTf]$ (right). Thermal ellipsoids are at the 50% probability level, hydrogen atoms are omitted for clarity.

The Ge-P interatomic distances for $[dmpe(Et_3Ge)_2][OTf]_2$ (2.3572(7) Å, 2.3695(7) Å) are similar to those for $[Cy_3PEt_3Ge][AlCl_4]$ (2.3822(7) Å, 2.3743(7) Å) and $[Me_3PPh_3Ge][OTf]$ (2.3538(6) Å), only slightly outside the sum of the covalent radii (2.28 Å). On the other hand, $[Cy_3PEt_3Ge][AlCl_4]$ has a slightly longer Ge-P interatomic distance in comparison to the other salts even though $Cy_3P$ is a better Lewis Base compared to $Me_3P$. Perhaps the dative bond distance is longer as a result of steric repulsion between the ethyl and cyclohexyl groups in the cation. In the lattice of $[Cy_3PEt_3Ge][AlCl_4]$ the aluminate is located in the proximity of the germanium center. This indicates that germanium bears the positive charge. The anion-cation ($A^-C^+$) interactions present in the majority of the salt show that there is not direct interaction of the anion with germanium, this is most likely due to the smaller atomic radius of germanium. This is in contrast with the tin studies (chapter 4-6) where tin normally has an interaction with the anions; this again can be accounted for by the atomic size of germanium (1.25 Å) versus tin (1.45 Å).

Table 3.3.1 Selected structural parameters for $[Cy_3PEt_3Ge][AlCl_4]$, $[dmpe(Et_3Ge)_2][OTf]_2$, and $[Me_3PPh_3Ge][OTf]$

| | **$[Cy_3PEt_3Ge][AlCl_4]$** | **$[dmpe(Et_3Ge)_2][OTf]_2$** | **$[Me_3PPh_3Ge][OTf]$** |
|---|---|---|---|
| Ge–P (Å) | 2.3822(7)<br>2.3743(7) | 2.3572(7)<br>2.3695(7) | 2.3538(6) |
| Nearest $A^-C^+$ Interaction (Å) | 2.945, 2.902<br>[H···Cl] | 2.654<br>[O···H] | 2.708, 2.679<br>[O···H] |
| Σ C–Ge–C (°) | 331.5(2)<br>337.6(2) | 339.9(5)<br>335.5(2) | 336.10(13) |

## 3.4 Summary and Conclusion

A small but diverse library of the first salts of phosphine stabilized germylium cations, digermylium dications, and a germyldiylium dication were synthesized, isolated and characterized by multinuclear NMR spectroscopy. Additionally, the data collected were complemented by single crystal X-Ray diffraction for most of the complexes discussed; the remaining salts were not characterized by X-Ray diffraction due to the poor crystallinity of the material. Salts can be made where germanium has alkyl or aryl functionality in addition to having one or two chlorides abstracted from the germane. The germanium cations were complexed with monophosphines $Me_3P$, $iPr_3P$, and $Cy_3P$ along with the diphosphine dmpe.

# CHAPTER 4 A PHOSPHINE STABILIZED CHLOROSTANNYLIUM CATION AND A CHLOROSTANNYLDIYLIUM DICATION

## 4.1 Background

Complexes of tin(IV) halides have been reported to form dative interactions with ligands such as phosphines (monodentate and bidentate),[74,75,76] phosphine oxides (coordination with the oxygen atom),[74] sulphides,[76] ethers,[75] pyridines,[74] and amines.[74] Examples of these frameworks are highlighted in Figure 4.1.1. The common feature of all the structures is that all the tin centers have halide groups present; without electron withdrawing group functionality the stannane is not acidic enough to undergo coordination chemistry. All of the compounds featured in Figure 4.1.1 involve two monodentate interactions or two interactions from a bidentate ligand. The orientation of each of the ligands in **B**, **E**, and **F** are *trans* and the ligands in **A**, **C**, and **D** are *cis* for the chelate ligands. Not surprising is that bidentate ligands like **G**, and **H** are disfavored. However, an exception would be when a bidentate ligand is predisposed to a configuration where chelation was not possible. This chapter looks at diversifying tin coordination chemistry where the syntheses involve $SnCl_4$ and two equivalents of $PMe_3$ with varying stiochiometries of $AlCl_3$ to generate a neutral, a cationic and a dicationic framework.

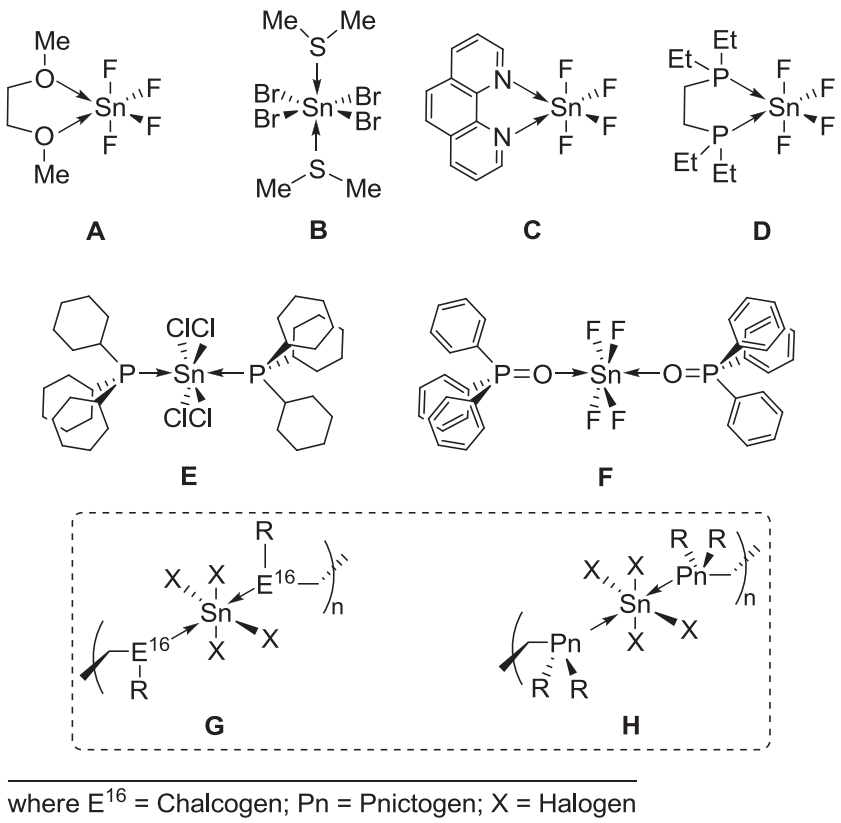


Figure 4.1.1 Examples of tin(IV) halides forming coordination complexes with ethers (**A**), sulfides (**B**), pyridines (**C**), diphosphines (**D**), phosphines (**E**) and phosphine oxides (**F**). Coordination complexes in the dashed box (**G** and **H**) are not observed.

Vibrational spectroscopic studies on the neutral complex $(PMe_3)_2SnCl_4$ were completed previously,[77,32] however solid state $^{31}P$ NMR data and X-Ray diffraction data were not collected on $(Me_3P)_2SnCl_4$ during the initial investigations. We sought to complete the characterization of $(PMe_3)_2SnCl_4$ for comparison with $[(Me_3P)_2SnCl_3][AlCl_4]$ and $[(Me_3P)_2SnCl_2][AlCl_4]_2$ to examine the full molecular series.

## 4.2 Synthesis, Isolation, and Characterization

Reaction mixtures of $Me_3P$ with $SnCl_4$ give $SnCl_4(PMe_3)_2$ (equation 4.1) in high yield independent of the stoichiometry of the mixture. The reaction yields a colorless precipitate with a colorless clear supernatant. After an hour a $^{31}P\{^1H\}$ NMR spectrum was recorded on the supernatant which revealed a new resonance at 1.6 ppm and a triplet resonance at -554 ppm in the $^{119}Sn\{^1H\}$NMR spectrum. These new resonances were confirmed to be $(Me_3P)_2SnCl_4$. The NMR data deviated from the previously reported $(Me_3P)_2SnCl_4$ at 6.8 ppm ( $^1J_{PSn}$ 2720 Hz).[77] In the same data the *cis* isomer was reported to be at 3.6 ppm; however during my investigations, the *trans* isomer was the exclusive product. Solid state $^{31}P$ CP/MAS NMR spectra of the bulk precipitate obtained from the reaction mixture were identical to the NMR spectra obtained for the crystals of $(PMe_3)_2SnCl_4$. Spectral data on the bulk solids was difficult to obtain due to the low solubility of the material in chlorocarbon solvents. Solvation in $CH_3CN$ resulted in an exchange reaction to generate $(CH_3CN)_2SnCl_4$.[78] Crystals were confirmed to be the same material as the bulk precipitate as the $^{31}P$ CP/MAS NMR chemical shifts and coupling constants matched perfectly. The solid state $^{31}P$ CP/MAS NMR (6.7 ppm, $^1J_{Sn-P}$ = 2772 Hz) and solution $^{31}P\{^1H\}$ NMR (1.6 ppm, $^1J_{Sn-P}$ = 2635/2517 Hz) chemical shifts of $(Me_3P)_2SnCl_4$ differ slightly (Figure 4.2.1). A possibility to account of the difference between solution and solid state is that the solution NMR could have solvent ($CH_2Cl_2$) interactions with $(Me_3P)_2SnCl_4$ where the chlorine atoms could provide shielding to the phosphorus nuclei via proximity.

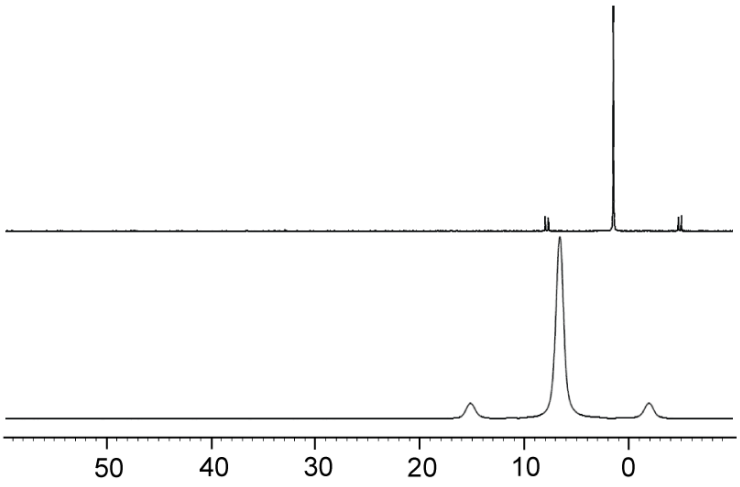


Figure 4.2.1 Dichloromethane-$d_2$ solution $^{31}P\{^1H\}$ NMR spectrum (top) and solid state $^{31}P$ CP/MAS NMR spectrum (bottom) of $(PMe_3)_2SnCl_4$.

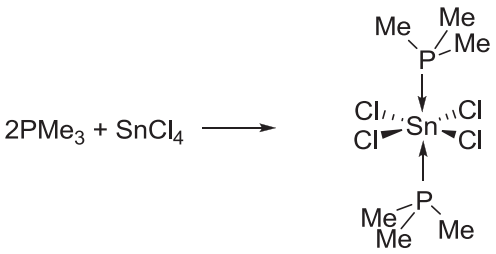


(**4.1**)

In the presence of one equivalent of $AlCl_3$, mixtures of $Me_3P$ with $SnCl_4$ give the ionic compound $[SnCl_3(PMe_3)_2][AlCl_4]$ in high yield (equation 4.2) which exhibit a single resonance at 10.8 ppm in the $^{31}P\{^1H\}$ NMR spectrum and a triplet at -456 ppm in the $^{119}Sn\{^1H\}$ NMR spectrum. Consistently, $(PMe_3)_2SnCl_4$ reacts with one equivalent of $AlCl_3$ to yield $[SnCl_3(PMe_3)_2][AlCl_4]$ with matching phosphorus and tin NMR resonances. Solid state $^{31}P$ CP/MAS NMR spectra acquired on both the bulk precipitate isolated from the reaction mixture and the slowly grown crystals confirmed that the two components had matching resonances at 15.9 ppm ($^1J_{Sn\text{-}P}$ 2706 Hz). The solution (10.8 ppm) and solid state (15.9 ppm) NMR spectra are compared in Figure 4.2.2 and as for

$(Me_3P)_2SnCl_4$, the chlorine atoms from $CH_2Cl_2$ could provide shielding to the phosphines which can result in a 5 ppm difference between the solution and the solid phase NMR.

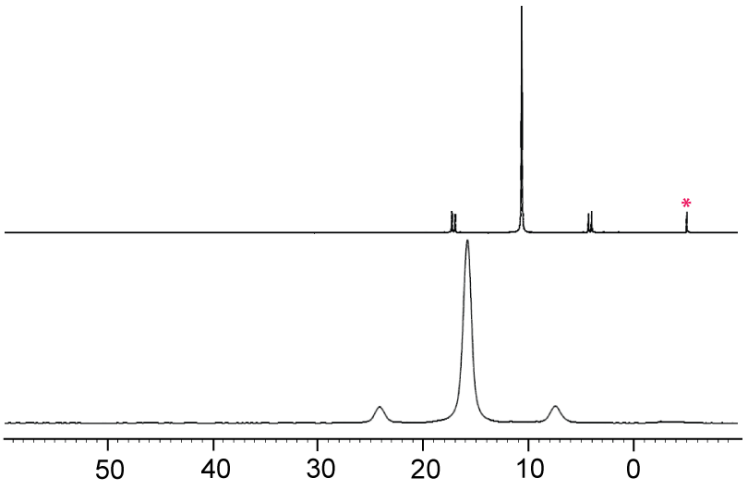


Figure 4.2.2 Dichloromethane-$d_2$ solution $^{31}P\{^1H\}$ NMR spectrum (top) and solid state $^{31}P$ CP/MAS NMR spectrum (bottom) of $[SnCl_3(PMe_3)_2][AlCl_4]$. Asterisk indicates a small $[Me_3PH]^+$ impurity present in the top spectrum.

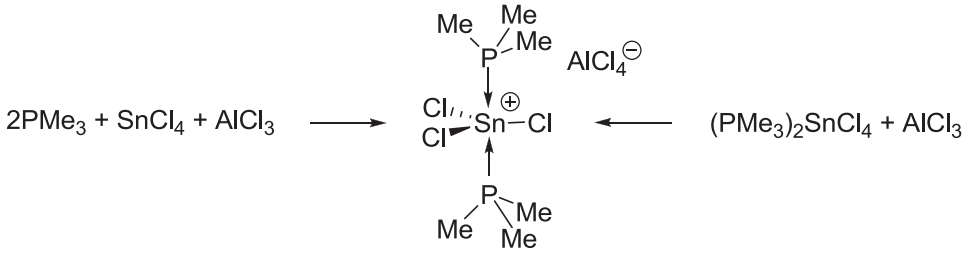


(**4.2**)

In the presence of two equivalents of $AlCl_3$, mixtures of $Me_3P$ with $SnCl_4$ give the ionic compound $[SnCl_2(PMe_3)_2][AlCl_4]_2$ in high yield (equation 4.3) as confirmed by a resonance at 16.9 ppm in the $^{31}P\{^1H\}$ NMR spectrum and a corresponding triplet at -333 ppm in the $^{119}Sn\{^1H\}$ NMR spectrum. Consistently, $(PMe_3)_2SnCl_4$ reacted with two equivalents of $AlCl_3$ to give the same $^{31}P\{^1H\}$ and $^{119}Sn\{^1H\}$ NMR chemical shifts. Solid state $^{31}P$ NMR spectra for both the bulk precipitate from the reaction and crystals exhibit

similar resonances at *c.a.* 46 ppm. Solid state and solution NMR spectra for $[(PMe_3)_2SnCl_2][AlCl_4]_2$ exhibit a 28 ppm difference in chemical shift (Figure 4.2.3) perhaps due to solvent or aluminate anion interactions. The $^{31}P$ CP/MAS NMR spectrum of $[(Me_3P)_2SnCl_2][AlCl_2]$ show two unique phosphorus environments (46.3 ppm and 45.8 ppm) consistent with two crystallographically distinct phosphorus atoms.

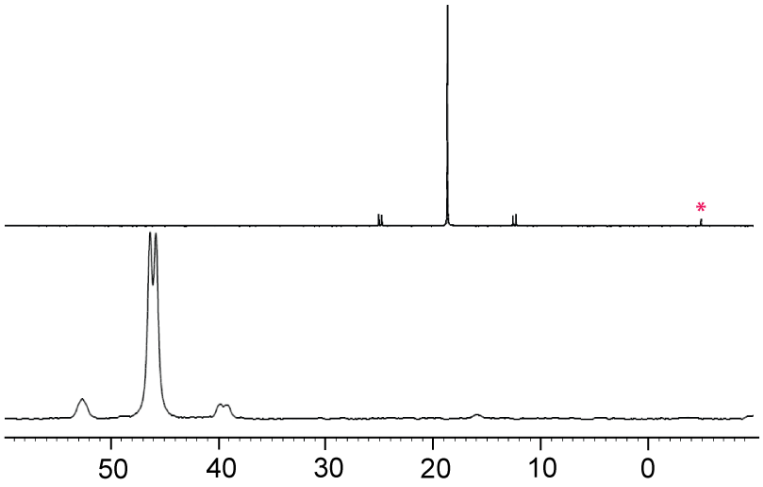


Figure 4.2.3 Dichloromethane-$d_2$ solution $^{31}P\{^1H\}$ NMR spectrum (top) and solid state $^{31}P$ CP/MAS NMR spectrum (bottom) of $[SnCl_2(PMe_3)_2][AlCl_4]_2$.

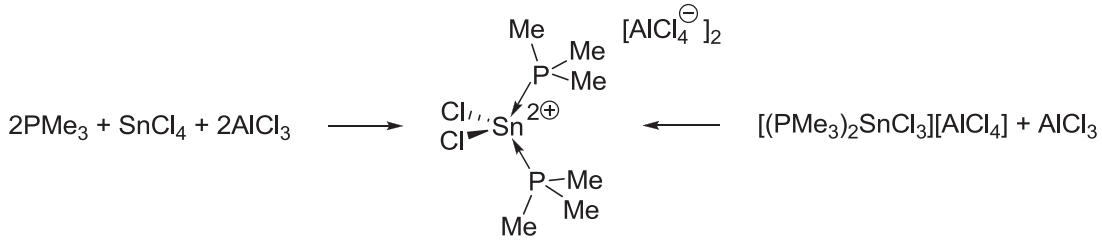


(**4.3**)

Table 4.2.1 Selected NMR data for $SnCl_4(PMe_3)_2$, $[SnCl_3(PMe_3)_2][AlCl_4]$ and $[SnCl_2(PMe_3)_2][AlCl_4]_2$

| | **$SnCl_4(PMe_3)_2$** | **$[SnCl_3(PMe_3)_2][AlCl_4]$** | **$[SnCl_2(PMe_3)_2][AlCl_4]_2$** |
|---|---|---|---|
| $^{31}P\{^1H\}$ NMR<br>δ, ppm ($CD_2Cl_2$)<br>($^1J_{PSn}$,119/117 Hz) | 1.6<br>(2635/2517) | 10.8<br>(2725/2604) | 16.9<br>(2591/2476) |
| $^{31}P$ CP/MAS<br>δ, ppm<br>($^1J_{PSn}$, Hz) | 6.7<br>(2772) | 15.9<br>(2706) | 46.3 (2125)<br>45.8 (2125) |
| $^{119}Sn$ NMR<br>δ, ppm ($CD_2Cl_2$)<br>($^1J_{PSn}$, Hz) | -554[a]<br>(2635) | -456[a]<br>(2725) | -333[a]<br>(2591) |

[a] triplet resonance

## 4.3 Molecular Structures

Crystals of $(PMe_3)_2SnCl_4$, $[(PMe_3)_2SnCl_3][AlCl_4]$, and $[(PMe_3)_2SnCl_2][AlCl_4]_2$ were grown by slow evaporation of the supernatant decanted from the reaction mixture. Figure 4.3.1 best illustrates how the slow evaporation apparatus in an evacuated vessel is set up for air and water sensitive substrates. Additionally, the colorless solid was washed with $CH_2Cl_2$ and the washings were then combined with the supernatant in the bulb. Over the course of a week the $CH_2Cl_2$ slowly transfers to the vacant bulb submerged in the water bath to leave behind X-Ray quality crystals. Although this set up was exclusively used for the compounds in this chapter, this slow evaporation method works well for large scale isolations in general.

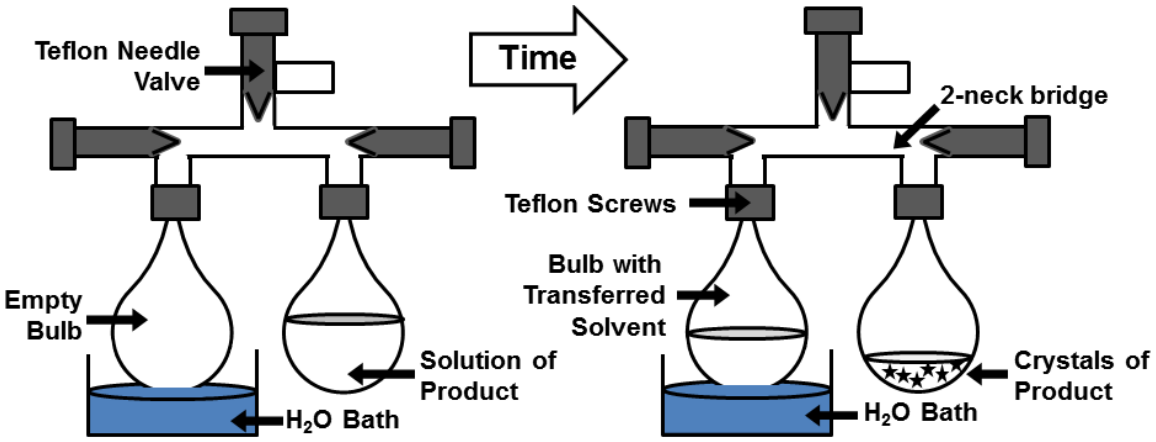


Figure 4.3.1 Evacuated two bulb vessel setup for large scale crystallizations toward the isolation of chlorostannylphosphine complexes. The dark areas represent Teflon connections and stars represent crystals of the product of interest.

Single crystal X-Ray diffraction studies have been completed on each of the complexes where Figure 4.3.2 provides views of the structures with selective bond lengths and angles summarized in Table 4.3.1. The geometry of tin in $(PMe_3)_2SnCl_4$ is distorted octahedral with the trimethylphosphine in the axial positions. The pentacoodinate environment for tin in $[(PMe_3)_2SnCl_3][AlCl_4]$ is a distorted trigonal bypyramidal configuration with the trimethylphosphine groups occupying the axial positions. The dication in $[(PMe_3)_2SnCl_2][AlCl_4]_2$ on the other hand, formally exhibits hexacoordinate tin with the counterion contacts in *cis* confirmation creating a distorted octahedral geometry with the phosphine groups in the axial positions. The dication is the only complex of the series of compounds that does not follow VSEPR geometry. However it should be noted that computational investigations have the cation geometry optimized as distorted tetrahedral in the absence of anion interactions.[79, 80]

The Sn-P distances are very similar in all three compounds, with a noticeable contraction in Sn-Cl covalent bonds with an increase in the electropositivity at tin. The Sn···Cl contacts between the dication and the aluminate anions (2.9942(15) Å and 2.9245(15) Å) are well outside the sum of the Sn-Cl covalent radii (2.40Å) however are well inside the sum of the van der Waals radii (3.92 Å). Sn···Cl interactions from the aluminate are not present in the less acidic $[(Me_3P)_2SnCl_3][AlCl_4]$ salt. Gas phase calculations were completed for each of the complexes which revealed the optimized geometries were consistent with the experimental observations.[79]

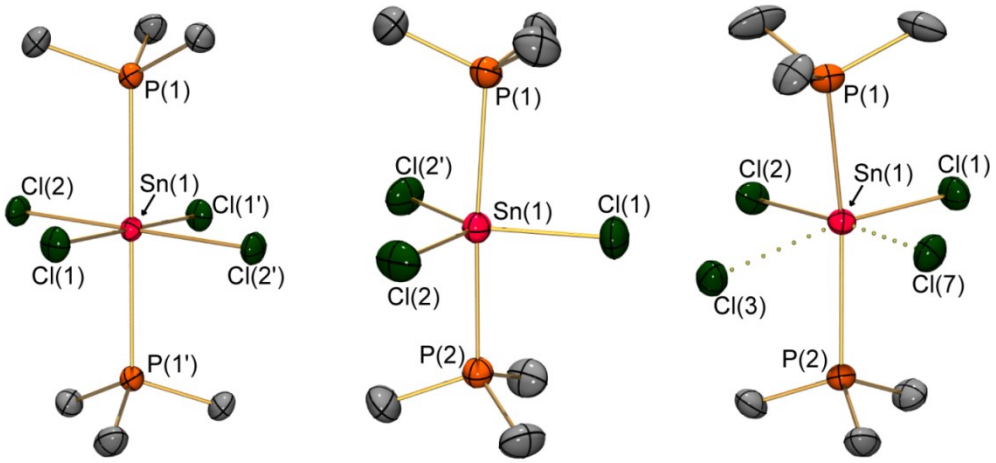


Figure 4.3.2 POV-Ray views of $SnCl_4(PMe_3)_2$, the cation in $[SnCl_3(PMe_3)_2][AlCl_4]$ and the dication in $[SnCl_2(PMe_3)_2][AlCl_4]_2$ including the anion contacts between tin and chlorine atoms of the aluminates. Thermal ellipsoids are at the 50% probability level, hydrogen atoms and anions are omitted for clarity.

Table 4.3.1 Selected structural parameters for $SnCl_4(PMe_3)_2$, $[SnCl_3(PMe_3)_2][AlCl_4]$ and $[SnCl_2(PMe_3)_2][AlCl_4]_2$

| | **$SnCl_4(PMe_3)_2$** | **$[SnCl_3(PMe_3)_2][AlCl_4]$** | **$[SnCl_2(PMe_3)_2][AlCl_4]_2$** |
|---|---|---|---|
| Sn–P (Å) | 2.5654(7) | 2.5439(12) *P(1)*<br>2.5347(12) *P(2)* | 2.5420(16) *P(1)*<br>2.5454(15) *P(2)* |
| Sn–Cl (Å) | 2.4762(6) *Cl(1)*<br>2.4565(7) *Cl(2)* | 2.3490(12) *Cl(1)*<br>2.3955(10) *Cl(2)* | 2.3362(15) *Cl(1)*<br>2.3568(14) *Cl(2)* |
| Sn···Cl (Å) | - | - | 2.9942(15) *Cl(3)*<br>2.9245(15) *Cl(7)* |
| P–Sn–P (°) | 180 | 172.67(4) | 157.45(5) |
| Σ Cl–Sn–Cl (°) | 360.00(2) | 359.98(2) | 360.2(5) |

## 4.4 Summary and Conclusion

A series of phosphine stabilized $SnCl_4$, $[SnCl_3]^+$, and $[SnCl_2]^{2+}$ complexes were synthesized and characterized by solution and solid state NMR spectroscopy in conjunction with single crystal X-Ray diffraction. $^{119}Sn\{^1H\}$ NMR spectroscopy was a better diagnostic tool than $^{31}P\{^1H\}$ NMR spectroscopy to distinguish between each of the structures as the chemical shift range in the phosphorus NMR was relatively narrow. This study showed that by sequential abstraction of a chloride from $SnCl_4$ resulted in contraction of the remaining covalent Sn-Cl bonds as a means to sustain the enhanced electrophilicity (Lewis acidity) at the tin center.[81] Additionally, the Sn-P dative bonds remain consistent throughout the series providing evidence that the Sn-Cl bonds are influenced by the charge present on tin.

# CHAPTER 5 PHOSPHINE STABILIZED ALKYLSTANNYLIUM CATIONS AND ALKYLSTANNYLDIYLIUM DICATIONS

## 5.1 Background

Complexes with $[R_3Sn]^+$ [68-71] that are stabilized by phosphines are rare in the literature, particularly in comparison to the uncommon pnictogen (Pn = P and As) adducts of $SnX_4$ (X = F, Cl, Br, and I). A couple of representative intramolecular Sn-P complexes with alkyl groups on tin have been published[48,51] which involve syntheses with many steps and long reaction times to obtain the target P→Sn interaction (chapter 1, section 1.3.1). [82] Figure 5.1.1 illustrates that $[(Me_3Sn)_4P][OTf]$[65] can be viewed as alternating $[(Me_3Sn)_3P{\rightarrow}SnMe_3][OTf]$ interactions to give an average Sn-P interatomic distance of 2.547(1) Å. One of the fascinating features about this cation is that it is readily synthesized in two steps. The first combines $Me_3SnBr$ with AgOTf to generate $Me_3SnOTf$ and AgBr in a salt elimination reaction. The second and last step involves reacting $Me_3SnOTf$ in the presence of $(Me_3Sn)_3P$ to generate $[(Me_3Sn)_4P][OTf]$. [65]This chapter looks at a similar methodology without the need to isolate substrates like $Me_3SnOTf$ before proceeding with the reaction. The syntheses herein look at one pot, two step approach to easily generate a variety phosphine stabilized tin cations and dications.

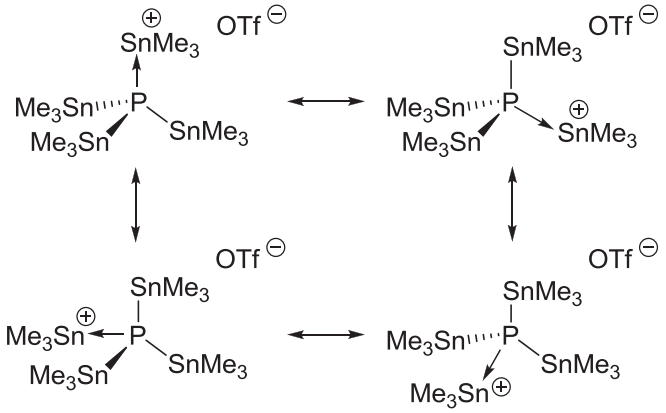


Figure 5.1.1 An example of an intermolecular $[Me_3Sn]^+$ stabilized by $(Me_3Sn)_3P$ which has a Sn-P interatomic distance of 2.547(1) Å.

## 5.2 Phosphine Complexes of Stannylium Cations

### 5.2.1 Synthesis, Isolation, and Characterization

Reaction mixtures of $Me_3SnCl$ and $AlCl_3$ give a $^{119}Sn\{^1H\}$ signal at 255 ppm within 10 mins. A $Me_3P$ solution was added dropwise to the clear, pale yellow solution to produce a colorless clear reaction mixture $[Me_3PMe_3Sn][AlCl_4]$ (equation **5.1a**) with a single resonance at -36.8 ppm in the $^{31}P\{^1H\}$ NMR spectrum and a triplet resonance at 43 ppm in the $^{119}Sn\{^1H\}$ NMR spectrum. Colorless parallelepiped crystals of $[Me_3PMe_3Sn][AlCl_4]$ were grown by layering the reaction mixture with hexane or $Et_2O$ over the course of 2 days at -20°C. Salts of the type $[R_3PMe_3Sn][AlCl_4]$ (where R = iPr (**5.1b**), Cy (**5.1c**), and tBu(**5.1d**)) were synthesized by using procedure above with an alternate $R_3P$ to get the corresponding phosphine stabilized stannylium salt. Monitoring these reactions by $^{31}P\{^1H\}$ NMR and $^{119}Sn\{^1H\}$ NMR showed consumption of all the phosphine starting material and full conversion to a new resonance (Table 5.2.1.1). Equimolar mixtures of $Me_3SnCl$, TMSOTf, and $Me_3P$ produced $[Me_3PMe_3Sn][OTf]$ (equation 5.2) with a  resonance at -36.3 ppm in the $^{31}P\{^1H\}$ NMR spectrum and a triplet

resonance at 7 ppm in the $^{119}Sn\{^{1}H\}$ NMR spectrum. Colorless prism crystals of $[Me_3PMe_3Sn][OTf]$ were grown by slow evaporation of $CH_3CN$ over the course of 5 days.

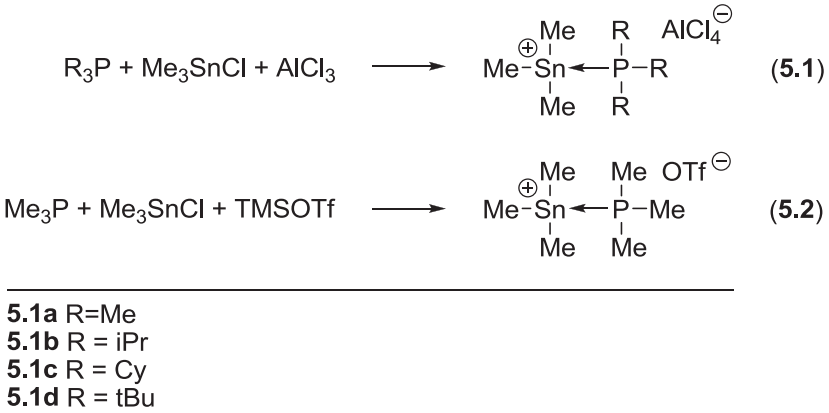


Table 5.2.1.1 $^{31}P\{^{1}H\}$ and $^{119}Sn\{^{1}H\}$ NMR data for $[R_3PMe_3Sn][AlCl_4]$ (where R = Me, iPr, Cy and tBu) and $[Me_3PMe_3Sn][OTf]$

| **Compound** | **$^{31}P\{^{1}H\}$ NMR: δ, ppm ($^{1}J_{PSn}$ 119/117)** | **$^{119}Sn\{^{1}H\}$ NMR: δ, ppm ($^{1}J_{PSn}$)** |
|---|---|---|
| $[Me_3PMe_3Sn][AlCl_4]$ | -36.8 (322/308) | 43 (322) |
| $[Me_3PMe_3Sn][OTf]$ | -36.3[a] | 7[a] |
| $[iPr_3PMe_3Sn][AlCl_4]$ | 23.5[a] | 25[a] |
| $[Cy_3PMe_3Sn][AlCl_4]$ | 14.1[a] | 22[a] |
| $[tBu_3PMe_3Sn][AlCl_4]$ | 29.0[a] | - |

[a] Broad resonances were present in both $^{31}P$ and $^{119}Sn$ NMR therefore no coupling data were obtained for these complexes.

## 5.2.2 Molecular Structures

Single crystal X-Ray diffraction studies have been completed on each of the aluminate salts (Figure 5.2.2.1) as well as the trimethylstannylium salt with a triflate anion (Figure 5.2.2.2) with selected bond lengths and angles summarized in Table 5.2.2.1 and Table

5.2.2.2. The geometry at tin in $[Me_3PMe_3Sn][AlCl_4]$ is a distorted tbp with $Me_3P$ and $AlCl_4$ occupying the axial positions and the methyl groups located in the equatorial plane. A similar geometry is observed for $[iPr_3PMe_3Sn][AlCl_4]$ and $[Me_3PMe_3Sn][OTf]$. However, for compounds with the bulkier phosphines $Cy_3P$ and $tBu_3P$, the tin atom is four coordinate with a distorted tetrahedral geometry. This is reflected when the nearest $A^-C^+$ interaction is between the aluminate chlorine and the alkyl hydrogen groups (H···Cl) (Table 5.2.2.1). Methyl groups are found to pack in the crystals lattice in such a way that the Sn-P bond adopts an eclipsed confirmation. The C-Sn-P-C torsion angles in $[Me_3PMe_3Sn][AlCl_4]$ are eclipsed (0.4°) whereas the examples with bulkier phosphines ($Cy_3P$, $iPr_3P$, $tBu_3P$) reveal a staggered (36°) arrangement. The sum of the three C-Sn-C angles for $[Me_3SnMe_3P][AlCl_4]$, $[Me_3PMe_3Sn][OTf]$ and $[iPr_3Me_3Sn][AlCl_4]$ are close to an ideal 360° for the equatorial groups and the P-Sn-Cl (or P-Sn-O) angles are near 180° for axial groups. $[Cy_3PMe_3Sn][AlCl_4]$ on the other hand is close to the ideal tetrahedral (3 angle sum of 328.5°) with a C-Sn-C angle sum of 337.3(5)°.

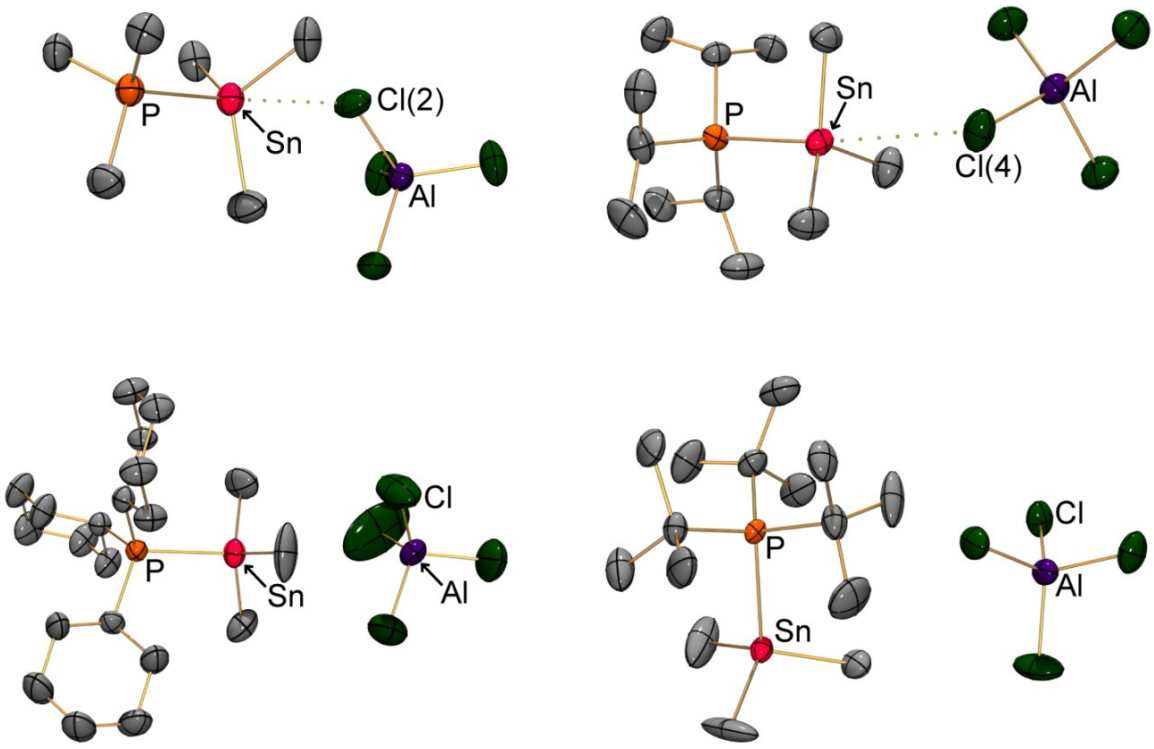


Figure 5.2.2.1 POV-Ray representation of the molecular structures containing a $[Me_3Sn]^+$ unit base stabilized by phosphines of varying steric bulk. Thermal ellipsoid plots are at the 50% probability level with hydrogen atoms omitted for clarity.

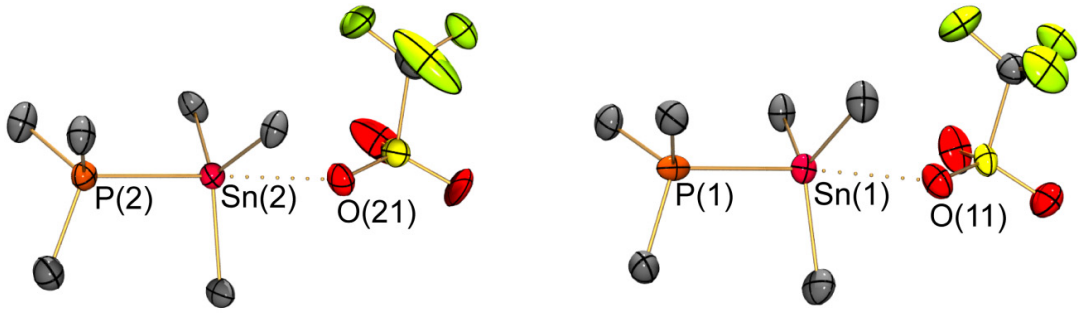


Figure 5.2.2.2 POV-Ray representation of the two unique salts located in the unit cell of $[Me_3PMe_3Sn][OTf]$. Thermal ellipsoids are at the 50% probability level with hydrogen atoms omitted for clarity.

The Sn-P interatomic distances for this series of compounds reveal narrow range of values (Table 5.2.2.1) even when one would expect that the larger alkyl groups to be stronger Lewis bases by virtue of the inductive ability to strengthen the P→Sn

interaction. However, inductive effects bear a miniscule influence on the dative bond. The Sn···Cl contact for $[Me_3PMe_3Sn][AlCl_4]$ and $[iPr_3PMe_3Sn][AlCl_4]$ have interatomic distances of 3.596 Å and 3.616 Å respectively. The Sn···Cl distances were inside the sum of the van der Waals radii (3.92 Å) but well outside the sum of the covalent radii (2.40 Å).[83] The Sn···O interatomic distances in $[Me_3PMe_3Sn][OTf]$ are 2.823 Å and 2.796 Å which are inside the sum of the van der Waals radii (3.69 Å) and outside the sum of the covalent radii (2.14 Å).[4] A common feature with these salts is that the anion is in proximity to the tin atom which indicates that the positive charge resides on tin. No specific structural features can be discussed for $[tBu_3PMe_3Sn][AlCl_4]$ as the X-Ray data were only sufficient to confirm connectivity.

Table 5.2.2.1 Selected interatomic distances (Å) for $[R_3PMe_3Sn][AlCl_4]$ (where R = Me, iPr, Cy and tBu) and $[Me_3PMe_3Sn][OTf]$

| **Compound** | **Sn-P** | **Nearest $A^-C^+$ Interaction** |
|---|---|---|
| $[Me_3PMe_3Sn][AlCl_4]$ | 2.5861(9) | 3.596 [Sn···Cl] |
| $[Me_3PMe_3Sn][OTf]$ | 2.6624(18), 2.6282(16) | 2.823, 2.796 [Sn···O] |
| $[iPr_3PMe_3Sn][AlCl_4]$ | 2.5729(8) | 3.616 [Sn···Cl] |
| $[Cy_3PMe_3Sn][AlCl_4]$ | 2.5808(11) | 2.695 [H···Cl][a] |

[a] hydrogen bonded with the Cy groups on phosphorus.

Table 5.2.2.2 Selected interatomic and torsion angles (°) for $[R_3PMe_3Sn][AlCl_4]$ (where R = Me, iPr, Cy and tBu) and $[Me_3PMe_3Sn][OTf]$

| Compound | ∑ 3(C-Sn-C) | C-Sn-P-C |
|---|---|---|
| $[Me_3PMe_3Sn][AlCl_4]$ | 344.4(2) | 0.4(1) |
| $[Me_3PMe_3Sn][OTf]$ | 352.7(5), 352.8(5) | 1.0(4), 1.5(4) |
| $[iPr_3PMe_3Sn][AlCl_4]$ | 342.7(2) | 36.9(1) |
| $[Cy_3PMe_3Sn][AlCl_4]$ | 337.3(5) | 36.7(3) |

## 5.3 Diphosphine Complexes of Stannylium Cations and Distannylium Dications

### 5.3.1 Synthesis, Isolation, and Characterization

Equimolar mixtures of dmpe, $Me_3SnCl$ and $AlCl_3$ produced a colorless, clear reaction mixture containing $[(dmpe)Me_3Sn][AlCl_4]$ as the only phosphorus containing product (equation 5.3) as confirmed by a broad resonance at -37.1 ppm in the $^{31}P\{^1H\}$ NMR spectrum and corresponding broad resonance at 32 ppm in the $^{119}Sn\{^1H\}$ NMR spectrum. Colorless block crystals of $[(dmpe)Me_3Sn][AlCl_4]$ were grown by layering the reaction mixture with $Et_2O$ which was left at room temperature over the course of 2 days. Two equivalents of $Me_3SnCl$ and TMSOTf in the presence of dmpe produced a colorless precipitate with a colorless clear supernatant containing $[dmpe(Me_3Sn)_2][OTf]_2$ (equation 5.4) confirmed by a broad resonance -30.3 ppm in the $^{31}P\{^1H\}$ NMR spectrum and 6.7 ppm in the $^{119}Sn\{^1H\}$ NMR spectrum. Colorless rod crystals of $[dmpe(Me_3Sn)_2][OTf]_2$ were grown by layering the supernatant with $Et_2O$ which mixed over the course of 2 days at room temperature. An interesting feature about these salts is that they are thermodynamic products for their respective reactions, meaning that alternate reaction

stiochiometries still produce $[(dmpe)Me_3Sn][AlCl_4]$ and $[dmpe(Me_3Sn)_2][OTf]_2$ exclusively. This was confirmed by $^{31}P\{^1H\}$ NMR and $^{119}Sn\{^1H\}$ NMR spectroscopy along with single crystal X-Ray diffraction.

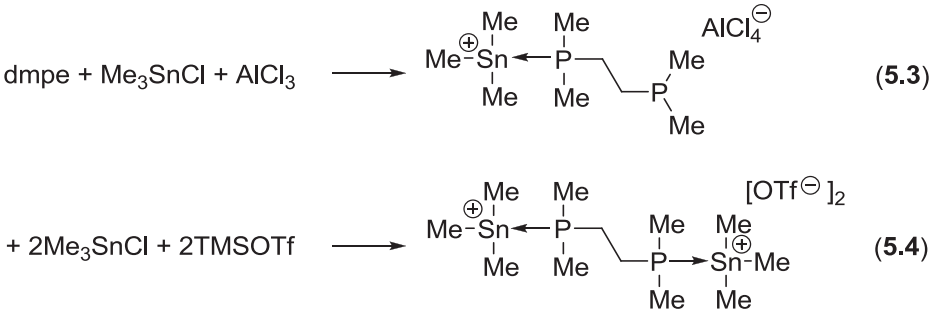


Equimolar amounts of dmpm, $Me_3SnCl$, and $AlCl_3$ produce a colorless, clear reaction mixture to give the complex $[(dmpm)Me_3Sn][AlCl_4]$ (equation 5.5) confirmed by a broad resonance at -39.1 ppm in the $^{31}P\{^1H\}$ NMR spectrum and a broad resonance at -46 ppm in the $^{119}Sn\{^1H\}$ NMR spectrum. Colorless irregular crystals of $[(dmpm)Me_3Sn][AlCl_4]$ were grown by layering the reaction mixture with $Et_2O$ to slowly mix over the course of 2 days at room temperature. In contrast, a mixture of one equivalent of dmpm with two equivalents of $Me_3SnCl$ and $AlCl_3$ immediately produces a colorless precipitate with a colorless clear supernatant contains $[dmpm(Me_3Sn)_2][AlCl_4]_2$ (equation 5.6) confirmed by a broad resonance at -40.8 ppm in the $^{31}P\{^1H\}$ NMR spectrum and a broad resonance at 72 ppm in the $^{119}Sn\{^1H\}$ NMR spectrum. Colorless irregular crystals of $[dmpm(Me_3Sn)_2][AlCl_4]_2$ were grown by layering the reaction mixture with $Et_2O$ to slowly diffuse over the course of 2 days at room temperature. A summary of the NMR data for the aforementioned compounds in this section can be found in Table 5.3.1.1.

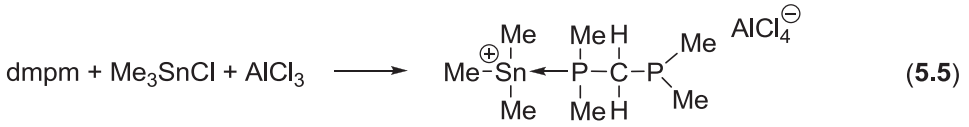


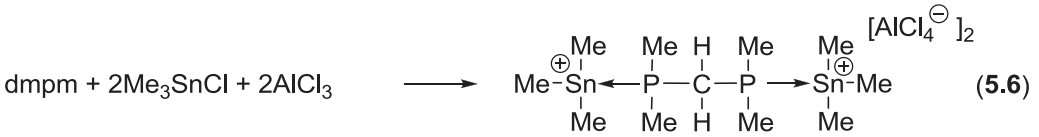


Table 5.3.1.1 $^{31}P\{^{1}H\}$ and $^{119}Sn\{^{1}H\}$ NMR data for $[(dmpe)Me_3Sn][AlCl_4]$, $[(dmpm)Me_3Sn][AlCl_4]$, $[dmpe(Me_3Sn)_2][OTf]_2$, and $[dmpm(Me_3Sn)_2][AlCl_4]_2$.

| Compound | $^{31}P\{^{1}H\}$ NMR δ, ppm | $^{119}Sn\{^{1}H\}$ NMR δ, ppm |
|---|---|---|
| $[(dmpe)Me_3Sn][AlCl_4]$ | -37.1[a] | 3[a] |
| $[(dmpm)Me_3Sn][AlCl_4]$ | -30.3[a] | 7[a] |
| $[dmpe(Me_3Sn)_2][OTf]_2$ | -39.1[a] | -46[a] |
| $[dmpm(Me_3Sn)_2][AlCl_4]_2$ | -40.8[a] | 72[a] |

[a] Broad resonances were present in both $^{31}P$ and $^{119}Sn$ NMR spectra and Sn-P J-coupling were not observed.

## 5.3.2 Molecular Structures

Single crystal X-Ray diffraction studies have been completed on $[(dmpe)Me_3Sn][AlCl_4]$ and $[(dmpm)Me_3Sn][AlCl_4]$ (Figure 5.3.2.1) $[dmpe(Me_3Sn)_2][OTf]_2$ and $[dmpm(Me_3Sn)_2][AlCl_4]_2$ (Figure 5.3.2.2). Selected interatomic distances and angles are summarized in Table 5.3.2.1 and Table 5.3.2.2.The geometry at tin in $[(dmpe)Me_3Sn][AlCl_4]$ is tbp with the two phosphorus atoms in the axial positions and the methyl groups occupying the equatorial plane. Notably this cation is unique in that the crystalline solid is a P-Sn-P polymer. The connectivity observed in the solid state is possibly a packing effect of $[(dmpe)Me_3Sn][AlCl_4]$. The corresponding salts $[(dmpm)Me_3Sn][AlCl_4]$, $[dmpe(Me_3Sn)_2][OTf]_2$, and $[dmpm(Me_3Sn)_2][AlCl_4]_2$ also have

a tbp geometry at the tin center and forms solid state polymer by $A^{-}C^{+}$ interactions between tin and anions (Sn··· O or Sn···Cl interactions: Figure 5.3.2.2).

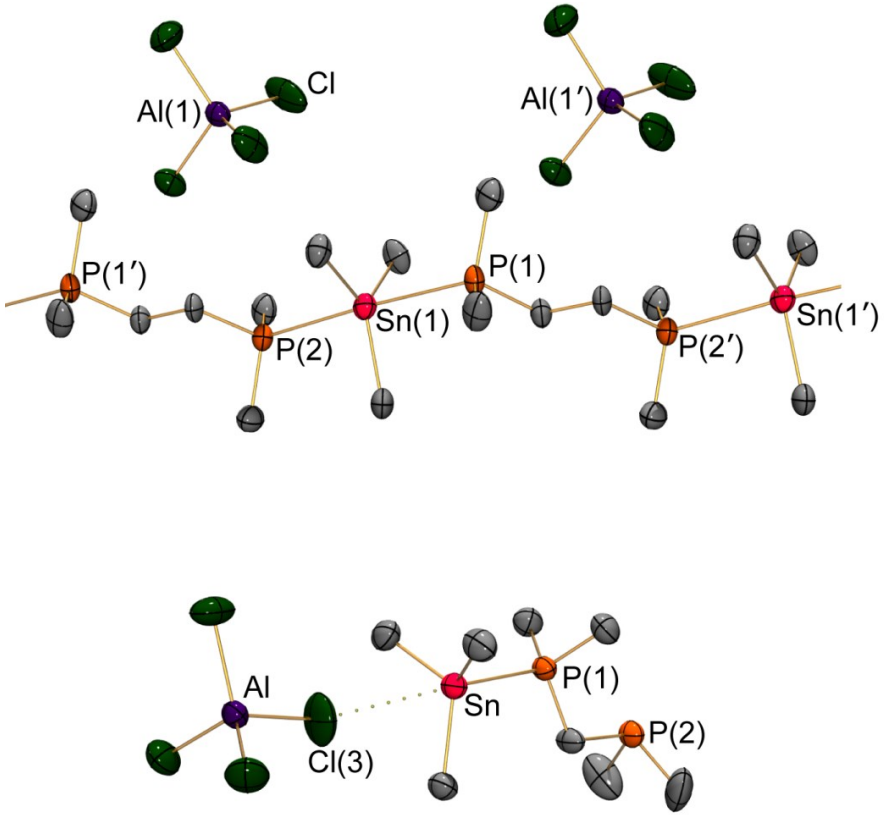


Figure 5.3.2.1 POV-Ray representation of the molecular structures of $[(dmpe)Me_3Sn][AlCl_4]$ (top, with 2-units showing) and $[(dmpm)Me_3Sn][AlCl_4]$ (bottom). Thermal ellipsoid plots are at the 50% probability level with hydrogen atoms omitted for clarity.

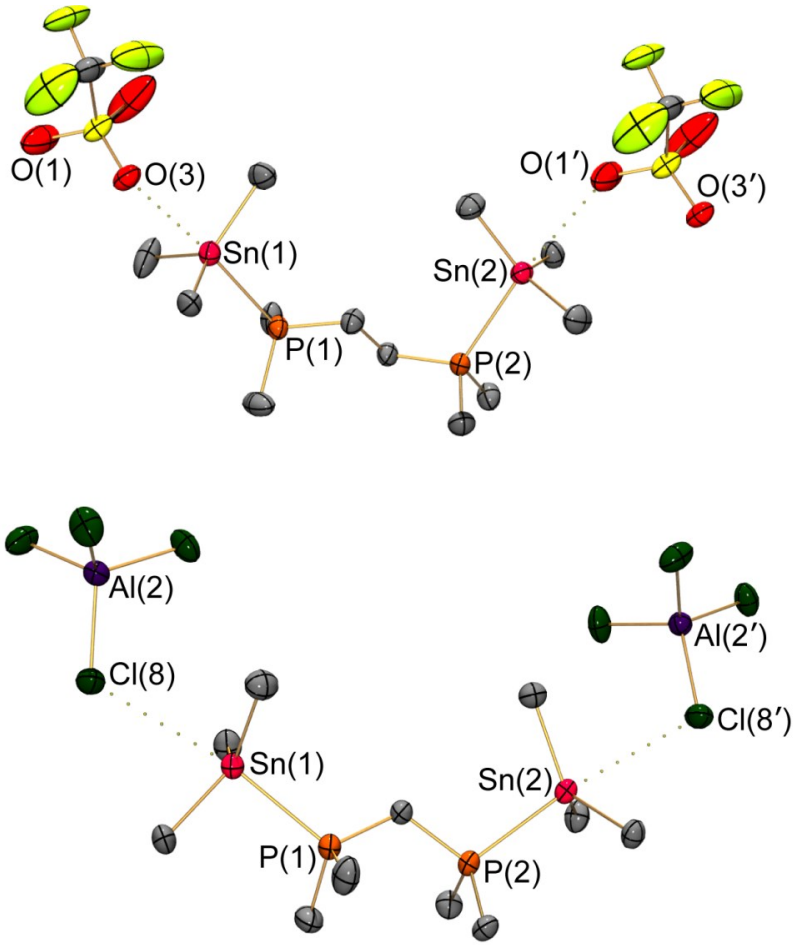


Figure 5.3.2.2 POV-Ray representation of the molecular structures of $[dmpe(Me_3Sn)_2][OTf]_2$ (top) and $[dmpm(Me_3Sn)_2][AlCl_4]_2$ (bottom). Thermal ellipsoid plots are at the 50% probability level with hydrogen atoms omitted for clarity.

The Sn-P dative bonds in this series of complexes have shown consistent interatomic distances with the exclusion of $[(dmpe)Me_3Sn][AlCl_4]$. The Sn-P interatomic distance for $[(dmpe)Me_3Sn][AlCl_4]$ was determined to be 2.8221(17) Å and 2.8626(17) Å which were larger values compared to the other cations that spanned 2.5805(13) Å-2.6257(12) Å. This longer Sn-P dative bond in $[(dmpe)Me_3Sn][AlCl_4]$ can be attributed to the axial phosphine groups exhibiting a *trans* influence. The longer than average interatomic distances are outside the covalent radii (2.47 Å) but are well within the sum of the van

der Waals radii (3.97 Å). $[dmpe(Me_3Sn)_2][OTf]_2$ exhibits Sn···O contacts with interatomic distances of 2.994 Å and 3.416 Å. These values are still well outside the sum of the Sn-O covalent radii (2.14 Å) and are within the sum of the van der Waals radii (3.69 Å). Lastly, the anion contacts for $[dmpm(Me_3Sn)_2][AlCl_4]_2$ and $[(dmpm)Me_3Sn][AlCl_4]$ are 3.428Å, 3.528 Å and 3.580 Å respectively. The Sn-Cl interatomic distances are within the sum of the van der Waals radii (3.92 Å) and are well outside the sum of the covalent radii (2.40 Å).

Table 5.3.2.1 Selected interatomic distances (Å) for $[(dmpe)Me_3Sn][AlCl_4]$, $[(dmpm)Me_3Sn][AlCl_4]$, $[dmpe(Me_3Sn)_2][OTf]_2$, and $[dmpm(Me_3Sn)_2][AlCl_4]_2$.

| **Compound** | **Sn-P** | **Nearest $A^-C^+$ Interaction** |
|---|---|---|
| $[(dmpe)Me_3Sn][AlCl_4]$ | 2.8221(17)<br>2.8626(17) | 2.945<br>[H···Cl] |
| $[(dmpm)Me_3Sn][AlCl_4]$ | 2.5805(13) | 3.580<br>[Sn···Cl] |
| $[dmpe(Me_3Sn)_2][OTf]_2$ | 2.6146(12)<br>2.6257(12) | 2.994, 3.416<br>[Sn···O] |
| $[dmpm(Me_3Sn)_2][AlCl_4]_2$ | 2.6179(12)<br>2.6100(11) | 3.428, 3.528<br>[Sn···Cl] |

Table 5.3.2.2 Selected interatomic angles (°) for $[(dmpe)Me_3Sn][AlCl_4]$, $[(dmpm)Me_3Sn][AlCl_4]$, $[dmpe(Me_3Sn)_2][OTf]_2$, and $[dmpm(Me_3Sn)_2][AlCl_4]_2$.

| Compound | ∑ C-Sn-C |
|---|---|
| $[(dmpe)Me_3Sn][AlCl_4]$ | 359.7(5) |
| $[(dmpm)Me_3Sn][AlCl_4]$ | 343.0(3) |
| $[dmpe(Me_3Sn)_2][OTf]_2$ | 348.5(3), 353.6(5) |
| $[dmpm(Me_3Sn)_2][AlCl_4]_2$ | 350.1(2), 351.2(2) |

## 5.4 Cyclic Diphosphine Complexes of Stannyldiylium Dications

### 5.4.1 Synthesis, Isolation, and Characterization

Reaction mixtures of $Bu_2SnCl_2$ with two equivalents of $AlCl_3$ produced a pale yellow clear mixture with a characteristic $^{119}Sn\{^1H\}$ NMR signal at -40 ppm. A $CH_2Cl_2$ solution of dmpe was added to the mixture which produced a colorless precipitate with a clear colorless supernatant which was grown to contain the cyclic dication $[(dmpe)Bu_2Sn][AlCl_4]_2$ (equation 5.7) with a $^{31}P\{^1H\}$ NMR resonance at -27.7 ppm and a $^{119}Sn\{^1H\}$ NMR resonance at -230 ppm. Colorless irregular crystals of $[(dmpe)Bu_2Sn][AlCl_4]_2$ were grown by leaving the supernatant at room temperature for 14 days. Two equivalents of TMSOTf in the presence of one equivalent of $Bu_2SnCl_2$ and dmpe immediately produced a colorless precipitate with a colorless clear supernatant containing $[(dmpe)Bu_2Sn][OTf]_2$ (equation 5.8) as confirmed by a singlet at -15.2 ppm in the $^{31}P\{^1H\}$ NMR spectrum and a corresponding triplet in the $^{119}Sn\{^1H\}$ NMR spectrum at -197 ppm. Colorless parallelepiped crystals of $[(dmpe)Bu_2Sn][OTf]_2$ were grown by decanting the supernatant and allowing the solution to stand at room temperature for 14 days.

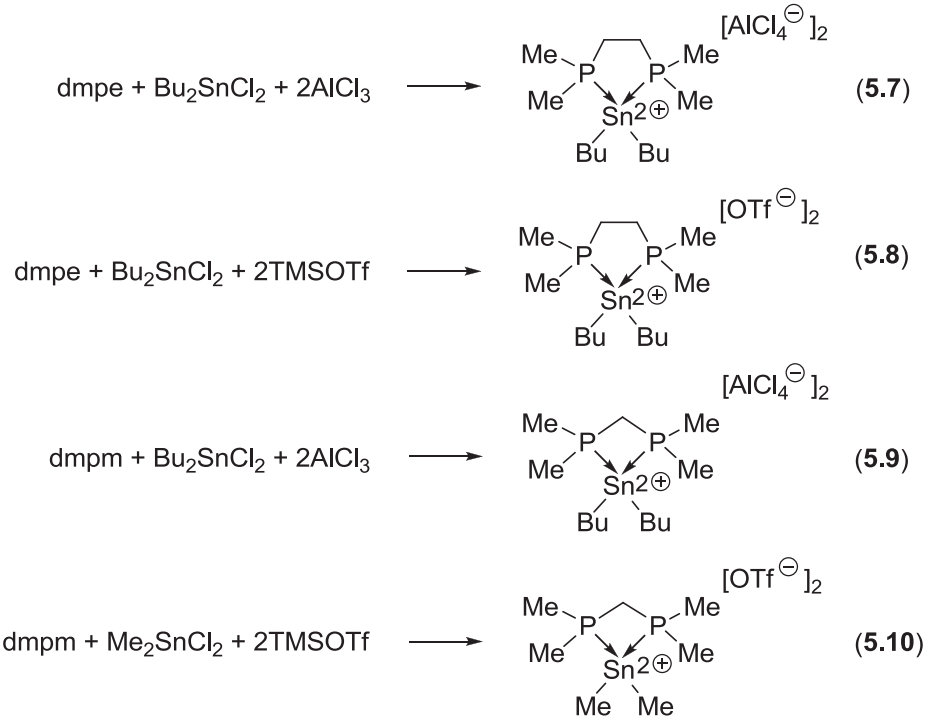


The diphosphine ligand, dmpm, was used to generate cations with a four membered ring structure. In the presence of two equivalents of $AlCl_3$, one equivalent of $Bu_2SnCl_2$ and dmpm were combined to produce a colorless clear solution with a $^{31}P\{^1H\}$ NMR resonance at -29.4 ppm and a $^{119}Sn\{^1H\}$ NMR resonance at 63 ppm assigned to be $[(dmpe)Bu_2Sn][AlCl_4]$ (equation 5.9). Colorless rod crystals of $[(dmpm)Bu_2Sn][AlCl_4]_2$ were grown by layering the reaction mixture with $Et_2O$ and at room temperature for 14 days. Two equivalents of TMSOTf in the presence of one equivalent of $Me_2SnCl_2$ and dmpm immediately produced a colorless precipitate with a colorless clear supernatant containing $[(dmpm)Me_2Sn][OTf]_2$ (equation 5.10) as confirmed by a broad resonance at -30.2 ppm in the $^{31}P\{^1H\}$ NMR spectrum and a $^{119}Sn\{^1H\}$ NMR resonance at -70 ppm. Crystals of $[(dmpm)Me_2Sn][OTf]_2$ were grown by slow evaporation after dissolving the material in a minimal amount of $CH_3CN$. Over the course of 14 days, colorless irregular

crystals formed which were confirmed to be $[(dmpe)Bu_2Sn][OTf]_2$. The multinuclear NMR data for the complexes discussed in this section are summarized in Table 5.4.1.1.

Table 5.4.1.1 $^{31}P\{^1H\}$ and $^{119}Sn\{^1H\}$ NMR data for $[(dmpe)Bu_2Sn][AlCl_4]_2$, $[(dmpe)Bu_2Sn][OTf]_2$, $[(dmpm)Bu_2Sn][AlCl_4]_2$,and $[(dmpm)Me_2Sn][OTf]_2$

| Compound | $^{31}P\{^1H\}$ NMR δ, ppm ($^1J_{PSn}$ 119/117) | $^{119}Sn\{^1H\}$ NMR δ, ppm ($^1J_{Sn-P}$) |
|---|---|---|
| $[(dmpe)Bu_2Sn][AlCl_4]_2$ | -27.7[a] | -230[a] |
| $[(dmpe)Bu_2Sn][OTf]_2$ | -15.2 (452/432) | -197[b] (452) |
| $[(dmpm)Bu_2Sn][AlCl_4]_2$ | -29.4[a] | 63[a] |
| $[(dmpm)Me_2Sn][OTf]_2$ | -30.2[a] | -70[a] |

[a] Broad resonances were present in both $^{31}P$ and $^{119}Sn$ NMR and tin satellites were not observed.
[b] Triplet resonance

## 5.4.2 Molecular Structures

Single crystal X-Ray diffraction studies have been completed on the cyclic compounds (Figure 5.4.2.1). Selected interatomic distances and angles are summarized in Table 5.4.2.1 and Table 5.4.2.2.The local geometry at tin in the aforementioned cations is a distorted tetrahedral within the dication with two weak contacts between tin and the anion. The anion interactions are perpendicular to the substituents at tin and essentially are coplanar with the phosphorus centers of the chelating ligand. Structural features of $[(dmpm)Me_2Sn][OTf]_2$ and $[(dmpe)Bu_2Sn][OTf]_2$ will not be discussed in detail as the structures are disordered, however the connectivity within the cations has been confirmed.

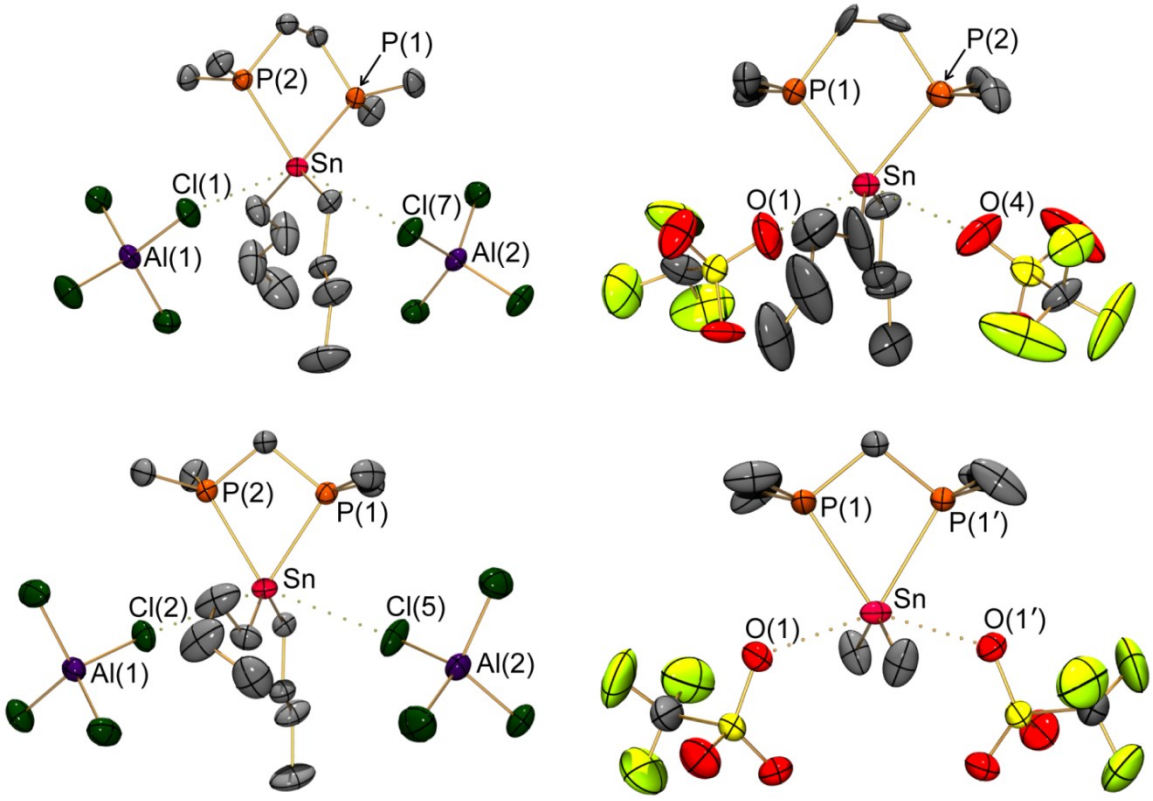


Figure 5.4.2.1 POV-Ray representation of the molecular structures of $[(dmpe)Bu_2Sn][AlCl_4]_2$ (top left), $[(dmpe)Bu_2Sn][OTf]_2$ (top right), $[(dmpm)Bu_2Sn][AlCl_4]_2$ (bottom left), and $[(dmpm)Me_2Sn][OTf]_2$ (bottom right). Thermal ellipsoid plots are at the 50% probability level with hydrogen atoms omitted for clarity.

The Sn-P interatomic distances for $[(dmpe)Bu_2Sn][AlCl_4]_2$ and $[(dmpm)Bu_2Sn][AlCl_4]_2$ are 2.5654(9) Å, 2.5731(9) Å and 2.5817(6) Å, 2.5910(6) Å which are just outside the sum of the Sn-P covalent radii (2.47Å) indicating that there is a significant dative bond. In addition, these complexes have a P-Sn-P bite angle of 82.59(3)° for $[(dmpe)Bu_2Sn][AlCl_4]_2$) and 68.498(18)° for $[(dmpm)Bu_2Sn][AlCl_4]_2$. $[(dmpm)Bu_2Sn][AlCl_4]_2$ has a smaller bite angle compared to $[(dmpe)Bu_2Sn][AlCl_4]_2$, this can be attributed to using dmpe to make a five membered ring whereas dmpm generates a four membered ring. The strain of forming a four membered ring was

reflected in the longer Sn-P interatomic distance of $[(dmpm)Bu_2Sn][AlCl_4]_2$ and shorter anion contacts compared to $[(dmpe)Bu_2Sn][AlCl_4]_2$. The Sn···Cl interatomic distances for $[(dmpe)Bu_2Sn][AlCl_4]_2$ were found to be 3.474 Å and 3.498 Å and in the case of $[(dmpm)Bu_2Sn][AlCl_4]_2$ Sn···Cl values were 3.262 Å and 3.285 Å. The aluminate interactions were determined to be van der Waals interactions (3.92 Å) and not Sn-Cl covalent bonds (2.40 Å). This series of complexes containing dmpm was found to chelate to form four membered rings even though this typically can cause strain in the backbone of the structure where P-C-P angle was 105.10(12)° instead of the typical 109.5° for an $sp^3$ carbon center.

Table 5.4.2.1 Selected interatomic distances (Å) for $[(dmpe)Bu_2Sn][AlCl_4]_2$ and $[(dmpm)Bu_2Sn][AlCl_4]_2$.

| Compound | Sn-P | Nearest $A^-C^+$ Interaction |
|---|---|---|
| $[(dmpe)Bu_2Sn][AlCl_4]_2$ | 2.5654(9)<br>2.5721(9) | 3.474, 3.498<br>[Sn···Cl] |
| $[(dmpm)Bu_2Sn][AlCl_4]_2$ | 2.5817(6)<br>2.5910(6) | 3.262, 3.285<br>[Sn···Cl] |

Table 5.4.2.2 Selected interatomic angles (°) for $[(dmpe)Bu_2Sn][AlCl_4]_2$ and $[(dmpm)Bu_2Sn][AlCl_4]_2$.

| Compound | C-Sn-C | P-Sn-P |
|---|---|---|
| $[(dmpe)Bu_2Sn][AlCl_4]_2$ | 126.10(13) | 82.59(3) |
| $[(dmpm)Bu_2Sn][AlCl_4]_2$ | 127.53(9) | 68.498(18) |

## 5.5 Summary and Conclusion

A variety of phosphine stabilized stannylium cations were synthesized and comprehensively characterized by multinuclear NMR and X-Ray crystallography. Notably the $R_3P$ (where R = Me, iPr, Cy, tBu) complexes synthesized showed that with increasing steric bulk on phosphorus, the Sn-P interatomic distance remained relatively unaffected. Meanwhile the $A^-C^+$ interaction gradually elongated to the point where the anion hydrogen bonded to the alkyl groups on phosphorus. When diphosphines were employed a variety of stannylium cations and distannylium dications were synthesized and fully characterized. The salt $[(dmpe)Me_3Sn][AlCl_4]$ is unique where the crystallization of the cation created a solid state coordination polymer with P-Sn-P interactions. When the diphosphine ligand dmpm is used the subtle modification in the backbone length changes how the cation crystallizes and the P-Sn-P linkage is no longer present. Two other coordination polymers were observed in this series, $[dmpe(Me_3Sn)_2][OTf]_2$ and $[dmpm(Me_3Sn)_2][AlCl_4]_2$, by the $A^-C^+$ interactions in the crystal lattice. Diphosphines are effectively used to make a series of stannyldiylium dications where the ligand chelated the tin center to generate ring structures.

## CHAPTER 6 PHOSPHINE AND DIPHOSPHINE STABILIZED DIALKYLCHLOROSTANNYLIUM CATIONS

### 6.1 Background

Neutral frameworks containing Sn-P interaction to a Sn-Cl center have been previously isolated with selected examples illustrated in Figure 6.1.1 (and chapter 1 section 1.3.1).[48,51,84] The most relatable literature example that resembles the complexes discussed in this chapter is $R_2P(Me_2SnCl)Me_2SnCl_2$ where there are two chlorine groups present on tin.[84] This can be viewed as a coordination complex of $R_2PMe_2SnCl$ with $Me_2SnCl_2$. To the best of my knowledge, there are no examples of cationic complexes of phosphines ligands with a $[R_2SnCl]^+$ or $[RSnCl_2]^+$ moiety. This chapter describes the syntheses and characterization of phosphine stabilized alkylchlorostannylium salts with $Me_3P$, dmpe, or dmpm ligands.

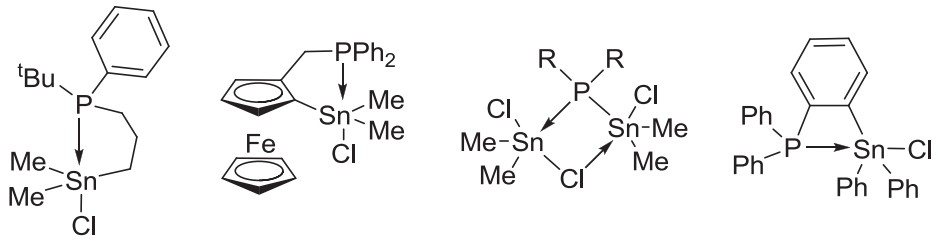


Figure 6.1.1 Representative examples of neutral compounds involving Sn-P dative bonds where there are one or more chlorine atoms present on tin.

### 6.2 Synthesis, Isolation, and Characterization

A reaction mixture of dmpe and $Me_2SnCl_2$ produces a saturated colorless solution with a $^{31}P\{^1H\}$ NMR resonance at -24.6 ppm and a $^{119}Sn\{^1H\}$ NMR signal at -208 ppm assigned

to dmpe($Me_2SnCl_2$)$_2$ (equation 6.1). Crude product was precipitated by adding hexane to the reaction mixture to precipitate colorless solid. Colorless plate crystals of dmpe($Me_2SnCl_2$)$_2$ were grown by dissolving the crude material in $CH_3CN$ and allowing the solvent to slowly evaporate over the course of 6 days at room temperature. Equimolar mixtures of $Me_2SnCl_2$ and $AlCl_3$ give a $^{119}Sn\{^1H\}$ signal at 56.7 ppm within minutes of mixing. A solution of $Me_3P$ was added to the clear pale yellow $Me_2SnCl_2/AlCl_3$ mixture to produce a colorless clear solution with a broad resonance at -15.0 ppm in the $^{31}P\{^1H\}$ NMR spectrum and a resonance at -49 ppm in the $^{119}Sn\{^1H\}$ NMR spectrum assigned to [$Me_3PMe_2SnCl$][$AlCl_4$] (equation 6.2). Colorless rod crystals of [$Me_3PMe_2SnCl$][$AlCl_4$] are grown by layering the solution with hexane which slowly mixed over the course of 2 days at -25°C.

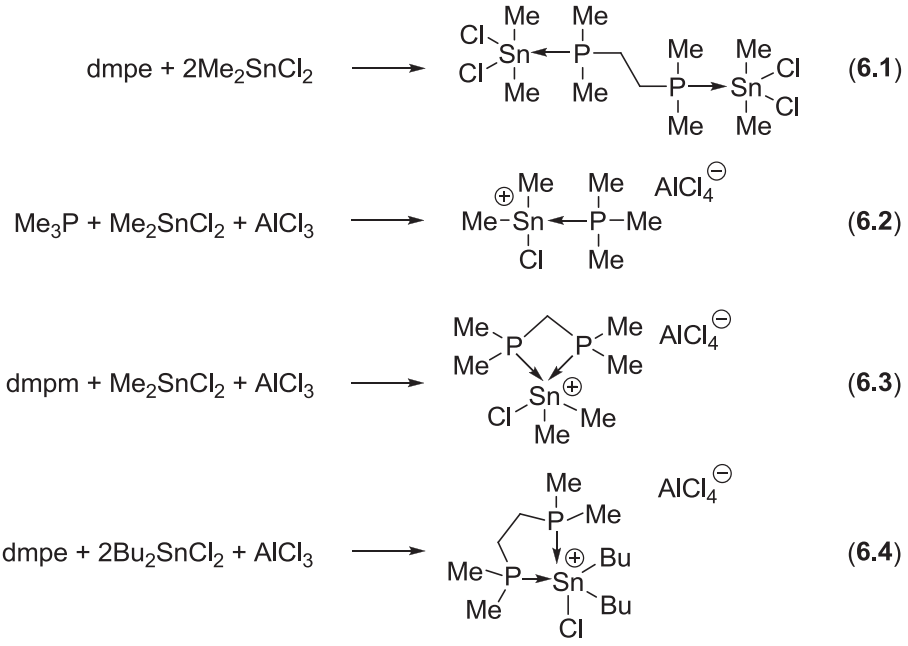


Equimolar mixtures of dmpm, $Me_2SnCl_2$, and $AlCl_3$ produce a colorless precipitate with a colorless clear supernatant determined to be [(dmpm)$Me_2SnCl$][$AlCl_4$] (equation 6.3)

with a $^{31}P\{^1H\}$ NMR resonance at -30.4 ppm and a $^{119}Sn\{^1H\}$ NMR resonance at -42 ppm. Adding hexane to the reaction mixture produces more colorless precipitate which was isolated for crystallization. Colorless irregular crystals of $[(dmpm)Me_2SnCl][AlCl_4]$ were grown by dissolving the crude material in $CH_3CN$ and allowing the solvent to slowly evaporate over the course of 6 days at room temperature.

Equimolar mixtures of $Bu_2SnCl_2$ and $AlCl_3$ give a $^{119}Sn\{^1H\}$ NMR signal at 100 ppm within 10 minutes of mixing. A solution of dmpe was added to the $Bu_2SnCl_2/AlCl_3$ mixture which produced a colorless precipitate with a colorless clear supernatant having a $^{31}P\{^1H\}$ NMR resonance at -31.3 ppm and a $^{119}Sn\{^1H\}$ NMR resonance at -216 ppm confirmed to be $[(dmpe)Bu_2SnCl][AlCl_4]$ (equation 6.4). Colorless plate crystals of $[(dmpe)Bu_2SnCl][AlCl_4]$ were grown by decanting the supernatant and allowing the solution to remain at room temperature for 14 days. Selected multinuclear NMR data for the compounds synthesized in this chapter are shown in Table 6.2.1.

Table 6.2.1 $^{31}P\{^1H\}$NMR data for $dmpe(Me_2SnCl_2)_2$, $[Me_3PMe_2SnCl][AlCl_4]$, $[(dmpe)Bu_2SnCl][AlCl_4]$, and $[(dmpm)Me_2SnCl][AlCl_4]$

| Compound | $^{31}P\{^1H\}$: δ, ppm | $^{119}Sn\{^1H\}$: δ, ppm |
|---|---|---|
| $dmpe(Me_2SnCl_2)_2$ | -24.6[a] | -208[a] |
| $[Me_3PMe_2SnCl][AlCl_4]$ | -15.0[a] | -49[a] |
| $[(dmpe)Bu_2SnCl][AlCl_4]$ | -31.3[a] | -216[a] |
| $[(dmpm)Me_2SnCl][AlCl_4]$ | -30.4[a] | -42[a] |

[a] Broad resonances were present in both $^{31}P$ and $^{119}Sn$ NMR spectra and coupling data could not be obtained for these complexes.

## 6.3 Molecular Structures

Single crystal X-Ray diffraction studies have been completed on each of the salts and dmpe($Me_2SnCl_2$)$_2$ (Figure 6.3.1 and Figure 6.3.2) with selected bond lengths and angles summarized in Table 6.3.1 and Table 6.3.2. The geometry of tin in dmpe($Me_2SnCl_2$)$_2$ is distorted tbp with the chlorine atoms in the axial positions. The chlorine atoms are bent toward the phosphine ligand with a Cl-Sn-Cl angle of 168.35(2)°. The molecular structure of [$Me_3PMe_2SnCl$][$AlCl_4$] has a dimeric arrangement with a $Sn_2Cl_2$ parallelogram. In addition, there is a chlorine contact from the aluminate anion which imposes a distorted octahedral geometry. The tin center in [(dmpe)$Bu_2SnCl$][$AlCl_4$] has a distorted tbp geometry at tin with the chorine atom in the axial position and the chelating phosphine ligand interacting in an axial-equatorial manner. The Sn-P interactions are asymmetric where the equatorial P(1) has a shorter bond to tin compared to axial P(2); the P-Sn-P bite angle is 77.15(3)°. Notably P(2) has a *trans* chlorine group (P-Sn-Cl = 158.1(3)°) whereas P(1) bears no *trans* functional groups. [(dmpm)$Me_2SnCl$][$AlCl_4$] involves a chelating phosphine; however there is an interaction from the aluminate anion which gives tin a coordination number of six, albeit the tin atom did not have an octahedral geometry. Additionally, the dmpm ligand has an asymmetric interaction with tin where P(1) has a stronger dative bond compared to P(2).

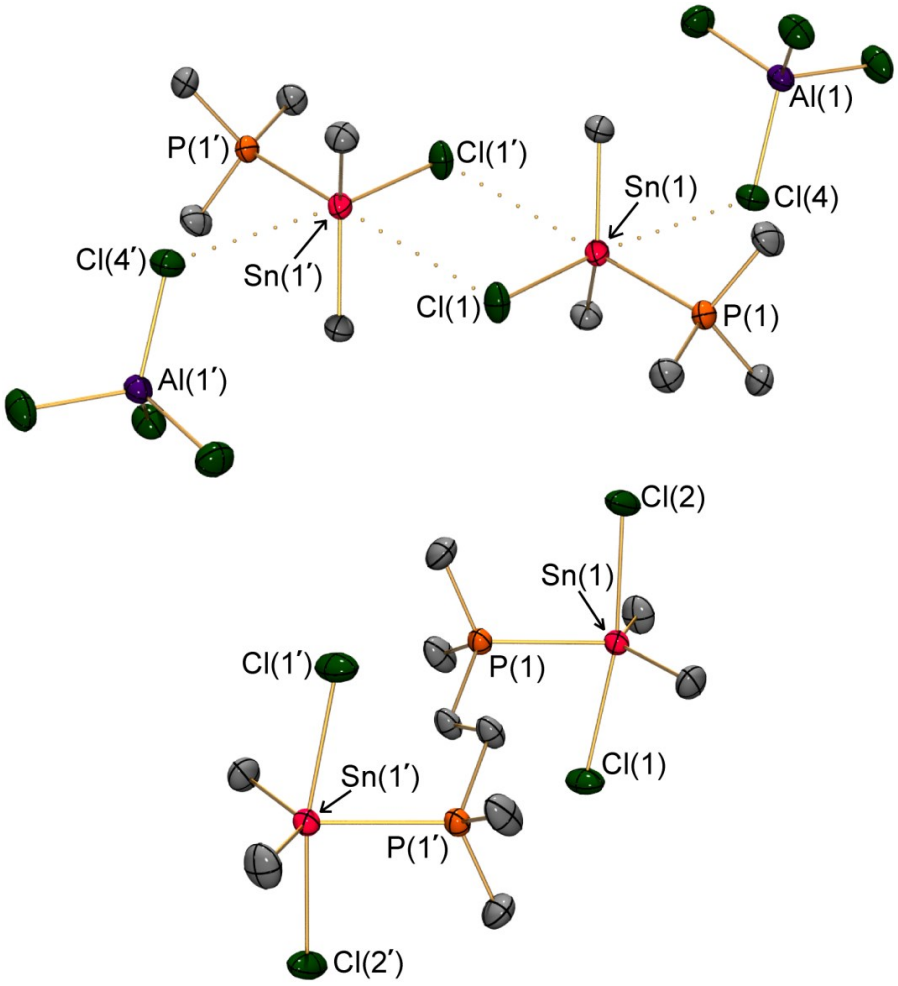


Figure 6.3.1 POV-Ray representation of dmpe($Me_2SnCl_2$)$_2$ (bottom) and [$Me_3PMe_2SnCl$][$AlCl_4$] (Top). Thermal ellipsoids are at the 50% probability level, hydrogen atoms are omitted for clarity.

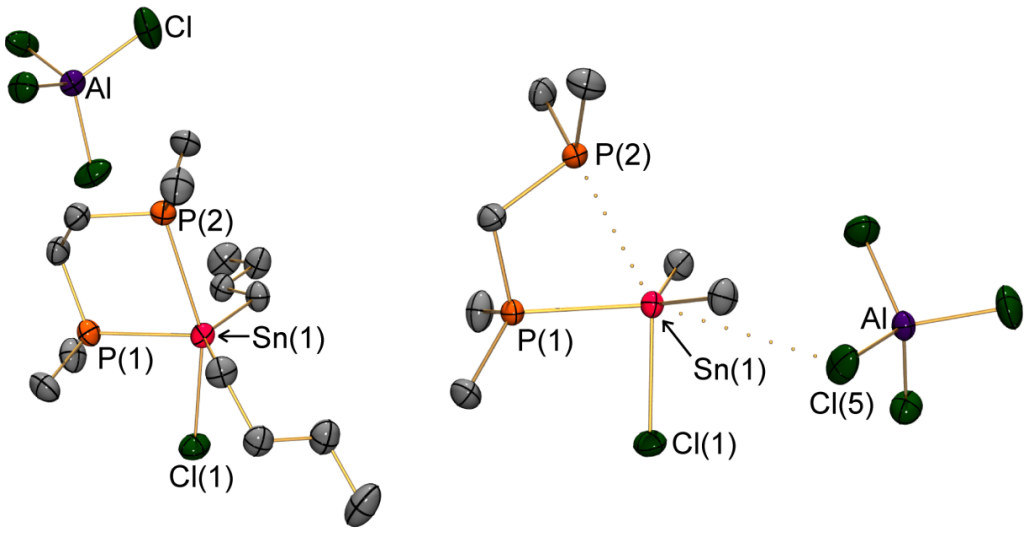


Figure 6.3.2 POV-Ray representation of $[(dmpe)Bu_2SnCl][AlCl_4]$ (left) and $[(dmpm)Me_2SnCl][AlCl_4]$ (right), thermal ellipsoids are at the 50% probability level, hydrogen atoms are omitted for clarity.

As previously mentioned, $dmpe(Me_2SnCl_2)_2$ was synthesized for comparison to $[Me_3PMe_2SnCl][AlCl_4]$, $[(dmpm)Me_2SnCl][AlCl_4]$, and $[(dmpe)Bu_2SnCl][AlCl_4]$ to see if either the Sn-P dative bonds or the remaining Sn-Cl covalent interatomic distances would be affected by the loss of a chloride. The Sn-P interatomic distance in $dmpe(Me_2SnCl_2)$ is 2.5463(8) Å and the Sn-Cl distances are 2.5256(7) Å and 2.6068(7) Å. In the dimeric structure $[Me_3PMe_2SnCl][AlCl_4]$, the Sn-Cl distances in the $Sn_2Cl_2$ parallelogram are 2.3698(5) Å and 3.5771(5) Å. The nearest $A^-C^+$ interaction between tin and the aluminate chlorine was 3.461 Å which is within the sum of the van der Waals radii (3.92 Å) and well outside the sum of the covalent radii (2.40 Å). The Sn-P dative bond was found to be 2.5585 Å, this was longer than the interatomic distance in $dmpe(Me_2SnCl_2)_2$. Perhaps this is due to the fact that tin in $dmpe(Me_2SnCl_2)_2$ has five interactions whereas in $[Me_3PMe_2SnCl][AlCl_4]$ tin has six interactions, even though the $[Me_2SnCl]^+$ core is more acidic than the $Me_2SnCl_2$ moiety.

The cyclic cation in [(dmpe)$Bu_2$SnCl][$AlCl_4$] has a Sn-Cl interatomic distance of 2.5756(8) Å which is longer than the sum of the covalent radii for Sn-Cl (2.40 Å) bonds this could be due to the influence of P(2), the *trans* phosphine substituent. The Sn-P dative interactions in [(dmpe)$Bu_2$SnCl][$AlCl_4$] are 2.5696(8) Å (equatorial) and 2.7601(8) Å (axial) and are values outside the sum of the covalent radii (2.47 Å) but within the sum of the van der Waals radii (3.97 Å). When the ring size in the chelating phosphine is four rather than five in [(dmpm)$Me_2$SnCl][$AlCl_4$]; there is no longer a well-defined cyclic system. The Sn-P interatomic distances in [(dmpm)$Me_2$SnCl][$AlCl_4$] are 2.5611(8) Å and 2.9603(8) Å; the latter being a weaker interaction nevertheless within the Sn-P van der Waals radii (3.97 Å). The Sn-Cl bond length is 2.4509(7) Å and the aluminate chlorine contact distance (Sn···Cl) is 3.834 Å the latter best described as a van der Waals interaction.

Table 6.3.1 Selected interatomic distances (Å) for [$Me_3PMe_2$SnCl][$AlCl_4$], [(dmpe)$Bu_2$SnCl][$AlCl_4$], [(dmpm)$Me_2$SnCl][$AlCl_4$], and dmpe($Me_2SnCl_2$)$_2$.

| **Compound** | **Sn-P** | **Sn-Cl** | **Nearest $A^-C^+$ Interaction** |
|---|---|---|---|
| dmpe($Me_2SnCl_2$)$_2$ | 2.5463(8) | 2.5256(7)<br>2.6068(7) | - |
| [$Me_3PMe_2$SnCl][$AlCl_4$] | 2.5585(5) | 2.3698(5)<br>3.5771(5)[a] | 3.461<br>[Sn···Cl] |
| [(dmpe)$Bu_2$SnCl][$AlCl_4$] | 2.5696(8)[b]<br>2.7601(8)[c] | 2.5756(8) | 2.853<br>[H···Cl] |
| [(dmpm)$Me_2$SnCl][$AlCl_4$] | 2.5611(8)[b]<br>2.9603(10)[c] | 2.4509(7) | 3.834<br>[Sn···Cl] |

[a] Sn···Cl interaction from the dimeric core
[b] P(1)
[c] P(2)

Table 6.3.2 Selected interatomic angles (°) for $[Me_3PMe_2SnCl][AlCl_4]$, $[(dmpe)Bu_2SnCl][AlCl_4]$, $[(dmpm)Me_2SnCl][AlCl_4]$, and $dmpe(Me_2SnCl_2)_2$.

| Compound | P-Sn-P | Cl-Sn-Cl | C-Sn-C |
|---|---|---|---|
| $dmpe(Me_2SnCl_2)_2$ | - | 168.35(2) | 129.25(10) |
| $[Me_3PMe_2SnCl][AlCl_4]$ | - | 76.41(3)[a]<br>52.38(3)[b]<br>93.43(3)[c] | 129.49(7) |
| $[(dmpe)Bu_2SnCl][AlCl_4]$ | 77.15(3) | - | 133.68(12) |
| $[(dmpm)Me_2SnCl][AlCl_4]$ | 63.09(3) | - | 125.06(8) |

[a] Cl(1)-Sn-Cl(1′)
[b] Cl(4)···Sn-Cl(1)
[c] Cl(4)-Sn-Cl(1′)

## 6.4 Summary and Conclusion

Three new phosphine stabilized alklychlorostannylium salts were synthesized, isolated and characterized by multinuclear NMR spectroscopy and single crystal X-Ray diffraction; the neutral adduct $dmpe(Me_2SnCl_2)_2$ was synthesized for comparison. All the compounds mentioned can be readily synthesized and with moderate yields. The $[R_2SnCl]^+$ moiety was determined to have enhanced electrophilicity at tin compared to $Me_2SnCl_2$ and $[R_3Sn]^+$ which allowed for shorter interatomic distance between tin and phosphorus. The Sn-P interactions in $[(dmpm)Me_2SnCl][AlCl_4]$ showed an asymmetric interaction of diphosphine ligand; this is attributed to a less acidic tin center. When a second chlorine is abstracted from $[Me_2SnCl]^+$ to generate $[Me_2Sn]^{2+}$, diphosphines are found to have a better interaction with the tin center. This is supported by the results discussed in chapter 5, section 4 where salts of the type $[(PCP)R_2Sn][A]_2$ (where PCP =

dmpe or dmpm; A = anion) showed an improved and symmetric interaction of the diphosphine ligand with tin.

# CHAPTER 7 CONCLUSIONS AND FUTURE WORK

## 7.1 Thesis Summary

Contributions from this dissertation highlight the use of halide abstracting agents to increase the Lewis acidity of tin and germanium to favor the Sn-P and Ge-P dative interactions by virtue of introducing a positive charge on tin or germanium. The work presented shows the first examples of germyldiylium and stannyldiylium dications with phosphine ligands along with an expanded library of base stabilized stannylium and germylium cations. Additionally, when chlorine functionality is retained on a germylium or stannylium moiety, this causes the E-$Cl_{cov}$ (E = Sn, Ge) bond to contract in comparison to neutral compounds. The use of diphosphine ligands has enabled the synthesis, isolation, and characterization of a number of linear dications and cyclic (chelate) dications. This report represents a significant contribution toward the development of p-block Sn-P and Ge–P cationic and dicationic coordination complexes.

## 7.2 Future Work

### 7.2.1 Phosphine-Stannane Complexes and Phosphine Stabilized Stannylium Cations

Chapters 4, 5, and 6 have highlighted all of the phosphine stabilized stannylium cations, distannylium dications, and stannyldiylium dications isolated and characterized thus far. However, a study could be carried out to investigate the effect of substituents on tin, for example using different alkyl groups on tin (iPr, tBu). A preliminary example has been synthesized thus far but there is further exploration that still needs to be done. The neutral complex dmpe($iPr_3OTf)_2$ was synthesized by reacting one equivalent of dmpe in the

presence of two equivalents of $iPr_3SnCl$ and TMSOTf to generate dmpe$(iPr_3SnOTf)_2$. Preliminary results in this regard indicate that an exchange reaction occurs as opposed to generating cationic frameworks (Figure 7.2.1.1). This is also highlighted in the interatomic distances for this new neutral complex. The Sn···O distances for $[Me_3PMe_3Sn][OTf]$ and dmpe$(Me_3Sn)_2][OTf]_2$ have been included in Table 7.2.1.1 for comparison. The Sn-O interaction in dmpe$(iPr_3SnOTf)_2$ was better described as a covalent interaction as opposed to a van der Waals interaction (3.69 Å) as the interatomic distance resembles a covalent interaction (2.14 Å). There is only one example of this type of framework isolated and further investigation with other halide abstracting agents along with other phosphines such as $Me_3P$, $Cy_3P$ and $tBu_3P$ would need to be completed. A possibility is that bulkier groups on phosphorus will impede Sn-P interactions where there was a significant contribution from the triflate in dmpe$(iPr_3SnOTf)_2$.

Table 7.2.1.1 Selected interatomic distances (Å) for dmpe$(iPr_3SnOTf)_2$, $[Me_3PMe_3Sn][OTf]$, and dmpe$(Me_3Sn)_2][OTf]_2$.

| Compound | Sn-O | Sn-P |
|---|---|---|
| dmpe$(iPr_3SnOTf)_2$ | 2.4614(18) | 2.7094(7) |
| $[Me_3PMe_3Sn][OTf]$ | 2.823<br>2.796 | 2.6624(18)<br>2.6282(16) |
| dmpe$(Me_3Sn)_2][OTf]_2$ | 2.994<br>3.416 | 2.6146(12)<br>2.6257(12) |

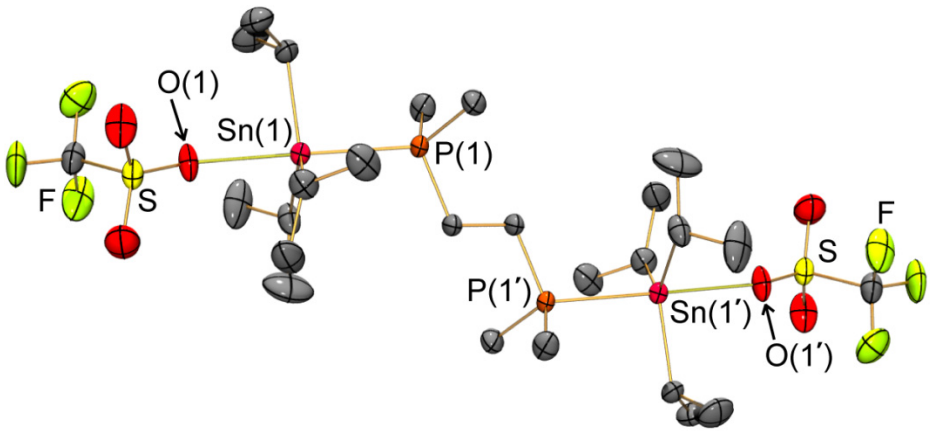


Figure 7.2.1.1 POV-Ray view of the molecular structure of dmpe($iPr_3SnOTf)_2$. Thermal ellipsoids are drawn at the 50% probability level and hydrogen atoms were omitted for clarity.

Other ambitious endeavors include attempting the synthesis of $[RSnCl_2]^+$ cations and $[RSnCl]^{2+}$ dications with examples seen in equations 7.1 and 7.2. Chapter 4,5, and 6 show examples of frameworks containing $[R_3Sn]^+$, $[R_2Sn]^{2+}$, $[R_2SnCl]^+$, $[SnCl_3]^+$, and $[SnCl_2]^{2+}$ moieties. Examining phosphine stabilized $[RSnCl_2]^+$ and $[RSnCl]^{2+}$ salts would complete the study of the effects of halide abstraction of $R_nSnCl_{4-n}$ (n = 0,1,2, or 3) used to make stannylium and stannyldiylium dications.

$$R_3P + RSnCl_3 + AlCl_3 \longrightarrow \text{Cl–Sn(R)(Cl)–P(R)(R)–R}\ AlCl_4^{\ominus} \qquad (7.1)$$

$$R_2PCH_2CH_2PR_2 + RSnCl_3 + 2AlCl_3 \longrightarrow \text{[Sn(Cl)(R)–P(R)(R)–CH}_2\text{–CH}_2\text{–P(R)(R)]}^{2\oplus}\ [AlCl_4^{\ominus}]_2 \qquad (7.2)$$

Reduction reactions were attempted on frameworks that retained a minimum of one chlorine atom on tin. The concept was to reductively couple two tin atoms together; however, the reactions so far have been unsuccessful. One-electron reducing agents such

as cobaltocene are found to reduce the tin center and break the Sn-P dative bonds which generated a tin(II) dianion. For example, when equimolar amounts of $[(Me_3P)_2SnCl_2][AlCl_4]_2$ and $CoCp_2$ were reacted together, a dark purple reaction mixture was produced within 30 mins of stirring. Yellow, irregular crystals were grown by layering the solution with hexane and the yellow crystals were confirmed to be $[CoCp_2]_2[SnCl_4]$ (Figure 7.2.1.2). $[CoCp_2]_2[SnCl_4]$ can be made independently by reacting $SnCl_4$ in the presence of two equivalents of cobaltocene; selected interatomic distances and angles are listed in Table 7.2.1.2. There are only a few instances of the diphenoidal $[SnCl_4]^{2-}$ in the literature with most examples involving $[SnCl_4]^{2-}$ as a dianion for ionic liquids.[85,86,87] The Sn-Cl interatomic distances and angles are consistent with the other examples currently present in the literature.[85-87] Redox chemistry with one electron reducing agents is not a viable route toward the synthesis of Sn-Sn cations however, it might be possible that another agent such as $SbPh_3$ or $Bu_3Sb$ could have a different outcome and potentially form a Sn-Sn bond.

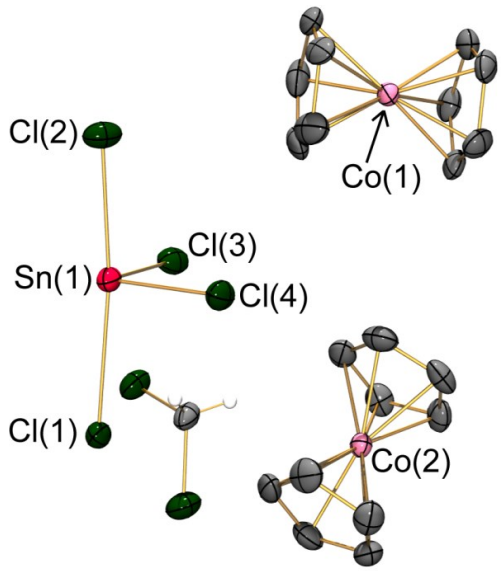


Figure 7.2.1.2 POV-Ray view of the molecular structure of $[CoCp_2]_2[SnCl_4]\cdot CH_2Cl_2$. Thermal ellipsoids are drawn at the 50% probability level and hydrogen atoms on everything but $CH_2Cl_2$ were omitted for clarity.

Table 7.2.1.2 Selected structural parameters for $[CoCp_2]_2[SnCl_4]$.

| Compound | Atom | Sn-Cl (Å) | Cl-Sn-Cl (°) |
|---|---|---|---|
| $[CoCp_2]_2[SnCl_4]$ | Cl(4) | 2.4702(14) | 90.92(5)[a]<br>92.41(5)[b]<br>92.81(5)[c] |
| | Cl(3) | 2.5225(19) | 93.89(5)[b]<br>90.65(5)[c] |
| | Cl(2) | 2.6558(15) | 173.02(5)[c] |
| | Cl(1) | 2.9344(14) | - |

[a] Cl(3)
[b] Cl(2)
[c] Cl(1)

Reactions involving $Me_3P$ and $Me_3SnCl$ in the absence of a halide abstracting agent were investigated. When a $^{31}P\{^1H\}$ NMR and $^{119}Sn\{^1H\}$ NMR spectra were recorded at room

temperature, there was a new resonance that made up approximately 3% of the total integration while the other 97% was $Me_3P$. The reaction mixture was cooled to -25°C which had colorless plate crystals form over the course of hours. The crystals were confirmed to be the adduct $Me_3P(Me_3SnCl)_2$ illustrated in Figure 7.2.1.3 with selected bond lengths and angles in Table 7.2.1.3. To the best of my knowledge, there is only one similar structure in the literature which is $Me_3SnCl(Ph_3PO)$ which has the phosphine oxide (P=O) interacting with the tin center. In the tbp structure of $Me_3SnCl(Ph_3PO)$, the P=O···Sn interaction is *trans* to Cl with the methyl substituents in the equatorial plane.[88] With the isolation of $Me_3P(Me_3SnCl)_2$, follow up work would need to be carried out to make more examples of this type as well as attempt to make germanium analogues.

Table 7.2.1.3 Selected structural parameters for $Me_3P(Me_3SnCl)_2$.

| | **$Me_3P(Me_3SnCl)_2$** |
|---|---|
| Sn-Cl (Å) | 2.8910(8)[a]<br>2.5407(10)[b]<br>2.7852(9)[c] |
| Sn-P (Å) | 2.6511(8) |
| Cl-Sn-Cl (°) | 179.30(3) |
| Sn-Cl-Sn (°) | 121.29(3) |
| Cl-Sn-P (°) | 178.49(2) |
| C-Sn-C (°) | 119.24(13), 118.48(15), 120.82(13)<br>117.44(19), 119.15(17), 122.48(19) |

[a] Sn(1)-Cl(1)
[b] Sn(2)-Cl(1)
[c] Sn(2)-Cl(2)

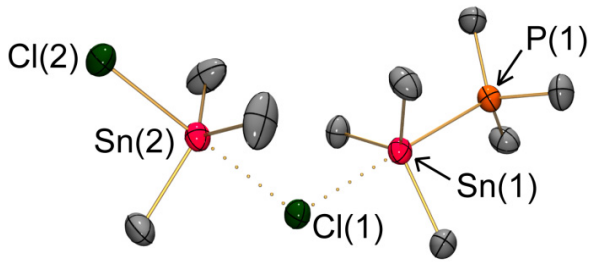


Figure 7.2.1.3 POV-Ray view of the molecular structure of $Me_3P(Me_3SnCl)_2$. Thermal ellipsoids are drawn at the 50% probability level and hydrogen atoms were omitted for clarity.

### 7.2.2 Arsine Stabilized Stannylium Cations

Arsenic was explored as a possible Lewis base toward the isolation of arsine stabilized stannylium cations with good preliminary evidence suggesting that arsenic is a viable ligand. Equimolar amounts of $Et_3As$, $Me_3SnCl$, and $AlCl_3$ can be combined together to produce a colorless clear reaction mixture with a $^{119}Sn\{^1H\}$ NMR resonance at 60 ppm. By layering the solution with hexane, crystals can be grown over the course of 2 days to give the corresponding salt $[Et_3AsMe_3Sn][AlCl_4]$. The crystals that were isolated were too soft and did not diffract well, regrettably no X-Ray data were collected on the material. The $^{119}Sn\{^1H\}$ NMR resonance was in the range of the analogous $[Me_3PMe_3Sn][AlCl_4]$ cation which had $^{119}Sn\{^1H\}$ NMR chemical shift at 43 ppm.

### 7.2.3 Phosphine Stabilized Germylium Cations and Germyldiylium Dications

The development of phosphine stabilized germylium cations and germyldiylium dications have seen many new frameworks emerge. However, many of the germanium salts have a few of drawbacks where there is a tendency for some of the salts to be isolated as an oil. Nonetheless, some of the oils can give solids upon sonication and can then be

recrystallized to produce X-Ray quality crystals. The coordination chemistry involving $GeCl_4$ is not viable since $GeCl_4$ preferentially undergoes redox reactions with phosphorus.[89] Lastly, it would be of interest to make germanium cations of the type $[RGeCl_2]^+$ and $[RGeCl]^{2+}$ by similar methods mentioned in section 7.2.1 toward the isolation of tin analogues (equation 7.3 and 7.4).

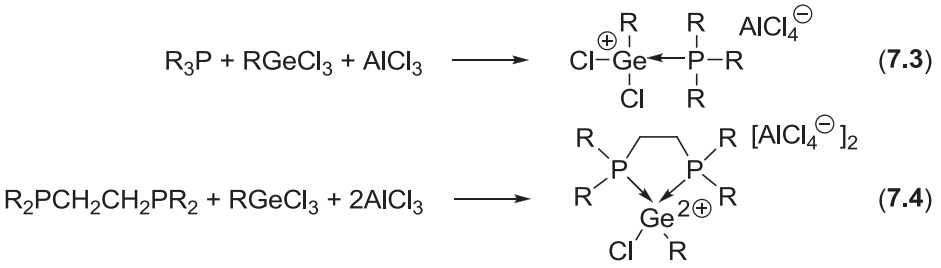


## 7.2.4 Phosphine Stabilized Germyliumylidene Cation and Germyliumdiylidene Dication

Investigations using $GeCl_4$ in an attempt to make phosphine-stabilized germylium cations with $Me_3P$ and TMSOTf lead to the serendipitous discovery and isolation of $[(Me_3P)_2Ge][OTf]_2$, a product observed to be independent of the reaction stiochiometry. However, this was one product of many with other confirmed isolated materials such as $[Me_3PCl][GeCl_3]$[89], $[Me_3PMe_3P][OTf]$[90], and $Ge_6Cl_{16}$[91]. I have proposed that a Ge(II) species is formed through the halide abstraction of a $[GeCl_3]^-$ intermediate which is produced from the direct reaction of $Me_3P$ with $GeCl_4$. Conceivably, three equivalents of TMSOTf could subsequently remove the three chlorine groups with two $Me_3P$ units, evolve volatile TMSCl, and stabilize the $[Ge]^{2+}$ core giving the dication $[(Me_3P)_2Ge][OTf]_2$. Since the reaction gave a Ge(II) product along with many other undesired products, another approach was devised where the reaction would start by using a Ge(II) starting material with the aim of reproducing the Ge(II) dication. One

equivalent of $GeCl_2$[1,4-dioxane] was reacted with two equivalents $Me_3P$ and TMSOTf believed to produce the dication $[(Me_3P)_2Ge][OTf]_2$ (Figure 7.2.4.1, left) with no evidence of unwanted redox chemistry occurring; although verification of the target product remains unconfirmed. This seems to be a viable method since the isolation of a related product [(dmpe)GeCl][OTf] which was crystallized from a reaction mixture consisting of equimolar amounts of dmpe, $GeCl_2$[1,4-dioxane] and excess TMSOTf (Figure 7.2.4.1, right). Selected interatomic distances and angles for $[(Me_3P)_2Ge][OTf]_2$ and [(dmpe)GeCl][OTf] are summarized in Table 7.2.4.1.

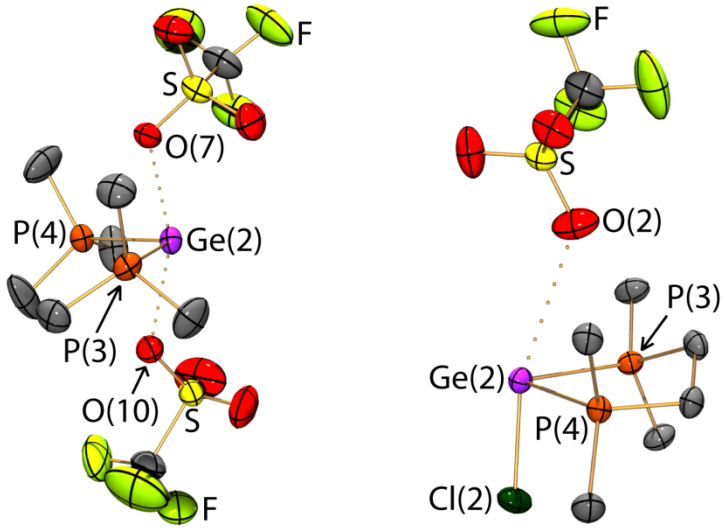


Figure 7.2.4.1 POV-Ray view of the molecular structure of $[(Me_3P)_2Ge][OTf]_2$ (left) and [(dmpe)GeCl][OTf] (right). Thermal ellipsoids are drawn at the 50% probability level and hydrogen atoms were omitted for clarity.

Table 7.2.4.1 Selected interatomic distances (Å) and angles (°) for $[(Me_3P)_2Ge][OTf]_2$ and [(dmpe)GeCl][OTf].

| Compound | Ge-P | P-Ge-P | Nearest $A^-C^+$ |
|---|---|---|---|
| $[(Me_3P)_2Ge][OTf]_2$ | 2.4182(11)<br>2.4160(11)<br>2.4191(12)<br>2.4176(11) | 98.91(4)<br>101.63(4) | 2.253, 2.239<br>[Ge···O] |
| [(dmpe)GeCl][OTf][a] | 2.4406(11)<br>2.4461(10)<br>2.4678(10)<br>2.4696(11) | 81.08(4)<br>80.91(4) | 3.036, 3.058<br>[Ge···O] |

[a] Ge-Cl interatomic distances are 2.2869(11) Å and 2.2917(11)Å

### 7.2.5 Diphosphines, Triphosphines and Cyclophosphines as Ligands for Stannylium and Germylium Cations

Diphosphines can offer structural versatility demonstrated by tethering diphosphines (chapter 5) but with the added potential to produce polymeric products with a completely inorganic backbone. Complexes of P-P bonded diphosphine ligands with $[R_3E]^+$ (where E = Sn, Ge) cations could produce many different compounds, like the products shown in Scheme 7.2.5.1. The stoichiometry of a 1:2:2 mixture (*diphosphine: tetrel: TMSOTf*), could give dications like the one shown in **7.5**, where each end of the diphosphine interacts with a different tetrel center. If a 2:1:1 mixture were used, there is the possibility for two diphosphine interactions with one tetrel to form a cation like the one shown in **7.6** with the tetrel having a coordination number of five; this is a derivative of $[(dmpm)Me_3Sn][AlCl_4]$. Having electron withdrawing groups present on germanium and tin would readily lead to the structure in **7.6**, an analogue of $[(Me_3P)_2SnCl_3][AlCl_4]$. When the reaction is conducted in a 1:1:1 manner there are two ways for the diphosphine

to interact with the tetrel; in the first situation both ends of the diphosphine can interact with the tetrel to generate a ring structure (**7.7**) or alternatively only one of the phosphorus atoms forms a dative bond to create a framework similar to the product in **7.8**.

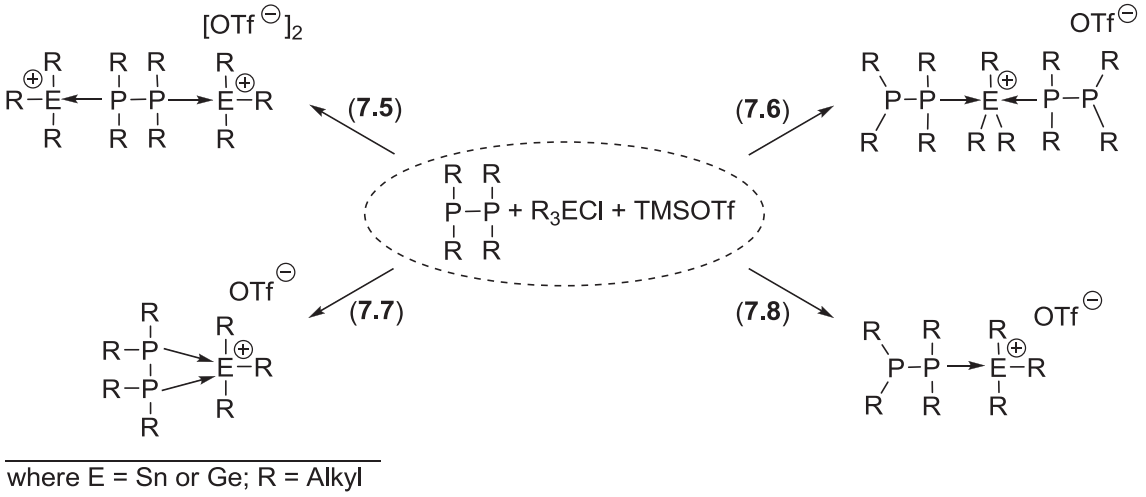


Scheme 7.2.5.1 Potential products from a reaction mixture containing $R_2PR_2P$, $R_3ECl$, and TMSOTf.

Tridentate phosphines could produce many types of unique structures, as well as form some of the first examples of phosphorus complexes of tetrel trications (Figure 7.2.5.1). A cation like $[P_3(ER_3)_3]^{3+}$ is possible where each phosphorus atom on a tridentate ligand is interacting with a separate $[ER_3]^+$ moiety. The salt containing $[P_3(ER_3)_3]^{3+}$ could be synthesized by reacting one equivalent of $P_3$ (triphosphine pincer ligand) with three equivalents of $R_3ECl$ and TMSOTf. A pincer complex like $[(P_3)ER]^{3+}$ could be synthesized reacting $P_3$ and $Cl_3ER$ with three equivalents of TMSOTf. Other pincer complexes such as the dication $[(P_3)ER_2]^{2+}$ could be made by reacting equimolar amounts of $P_3$ and $R_2ECl_2$ in the presence of two equivalents of TMSOTf to potentially form the

5-coordinate dication. A different tetrel framework could be generated by reacting equimolar amounts of $P_3$, $R_3ECl$, and TMSOTf to produce a cation like $[(P_3)ER_3]^+$ where germanium or tin would be surrounded by six substituents.

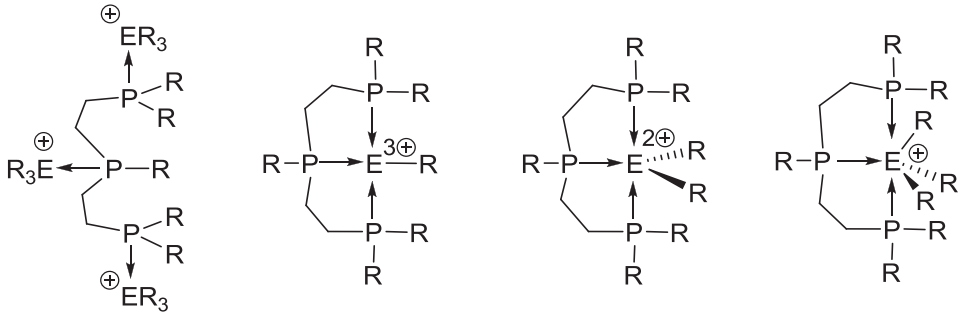


Figure 7.2.5.1 Tethering phosphines as a way to generate unique trications, dications with a coordination number of 5 and cations with a coordination number of 6.

Organocyclophosphines behave as ligands for germanium or tin to make some unique tetrelphosphonium cations. Equimolar amounts of $tBu_3P_3$, $Me_2GeCl_2$, and $AlCl_3$ form a pale yellow clear reaction mixture unconfirmed to be the cation $[(tBu_3P_3)Me_2GeCl][AlCl_4]$ (equation 7.9). The $^{31}P\{^1H\}$ NMR spectrum (Figure 7.2.5.2) suggests the $tBu_3P_3$ ring is involved in a dative interaction since there are three unique phosphorus environments. The peak signal has similar splitting patterns to $[tBu_3P_3Me][OTf]$.[92,6] Other organocyclophosphines are expected to work as there is literature precedent involving organocyclophosphine as ligands with examples of $Cy_4P_4$ effectively used to create Sb-P and As-P dative interactions.[14] Some of the ideal candidates toward this synthesis are $tBu_3P_3$,[93] $Cy_4P_4$,[94] $Ph_4P_4$,[95] $tBu_4P_4$,[96] $Ph_5P_5$,[94] and. $Me_5P_5$.[93]

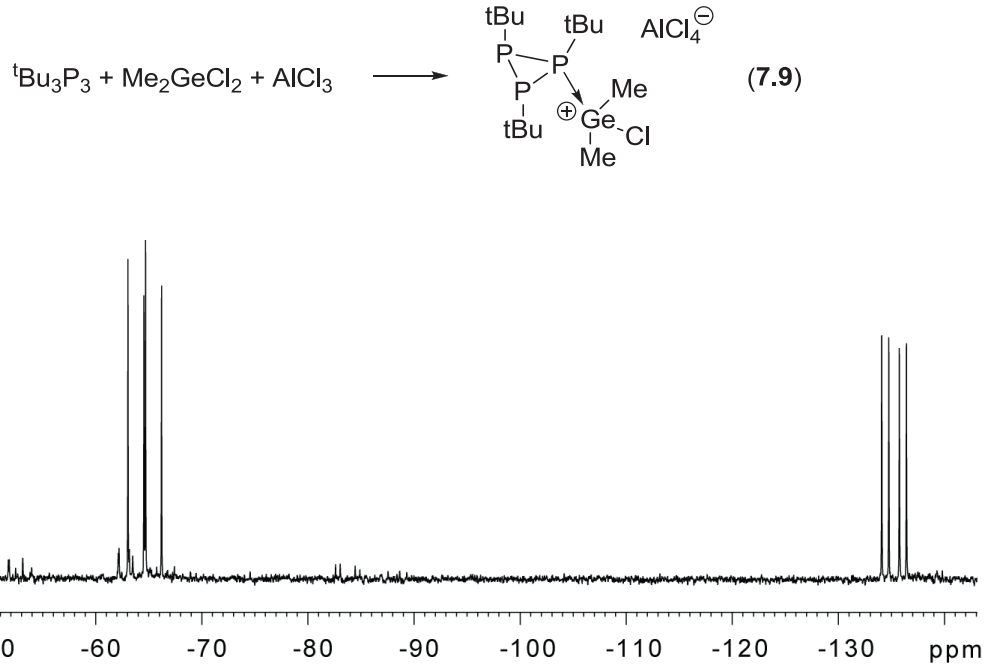


$^{t}Bu_3P_3 + Me_2GeCl_2 + AlCl_3$ → (**7.9**)

Figure 7.2.5.2 $^{31}P\{^{1}H\}$ NMR (202.5 MHz) of a reaction mixture containing $tBu_3P_3$, $Me_2GeCl_2$ and $AlCl_3$.

# CHAPTER 8 EXPERIMENTAL

## 8.1 General

Small scale reactions were carried out in an IT System One Manual glovebox with an inert $N_2$ atmosphere containing less than 10 ppm of oxygen and less than 5 ppm water. Initial reactions were completed in 4-dram glass vials with Teflon-lined caps and larger scale reactions used 100 mL round Schlenk glassware with Teflon needle valves and ground glass joint stoppers. All glassware was stored overnight in an oven at 170 °C and pumped into the glove-box while hot, or was flame-dried under vacuum prior to use.

Solvents were deoxygenated by sparging with $N_2$(g) for 45 mins and collected by a double column MBraun solvent purification system which had solvent pass over one column packed with alumina/copper-Q5 then passed through a second column with 4 Å sieves. $CH_3CN$, $CD_3CN$ and $CD_2Cl_2$ were dried by heating at reflux temperature over $CaH_2$ under Ar(g). $Et_2O$ was dried by heating at reflux temperature over sodium/benzophenone. All solvents were stored over 4 Å molecular sieves for 24 hours prior to use. $SnCl_4$ (99%), $Me_2SnCl_2$ (97%), $AlCl_3$ (99.99%), $PMe_3$ (98%), $Ph_3GeCl$ (99%), $iPr_3SnCl$ (97%), $GeCl_2$[1,4-dioxane], $GeCl_4$ (99.99%), $tBu_3P$ (98%), $PCy_3$ were purchased from Aldrich and used as received. $Et_3GeCl$ (98%), $Me_2GeCl_2$ (99%), dmpe (98%), dmpm (99%), and $AsEt_3$ (99%) were purchased from Strem Chemicals and used as received. $Me_3SnCl$ (97%), $Bu_2SnCl_2$ (97%), and $GaCl_3$ (99.99%) were purchased from Aldrich and sublimed prior to use. $iPr_3P$ (97%) and TMSOTf (99%) were purchased from Aldrich and distilled prior to use.

Solution $^{1}H$, $^{13}C$, $^{19}F$, $^{31}P$ and $^{119}Sn$ NMR spectra were collected at the indicated temperature on the Bruker Avance 500 NMR spectrometer. Chemical shifts are reported in ppm relative to an external reference standard [100% $SiMe_4$ ($^{1}H$, $^{13}C$), 100% $CFCl_3$ ($^{19}F$), 85% $H_3PO_4$ ($^{31}P$), and 90% $SnMe_4$ or 90% $SnCl_4$ ($^{119}Sn$)]. NMR spectra of reaction mixtures were obtained by transferring an aliquot of the bulk solution to a 5mm NMR tube. Tubes were then capped tightly and covered with parafilm and Teflon tape.

The $^{31}P$ CP/MAS NMR experiments were carried out on a Bruker DSX Avance NMR spectrometer with a 9.4T magnet (400.2 MHz proton Larmor frequency, 162.02 MHz $^{31}P$ Larmor frequency) using a probe head for rotors of 4 mm diameter. The samples were spun at 5.0 kHz, 9.0 kHz and 11.0 kHz to determine center bands and to identify spinning sidebands. Relaxation times for the $^{1}H$ NMR experiments were determined by inversion recovery sequences. From these experiments recycle delays between 4 and 12 seconds for the $^{31}P$ cross-polarization (CP) / magic angle spinning (MAS) were determined. The other parameters for the $^{31}P$ CP/MAS experiments with TPPM proton decoupling were optimized on $NH_4H_2PO_4$, whose resonance also served as external, secondary chemical shift standard at 0.81 ppm. For the CP/MAS NMR spectrum up to 32 scans were accumulated, using 500 microseconds CP contact times. All solid state NMR data were collected by Dr. Ulrike Werner-Zwanziger at Dalhousie University.

Infrared spectra were collected on samples prepared as nujol mulls between CsI plates using a Bruker Vector FT-IR spectrometer. Raman spectra were collected using a Bruker RFS 100 FT-Raman spectrometer on samples sealed in 1.5-1.8 mm capillaries under dry nitrogen. Peaks are reported in wavenumbers ($cm^{-1}$) with relative intensities (strong[s], medium[m], weak[w]) in parentheses.

Melting points were obtained on samples in pipettes with the tip sealed. The top of the pipette was wrapped with parafilm, capped by a pipette bulb, and wrapped again with parafilm under dry $N_2$(g). Melting points were carried out by use of an electrothermal apparatus with all values reported uncorrected. Elemental analyses (C, H) were performed by Canadian Microanalytical Services Ltd. Delta, British Columbia, Canada. Elemental analysis was conducted on representative complexes.

Single crystal X-Ray diffraction data were collected using a Bruker AXS P4/SMART 1000 diffractometer. All measurements were made with graphite monochromatic Mo-Kα radiation (0.71073 Å). The data were reduced (SAINT)[97] and corrected for absorption (SADABS)[98] and were corrected for Lorentz and polarization effects. The structures were solved by direct methods and expanded using Fourier techniques. Full matrix least squares refinement was carried out on F2 data using the program SHELXTL.[99] All crystallographic data collection and refinement was performed by Dr. Andreas Decken at the University of New Brunswick.

## 8.2 Preparation and Characterization of Compounds in Chapter 2

FT-IR and FT-Raman data were not collected on the complexes contained in this section. Due to the instability of the crystalline complexes, elemental analysis was not conducted on the material, granted the crystals are most stable stored under hexane at -25°C.

### 8.2.1 $Me_3SnClAlCl_3$

$Me_3SnCl$ (120 mg, 0.6 mmol) and $AlCl_3$ (80 mg, 0.6 mmol) in $CH_2Cl_2$ (5 mL) were stirred together resulting in dissolution of $AlCl_3$ within 5 mins and causing the previously

colorless cloudy reaction mixture to become pale yellow and clear. This was left stirring for 1 hour to ensure the completion of the reaction. X-Ray quality crystals were grown by layering with hexane and cooling the reaction mixture to -25℃ for 4 days. Solvent was decanted and crystals were then washed with 2 x 3 mL of hexane and dried in vacuo.

**Yield:** 172 mg (0.52 mmol, 86% crystalline material)

**M.p.** 84-87 °C

**$^{1}$H NMR** (500.1 MHz, $CD_2Cl_2$, 295K): δ 1.28 ppm (9H, *s,* $Sn[CH_3]_3$) tin satellites observed to overlap for $^{119}$Sn and $^{117}$Sn (*d*, $^{2}J_{Sn-H}$ = 57.8 Hz)

**$^{13}$C NMR** (125.8 MHz, UDEFT, $CD_2Cl_2$, 295K): δ 5.75 ppm (*s*, $Sn[CH_3]_3$) tin satellites observed (*d*, $^{1}J_{119Sn-H}$ = 352.5 Hz; *d*, $^{1}J_{117Sn-H}$ = 336.5 Hz)

**$^{119}$Sn{$^{1}$H} NMR** (186.5 MHz, $CD_2Cl_2$, 295K): δ 255 ppm (*s*)

**Crystal Data:** see Table 8.9.1

### 8.2.2 $Me_2SnCl_2AlCl_3$

$Me_2SnCl_2$ (132 mg, 0.6 mmol) and $AlCl_3$ (80 mg, 0.6 mmol) in $CH_2Cl_2$ (5 mL) were stirred together resulting in dissolution of $AlCl_3$ within 5 mins and causing the previously colorless cloudy reaction mixture to become yellow and clear. This was left stirring for 1 hour to ensure the completion of the reaction. X-Ray quality crystals were grown by layering with hexane and cooling the reaction mixture to -25℃ for 4 days. Solvent was decanted and crystals were then washed with 2 x 3 mL of hexane and dried in vacuo.

**Yield:** 76 mg (0.14 mmol, 23% crystalline material)

**M.p.** 59-61 °C

**$^{1}$H NMR** (500.1 MHz, $CD_2Cl_2$, 295K): δ 1.27 ppm (6H, *s*, Sn[C$H_3$]$_2$) tin satellites observed (*d*, $^{2}J_{119Sn-H}$ = 58 Hz; *d*, $^{2}J_{117Sn-H}$ = 57 Hz)

**$^{13}$C NMR** (125.8 MHz, UDEFT, $CD_2Cl_2$, 295K): δ 5.35 ppm (*s*, Sn[$CH_3$]$_2$) tin satellites observed (*d*, $^{1}J_{119Sn-C}$ = 347 Hz; *d*, $^{1}J_{117Sn-C}$ = 333 Hz)

**$^{119}$Sn{$^{1}$H} NMR** (186.5 MHz, $CD_2Cl_2$, 295K): δ 107 ppm (*s*)

**Crystal Data:** see Table 8.9.1

### 8.2.3 $Bu_2SnCl_2AlCl_3$

$Bu_2SnCl_2$ (182 mg, 0.6 mmol) and $AlCl_3$ (80 mg, 0.6 mmol) in $CH_2Cl_2$ (5 mL) were stirred together resulting in dissolution of $AlCl_3$ within 5 mins and causing the previously colorless, cloudy reaction mixture to become pale yellow and clear. This was left stirring for 1 hour to ensure the completion of the reaction. X-Ray quality crystals were grown by layering with hexane and cooling the reaction mixture to -25℃ for 4 days. Solvent was decanted and crystals were then washed with 2 x 3 mL of hexane and dried in vacuo.

**Yield:** 35 mg (0.08 mmol, 13% crystalline material)

**M.p.** 59-61 °C

**$^{1}$H NMR** (500.1 MHz, $CD_2Cl_2$, 295K): δ 2.48 ppm (4H, *m*, "apparent 1:1:1 triplet", $CH_3CH_2CH_2CH_2Sn$); 1.98 ppm (4H, *pentet*, $CH_3CH_2CH_2CH_2Sn$, $^{3}J_{H-H}$ = 7.3 Hz) tin

satellites observed to overlap for $^{119}$Sn and $^{117}$Sn (*doublet* of *pentet*, $^{3}J_{Sn-H}$ = 106 Hz); 1.51 ppm (4H, *sextet*, $CH_3CH_2CH_2CH_2Sn$, $^{3}J_{H-H}$ = 7.3 Hz); 1.02 ppm (6H, *t*, $^{3}J_{H-H}$ = 7.3 Hz)

**$^{13}$C NMR** (125.8 MHz, UDEFT, $CD_2Cl_2$, 295K): δ 35.77 ppm (*s*, $CH_3CH_2CH_2CH_2Sn$) tin satellites observed (*d*, $^{1}J_{119Sn-C}$ = 354 Hz; *d*, $^{1}J_{117Sn-C}$ = 339 Hz); 27.17 ppm (*s*, $CH_3CH_2CH_2CH_2Sn$) tin satellites observed to overlap for $^{119}$Sn and $^{117}$Sn (*d*, $^{3}J_{Sn-C}$ = 42 Hz); 26.02 ppm (s, $CH_3CH_2CH_2CH_2Sn$) tin satellites observed to overlap for $^{119}$Sn and $^{117}$Sn (*d*, $^{2}J_{SnC}$ = 105 Hz); 13.14 ppm (*s*, $CH_3CH_2CH_2CH_2Sn$)

**$^{119}$Sn{$^{1}$H} NMR** (186.5 MHz, $CD_2Cl_2$, 295K): δ 100 ppm (*s*)

**Crystal Data**: See Table 8.9.1

### 8.2.4 General Preparation of $R_3SnClAlCl_3$ for NMR Studies

$R_3SnCl$ (0.3 mmol) and $AlCl_3$ (40 mg, 0.3 mmol) in $CH_2Cl_2$ (5 mL) were stirred together resulting in dissolution of $AlCl_3$ within 5 mins. This was left stirring for 1 hour to ensure the completion of the reaction. An aliquot can be removed from the reaction mixture for multinuclear NMR studies and a $C_6D_6$ capillary can be inserted into the NMR tube for locking and shimming.

### 8.2.5 General Preparation of $R_2SnCl_2AlCl_3$ for NMR Studies

$R_2SnCl_2$ (0.3 mmol) and $AlCl_3$ (40 mg, 0.3 mmol) in $CH_2Cl_2$ (5 mL) were stirred together resulting in dissolution of $AlCl_3$ within 5 mins. This was left stirring for 1 hour to ensure the completion of the reaction. An aliquot can be removed from the reaction mixture for

multinuclear NMR studies and a $C_6D_6$ capillary can be inserted into the NMR tube for locking and shimming.

### 8.2.6 General Preparation of $R_2SnCl_2(AlCl_3)_2$ for NMR Studies

$R_2SnCl_2$ (0.3 mmol) and $AlCl_3$ (80 mg, 0.6 mmol) in $CH_2Cl_2$ (5 mL) were stirred together resulting in dissolution of $AlCl_3$ within 5 mins. This was left stirring for 1 hour to ensure the completion of the reaction. An aliquot can be removed from the reaction mixture for multinuclear NMR studies and a $C_6D_6$ capillary can be inserted into the NMR tube for locking and shimming.

## 8.3 Preparation and Characterization of Compounds in Chapter 3

### 8.3.1 $[Me_3PMe_2GeCl][AlCl_4]$

$Me_2GeCl_2$ (520 mg, 3 mmol) and $AlCl_3$ (400 mg, 3 mmol) in 5 mL of $CH_2Cl_2$ were stirred together for 10 mins resulting in dissolution of $AlCl_3$. $PMe_3$ (228 mg, 3 mmol), in 7 mL of $CH_2Cl_2$, was added dropwise to the $Me_2GeCl_2/AlCl_3$ mixture. After 1 hour the reaction was layered with $Et_2O$ and crystallized over 2 days at -25 °C to yield crystals suitable for X-Ray experiments. Crystals not submitted for X-Ray diffraction were washed with ether (2 x 5 mL), and dried in vacuo.

**Yield:** 832 mg (2.17 mmol, 72% crystalline material)

**M.p.** 160-163 °C

**E.A.** actual (calculated) C 15.18% (15.68%), H 4.24% (3.95%)

**FT-IR**: (nujol mull, CsI plates, $cm^{-1}$, [relative intensities]): 2915[bs], 1464[s], 1415[ms], 1377[ms], 1299[m], 1249[w], 962[s], 861[m], 821[ms], 768[m], 722[w], 671[vw], 635[mw], 590[mw], 478[bs]

**FT-Raman** (capillary tube - 1mm, $cm^{-1}$, [relative intensities]): 2988[m], 2912[s], 1416[vw], 1400[w], 769[vw], 672[w], 635[vw], 591[w], 397[vw], 372[w], 348[w], 264[w], 173[w], 122[w]

**$^{1}$H NMR** (500.1 MHz, $CD_3CN$, 295K): δ 2.02 ppm (9H, *d*, $PCH_3$, $^{2}J_{P\text{-}H}$ = 12.9 Hz); 1.39 ppm (6H, *s*, $[CH_3]_2Ge$)

**$^{13}$C NMR** (125.8 MHz, UDEFT, $CD_3CN$, 295K): δ 7.79 ppm (*d*, $PCH_3$, $^{1}J_{P\text{-}C}$ = 37.6 Hz); 4.22 ppm (*s*, $[CH_3]_2Ge$)

**$^{31}$P{$^{1}$H} NMR** (202.5 MHz, $CD_3CN$, 295K): δ -15.3 ppm (*s*)

**Crystal Data:** See Table 8.9.3

### 8.3.2 $[Cy_3PEt_3Ge][AlCl_4]$

$Et_3GeCl$ (585 mg, 3 mmol) and $AlCl_3$ (400 mg, 3 mmol) in 5 mL of $CH_2Cl_2$ were stirred for 10 mins resulting in dissolution of $AlCl_3$ which generated a yellow clear reaction mixture. $PCy_3$ (342 mg, 3 mmol), in 7 mL of $CH_2Cl_2$, was added dropwise to the $Et_3GeCl/AlCl_3$ mixture. After 1 hour the colorless, clear reaction mixture was layered with hexane and crystallized over 2 days at -25 °C to yield a few crystals suitable for X-Ray experiments along with some pale yellow oil. Since the purity of the sample could not be determined: yield, melting point, IR, Raman, and elemental analysis were not

collected on the sample.

**$^{31}P\{^{1}H\}$ NMR** (202.5 MHz, $CH_2Cl_2$, $C_6D_6$ capillary, 295K): δ 13.6 ppm (*s*)

**Crystal Data:** See Table 8.9.2

### 8.3.3 $[Me_3PEt_3Ge][AlCl_4]$

$Et_3GeCl$ (585 mg, 3 mmol) and $AlCl_3$ (400 mg, 3 mmol) in 5 mL of $CH_2Cl_2$ were stirred for 10 mins resulting in dissolution of $AlCl_3$ and creating a yellow clear reaction mixture. $PMe_3$ (228 mg, 3 mmol), in 7 mL of $CH_2Cl_2$, was added dropwise to the $Et_3GeCl/AlCl_3$ mixture. After 1 hour the colorless clear reaction mixture was layered with $Et_2O$ and crystallized over 2 days at -25 °C to yield crystals suitable for X-Ray experiments. Crystals not submitted for X-Ray diffraction were washed with hexane (2 x 5 mL), and dried in vacuo. FT-IR data were not collected on the sample and the crystals submitted for X-Ray experiments did not diffract well therefor no molecular information on this salt was determined.

**Yield:** 605 mg (1.45 mmol, 48% crystalline material)

**M.p.** 176-178 °C

**E.A.** actual (calculated) C 22.24% (26.71%), H 5.83% (5.98%)

**FT-Raman** (capillary tube - 1mm, $cm^{-1}$, [relative intensities]): 2987[m], 2956[mw], 2909[s], 2865[mw], 1462[vw], 1407[vw], 1230[w], 761[w], 672[mw], 586[w], 536[mw], 349[mw], 203[w], 121[m]

**$^{1}$H NMR** (500.1 MHz, $CH_2Cl_2$, $C_6D_6$ capillary, 295K): δ 1.85 ppm (9H, *d*, PC*H*$_3$, $^{2}J_{P\text{-}H}$ = 11.8 Hz); 1.40 ppm (6H, *q*, $CH_3CH_2Ge$, $^{3}J_{H\text{-}H}$ = 7.65 Hz); 1.25 ppm (9H, *t*, $CH_3CH_2Ge$, $^{3}J_{H\text{-}H}$ = 7.65 Hz)

**$^{13}$C NMR** (125.8 MHz, UDEFT, $CH_2Cl_2$, $C_6D_6$ capillary, 295K): δ 9.22 ppm (*d*, P*C*H$_3$, $^{1}J_{P\text{-}C}$ = 34.7 Hz); 8.77 ppm (*s*, $CH_3CH_2Ge$); 4.56 ppm (*s*, $CH_3CH_2Ge$)

**$^{31}$P{$^{1}$H} NMR** (202.5 MHz, $CH_2Cl_2$, $C_6D_6$ capillary, 295K): δ -21.7 ppm (*s*)

### 8.3.4 [iPr$_3$PMe$_2$GeCl][OTf]

$Me_2GeCl_2$ (520 mg, 3 mmol) and TMSOTf (667 mg, 3 mmol) in 5 mL of $CH_2Cl_2$ were stirred for 10 mins resulting in a colorless, clear reaction mixture. $iPr_3P$ (480 mg, 3 mmol), in 5 mL of $CH_2Cl_2$, was added dropwise to the $Me_2GeCl_2$/TMSOTf mixture. After 1 hour the colorless clear reaction mixture was layered with $Et_2O$ and crystallized over 2 days at -25 °C to yield crystals suitable for X-Ray experiments. Crystals not submitted for X-Ray diffraction were washed with hexane (2 x 3 mL), and dried in vacuo.

**Yield:** 1.054 g (2.18 mmol, 79% crystalline material)

**M.p.** 171-173 °C

**E.A.** actual (calculated) C 32.45% (32.21%), H 6.15% (6.08%)

**FT-IR**: (nujol mull, CsI plates, cm$^{-1}$, [relative intensities]): 2922[bs], 1463[s], 1398[w], 1377[ms], 1268[bs], 1224[s], 1150[bs], 1092[w], 1062[w], 1030[s], 935[w], 884[m],

856[m], 829[m], 754[w], 722[vw], 690[w], 667[w], 638[s], 586[w], 572[m], 517[m], 489[w]

**FT-Raman** (capillary tube - 1mm, $cm^{-1}$, [relative intensities]):2981[m], 2948[m], 2917[s], 1468[w], 1224[vw], 1030[m], 880[w], 755[w], 627[w], 606[m], 586[w], 490[w], 395[w], 348[w], 313[w], 192[w], 133[w]

**$^{1}$H NMR** (500.1 MHz, $CH_2Cl_2$, $C_6D_6$ capillary, 295K): δ 3.01-2.93 ppm (3H, *m*, $[CH_3]_2CHP$); 1.46 ppm (18H, *dd*, $[CH_3]_2CHP$, $^{3}J_{H-H}$ = 7.25 Hz, $^{3}J_{P-H}$ = 16.9 Hz); 1.41 ppm (6H, *s*, $[CH_3]_2Ge$)

**$^{13}$C NMR** (125.8 MHz, UDEFT, $CH_2Cl_2$, $C_6D_6$ capillary, 295K): δ 120.82 ppm (*q*, $^{1}J_{C-F}$ = 321 Hz, $O_3SCF_3$); 22.39 ppm (*d*, $[CH_3]_2CHP$, $^{1}J_{P-C}$ = 24.9 Hz); 18.05 ppm (*d*, $[CH_3]_2CHP$, $^{2}J_{P-C}$ = 2.41 Hz); 9.26 ppm (*s*, $[CH_3]_2Ge$)

**$^{19}$F{$^{1}$H} NMR** (470.6 MHz, $CH_2Cl_2$, $C_6D_6$ capillary, 295K): δ -79.1 ppm (*s*)

**$^{31}$P{$^{1}$H} NMR** (202.5 MHz, $CH_2Cl_2$, $C_6D_6$ capillary, 295K): δ 26.5 ppm (*s*)

**Crystal Data:** See Table 8.9.2

### 8.3.5 $[Me_3PPh_3Ge][OTf]$

$Ph_3GeCl$ (679 mg, 2 mmol) and TMSOTf (444 mg, 2 mmol) in 5 mL of $CH_2Cl_2$ were stirred for 10 mins resulting in a colorless, slightly cloudy reaction mixture. $Me_3P$ (153 mg, 2 mmol) in 5 mL of $CH_2Cl_2$, was added dropwise to the $Ph_3GeCl$/TMSOTf mixture. After 1 hour the colorless slightly cloudy reaction mixture was filtered, layered with hexane, and crystallized over 2 days at -25 °C to yield material suitable for X-Ray

experiments. Crystals not submitted for X-Ray diffraction were washed with hexane (2 x 3 mL) and dried in vacuo. It was not possible to obtain analytically pure samples however E. A. was conducted on the material and the purity of the sample was inconclusive.

**Yield:** 721 mg (1.36 mmol, 68% crystalline material)

**M.p.** 213-215 °C

**E.A.** actual (calculated) C 46.98% (49.94%), H 4.27% (4.57%)

**FT-IR**: (nujol mull, CsI plates, $cm^{-1}$, [relative intensities]): 2956[s], 2921[s], 2853[s], 1485[w], 1462[m], 1433[m], 1377[mw], 1322[mw], 1303[m], 1278[bs], 1261[bs], 1224[m], 1152[ms], 1090[m], 1031[s], 997[mw], 964[m], 799[w], 748[ms], 738[m], 697[ms], 636[ms], 572[mw], 517[mw], 462[m]

**FT-Raman** (capillary tube - 1mm, $cm^{-1}$, [relative intensities]): 3184[vw], 3140[vw], 3053[mw], 2999[w], 2984[w], 2913[mw], 1582[mw], 1570[w], 1404[vw], 1224[vw], 1186[vw], 1164[vw], 1088[vw], 1033[mw], 1025[w], 999[s], 770[vw], 753[w], 677[w], 666[vw], 617[vw], 572[vw], 372[vw], 348[vw], 238[vw], 225[w], 199[vw], 168[w]

**$^{1}$H NMR** (500.1 MHz, $CD_2Cl_2$, 295K): δ 7.64-7.53 ppm (15H, *m*, $C_6H_5Ge$); 1.78 ppm (9H, *d*, $[CH_3]_3P$, $^{2}J_{P-H}$ = 12.5 Hz)

**$^{13}$C NMR** (125.8 MHz, UDEFT, $CD_2Cl_2$, 295K): δ 134.94 ppm (*s*, $CH[CHCH]_2CGe$); 131.84 ppm (*s*, $CH[CHCH]_2CGe$); 129.93 ppm (*s*, $CH[CHCH]_2CGe$); 126.99 ppm (*s*, $CH[CHCH]_2CGe$); 120.77 ppm (*q*, $^{1}J_{C-F}$ = 320 Hz, $O_3SCF_3$); 8.31 ppm (*d*, $[CH_3]_3P$, $^{1}J_{P-C}$ = 36.9 Hz)

**$^{19}F\{^{1}H\}$ NMR** (470.6 MHz, $CD_2Cl_2$, 295K): δ -78.9 ppm (*s*)

**$^{31}P\{^{1}H\}$ NMR** (202.5 MHz, $CD_2Cl_2$, 295K): δ -19.0 ppm (br)

**Crystal Data:** See Table 8.9.3

### 8.3.6 $[dmpe(Et_3Ge)_2][OTf]_2$

$Et_3GeCl$ (585 mg, 3 mmol) and TMSOTf (667 mg, 3 mmol) in 5 mL of $CH_2Cl_2$ were stirred for 10 mins resulting in a colorless clear reaction mixture. Dmpe (225 mg, 1.5 mmol) in 5 mL of $CH_2Cl_2$, was added dropwise to the $Et_3GeCl$/TMSOTf mixture. After 1 hour the colorless clear reaction mixture was layered with $Et_2O$ and crystallized over 2 days at -25 °C to yield crystals suitable for X-Ray experiments. Crystals not submitted for X-Ray diffraction were washed with hexane (2 x 3 mL), and dried in vacuo.

**Yield:** 1.796 g (2.33 mmol, 78% crystalline material)

**M.p.** 119-121 °C

**E.A.** actual (calculated) C 30.18% (31.28%), H 5.91% (6.04%)

**FT-IR**: (nujol mull, CsI plates, $cm^{-1}$, [relative intensities]): 2907[bs], 1464[s], 1377[ms], 1314[ms], 1301[ms], 1258[s], 1159[s], 1131[s], 1029[ms], 962[m], 929[m], 768[w], 756[w], 721[mw], 690[mw], 676[m], 637[mw], 584[mw], 572[w], 517[s]

**FT-Raman** (capillary tube - 1mm, $cm^{-1}$, [relative intensities]): 2994[m], 2983[m], 2960[s], 2937[s], 2913[m], 2879[vw], 1467[vw], 1457[vw], 1433[vw], 1427[vw], 1423[vw], 1252[vw], 1226[w], 1036[m], 776[vw], 757[mw], 696[w], 586[w], 573[w], 540[mw], 347[vw], 331[vw], 314[vw], 303[vw], 229[vw], 224[vw], 220[vw], 199[vw]

**$^{1}H\{^{31}P\}$ NMR** (500.1 MHz, $CH_2Cl_2$, $C_6D_6$ capillary, 295K): δ 2.55 ppm (4H, *s*, C*H*$_2$P); 1.90 ppm (12H, *s*, [C*H*$_3$]$_2$P); 1.45 ppm (12H, *q*, $CH_3CH_2Ge$, $^{3}J_{H-H}$ = 7.95 Hz); 1.23 ppm (12H, *t*, $CH_3CH_2Ge$, $^{3}J_{H-H}$ = 7.95 Hz)

**$^{13}C$ NMR** (125.8 MHz, UDEFT, $CH_2Cl_2$, $C_6D_6$ capillary, 295K): δ 120.81 ppm (*q*, $^{1}J_{C-F}$ = 320 Hz, $O_3SCF_3$); 14.90-14.74 ppm (*m*, virtual coupling, *C*$H_2$P); 8.64 ppm (*s*, $CH_3CH_2Ge$); 5.80-5.54 ppm (*m*, virtual coupling, *C*$H_3$P); 4.73 ppm (*s*, *C*$H_3CH_2Ge$)

**$^{19}F\{^{1}H\}$ NMR** (470.6 MHz, $CH_2Cl_2$, $C_6D_6$ capillary, 295K): δ -77.6 ppm (*s*)

**$^{31}P\{^{1}H\}$ NMR** (202.5 MHz, $CH_2Cl_2$, $C_6D_6$ capillary, 295K): δ -12.3 ppm (*s*)

**Crystal Data:** See Table 8.9.4

### 8.3.7 $[dmpe(Ph_3Ge)_2][OTf]_2$

$Ph_3GeCl$ (204 mg, 0.6 mmol) and TMSOTf (133 mg, 0.6 mmol) in 5 mL of $CH_2Cl_2$ were stirred for 10 mins resulting in a colorless, clear reaction mixture. dmpe (46 mg, 0.3 mmol), in 5 mL of $CH_2Cl_2$, was added dropwise to the $Ph_3GeCl$/TMSOTf mixture creating a saturated solution evident by the presence of a small amount of precipitate. After 1 hour, the mixture can be filtered through a pipette plugged by a Kimwipe until it becomes colorless and clear. The colorless, clear reaction mixture was layered with hexane and crystallized over 2 days at -25 °C to yield crystals suitable for X-Ray experiments. Crystals not submitted for X-Ray diffraction were washed with hexane (2 x 3 mL), and dried in vacuo. By multinuclear NMR spectroscopy, the crystals and the powder have matching NMR resonances confirming that they correspond to the same complex. If bulk material of the salt is desired, adding hexane to the reaction mixture

with some of the colorless precipitate will cause more material out of solution which can then be washed with 2 x 3 mL portions of hexane, then dried in vaccuo.

**Yield:** Synthesis was repeated in duplicate to obtain two yields; crystalline and bulk powder respectively. 83 mg (0.07 mmol, 26% crystalline material); 136 mg (0.12 mmol, 43% powder material)

**M.p.** 210-212°C

**$^{1}$H NMR** (500.1 MHz, $CD_3CN$, 295K): δ 7.72-7.67 ppm (6H, *m*, C*H*[CHCH]$_2$CGe); 7.65-7.61 (12H, *m*, CH[CHC*H*]$_2$CGe); 7.60-7.56 ppm (12H, *m*, CH[C*H*CH]$_2$CGe); 2.07-2.05 ppm (4H, *m*, virtual coupled, C$H_2$P); 1.61-1.57 ppm (12H, *m*, virtual coupled "apparent 1:1:1 triplet", C$H_3$P)

**$^{13}$C NMR** (125.8 MHz, UDEFT, $CD_3CN$, 295K): δ 136.44 ppm (*s*, CH[CH*C*H]$_2$CGe); 132.99 ppm (*s*, *C*H[CHCH]$_2$CGe); 130.94 ppm (*s*, CH[*C*HCH]$_2$CGe); 127.96 ppm (*s*, CH[CHCH]$_2$*C*Ge); 122.02 ppm (*q*, $^{1}J_{CF}$ = 321 Hz, $O_3SCF_3$); 17.63-17.29 ppm (*m*, virtual coupling "apparent 1:1:1 triplet", *C*H$_2$P); 7.18-6.76 ppm (*m*, virtual coupling "apparent 1:1:1 triplet", *C*H$_3$P)

**$^{19}$F{$^{1}$H} NMR** (470.6 MHz, $CD_3CN$, 295K): δ -79.2 ppm (*s*)

**$^{31}$P{$^{1}$H} NMR** (202.5 MHz, $CD_3CN$, 295K): δ -11.2 ppm (br)

**Crystal Data:** See Table 8.9.5

### 8.3.8 $[(dmpe)Me_2Ge][OTf]_2$

$Me_2GeCl_2$ (520 mg, 3 mmol) and TMSOTf (1.33 g, 6 mmol) in 5 mL of $CH_2Cl_2$ were stirred for 10 mins resulting in a colorless clear reaction mixture. Dmpe (450 mg, 3 mmol) in 5 mL of $CH_2Cl_2$ was added dropwise to the $Me_2GeCl_2$/TMSOTf mixture. After 1 hour the colorless clear reaction mixture was layered with $Et_2O$ and crystallized over 2 days at -25 °C to yield crystals suitable for X-Ray experiments. Crystals not submitted for X-Ray diffraction were washed with hexane (2 x 3 mL), and dried in vacuo.

**Yield:** 190 mg (0.30 mmol, 61% crystalline)

**M.p.** 299-301 °C

**E.A.** actual (calculated) C 21.30% (21.80%), H 3.97% (4.02%)

**FT-IR**: (nujol mull, CsI plates, $cm^{-1}$, [relative intensities]): 2923[s], 2853[s], 1461[m], 1426[mw], 1377[mw], 1318[mw], 1299[m], 1261[s], 1163[s], 1035[s], 998[w], 971[m], 953[m], 924[w], 866[mw], 806[w], 779[w], 759[w], 737[w], 646[s], 574[mw], 517[m]

**FT-Raman** (capillary tube - 1mm, $cm^{-1}$, [relative intensities]): 3006[mw], 2965[mw], 2929[s], 2524[mw], 1029[m], 758[mw], 742[w], 672[mw], 575[w], 349[w], 314[w], 119[w]

**$^1$H NMR** (500.1 MHz, $CD_3CN$, 295K): δ 2.67-2.65 (4H, *m*, virtual coupling, $CH_2P$); 2.00-1.97 ppm (12H, *m*, virtual coupling, $[CH_3]_2P$); 1.26 ppm (6H, *t*, $[CH_3]_2Ge$, $^3J_{P-H}$ = 6.90 Hz)

**$^{13}$C NMR** (125.8 MHz, UDEFT, $CD_3CN$, 295K): δ 121.90 ppm (*q*, $^1J_{C\text{-}F}$ = 320 Hz, $O_3SCF_3$); 21.09-20.80 ppm (*m*, virtual coupling "apparent triplet", $CH_2P$); 6.75-6.44 ppm (*m*, virtual coupling "apparent triplet", $[CH_3]_2P$; -1.05-(-1.17) ppm (*m*, virtual coupling "apparent triplet", $[CH_3]_2Ge$)

**$^{19}$F{$^1$H} NMR** (470.6 MHz, $CD_3CN$, 295K): δ -77.7 ppm (*s*)

**$^{31}$P{$^1$H} NMR** (202.5 MHz, $CD_3CN$, 295K): δ 2.60 ppm (*s*)

**Crystal Data:** See Table 8.9.4

## 8.4 Preparation and Characterization of Compounds in Chapter 4

### 8.4.1 $(PMe_3)_2SnCl_4$

$PMe_3$ (761 mg, 10 mmol) in $CH_2Cl_2$ (16 mL) was added dropwise to $SnCl_4$ (1.302 g, 5 mmol) stirring in $CH_2Cl_2$ (14 mL). After 1 hour the colorless opaque reaction mixture was concentrated producing colorless powder, the remaining solvent was decanted off and the colorless powder was dried in vacuo. Crystalline material was obtained by dissolving the slightly-soluble powder in $CH_2Cl_2$ (20 mL) from which the colorless supernatant was decanted and allowed to slowly evaporate (evacuated 2 bulb apparatus) for 6 days at room temperature; this yielded single crystals suitable for X-Ray diffraction experiments, the crystals were washed with hexane (3 x 7 mL) and dried in vacuo. By multinuclear NMR spectroscopy, the crystals and the powder have matching NMR resonances confirming that they correspond to the same complex. If bulk material of the salt is desired, adding hexane to the reaction mixture with some of the colorless

precipitate will cause more material out of solution which can then be washed with 2 x 3 mL portions of hexane, then dried in vaccuo.

**Yield:** Synthesis was repeated in duplicate to obtain two yields; crystalline and bulk powder respectively. 1.782 g (4.33 mmol, 86%, powder), 0.388 g (0.94 mmol, 19%, crystalline)

**M.p.** 201-204°C (powder), 202-204°C (crystalline)

**E.A.** calculated (actual) of crystalline material: C 17.46% (17.32%), H 4.40% (4.49%)

**FT-IR** (nujol mull on CsI plates, $cm^{-1}$, [relative intensities]): 2960[s], 2924[bs], 2871[s], 2854[s], 1465[s], 1460[s], 1394[m], 1376[m], 1293[w], 1250[m], 1209[w], 1199[w], 1158[m], 1091[m], 1056[m], 1034[m], 928[w], 881[m], 790[s], 681[m], 659[m], 598[w], 536 [m], 494 [bs]

**FT-Raman** (capillary tube - 1mm, $cm^{-1}$, [relative intensities]): 2985[m], 2910[s], 1403[w], 764[w], 667[w], 349[w], 334[w], 228[w], 267[w], 174[w]

**$^{1}$H NMR** (500.1 MHz, $CD_2Cl_2$, 295K): δ 1.80-1.83 ppm (18H, *m*, virtual coupling, P*C*$H_3$)

**$^{13}$C{$^{1}$H} NMR** (125.8 MHz, $CD_2Cl_2$, 295K): δ 10.15-10.39 ppm (*m*, virtual coupling "apparent 1:1:1 triplet", P*C*$H_3$)

**$^{31}$P{$^{1}$H} NMR** (202.5 MHz, $CD_2Cl_2$, 295K): δ 1.6 ppm (*s*), tin satellites observed (*d*, $^{1}J_{119Sn-P}$ = 2635 Hz, $^{1}J_{117Sn-P}$ = 2517 Hz)

**$^{119}$Sn NMR** (186.5 MHz, $CD_2Cl_2$, 295K): δ -554 ppm (*t*, $^{1}J_{P-Sn}$ = 2635 Hz)

**$^{31}$P CP/MAS** (62.02 MHz, 4mm rotor, 9.0 kHz spinning, 295K): 6.74 ppm (*s*) tin satellites observed to overlap for $^{119}$Sn and $^{117}$Sn (*d*, $^{1}J_{P\text{-}Sn}$ = 2772 Hz)

**Crystal Data**: See Table 8.9.6

### 8.4.2 $[(PMe_3)_2SnCl_3][AlCl_4]$

$PMe_3$ (761 mg, 10 mmol) in $CH_2Cl_2$ (13 mL) was added rapidly to a stirring mixture of $AlCl_3$ (667 mg, 5 mmol) and $SnCl_4$ (1.302 g, 5 mmol) in $CH_2Cl_2$ (32 mL). After 1 hour the pale yellow opaque reaction mixture was concentrated producing an off-white powder. Crystalline material was obtained by partially dissolving the slightly-soluble powder in $CH_2Cl_2$ (20 mL) from which the pale yellow supernatant was decanted and allowed to slowly evaporate over 6 days (evacuated 2 bulb apparatus) at room temperature; this yielded single crystals suitable for X-Ray diffraction experiments. By multinuclear NMR spectroscopy, the crystals and the powder have matching NMR resonances confirming that they correspond to the same complex. If bulk material of the salt is desired, adding hexane to the reaction mixture with some of the colorless precipitate will cause more material out of solution which can then be washed with 2 x 3 mL portions of hexane, then dried in vaccuo.

**Yield:** Synthesis was repeated in duplicate to obtain two yields; crystalline and bulk powder respectively. 2.482 g (4.56 mmol, 91%, powder), 0.772 g (1.42 mmol, 28%, crystalline)

**M.p.** 171-175°C (powder), 172-175°C (crystalline)

**E.A.** calculated (actual) of crystalline material: C 13.36% (13.20%), H 3.32% (3.32%)

**FT-IR** (nujol mull on CsI plates, $cm^{-1}$, [relative intensities]): 2955[s], 2924[bs], 2854[s], 1458[bm], 1422[m], 1410[s], 1377[m], 1304[w], 1295[m], 1288[m], 1268[w], 1010[w], 960[bs], 851[w], 842[w], 829[w], 759[m], 722[w], 664[w], 528[m], 495[s], 488[s], 444[w]

**FT-Raman** (capillary tube - 1mm, $cm^{-1}$, [relative intensities]): 2985[m], 2905[s], 1401[w], 759[w], 668[w], 338[w], 268[ms], 234[w], 201[w], 178[w]

**$^{1}$H NMR** (500.1 MHz, $CD_2Cl_2$, 295K): δ 1.93-1.96 ppm (18H, *m*, virtual coupling, PC*H*$_3$)

**$^{13}$C{$^{1}$H} NMR** (125.8 MHz, UDEFT, $CD_2Cl_2$, 295K): δ 10.14-10.39 ppm (*m*, virtual coupling "apparent 1:1:1 triplet", P*C*H$_3$)

**$^{31}$P{$^{1}$H} NMR** (202.5 MHz, $CD_2Cl_2$, 295K): δ 10.8 ppm (*s*), tin satellites observed (*d*, $^{1}J_{119Sn-P}$ = 2725 Hz, $^{1}J_{117Sn-P}$ = 2604 Hz)

**$^{119}$Sn NMR** (186.5 MHz, $CD_2Cl_2$, 295K): δ -456 ppm (*t*, $^{1}J_{P-Sn}$ = 2725 Hz)

**$^{31}$P CP/MAS** (62.02 MHz, 4 mm rotor, 9.0 kHz spinning, 295K): 15.9 ppm (*s*) tin satellites observed to overlap for $^{119}$Sn and $^{117}$Sn (*d*, $^{1}J_{P-Sn}$ = 2706 Hz)

**Crystal Data**: See Table 8.9.6.; Table 8.9.7 contains data on the gallate salt obtained for a Raman study; details are not discussed in this thesis.

### 8.4.3 $[(PMe_3)_2SnCl_2][AlCl_4]_2$

$PMe_3$ (761 mg, 10 mmol) in $CH_2Cl_2$ (16 mL) was added rapidly to a stirring mixture of $AlCl_3$ (1.333 g, 10 mmol) and $SnCl_4$ (1.302 g, 5 mmol) in $CH_2Cl_2$ (16 mL). After 2 hours

the yellow, opaque reaction mixture was allowed to separate revealing colorless precipitate with yellow, clear supernatant. Crystalline material was obtained by decanting the yellow clear supernatant which was left to slowly evaporate over 6 days (evacuated 2 bulb apparatus) at room temperature; this yielded single crystals suitable for X-Ray diffraction experiments. By multinuclear NMR spectroscopy, the crystals and the powder have matching NMR resonances confirming that they correspond to the same complex. If bulk material of the salt is desired, adding hexane to the reaction mixture with some of the colorless precipitate will cause more material out of solution which can then be washed with 2 x 3 mL portions of hexane, then dried in vaccuo.

**Yield:** Synthesis was repeated in duplicate to obtain two yields; crystalline and bulk powder respectively. 3.289 g (4.82 mmol, 96%, powder), 0.250 g (0.37 mmol, 7%, crystalline)

**D.p** 155–157 °C (decomposes to give a colorless powder that melts between 233-235 °C)

**E.A.** calculated (actual) of crystalline material: C 10.61% (10.54%), H 2.67% (2.64%)

**FT-IR** (nujol mull on CsI plates, $cm^{-1}$, [relative intensities]): 2956[s], 2921[bs], 2854[s], 1462[bm], 1418[m], 1403[s], 1377[m], 1311[w], 1296[s], 960[s], 947[s], 853[w], 762[s], 722[w], 664[s], 526[bs], 428[s]

**FT-Raman** (capillary tube - 1mm, $cm^{-1}$, [relative intensities]): 2996[m], 2981[m], 2919[ms], 2907[s], 1399[w], 763[w], 667[w], 329[m], 193[w], 174[m]

**$^1$H NMR** (500.1 MHz, $CD_2Cl_2$, 295K): δ 2.05-2.08 ppm (18H, *m*, virtual coupling, PC$H_3$)

**$^{13}C\{^1H\}$ NMR** (125.8 MHz, $CD_2Cl_2$, 2980K): δ 9.96-10.21 ppm (*m*, virtual coupling "apparent triplet", P*C*$H_3$)

**$^{31}P\{^1H\}$ NMR** (202.5 MHz, $CD_2Cl_2$, 295K): δ 16.9 ppm (*s*), tin satellites present (*d*, $^1J_{119Sn\text{-}P}$ = 2591 Hz, $^1J_{117Sn\text{-}P}$ = 2476 Hz)

**$^{119}Sn$ NMR** (186.5 MHz, $CD_2Cl_2$, 295K): ): δ -333 ppm (*t*, $^1J_{P\text{-}Sn}$ = 2591 Hz)

**$^{31}P$ CP/MAS** (62.02 MHz, 4 mm rotor, 9.0 kHz spinning, 295K): 46.3 ppm (*s*) tin satellites observed to overlap for $^{119}Sn$ and $^{117}Sn$ (*d*, $^1J_{P\text{-}Sn}$ = 2125 Hz); 45.8 ppm (*s*) tin satellites observed to overlap for $^{119}Sn$ and $^{117}Sn$ (*d*, $^1J_{P\text{-}Sn}$ = 2125 Hz)

**Crystal Data**: see Table 8.9.7

## 8.5 Preparation and Characterization of Compounds in Chapter 5

### 8.5.1 $[Me_3PMe_3Sn][AlCl_4]$

$Me_3SnCl$ (498 mg, 2.5 mmol) and $AlCl_3$ (333 mg, 2.5 mmol) in $CH_2Cl_2$ (20 mL) were stirred together for 20 mins resulting in dissolution of $AlCl_3$. $PMe_3$ (257.7 μL, 2.5 mmol) in $CH_2Cl_2$ (14 mL) was added dropwise to the mixture. After 1 hour the colorless clear reaction mixture was layered with ether and over 2 days at room temperature to yield a crystalline solid. This was washed with ether (3 x 10 mL) and pentane (3 x 10 mL) then dried in vacuo.

**Yield:** 460 mg (1.13 mmol, 45% crystalline material)

**M.p.** 176-180 °C

**E.A.** actual (calculated) C 16.60% (17.63%), H 4.15% (4.44%)

**FT-IR**: (nujol mull, CsI plates, $cm^{-1}$, [relative intensities]): 2955[bs], 2926[s], 2853[s], 1462[bs], 1430[m], 1377[ms], 1295[ms], 969[s], 957[s], 785[bs], 754[ms], 541[s], 496[s], 484[s]

**FT-Raman** (capillary tube - 1mm, $cm^{-1}$, [relative intensities]): 2992[m], 2921[ms], 1406[w], 1197[w], 783[w], 670[mw], 547[s], 512[w], 347[w], 262[w], 177[mw]

**$^{1}$H NMR** (500.1 MHz, $CD_2Cl_2$, 295K): δ 1.82 ppm (9H, *d*, $^{2}J_{P\text{-}H}$ = 11.4Hz, PC*H*$_3$) tin satellites are observed to overlap for $^{117}$Sn and $^{119}$Sn (*d*, $^{3}J_{Sn\text{-}H}$ = 10.6 Hz); 0.80 ppm (9H, *d*, $^{3}J_{PH}$ = 1.9 Hz, SnC*H*$_3$) tin satellites observed (*d*, $^{2}J_{119Sn\text{-}H}$ = 58.4 Hz; *d*, $^{2}J_{117Sn\text{-}H}$ = 55.7 Hz)

**$^{13}$C NMR** (125.8 MHz, UDEFT, $CD_2Cl_2$, 295K): δ 9.74 ppm (*d*, $^{1}J_{P\text{-}C}$ = 29.2 Hz, P*C*H$_3$); -5.96 ppm (*s*, Sn*C*H$_3$) tin satellites observed (*d*, $^{1}J_{119Sn\text{-}C}$ = 363 Hz; *d*, $^{1}J_{117Sn\text{-}C}$ = 344 Hz)

**$^{31}$P{$^{1}$H} NMR** (202.5 MHz, $CD_2Cl_2$, 295K): δ -36.8 ppm (*s*) tin satellites present (*d*, $^{1}J_{117Sn\text{-}P}$ = 308 Hz; *d*, $^{1}J_{119Sn\text{-}P}$ = 322 Hz)

**$^{119}$Sn{$^{1}$H} NMR** (186.5 MHz, $CD_2Cl_2$, 295K): δ 43 ppm (*d*, $^{1}J_{Sn\text{-}P}$ = 322 Hz)

**$^{31}$P CP/MAS** (162.02 MHz, 11.0 KHz spinning, 295K): δ -34.8 ppm (*s*) tin satellites observed to overlap for $^{119}$Sn and $^{117}$Sn (*d*, $^{1}J_{P\text{-}Sn}$ = 330 Hz)

**Crystal Data:** See Table 8.9.8

### 8.5.2 [$Me_3PMe_3Sn$][OTf]

$Me_3SnCl$ (996 mg, 5 mmol) and TMSOTf (1.111 g, 5 mmol) in 26 mL of $CH_2Cl_2$ were stirred together for 10 mins. $PMe_3$ (381 mg, 5 mmol), in 14 mL of $CH_2Cl_2$, was added dropwise to the $Me_3SnCl$/TMSOTf mixture. After 1 hour the colorless clear reaction mixture was layered with ether and crystallized over 2 days at -25 °C to yield crystals suitable for X-Ray experiments. Crystals not submitted for X-Ray diffraction were washed with ether (2 x 10 mL), and dried in vacuo.

**Yield:** 525 mg (1.35 mmol, 45% crystalline material)

**M.p.** 195-198 °C

**E.A.** actual (calculated) C 21.28% (21.67%), H 4.77% (4.66%)

**FT-IR**: (nujol mull, CsI plates, $cm^{-1}$, [relative intensities]): 2958[s], 2926[s], 2853[s], 1461[s], 1430[ms], 1377[m], 1274[s], 1260[s], 1150[s], 1029[s], 959[s], 858[w], 842[w], 796[s], 755[s], 723[s], 636[s], 571[m], 549[m], 514[s]

**FT-Raman** (capillary tube - 1mm, $cm^{-1}$, [relative intensities]): 2989[ms], 2916[s], 1414[w], 1223[w], 1188[w], 1026[s], 755[m], 703[w], 669[mw], 572[w], 548[mw], 515[s], 348[w], 314[w], 262[w], 171[bm]

**$^1$H NMR** (500.1 MHz, $CD_3CN$, 295K): δ 1.60 ppm (9H, *d*, $^2J_{P-H}$ = 11.4 Hz, P$CH_3$); 0.64 ppm (9H, *s*, Sn$CH_3$) tin satellites observed (*d*, $^2J_{119Sn-H}$ = 64.0 Hz; *d*, $^2J_{117Sn-H}$ = 61.3 Hz)

**$^{13}$C NMR** (125.8 MHz, UDEFT, $CD_3CN$, 295K): δ 121.99 ppm (*q*, $^1J_{C-F}$ = 320 Hz, $O_3SCF_3$); 9.51 ppm (*d*, $^1J_{P-C}$ = 28.4 Hz, P$CH_3$); -5.57 ppm (*s*, Sn$CH_3$)

**$^{19}F\{^{1}H\}$ NMR** (470.6 MHz, $CD_3CN$, 295K): δ -79.2 ppm (*s*)

**$^{31}P\{^{1}H\}$ NMR** (202.5 MHz, $CD_3CN$, 295K): δ -36.3 ppm (br)

**$^{119}Sn\{^{1}H\}$ NMR** (186.5 MHz, $CD_3CN$, 295K): δ 7 ppm (br)

**Crystal Data:** See Table 8.9.8

### 8.4.3 $[iPr_3PMe_3Sn][AlCl_4]$

$Me_3SnCl$ (996 mg, 5 mmol) and $AlCl_3$ (667 mg, 5 mmol) in 20 mL of $CH_2Cl_2$ were stirred together for 20 mins resulting in dissolution of $AlCl_3$. $iPr_3P$ (801 mg, 5 mmol), in 14 mL of $CH_2Cl_2$, was added dropwise to the $Me_3SnCl/AlCl_3$ mixture. After 1 hour the colorless clear reaction mixture was layered with $Et_2O$ and crystallized over 2 days at -25 °C to yield crystals suitable for X-Ray experiments. Crystals not submitted for X-Ray diffraction were washed with $Et_2O$ (2 x 7 mL), and dried in vacuo.

**Yield:** 492 mg (1 mmol, 20% crystalline material)

**M.p.** 290-292 °C

**E.A.** actual (calculated) C 29.11% (29.24%), H 6.32% (6.14%)

**FT-IR**: (nujol mull, CsI plates, $cm^{-1}$, [relative intensities]): 2957[bs], 2924[bs], 2869[bs], 2853[s], 1461[s], 1377[ms], 1250[w], 1091[w], 1034[w], 881[w], 790[ms], 722[], 681[w], 536[m], 493[s]

**FT-Raman** (capillary tube - 1mm, $cm^{-1}$, [relative intensities]): 2972[s], 2911[s], 2874[m], 1467[w], 1448[w], 1210[w], 1199[w], 879[w], 598[w], 537[m], 509[ms], 480[vw], 349[w]

**$^{1}$H NMR** (500.1 MHz, $CD_2Cl_2$, 295K): δ 2.72-2.61 ppm (3H, *m*, $[CH_3]_2CHP$), 1.43 ppm (18H, *dd*, $^{3}J_{H-H}$ = 7.2 Hz, $^{4}J_{PH}$ = 16.5 Hz, $[CH_3]_2CHP$), 0.84 ppm (9H, s, $CH_3Sn$) tin satellites observed (*d*, $^{2}J_{119Sn-H}$ = 56.7 Hz; *d*, $^{2}J_{117Sn-H}$ = 54.4 Hz)

**$^{13}$C NMR** (125.8 MHz, UDEFT, $CD_2Cl_2$, 295K): δ 22.31 ppm (*d*, $^{1}J_{C-P}$ = 20.6 Hz, *C*HP); 18.99 ppm (*s*, $[CH_3]_2CHP$); -4.28 ppm (*s*, $CH_3Sn$) tin satellites observed (*d*, $^{1}J_{119Sn-C}$ = 353 Hz; *d*, $^{1}J_{117Sn-C}$ = 338 Hz)

**$^{31}$P{$^{1}$H} NMR** (202.5 MHz, $CD_2Cl_2$, 295K): δ 23.5 ppm (br)

**$^{119}$Sn{$^{1}$H} NMR** (186.5 MHz, $CD_2Cl_2$, 295K): δ 25 ppm (br)

**Crystal Data:** See Table 8.9.9

### 8.5.4 $[Cy_3PMe_3Sn][AlCl_4]$

$Me_3SnCl$ (598 mg, 3 mmol) and $AlCl_3$ (400 mg, 3 mmol) in 7 mL of $CH_2Cl_2$ were stirred together for 10 mins resulting in dissolution of $AlCl_3$. $PCy_3$ (342 mg, 3 mmol), in 7 mL of $CH_2Cl_2$, was added dropwise to the $Me_3SnCl/AlCl_3$ mixture. After 1 hour the colorless clear reaction mixture was layered with $Et_2O$ and crystallized over 2 days at -25 °C to yield crystals suitable for X-Ray experiments. Crystals not submitted for X-Ray diffraction were washed with $Et_2O$ (2 x 5 mL), and dried in vacuo.

**Yield:** 612 mg (0.99 mmol, 33% crystalline material)

**M.p.** 222-224 °C

**E.A.** actual (calculated) C 41.20 % (41.14%), H 7.28% (6.91%)

**FT-IR**: (nujol mull, CsI plates, $cm^{-1}$, [relative intensities]): 2932[s], 2925[s], 2855[s], 1447[s], 1377[w], 1357[w], 1300[mw], 1269[w], 1199[w], 1177[w], 1113[w], 1004[w], 891[w], 850[w], 790[ms], 537[m], 494[s]

**FT-Raman** (capillary tube - 1mm, $cm^{-1}$, [relative intensities]): 2994[w], 2939[s], 2856[s], 1442[m], 1295[w], 1211[w], 1198[w], 1040[w], 1027[w], 847[w], 813[w], 699[w], 537[ms], 514[ms], 507[ms], 351[m], 216[m], 181[m]

**$^{1}$H NMR** (500.1 MHz, $CD_2Cl_2$, 295K): δ 2.41-2.35 ppm (3H, *m*); 1.98-1.96 ppm (12H, *m*); 1.85-1.83 ppm (3H, *m*); 1.56-1.29 ppm (15H, *m*); 0.82 ppm (9H, *s*, C$H_3$Sn) tin satellites observed (*d*, $^{2}J_{119Sn-H}$ = 56.2 Hz; *d*, $^{2}J_{117Sn-H}$ = 54.1 Hz)

**$^{13}$C NMR** (125.8 MHz, UDEFT, $CD_2Cl_2$, 295K): δ 31.88 ppm (*d*, $^{1}J_{C-P}$ = 19.3 Hz, *C*$H_2$P); 29.53 ppm (*s*, $CH_2$[*C*$H_2$C$H_2$]$_2$C$H_2$P); 26.72 ppm (*d*, $^{2}J_{C-P}$ = 11.6 Hz, [*C*$H_2$]$_2$C$H_2$P); 25.32 ppm (*s*, *C*$H_2$[C$H_2$C$H_2$]$_2$C$H_2$P); -4.12 ppm (*s*, *C*$H_3$Sn) tin satellites observed (*d*, $^{1}J_{119Sn-C}$ = 350 Hz; *d*, $^{1}J_{117Sn-C}$ = 337 Hz)

**$^{31}$P{$^{1}$H} NMR** (202.5 MHz, $CD_2Cl_2$, 295K): δ 14.1 ppm (br)

**$^{119}$Sn{$^{1}$H} NMR** (186.5 MHz, $CD_2Cl_2$, 295K): δ 22 ppm (br)

**Crystal Data:** See Table 8.9.9

### 8.5.5 $[tBu_3PMe_3Sn][AlCl_4]$

$Me_3SnCl$ (60 mg, 0.3 mmol) and $AlCl_3$ (40 mg, 0.3 mmol) in 5 mL of $CH_2Cl_2$ were stirred together for 20 mins resulting in dissolution of $AlCl_3$. $tBu_3P$ (60 mg, 0.3 mmol), in 3 mL of $CH_2Cl_2$, was added dropwise to the $Me_3SnCl/AlCl_3$ mixture. After 1 hour the colorless clear reaction mixture was layered with $Et_2O$ and crystallized over 2 days at -25 °C to yield crystals suitable for X-Ray experiments. Crystals not submitted for X-Ray diffraction were washed with $Et_2O$ (2 x 7 mL), and dried in vacuo.

**$^{31}P\{^1H\}$ NMR** (202.5 MHz, $CH_2Cl_2$, $C_6D_6$ capillary, 295K): δ 51.4 ppm (br) tin satellites observed to overlap for $^{119}Sn$ and $^{117}Sn$ (*d*, $^1J_{Sn-P}$ = 197 Hz)

**$^{119}Sn\{^1H\}$ NMR** (186.5 MHz, $CH_2Cl_2$, $C_6D_6$ capillary, 295K): δ 29 ppm (*d*, $^1J_{Sn-P}$ = 197 Hz)

**Crystal Data:** See Table 8.9.10

### 8.5.6 $[(dmpe)SnMe_3][AlCl_4]$

$Me_3SnCl$ (498 mg, 2.5 mmol) and $AlCl_3$ (333 mg, 2.5 mmol) in 20 mL of $CH_2Cl_2$ were stirred for 20 mins and then added to dropwise to dmpe (257.7 μL, 2.5 mmol), in 14 mL of $CH_2Cl_2$. $^{31}P\{^1H\}$ NMR spectrum of the reaction mixture established a *sextet* signal at -40 ppm along with a signal corresponding to the target compound at -37.1 ppm. Within 1 hour the reaction mixture was layered with ether and crystallized over 2 days at room temperature to yield crystals suitable for X-Ray experiments. Rhombohedral shape crystals corresponding to $[(dmpe)Me_3Sn][AlCl_4]$ and cube shape crystals corresponding to $[(dmpe)_2AlCl_2][AlCl_4]$ were isolated by decantation, washed with ether (3 x 15 mL)

and pentane (3 x 10 mL) then separated by crystal selection. Notably, the crystals were quite large with most of the rhombohedral shaped crystals averaged 0.5 cm with one of the larger crystals measuring around 4 cm in length making this process straight forward for obtaining a reasonable amount of material. Additionally by $^{31}P\{^{1}H\}$ NMR, the minor product $[(dmpe)_2AlCl_2][AlCl_4]$ contributed to 20% of the total phosphorus signal. $[(dmpe)_2AlCl_2][AlCl_4]$ can be synthesized independently if desired.

**Yield:** 600 mg (1.24 mmol, 50% crystalline)

**M.p.** 185-187 °C

**E.A.** actual (calculated): C 21.79% (22.39%), H 5.63% (5.22%)

**FT-IR**: (nujol mull, CsI plates, $cm^{-1}$, [relative intensities]): 2955[s], 2922[bs], 2853[s], 1462[ms], 1420[m], 1377[m], 1366[m], 1305[m], 1291[m], 1202[mw], 949[m], 932[mw], 908[mw], 767[w], 726[mw], 494[ms], 394[m]

**FT-Raman** (capillary tube - 1mm, $cm^{-1}$, [relative intensities]): 2989[m], 2910[s], 1412[mw], 1171[w], 684[mw], 518[m], 119[mw]

**$^{1}$H NMR** (500.1 MHz, $CD_3CN$, 295K): δ 1.78 ppm (4H, br, C*H*$_2$P); 1.33 ppm (12H, br, C*H*$_3$P); 0.66 ppm (9H, *s*, C*H*$_3$Sn) tin satellites observed (*d*, $^{2}J_{119Sn-H}$ = 63.6 Hz; *d*, $^{2}J_{117Sn-H}$ = 60.8 Hz)

**$^{13}$C NMR** (125.8 MHz, UDEFT, $CD_3CN$, 295K): δ 22.42 ppm (br, *C*H$_2$P); 10.24 ppm (br, *C*H$_3$P); -3.98 ppm (*s*, *C*H$_3$Sn), tin satellites observed (*d*, $^{1}J_{119Sn-C}$ = 409 Hz, $^{1}J_{117Sn-C}$ = 390 Hz)

**$^{31}P\{^{1}H\}$ NMR** (202.5 MHz, $CD_3CN$, 295K): δ -36.7 ppm (br)

**$^{119}Sn\{^{1}H\}$ NMR** (186.5 MHz, $CD_3CN$, 295K): δ 32 ppm (br)

**$^{31}P$ CP/MAS** (162.02 MHz, 9.0 KHz spinning, 295K): δ -38.4 ppm (*d*, $^{2}J_{P-P}$ = 158 Hz) tin satellites observed to overlap for $^{119}Sn$ and $^{117}Sn$ (*d*, $^{1}J_{P-Sn}$ = 950.3 Hz); -42.7 ppm (*d*, $^{2}J_{P-P}$ = 158 Hz) tin satellites observed to overlap for $^{119}Sn$ and $^{117}Sn$ (*d*, $^{1}J_{Sn-P}$ = 820.7 Hz)

**Crystal Data:** See Table 8.9.10

### 8.5.7 [(dmpm)$SnMe_3$][$AlCl_4$]

$Me_3SnCl$ (598 mg, 3 mmol) and $AlCl_3$ (400 mg, 6 mmol) in 7 mL of $CH_2Cl_2$ were stirred together for 10 mins. The $Me_3SnCl/AlCl_3$ mixture was added dropwise to dmpm (408 mg, 3 mmol), in 7 mL of $CH_2Cl_2$. Within 1 hour the reaction mixture was layered with $Et_2O$ and allowed to stand for 2 days at 25 °C to yield crystals for X-Ray experiments. Crystals not submitted for X-Ray diffraction were washed with $Et_2O$ (5 x 2 mL), and dried in vacuo.

**Yield:** 1.143 g (2.44 mmol, 81% crystalline)

**M.p.** 101-103 °C

**E.A.** actual (calculated): C 20.02% (20.50%), H 4.61% (4.95%)

**FT-IR**: (nujol mull, CsI plates, $cm^{-1}$, [relative intensities]): 2924[bs], 2854[s], 1458[ms], 1420[s], 1406[m], 1377[mw], 1359[mw], 1299[m], 1152[mw], 960[ms], 918[s], 889[mw], 843[mw], 782[s], 716[m], 710[m], 688[mw], 628[w], 540[m], 486[bs]

**FT-Raman** (capillary tube - 1mm, $cm^{-1}$, [relative intensities]): 2992[m], 2977[m], 2931[mw], 2908[s], 2887[m], 1424[vw], 1413[vw], 1212[w], 1196[w], 717[w], 710[w], 689[w], 629[w], 548[mw], 542[mw], 513[m], 348[w], 154[m]

**$^{1}$H NMR** (500.1 MHz, $CD_3CN$, 295K): δ 2.19-2.17 ppm (2H, *m*, virtual coupling "apparent triplet", C*H*$_2$P); 1.55 ppm (12H, *m*, virtual coupling [C*H*$_3$]$_2$P); 0.79 ppm (9H, *s*, C*H*$_3$Sn) tin satellites observed (*d*, $^{2}J_{119Sn-H}$ = 58.4 Hz; *d*, $^{2}J_{117Sn-H}$ = 56.3 Hz)

**$^{13}$C NMR** (125.8 MHz, UDEFT, $CD_3CN$, 295K): δ 25.41 ppm (*m*, virtual coupling, *C*H$_2$P); 12.45-12.33 ppm (*m*, virtual coupling "apparent triplet", [*C*H$_3$]$_2$P); -6.32 ppm (*s*, CH$_3$Sn) tin satellites observed (*d*, $^{1}J_{119Sn-C}$ = 358 Hz; *d*, $^{1}J_{117Sn-C}$ = 342 Hz)

**$^{31}$P{$^{1}$H} NMR** (202.5 MHz, $CD_3CN$, 295K): δ -39.1 ppm (br)

**$^{119}$Sn{$^{1}$H} NMR** (186.5 MHz, $CD_3CN$, 295K): δ -45.6 ppm (br)

**Crystal Data:** See Table 8.9.11

### 8.5.8 $[dmpe(SnMe_3)_2][OTf]_2$

$Me_3SnCl$ (996 mg, 5.0 mmol) and TMSOTf (1.111 g, 5.0 mmol) in 10 mL of $CH_2Cl_2$ were stirred together for 10 mins then added dropwise to dmpe (771 mg, 5.0 mmol), in 7 mL of $CH_2Cl_2$. After 1 hour the reaction had become saturated evident by the presence of a small amount of colorless precipitate. The colorless clear supernatant was decanted from the reaction mixture and allowed to stand for 14 days at 25 °C to yield crystals suitable for X-Ray experiments. Crystals not submitted for X-Ray diffraction were washed with ether (3 x 5 mL), and dried in vacuo. By multinuclear NMR spectroscopy,

the crystals and the powder have matching NMR resonances confirming that they correspond to the same complex. If bulk material of the salt is desired, adding hexane to the reaction mixture with some of the colorless precipitate will cause more material out of solution which can then be washed with 2 x 3 mL portions of hexane, then dried in vaccuo.

**Yield:** Synthesis was repeated in duplicate to obtain two yields; crystalline and bulk powder respectively. 1.56 g (2.0 mmol, 40% crystalline); 3.12 g (4.0 mmol, 80 % powder)

**M.p.** 148-150 °C

**E.A.** actual (calculated) of powder material C 21.32% (21.67%), H 4.39% (4.42%)

**FT-IR**: (nujol mull, CsI plates, $cm^{-1}$, [relative intensities]): 2957[s], 2924[bs], 2853[s], 1461[s], 1430[ms], 1377[ms], 1268[bs], 1167[s], 1152[s], 1034[s], 961[s], 918[ms], 846[m], 791[bs], 758[s], 636[bs], 573[m], 544[s], 516[s]

**FT-Raman** (capillary tube - 1mm, $cm^{-1}$, [relative intensities]): 2988[m], 2918[s], 1426[w], 1413[w], 1226[mw], 1205[mw] 1193[mw], 1032[m], 1026[m], 755[mw], 708[w], 660[w], 573[w], 543[m], 511[s], 348[w], 316[w], 158[bm],

**$^{1}$H NMR** (500.1 MHz, $CD_3CN$, 295K): δ 2.04 ppm (4H, br, C$H_2$P); 1.54 ppm (12H, br, [C$H_3$]$_2$P ); 0.68 ppm (18H, br, C$H_3$Sn) tin satellites observed to overlap for $^{119}$Sn and $^{117}$Sn (*d*, $^{2}J_{Sn-H}$ = 64 Hz)

**$^{13}$C NMR** (125.8 MHz, UDEFT, $CD_3CN$, 295K): δ 122.50 ppm (*q*, $^1J_{C\text{-}F}$ = 320 Hz, $O_3SCF_3$); 17.77 ppm (br, $CH_2P$); 6.68 ppm (br, $[CH_3]_2P$); 0.34 ppm (br, $CH_3Sn$)

**$^{19}$F{$^1$H} NMR** (470.6 MHz, CD3CN, 295K): δ -79.3 ppm (*s*)

**$^{31}$P{$^1$H} NMR** (202.5 MHz, $CD_3CN$, 295K): δ -30.3 ppm (br)

**$^{119}$Sn{$^1$H} NMR** (186.5 MHz, $CD_3CN$, 295K): δ 6.7 ppm (br)

**$^{31}$P CP/MAS** (162.02 MHz, 4 mm rotor, 11.0 KHz spinning, 295K): δ -29.6 ppm (*s*) tin satellites observed to overlap for $^{119}$Sn and $^{117}$Sn (*d*, $^1J_{P\text{-}Sn}$ = 571.8 Hz), -30.8 ppm (*s*) tin satellites observed to overlap for $^{119}$Sn and $^{117}$Sn (*d*, $^1J_{Sn\text{-}P}$ = 594.3 Hz)

**Crystal Data:** See Table 8.9.11

### 8.5.9 $[dmpm(SnMe_3)_2][AlCl_4]_2$

$Me_3SnCl$ (797 mg, 4 mmol) and $AlCl_3$ (533 mg, 4 mmol) in 5 mL of $CH_2Cl_2$ were stirred together for 10 mins. The $Me_3SnCl/AlCl_3$ mixture was added dropwise to a stirring solution of dmpm (272 mg, 2 mmol) in 5 mL of $CH_2Cl_2$. Within 1 hour, a large amount of colorless precipitate formed and hexane was added to the reaction mixture to precipitate any remaining product. X-Ray quality crystals can be grown by dissolving the colorless powder in $CH_3CN$ and allowing the solvent to slowly evaporate (evacuated 2 bulb apparatus). Crystals not submitted for X-Ray diffraction were washed with hexane (5 x 2 mL), and dried in vacuo.

**Yield:** 1.430 g (1.78 mmol, 89% crystalline)

**M.p.** 154-156°C

**E.A.** actual (calculated) crystalline material C 15.91% (16.49%), H 3.80% (4.03%)

**FT-IR**: (thin film, CsI plates, $cm^{-1}$, [relative intensities]): 2999[ms], 2965[ms], 2919[ms], 2902[ms], 2817[ms], 1428[ms], 1418[ms], 1368[mw], 1302[ms], 1207[w], 1194[w], 1145[mw], 1095[mw], 997[m], 956[ms], 918[ms], 898[m], 839[mw], 792[s], 758[m], 716[m], 702[m], 677[mw], 632[w], 538[s], 486[bs]

**FT-Raman** (capillary tube - 1mm, $cm^{-1}$, [relative intensities]): 3004[w], 2978[w], 2916[m], 2885[w], 1425[vw], 1399[vw], 1346[vw], 1206[w], 806[vw], 767[vw], 729[vw], 679[vw], 589[w], 548[m], 513[s], 428[vw], 348[w], 319[vw], 277[w], 177[mw], 151[m]

**$^{1}$H NMR** (500.1 MHz, $CD_3CN$, 295K): δ 2.11-2.08 ppm (2H, *m*, virtual coupling "apparent triplet", C*H*$_2$P); 1.44-1.43 ppm (12H, *m*, virtual coupling, [C*H*$_3$]$_2$P); 0.64 ppm (18H, *s*, C*H*$_3$Sn) tin satellites observed (*d*, $^{2}J_{119Sn-H}$ = 63.8 Hz; *d*, $^{2}J_{117Sn-H}$ = 61.1 Hz)

**$^{13}$C NMR** (125.8 MHz, UDEFT, $CD_3CN$, 295K): δ 25.59 ppm (*m*, virtual coupling, *C*H$_2$P); 12.52-12.41 ppm (*m*, virtual coupling, [*C*H$_3$]$_2$P); -2.20 ppm (*s*, $CH_3Sn$) tin satellites present (*d*, $^{1}J_{119Sn-C}$ = 404 Hz; *d*, $^{1}J_{117Sn-C}$ = 386 Hz)

**$^{31}$P{$^{1}$H} NMR** (202.5 MHz, $CD_3CN$, 295K): δ -40.8 ppm (br)

**$^{119}$Sn{$^{1}$H} NMR** (186.5 MHz, $CD_3CN$, 295K): δ 72 ppm (br)

**Crystal Data:** See Table 8.9.12

### 8.5.10 $[(dmpe)Bu_2Sn][AlCl_4]_2$

$Bu_2SnCl_2$ (760 mg, 2.5 mmol) and $AlCl_3$ (667 mg, 2.5 mmol) in 5 mL of $CH_2Cl_2$ were stirred together for 10 mins resulting in dissolution of $AlCl_3$. The $Bu_2SnCl_2/AlCl_3$ mixture was added dropwise to dmpe (385 mg, 2.5 mmol), in 7 mL of $CH_2Cl_2$. After 1 hour the reaction was saturated indicated by the presence of a small amount of colorless precipitate. The colorless clear supernatant was decanted from the reaction mixture and allowed to stand for 14 days at 25 °C to yield crystals suitable for X-Ray experiments. Crystals not submitted for X-Ray diffraction were washed with ether (2 x 5 mL), and dried in vacuo.

**Yield:** 1.487 g (2.06 mmol, 83% crystalline)

**M.p.** 168-170 °C

**E.A.** actual (calculated) crystalline material C 22.88% (23.33%), H 4.64% (4.76%)

**FT-IR**: (nujol mull, CsI plates, $cm^{-1}$, [relative intensities]): 2946[bs], 2850[bs], 1463[s], 1411[mw], 1377[ms], 1310[w], 1294[m], 1150[m], 953[ms], 939[ms], 905[w], 872[w], 846[w], 727[mw], 675[mw], 510[s], 490[s], 468[s]

**FT-Raman** (capillary tube - 1mm, $cm^{-1}$, [relative intensities]): 2984[mw], 2934[mw], 2911[s], 2872[mw], 1418[w], 1150[w], 725[w], 647[w], 601[w], 580[w], 504[w], 348[w], 241[mw], 169[mw], 119[mw]

**$^1H\{^{31}P\}$ NMR** (500.1 MHz, $CD_3CN$, 295K): δ 2.27 ppm (4H, *s*, $PCH_2$); 1.89-1.86 ppm (4H, *m*, $SnCH_2CH_2$); 1.81-1.75 ppm (4H, *m*, $SnCH_2CH_2$); 1.66 ppm (12H, *s*, $P[CH_3]_2$);

1.44 ppm (4H, *sextet*, $^{3}J_{H\text{-}H}$ = 7.35 Hz, $SnCH_2CH_2C\mathit{H}_2CH_3$); 0.97 ppm (6H, *t*, $^{3}J_{H\text{-}H}$ = 7.35 Hz, $SnCH_2CH_2CH_2C\mathit{H}_3$)

**$^{13}$C NMR** (125.8 MHz, UDEFT, $CD_3CN$, 295K): δ 28.88 ppm (*s*, $SnCH_2CH_2\mathit{C}H_2CH_3$) tin satellites observed to overlap for $^{119}$Sn and $^{117}$Sn (*d*, $^{2}J_{Sn\text{-}C}$ = 33.5 Hz); 27.09 ppm (*s*, $SnCH_2\mathit{C}H_2CH_2CH_3$) tin satellites observed to overlap for $^{119}$Sn and $^{117}$Sn (*d*, $^{1}J_{Sn\text{-}C}$ = 106 Hz); 24.90 ppm (br, $Sn\mathit{C}H_2CH_2CH_2CH_3$); 21.74-21.53 ppm (*m*, virtual coupling "apparent 1:1:1 triplet" $P\mathit{C}H_2$); 13.76 ppm (s, $SnCH_2CH_2CH_2\mathit{C}H_3$); 8.68-8.49 ppm (*m*, virtual coupling "apparent triplet" $P[\mathit{C}H_3]_2$)

**$^{31}$P{$^{1}$H} NMR** (202.5 MHz, $CD_3CN$, 295K): δ -27.7 ppm (br)

**$^{119}$Sn{$^{1}$H} NMR** (186.5 MHz, $CD_3CN$, 295K): δ -230 ppm (br)

**$^{31}$P CP/MAS** (162.02 MHz, 4 mm rotor, 11.0 KHz spinning, 295K): δ -8.9 ppm (*d*, $^{2}J_{P\text{-}P}$ = 65.1 Hz) tin satellites observed to overlap for $^{119}$Sn and $^{117}$Sn (*d*, $^{1}J_{P\text{-}Sn}$ = 607.5 Hz); -9.8 ppm (*d*, $^{2}J_{P\text{-}P}$ = 65.1 Hz) tin satellites observed to overlap for $^{119}$Sn and $^{117}$Sn (*d*, $^{1}J_{Sn\text{-}P}$ = 603.7 Hz)

**Crystal Data:** See Table 8.9.12

### 8.5.11 $[(dmpe)Bu_2Sn][OTf]_2$

$Bu_2SnCl_2$ (911 mg, 3 mmol) and TMSOTf (1.333 g, 6 mmol) in 5 mL of $CH_2Cl_2$ were stirred together for 10 mins. The $Bu_2SnCl_2$/TMSOTf mixture was added dropwise to dmpe (462 mg, 3 mmol), in 7 mL of $CH_2Cl_2$. After 1 hour the reaction was complete and the reaction mixture had become saturated as indicated by the presence of a colorless

precipitate. The colorless clear supernatant was decanted from the reaction mixture and allowed to stand for 14 days at 25 °C to yield crystals for X-Ray experiments. Crystals not submitted for X-Ray diffraction were washed with $Et_2O$ (2 x 5 mL), and dried in vacuo.

**Yield:** 1.644 g (2.4 mmol, 80% powder)

**M.p.** 120-122 °C

**E.A.** actual (calculated) C 27.65% (28.21%), H 5.54% (5.03%)

**FT-IR**: (nujol mull, CsI plates, $cm^{-1}$, [relative intensities]): 2955[s], 2923[s], 2869[s], 2853[s], 1463[s], 1422[s], 1377[s], 1235[s], 1221[s], 1023[s], 957[ms], 944[ms], 912[m], 886[m], 879[w], 767[w], 758[w], 726[w], 688[m], 635[s], 573[m], 516[s]

**FT-Raman** (capillary tube - 1mm, $cm^{-1}$, [relative intensities]): 2985[bm], 2941[ms], 2915[s], 2876[bw], 1448[w], 1424[w], 1162[w], 1027[ms], 757[m], 724[w], 649[w], 590[w], 573[w], 348[w], 315[w], 246[w], 175[bm]

**$^{1}H\{^{31}P\}$ NMR** (500.1 MHz, $CD_3CN$, 295K): δ 2.45 ppm (4H, *s*, $PCH_2$); 1.98-1.92 ppm (8H, *m*, $SnCH_2CH_2$); 1.83 ppm (12H, *s*, $P[CH_3]_2$); 1.44 ppm (4H, *sextet*, $^{3}J_{H-H}$ = 7.35 Hz, $SnCH_2CH_2CH_2CH_3$); 0.98 ppm (6H, *t*, $^{3}J_{H-H}$ = 7.35 Hz, $SnCH_2CH_2CH_2CH_3$)

**$^{13}C$ NMR** (125.8 MHz, UDEFT, $CD_3CN$, 295K): δ 121.75 ppm (*q*, $^{1}J_{C-F}$ = 320 Hz, $O_3SCF_3$); 28.78 ppm (*s*, $SnCH_2CH_2CH_2CH_3$) tin satellites observed to overlap for $^{119}Sn$ and $^{117}Sn$ (*d*, $^{2}J_{SnC}$ = 33.5 Hz); 27.40 ppm (*s*, $SnCH_2CH_2CH_2CH_3$) tin satellites observed to overlap for $^{119}Sn$ and $^{117}Sn$ (*d*, $^{1}J_{Sn-C}$ = 120 Hz); 22.61-22.48 ppm (*m*, virtual coupling

"apparent triplet", $SnCH_2CH_2CH_2CH_3$); 21.75-21.50 ppm (*m*, virtual coupling "apparent triplet", $PCH_2$); 13.60 ppm (s, $SnCH_2CH_2CH_2CH_3$); 7.93 ppm (*m*, virtual coupling "apparent triplet", $P[CH_3]_2$)

**$^{19}F\{^1H\}$ NMR** (470.6 MHz, $CD_3CN$, 295K): δ -78.2 ppm (*s*)

**$^{31}P\{^1H\}$ NMR** (202.5 MHz, $CD_3CN$, 295K): δ -15.2 ppm (*s*), tin satellites observed (*d*, $^1J_{119Sn-P}$ =452 Hz, $^1J_{117Sn-P}$ = 432 Hz)

**$^{119}Sn\{^1H\}$ NMR** (186.5 MHz, $CD_3CN$, 295K): δ -197 ppm (*t*, $^1J_{P-Sn}$ = 452 Hz)

**Crystal Data:** See Table 8.9.13

### 8.5.12 $[(dmpm)Bu_2Sn][AlCl_4]_2$

$Bu_2SnCl_2$ (91 mg, 3 mmol) and $AlCl_3$ (400 mg, 6 mmol) in 7 mL of $CH_2Cl_2$ were stirred together for 10 mins. The $Bu_2SnCl_2/AlCl_3$ mixture was added dropwise to dmpm (408 mg, 3 mmol) in 7 mL of $CH_2Cl_2$. Within 1 hour the reaction mixture was layered with $Et_2O$ and allowed to stand for 2 days at 25 °C to yield crystals for X-Ray experiments. Crystals not submitted for X-Ray diffraction were washed with $Et_2O$ (5 x 2 mL), and dried in vacuo.

**Yield:** 1.882 g (2.66 mmol, 89% crystalline)

**M.p.** 145-146 °C

**E.A.** actual (calculated) C 21.57% (22.10%), H 4.76% (4.56%)

**FT-IR**: (nujol mull, CsI plates, $cm^{-1}$, [relative intensities]): 2955[s], 2923[bs], 2853[s], 1462[ms], 1410[w], 1377[m], 1300[w], 1154[w], 991[mw], 955[w], 897[w], 721[w], 679[w], 489[bm]

**FT-Raman** (capillary tube - 1mm, $cm^{-1}$, [relative intensities]): 2987[m], 2958[mw], 2909[s], 2865[mw], 1495[vw], 1445[vw], 1414[vw], 1401[vw], 1332[vw], 1157[w], 1045[vw], 887[vw], 855[vw], 761[vw], 736[vw], 654[vw], 610[vw], 583[m], 361[mw], 349[mw]

**$^{1}$H NMR** (500.1 MHz, $CD_3CN$, 295K): δ 2.27-2.24 ppm (2H, *m*, "apparent doublet of triplets", PC*H*$_2$P); 1.91-1.88 ppm (4H, *m*, virtual coupling "apparent 1:1:1 triplet", Sn$C$*H*$_2$CH$_2$CH$_2$CH$_3$); 1.77 ppm (4H, *pentet*, SnCH$_2$C*H*$_2$CH$_2$CH$_3$, $^{3}J_{H\text{-}H}$ = 7.33 Hz); 1.54 ppm (12H, *m*, virtual coupling, P[C*H*$_3$]$_2$) ; 1.43 ppm (4H, *sextet*, SnCH$_2$CH$_2$C*H*$_2$CH$_3$, $^{3}J_{H\text{-}H}$ = 7.33 Hz); 0.96 ppm (4H, *t*, SnCH$_2$CH$_2$CH$_2$C*H*$_3$, $^{3}J_{H\text{-}H}$ = 7.33 Hz)

**$^{13}$C NMR** (125.8 MHz, UDEFT, $CD_3CN$, 295K): δ 28.36 ppm (*s*, SnCH$_2$CH$_2$*C*H$_2$CH$_3$), tin satellites observed to overlap for $^{119}$Sn and $^{117}$Sn (*d*, $^{3}J_{SnC}$ = 33.4 Hz); 27.53 ppm (br, Sn*C*H$_2$CH$_2$CH$_2$CH$_3$); 26.93 ppm (*s*, SnCH$_2$*C*H$_2$CH$_2$CH$_3$), tin satellites observed to overlap for $^{119}$Sn and $^{117}$Sn (*d*, $^{2}J_{Sn\text{-}C}$ = 99.2 Hz); 25.50 ppm (*m*, virtual coupling, P*C*H$_2$P); 13.76 ppm (*s*, SnCH$_2$CH$_2$CH$_2$*C*H$_3$); 12.77 ppm (*m*, virtual coupling, P[*C*H$_3$]$_2$)

**$^{31}$P{$^{1}$H} NMR** (202.5 MHz, $CD_3CN$, 295K): δ -29.4 ppm (br)

**$^{119}$Sn{$^{1}$H} NMR** (186.5 MHz, $CD_3CN$, 295K): δ -63 ppm (br)

**Crystal Data:** See Table 8.9.14

### 8.5.13 $[(dmpm)Me_2Sn][OTf]_2$

$Me_2SnCl_2$ (220 mg, 1.0 mmol) and TMSOTf (222 mg, 1.0 mmol) in $CH_2Cl_2$ (5 mL) were stirred together for 10 mins producing a colorless, clear reaction mixture. A $CH_2Cl_2$ (5 mL) solution of dmpm (68 mg, 0.5 mmol) was added dropwise to the $Me_2SnCl_2$/TMSOTf mixture which gradually producing colorless precipitate with a clear colorless supernatant. After 1 hour hexane was added to the mixture, decanted off where the remaining colorless solid was washed with 2 x 3 mL hexane and dried in vacuo. To obtain crystals of the product, the material was dissolved in $CH_3CN$ which was left at room temperature to slowly evaporate for 6 days to produce X-ray diffraction quality crystals.

**Yield:** 390 mg ( 0.65 mmol, 65% crystalline material)

**M.p.** 155-157°C

**$^{1}$H NMR** (500.1 MHz, $CD_2Cl_2$, 295K): δ 2.66-2.63 ppm (*m*, virtual coupling, "apparent triplet", PC*H*$_2$P); 1.76-1.74 ppm (*m*, virtual coupling, "apparent triplet", P[C*H*$_3$]$_2$); 1.33 ppm (*s*) tin satellites observed to overlap for $^{119}$Sn and $^{117}$Sn (*d*, $^{2}J_{Sn-H}$ = 80.5 Hz)

**$^{13}$C NMR** (125.8 MHz, UDEFT, $CD_2Cl_2$, 295K): δ 119.78 ppm (*q*, $^{1}J_{C-F}$ = 319 Hz, $O_3SCF_3$); 23.12-22.93 ppm (*m*, virtual coupling, "apparent triplet", P*C*H$_2$P); 10.72-10.52 ppm (*m*, virtual coupling, "apparent triplet", P[*C*H$_3$]$_2$); 5.31 ppm (br, Sn[*C*H$_3$]$_2$)

**$^{19}$F{$^{1}$H} NMR** (470.6 MHz, $CD_2Cl_2$, 295K): δ -78.8 ppm (*s*)

**$^{31}$P{$^{1}$H} NMR** (202.5 MHz, $CD_2Cl_2$, 295K): δ -30.2 ppm (br)

**$^{119}$Sn{$^{1}$H} NMR** (186.5 MHz, $CD_2Cl_2$, 295K): δ -70 ppm (br)

**Crystal Data:** See Table 8.9.14

## 8.6 Preparation and Characterization of Compounds in Chapter 6

### 8.6.1 dmpe($SnMe_2Cl_2$)$_2$

Dmpe (77 mg, 0.5 mmol) in $CH_2Cl_2$ (5 mL) was added dropwise to a stirring solution of $Me_2SnCl_2$ (220 mg, 1.0 mmol) in $CH_2Cl_2$ (5 mL) producing a small amount of colorless precipitate with an otherwise colorless clear reaction supernatant. After 1 hour hexane was added to the mixture producing more colorless precipitate, solvent was decanted where the remaining colorless solid was washed with 2 x 3 mL hexane and dried in vacuo. To obtain crystals of the product the material was dissolved in $CH_3CN$ which was left at room temperature to slowly evaporate for 6 days to produce X-Ray diffraction quality crystals.

**Yield:** 261 mg (0.44 mmol, 88% crystalline material)

**M.p.** 201-203 °C

**FT-IR**: (nujol mull, CsI plates, cm$^{-1}$, [relative intensities]): 2950[s], 2920[s], 2852[s], 1465[s], 1412[ms], 1406[ms], 1377[ms], 1312[w], 1299[m], 1260[vw], 1203[w], 1151[w], 1111[w], 960[ms], 937[ms], 925[mw], 909[mw], 873[mw], 853[w], 802[m], 789[ms], 767[ms], 724[m], 517[s], 501[s], 494[s], 456[s]

**FT-Raman** (capillary tube - 1mm, cm$^{-1}$, [relative intensities]): 2995[m], 2981[m], 2945[m], 2927[m], 2910[s], 1413[w], 1409[w], 1204[w], 762[w], 725[w], 644[w],

558[w], 519[s], 350[s], 322[w], 302[w], 252[ms], 185[s], 177[s], 157[w], 135[w], 131[mw]

**$^{1}$H NMR** (500.1 MHz, $CD_2Cl_2$, 295K): δ 2.34-2.33 ppm (4H, *m*, virtual coupling, P[C$H_2$]$_2$); 1.70-1.69 ppm (12H, *m*, virtual coupling "apparent triplet", P[C$H_3$]$_2$); 1.19 ppm (6H, *s*, $Cl_2$Sn[C$H_3$]$_2$), tin satellites are observed (*d*, $^{2}J_{119Sn-H}$ = 80.5 Hz; *d*, $^{2}J_{117Sn-H}$ = 77.2 Hz)

**$^{13}$C NMR** (125.8 MHz, UDEFT, $CD_2Cl_2$, 295K): δ 21.32-21.09 ppm (*m*, virtual coupling "apparent triplet", P[$C$H$_2$]$_2$); 7.83-7.61 ppm (*m*, virtual coupling "apparent triplet", P[$C$H$_3$]$_2$), $Me_2SnCl_2$ signal could not be located

**$^{31}$P{$^{1}$H} NMR** (202.5 MHz, $CD_2Cl_2$, 295K): δ -24.5 ppm (br)

**$^{119}$Sn{$^{1}$H} NMR** (186.5 MHz, $CD_2Cl_2$, 295K): δ -208 ppm (br)

**Crystal Data:** See Table 8.9.15

### 8.6.2 $[Me_3PMe_2SnCl][AlCl_4]$

$Me_2SnCl_2$ (110 mg, 0.5 mmol) and $AlCl_3$ (67 mg, 0.5 mmol) in $CH_2Cl_2$ (5 mL) were stirred together for 20 mins resulting in dissolution of $AlCl_3$ and causing the previously colorless, cloudy reaction mixture to be pale yellow and clear. Monitoring the reaction progress by $^{119}$Sn{$^{1}$H} NMR revealed a new signal at 56.7 ppm. $Me_3P$ (38 mg, 0.5 mmol) in $CH_2Cl_2$ (5 mL) was added dropwise to the mixture producing a colorless, clear reaction mixture. After 1 hour the reaction mixture was layered with hexane and left

standing at -25℃ to produce X-Ray quality crystals over the course of 2 days. The resulting crystals were washed with 2 x 3 mL hexane and dried in vacuo.

**Yield:** 115 mg (0.27 mmol, 53% crystalline material)

**M.p.** 96-98°C

**$^{1}$H NMR** (500.1 MHz, $CD_2Cl_2$, 295K): δ 2.51 ppm (*d*, $^{2}J_{P\text{-}H}$ = 12 Hz, PC*H*$_3$); 1.91 ppm (*s*, Sn[C*H*$_3$]$_2$) tin satellites observed (*d*, $^{2}J_{119Sn\text{-}H}$ = 78.7 Hz; *d*, $^{2}J_{117Sn\text{-}H}$ = 76.6 Hz )

**$^{13}$C NMR** (125.8 MHz, UDEFT, $CD_2Cl_2$, 295K): δ 9.62 ppm (*d*, $^{1}J_{P\text{-}C}$ = 32.4 Hz, P*C*H$_3$); 7.16 ppm (*s*, Sn[*C*H$_3$]$_2$) no tin satellites observed

**$^{31}$P{$^{1}$H} NMR** (202.5 MHz, $CD_2Cl_2$, 295K): δ -15.0 ppm (br)

**$^{119}$Sn{$^{1}$H} NMR** (186.5 MHz, $CD_2Cl_2$, 295K): δ -49 ppm (br)

**Crystal Data:** See Table 8.9.15

### 8.6.3 [(dmpe)$Bu_2SnCl$][$AlCl_4$]

$Bu_2SnCl_2$ (760 mg, 2.5 mmol) and $AlCl_3$ (333 mg, 2.5 mmol) in 5 mL of $CH_2Cl_2$ were stirred together for 10 mins resulting in dissolution of $AlCl_3$ and producing a yellow clear solution. A $CH_2Cl_2$ (7 mL) solution of dmpe (385 mg, 2.5 mmol), was added to the $Bu_2SnCl_2$/$AlCl_3$ mixture which produced a colorless, clear reaction mixture. After 1 hour the reaction was complete as indicated by the presence of a colorless precipitate. The colorless clear supernatant was decanted from the reaction mixture and allowed to stand for 14 days at 25 °C to yield crystals suitable for X-Ray experiments. Crystals not submitted for X-Ray diffraction were washed with ether (2 x 5 mL), and dried in vacuo.

**Yield:** 1.058 g (1.80 mmol, 72% crystalline material)

**M.p.** 239-241 °C

**E.A.** actual (calculated) C 28.65% (28.63%), H 5.75% (5.83%)

**FT-IR**: (nujol mull, CsI plates, $cm^{-1}$, [relative intensities]): 2956[s], 2924[bs], 2870[s], 2854[s], 1463[s], 1418[ms], 1377[ms], 1290[m], 1144[m], 953[s], 936[s], 922[mw], 904[mw], 872[mw], 736[m], 712[m], 510[s], 491[s], 485[s]

**FT-Raman** (capillary tube - 1mm, $cm^{-1}$, [relative intensities]): 2985[m], 2956[w], 2947[w], 2935[m] 2912[s], 2872[w], 2857[w], 1420[vw], 1408[vw], 648[vw], 602[vw], 505[vw], 348[vw], 345[vw], 242[vw], 182[vw]

**$^{1}$H{$^{31}$P} NMR** (500.1 MHz, $CD_2Cl_2$, 295K): δ 2.33 ppm (4H, *s*, PC*H*$_2$); 1.94-1.91 ppm (4H, *m*, SnC*H*$_2$CH$_2$); 1.84-1.77 ppm (4H, *m*, SnCH$_2$C*H*$_2$); 1.72 ppm (12H, *s*, P[C*H*$_3$]$_2$); 1.46 ppm (4H, *sextet*, $^{3}J_{H\text{-}H}$ = 7.35 Hz, SnCH$_2$CH$_2$C*H*$_2$CH$_3$); 0.99 ppm (6H, *t*, $^{3}J_{H\text{-}H}$ = 7.35 Hz, SnCH$_2$CH$_2$CH$_2$C*H*$_3$)

**$^{13}$C NMR** (125.8 MHz, UDEFT, $CD_2Cl_2$, 295K): δ 28.19 ppm (br, SnCH$_2$CH$_2$*C*H$_2$CH$_3$) tin satellites observed to overlap for $^{119}$Sn and $^{117}$Sn (*d*, $^{2}J_{Sn\text{-}C}$ = 34.4 Hz); 26.41 ppm (br, SnCH$_2$*C*H$_2$CH$_2$CH$_3$) tin satellites observed to overlap for $^{119}$Sn and $^{117}$Sn (*d*, $^{1}J_{Sn\text{-}C}$ = 101 Hz); 25.18 ppm (br, Sn*C*H$_2$CH$_2$*C*H$_2$CH$_3$); 22.04-21.85 ppm (*m*, virtual coupling "apparent 1:1:1 triplet", P*C*H$_2$); 13.32 ppm (*s*, SnCH$_2$CH$_2$CH$_2$*C*H$_3$); 9.03-8.86 ppm (*m*, virtual coupling "apparent triplet", P[*C*H$_3$]$_2$)

**$^{31}$P{$^{1}$H} NMR** (202.5 MHz, $CD_2Cl_2$, 295K): δ -31.3 ppm (br)

**$^{119}$Sn{$^{1}$H} NMR** (186.5 MHz, $CD_2Cl_2$, 295K): δ -216 ppm (br)

**$^{31}$P CP/MAS** (162.02 MHz, 4 mm rotor, 11.0 KHz spinning, 295K): δ -29.6 ppm (*s*) tin satellites present but not distinguishable (*d*, $^{1}J_{P\text{-}Sn}$ = 571.8 Hz); -30.8 ppm (*s*) tin satellites present but not distinguishable (*d*, $^{1}J_{Sn\text{-}P}$ = 594.3 Hz)

**Crystal Data:** See **Table 8.9.16**

### 8.6.4 [(dmpm)$Me_2SnCl$][$AlCl_4$]

$Me_2SnCl_2$ (110 mg, 0.5 mmol) and $AlCl_3$ (67 mg, 0.5 mmol) in $CH_2Cl_2$ (5 mL) were stirred together for 20 mins resulting in dissolution of $AlCl_3$ and causing the previously colorless, cloudy reaction mixture to be pale yellow and clear. Monitoring the reaction progress by $^{119}$Sn{$^{1}$H} NMR revealed a new signal at 56.7 ppm. A $CH_2Cl_2$ (5 mL) solution of dmpm (68 mg, 0.5 mmol) was added dropwise to the mixture producing colorless precipitate with a clear, colorless supernatant. After 1 hour hexane was added to the mixture, decanted, and the remaining colorless solid was washed with 2 x 3 mL hexane and dried in vacuo. To obtain crystals of the product the material was dissolved in $CH_3CN$ which was left at room temperature to slowly evaporate for 6 days to produce X-Ray diffraction quality crystals.

**Yield:** 278 mg (0.44 mmol, 89% crystalline material)

**M.p.** 221-222 °C

**FT-IR**: (nujol mull, CsI plates, $cm^{-1}$, [relative intensities]): 2923[s], 2852[s], 1461[ms], 1377[m], 1241[s], 1160[s], 1027[s], 965[m], 946[m], 913[mw], 878[mw], 856[mw], 810[m], 768[w], 726[w], 637[s], 757[m], 517[s]

**FT-Raman** (capillary tube - 1mm, $cm^{-1}$, [relative intensities]): 2985[m], 2963[mw], 2911[s], 1413[w], 1202[w], 1195[w], 761[w], 740[w], 701[w], 740[w], 701[w], 655[w], 558[w], 552[w], 523[m], 515[m], 470[vw], 361[m], 350[m], 259[mw], 232[m]

**$^{1}$H NMR** (500.1 MHz, $CD_2Cl_2$, 295K): δ 2.29-2.27 ppm (2H, *m*, virtual coupling "apparent triplet", PC$H_2$); 1.57-1.52 ppm (12H, *m*, virtual coupling, P[C$H_3$]$_2$); 1.22 ppm (6H, *s*), tin satellites observed (*d*, $^{2}J_{119Sn-H}$ = 79.6 Hz; *d*, $^{2}J_{117Sn-H}$ = 76.1 Hz)

**$^{13}$C NMR** (125.8 MHz, UDEFT, $CD_2Cl_2$, 295K): δ 25.09-24.85 ppm (*m*, virtual coupling, P*C*H$_2$); 12.49-12.36 ppm (*m*, virtual coupling, P[*C*H$_3$]$_2$); 8.04 ppm (*s*, Sn[*C*H$_3$]$_2$), tin satellites observed (*d*, $^{1}J_{119Sn-C}$ = 559 Hz; *d*, $^{1}J_{117Sn-C}$ = 533 Hz)

**$^{31}$P{$^{1}$H} NMR** (202.5 MHz, $CD_2Cl_2$, 295K): δ -30.4 ppm (br)

**$^{119}$Sn{$^{1}$H} NMR** (186.5 MHz, $CD_2Cl_2$, 295K): δ -42 ppm (br)

**Crystal Data:** See Table 8.9.16

## 8.7 Preparation and Characterization of Compounds in Chapter 7

The compounds described below are incompletely characterized. The future work section looks at some compounds isolated serendipitously or were interesting but not pursued in much detail.

### 8.7.1 dmpe($iPr_3SnOTf)_2$

$iPr_3SnCl$ (283 mg, 1.0 mmol) and TMSOTf (222 mg, 1.0 mmol) in $CH_2Cl_2$ (5 mL) were stirred together for 20 mins resulting in a colorless, clear reaction mixture. dmpe (77 mg, 0.5 mmol) in $CH_2Cl_2$ (5 mL) was added dropwise to the mixture gradually producing a colorless precipitate with a clear colorless supernatant. After 1 hour hexane was added to the mixture, decanted, and the remaining colorless solid was washed with 2 x 3 mL hexane and dried in vacuo. To obtain crystals of the product, the material was dissolved in $CH_3CN$ which was left at room temperature to slowly evaporate for 6 days to produce X-Ray diffraction quality crystals.

**Yield:** 219 mg (0.23 mmol, 46% crystalline material)

**M.p.** 169-171 °C

**FT-IR**: (nujol mull, CsI plates, $cm^{-1}$, [relative intensities]): 2962[s], 2921[s], 2915[s], 2853[ss], 1577[vw], 1539[w], 1464[ms], 1410[ms], 1377[ms], 1365[m], 1343[w], 1305[w], 1293[m], 1203[mw], 1131[mw], 955[ms], 943[ms], 899[m], 819[m], 795[m], 767[m], 756[m], 503[s], 489[s]

**FT-Raman** (capillary tube - 1mm, $cm^{-1}$, [relative intensities]): 2995[m], 2964[mw], 2922[s], 1424[w], 1278[w], 1237[w], 1229[w], 1205[w], 1198[w], 1173[w], 1032[s], 1026[m], 761[m], 757[m], 727[mw], 649[m], 574[w], 562[m], 524[s], 348[m], 314[vw], 248[mw]

**Crystal Data:** See Table 8.9.17

### 8.7.2 $[SnCl_4][CoCp_2]$

$SnCl_4$ (130 mg, 0.5 mmol) and $CoCp_2$ (94 mg, 0.5 mmol) in $CH_2Cl_2$ (5 mL) were stirred together for 1 hour resulting in the dark purple, clear solution to becoming an opaque dark green solution. After 2 hours, the reaction mixture was filtered through a pipette and the remaining dark green, clear solution was layered with hexane and stored at -25°C to produce X-Ray quality crystals over the course of 2 days.

**Crystal Data:** See Table 8.9.17

### 8.7.3 $Me_3P(Me_3SnCl)_2$

$Me_3P$ (23 mg, 0.3 mmol) and $Me_3SnCl$ (40 mg, 0.3 mmol) in hexane (5 mL) were stirred together resulting in dissolution of $AlCl_3$ within 10 mins and causing the previously colorless cloudy reaction mixture to become clear. This was left stirring for 1 hour to ensure the completion of the reaction. X-Ray quality crystals were grown by cooling the reaction mixture to -22℃ for 2 days. Solvent was decanted and the crystals were then washed with 2 x 3 mL of hexane and dried in vacuo. Note: the reaction was intentionally done in a 1:1 ratio albeit the molecular structure reveals the compound to crystallize in a 1:2 ratio.

**$^{31}P\{^1H\}$ NMR** (202.5 MHz, $CH_2Cl_2$, $C_6D_6$ capillary, 295K): δ 28.5 ppm (*s*) tin satellites observed to overlap for $^{119}Sn$ and $^{117}Sn$ (*d*, $^1J_{Sn-P}$ = 64 Hz)

**$^{119}Sn\{^1H\}$ NMR** (186.5 MHz, $CH_2Cl_2$, $C_6D_6$ capillary, 295K): δ 17 ppm (*d*, $^1J_{Sn-P}$ = 64Hz)

**Crystal Data:** See Table 8.9.18

### 8.7.4 $[Et_3AsMe_3Sn][AlCl_4]$

$Me_3SnCl$ (598 mg, 3 mmol) and $AlCl_3$ (400 mg, 3 mmol) in $CH_2Cl_2$ (7 mL) were stirred together for 20 mins resulting in dissolution of $AlCl_3$. $AsEt_3$ (544 mg, 3 mmol) in $CH_2Cl_2$ (7 mL) was added dropwise to the mixture. After 1 hour the colorless clear reaction mixture was layered with hexane and over 2 days at -20 °C yielded a crystalline solid which was washed with ether (3 x 10 mL) then dried in vacuo. This material was not crystalline enough for single crystal X-Ray diffraction experiments.

**Yield:** 873 mg (1.76 mmol, 58% crystalline material)

**M.p.** 262-264 °C

**E.A.** actual (calculated) C 21.49 (21.85%), H 4.93 (4.89%)

**FT-IR**: (nujol mull, CsI plates, $cm^{-1}$, [relative intensities]): 2950[s], 2927[s], 2853[s], 1458[s], 1417[mw], 1377[m], 1239[mw], 1209[w], 1036[m], 974[w], 790[s], 746[ms], 592[w], 542[ms], 497[s]

**FT-Raman** (capillary tube - 1mm, $cm^{-1}$, [relative intensities]): 2970[s], 2926[s], 2878[ms], 1461[vw], 1210[vw], 1198[vw], 592[vw], 543[m], 510[s], 349[w]

**$^1$H NMR** (500.1 MHz, $CD_2Cl_2$, 295K): δ 2.26 ppm (6H, *q*, $^3J_{H\text{-}H}$ = 7.7 Hz, $CH_3CH_2As$); 1.35ppm (9H, *t*, $^3J_{H\text{-}H}$ = 7.7 Hz, $CH_3CH_2As$); 0.90 ppm (9H, s, $CH_3Sn$) tin satellites observed (*d*, $^2J_{119Sn\text{-}H}$ = 57.9 Hz; *d*, $^2J_{117Sn\text{-}H}$ = 55.6 Hz)

**$^{13}$C NMR** (125.8 MHz, UDEFT, $CD_2Cl_2$, 295K): δ 14.3 ppm (*s*, $CH_3CH_2As$); 9.3 ppm (*s*, $CH_3CH_3As$); -4.8 ppm (*s*, $CH_3Sn$) tin satellites present (*d*, $^1J_{119Sn-C}$ = 354 Hz; *d*, $^1J_{117Sn-C}$ = 338 Hz)

**$^{119}$Sn{$^1$H} NMR** (186.5 MHz, $CD_2Cl_2$, 295K): δ 60 ppm (*s*)

### 8.7.5 $[(Me_3P)_2Ge][OTf]_2$

$GeCl_2$[1,4-dioxane] (204 mg, 0.3 mmol) and $Me_3P$ (46 mg, 0.6 mmol) in 5 mL of $CH_2Cl_2$ were stirred for 15 mins resulting in the dissolution of the $GeCl_2$[1,4-dioxane] producing a colorless clear reaction mixture with a $^{31}P\{^1H\}$ resonance at -36.6 ppm. TMSOTf (133 mg, 0.6 mmol), in 5 mL of $CH_2Cl_2$, was added dropwise to the $GeCl_2$/$Me_3P$ mixture. After 1 hour the colorless, clear reaction mixture was layered with hexane and crystallized over 2 days at -25 °C to yield crystals suitable for X-Ray experiments. Crystals not submitted for X-Ray diffraction were washed with hexane (2 x 3 mL), and dried in vacuo.

**$^{31}$P{$^1$H} NMR** (202.5 MHz, $CD_3CN$, 295K): δ -13.1 ppm (br) (*unconfirmed*) or -14.5 ppm (br) (*unconfirmed*)

**Crystal Data:** See Table 8.9.18

### 8.7.6 [(dmpe)GeCl][OTf]

$GeCl_2$[1,4-dioxane] (204 mg, 0.3 mmol) and dmpe (46 mg, 0.3 mmol) in 5 mL of $CH_2Cl_2$ were stirred for 15 mins resulting in the formation of a colorless solid and a $^{31}P\{^1H\}$ resonance at 18.5 ppm. TMSOTf (200 mg, 0.9 mmol), in 5 mL of $CH_2Cl_2$, was added

dropwise to the $GeCl_2$/dmpe mixture. After 1 hour the supernatant was decanted and cooled to -25 °C and over the course of 2 days yielded crystals suitable for X-Ray experiments. Crystals not submitted for X-Ray diffraction were washed with hexane (2 x 3 mL), and dried in vacuo.

**$^{31}P\{^{1}H\}$ NMR** (202.5 MHz, $CD_3CN$, 295K): δ 19.38 ppm (br) (*unconfirmed*)

**Crystal Data**: See Table 8.9.19

### 8.7.7 $[Me_3PCl][GeCl_3]$

$GeCl_4$ (64 mg, 0.3 mmol) and $Me_3P$ (23 mg, 0.3 mmol) in 3 mL of $CH_2Cl_2$ were stirred together resulting in the immediate formation of a colorless precipitate. This solution was left stirring for 1 hour to ensure the reaction was complete. After 1 hour solvent was decanted, the remaining solid was washed with 2 x 5 mL of hexane and dried in vacuo. X-Ray quality crystals can be grown by dissolving the solid in $CH_3CN$ and allowing the solvent to slowly evaporate over the course of 6 days at room temperature. Alternatively, the supernatant from the reaction can be decanted from the precipitate and cooled -25°C over the course of 2 days to produce X-Ray quality crystals.

**Yield:** 68 mg (0.23 mmol, 78% powder material)

**M.p.** 211-213°C

**$^{1}H$ NMR** (500.1 MHz, $CD_3CN$, 295K): δ 2.47 ppm (9H, *d*, $^{2}J_{P-H}$ = 14 Hz, $P[CH_3]_3$)

**$^{13}C$ NMR** (125.8 MHz, UDEFT, $CD_3CN$, 295K): δ 17.04 ppm (*d*, $^{1}J_{P-C}$ = 52 Hz, $P[CH_3]_3$)

**$^{31}P\{^{1}H\}$ NMR** (202.5 MHz, $CD_3CN$, 295K): δ 93.9 ppm (*s*)

**Crystal Data:** See Table 8.9.19

### 8.7.8 $[(tBu_3P_3)Me_2GeCl][AlCl_4]$

$Me_2GeCl_2$ (35 mg, 0.2 mmol) and $AlCl_3$ (26 mg, 0.2 mmol) in 3 mL of $CH_2Cl_2$ were stirred for 10 mins resulting in dissolution of $AlCl_3$. $tBu_3P_3$ ( 51 mg, 0.2 mmol), in 2 mL of $CH_2Cl_2$, was added dropwise to the $Me_2GeCl_2/AlCl_3$ mixture. After 1 hour hexane was added to the yellow, clear reaction mixture to produce yellow oil, solvent was decanted and any residual solvent was removed in vacuo.

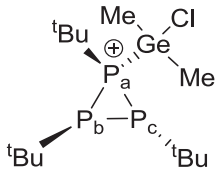


**$^{31}P\{^{1}H\}$ NMR** (202.5 MHz, $CH_2Cl_2$, $C_6D_6$ capillary, 298K): δ -46.3 ppm (*dd*, $^{1}J_{Pa\text{-}Pb}$ = 305 Hz; $^{1}J_{Pa\text{-}Pc}$ = 135 Hz, $P_a$), -64.6 ppm (*dd*, $^{1}J_{Pb\text{-}Pa}$ = 305 Hz; $^{1}J_{Pb\text{-}Pc}$ = 337 Hz, $P_b$), -135.2 ppm (*dd*, $^{1}J_{Pc\text{-}Pa}$ = 135 Hz; $^{1}J_{Pc\text{-}Pb}$ = 337 Hz, $P_c$)

## 8.8 Preparation and Characterization of a byproduct from the reaction of dmpe with $AlCl_3$

### 8.8.1 $[(dmpe)_2AlCl_2][AlCl_4]$

$AlCl_3$ (133 mg, 1 mmol) and dmpe (154 mg, 1 mmol) were stirred together in $CH_2Cl_2$ (10 mL) for 1 hour. After 1 hour the reaction mixture was layered with ether and stored at −25°C for 2 days producing cubic colorless crystals. Crystal not submitted for X-Ray analysis were washed with ether (3x 3 mL) and dried in vacuo.

**Yield**: 222 mg (0.39 mmol, 39% crystalline material)

**M.p.** 239-241 °C

**FT-IR**: (nujol mull, CsI plates, $cm^{-1}$, [relative intensities]): 2923[bs], 2853[bs], 1462[ms], 1419[s], 1377[ms], 1306[ms], 1291[ms], 1142[w], 1097[w], 993[w], 949[s], 932[s], 899[mw], 868[mw], 837[mw], 752[m], 717[m], 634[w], 494[s], 481[s], 438[s]

**FT-Raman** (capillary tube - 1mm, $cm^{-1}$, [relative intensities]): 2994[mw], 2980[mw], 2940[mw], 2913[s], 1421[w], 748[w], 720[w], 348[w], 255[w], 120[w]

**$^{1}$H NMR** (500.1 MHz, $CD_2Cl_2$, 295K): δ 2.05 ppm (8H, br, PC*H*$_2$); 1.48 ppm (24H, b*s*, PC*H*$_3$)

**$^{13}$C NMR** (125.8 MHz, UDEFT, $CD_2Cl_2$, 295K): δ 21.33-21.22 ppm (br, *C*$H_2$P); 9.25-9.16 ppm (b*s*, *C*$H_3$P)

**$^{31}$P{$^{1}$H} NMR** (202.5 MHz, $CD_2Cl_2$, 295K): δ -41.2 ppm (1:1:1:1:1:1 *sextet*, $^{1}J_{P\text{-}Al}$ = 163 Hz)

**Crystal Data**: See Table 8.9.20

## 8.9 Crystallographic Experimental Details

Table 8.9.1 Selected crystallographic data and collection parameters for compounds in chapter 2.

| | $Me_2SnCl_2AlCl_3$ | $Me_3SnClAlCl_3$ | $Bu_2SnCl_2AlCl_3$[a] |
|---|---|---|---|
| Empirical formula | $C_2H_6AlCl_5Sn$ | $C_3H_9AlCl_4Sn$ | $C_{16}H_{36}Al_2Cl_{10}Sn_2$ |
| Fw (g/mol) | 352.99 | 332.57 | 874.29 |
| T (K) | 188(1) | 173(1) | 173(1) |
| λ( Mo Kα) (Å) | 0.71073 | 0.71073 | 0.71073 |
| color and habit | Colorless, plate | Colorless, irregular | Pale yellow, irregular |
| cryst syst | Monoclinic | Triclinic | Triclinic |
| space group | $P2_1/c$ | P1 | P-1 |
| a (Å) | 13.126(5) | 6.9854(9) | 7.0371(14) |
| b (Å) | 6.866(3) | 14.376(2) | 11.089(2) |
| c (Å) | 13.668(5) | 18.392(2) | 11.592(2) |
| α (deg) | 90 | 73.172(2) | 69.846(2) |
| β (deg) | 113.250(5) | 81.094(2) | 87.617(2) |
| γ (deg) | 90 | 76.196(2) | 80.396(2) |
| V ($Å^3$) | 1131.8(8) | 1709.5(4) | 837.2(3) |
| Z | 4 | 6 | 1 |
| cryst size ($mm^3$) | 0.40 x 0.30 x 0.08 | 0.65 x 0.50 x 0.30 | 0.40 x 0.40 x 0.40 |
| abs coeff ($mm^{-1}$) | 3.448 | 3.191 | 2.349 |
| reflens colled | 5202 | 100743 | 5777 |
| indpndt reflens | 2434 | 10074 | 3624 |
| $R_{int}$ | 0.0326 | 0.0289 | 0.0142 |
| $\theta_{max}$ (deg) | 25.81 | 25.83 | 25.63 |
| GoF[b] | 1.156 | 1.032 | 1.131 |
| Data/ restraints/ parameters | 2434/ 0/ 84 | 10074/ 3/ 138 | 3624/ 0/ 138 |
| R1(all data)[c] | 0.0687 | 0.0257 | 0.0232 |
| wR2 (all data)[d] | 0.1333 | 0.0655 | 0.0582 |
| largest diff peak and hole (e $Å^{-3}$) | 1.655 and -1.309 | 0.844 and -0.971 | 1.083 and -0.329 |

[a] The crystal was twinned and the orientation matrixes for the major component was determined (CELL NOW[100]) The data were reduced and corrected for absorption (TWINABS[101]).

[b] $GOF = [\sum w(|F_o| - |F_c|)^2/(n-p)]^{1/2}$, where n = number of reflections, and p = number of parameters.

[c] $R1 = \sum ||F_o| - |F_c|| / \sum |F_o|$

[d] $wR2 = (\sum[w(F_o^2-F_c^2)^2]/\sum[wF_o^4])^{1/2}$, $w = [\sigma^2(F_o^2) + (0.0329P)^2 + (0.2239\ P)]^{-1}$, where $P = (\max(F_o^2, 0) + 2[F_c^2])/3$

Table 8.9.2 Selected crystallographic data and collection parameters for compounds in chapter 3.

| | **[$iPr_3PMe_2GeCl$][OTf][a]** | **[$Cy_3PEt_3Ge$][$AlCl_4$]** |
|---|---|---|
| Empirical formula | $C_{12}H_{27}ClF_3GeO_3PS$ | $C_{24}H_{48}AlCl_4GeP$ |
| Fw (g/mol) | 447.41 | 608.96 |
| T (K) | 198(1) | 198(1) |
| λ( Mo Kα) (Å) | 0.71073 | 0.71073 |
| color and habit | Colorless, prallelepiped | Colorless, block |
| cryst syst | Orthorhombic | Monoclinic |
| space group | $Pna2_1$ | $P2_1/c$ |
| a (Å) | 23.852(2) | 19.3598(16) |
| b (Å) | 9.2096(8) | 15.7332(12) |
| c (Å) | 8.9435(7) | 20.1828(16) |
| α (deg) | 90 | 90 |
| β (deg) | 90 | 92.6920(10) |
| γ (deg) | 90 | 90 |
| V ($Å^3$) | 1964.6(3) | 6140.7(8) |
| Z | 4 | 8 |
| cryst size ($mm^3$) | 0.50 x 0.40 x 0.30 | 0.40 x 0.40 x 0.20 |
| abs coeff ($mm^{-1}$) | 1.915 | 1.438 |
| reflens colled | 12935 | 42245 |
| indpndt reflens | 3941 | 13443 |
| $R_{int}$ | 0.0311 | 0.0298 |
| $\theta_{max}$ (deg) | 25.13 | 25.86 |
| GoF[b] | 1.050 | 1.066 |
| Data/ restraints/ Parameters | 3941/ 5/ 216 | 13443/ 0/ 565 |
| R1(all data)[c] | 0.0699 | 0.0607 |
| wR2 (all data)[d] | 0.1856 | 0.1000 |
| largest diff peak and hole (e $Å^{-3}$) | 2.525 and -1.539 | 1.104 and -0.765 |

[a] The $GeClMe_2$ moiety was disordered over two positions and the site occupancies determined using an isotropic model and fixed in subsequent refinement cycles. Ge- Cl distances were fixed at 2.2 Å, Ge-C(2) and Ge-C(2a) fixed at 1.95 Å and Ge-C(1) and Ge-C(1a) distances fixed at equal values. Due to the proximity of the two positions of the disordered group, thermal parameters of close atoms were fixed to be equal. Damping was required to force refinement of thermal parameters of C(1) and C(1a) to converge.

[b] $GOF = [\sum w(|F_o| - |F_c|)^2/(n-p)]^{1/2}$, where n = number of reflections, and p = number of parameters.

[c] $R1 = \sum ||F_o| - |F_c|| / \sum |F_o|$

[d] $wR2 = (\sum[w(F_o^2-F_c^2)^2]/\sum[wF_o^4])^{1/2}$, $w = [\sigma^2(F_o^2) + (0.0329P)^2 + (0.2239\ P)]^{-1}$, where $P = (\max(F_o^2, 0) + 2[F_c^2])/3$

Table 8.9.3 Selected crystallographic data and collection parameters for compounds in chapter 3.

| | **$[Me_3P(Ph_3Ge)][OTf]$** | **$[Me_3PMe_2GeCl][AlCl_4]$[a]** |
|---|---|---|
| Empirical formula | $C_{22}H_{24}F_3GeO_3PS$ | $C_5H_{15}AlCl_5GeP$ |
| Fw (g/mol) | 529.03 | 382.96 |
| T (K) | 188(1) | 213(1) |
| λ( Mo Kα) (Å) | 0.71073 | 0.71073 |
| color and habit | Colorless, plate | Colorless, parallelepiped |
| cryst syst | Monoclinic | Monoclinic |
| space group | $P2_1/n$ | $P2_1/c$ |
| a (Å) | 7.6784(7) | 7.6736(12) |
| b (Å) | 11.7723(10) | 11.3461(17) |
| c (Å) | 26.660(2) | 18.388(3) |
| α (deg) | 90 | 90 |
| β (deg) | 98.1550(10) | 95.861(2) |
| γ (deg) | 90 | 90 |
| V ($Å^3$) | 2385.5(4) | 1592.6(4) |
| Z | 4 | 4 |
| cryst size ($mm^3$) | 0.45 x 0.45 x 0.15 | 0.45 x 0.35 x 0.20 |
| abs coeff ($mm^{-1}$) | 1.474 | 2.882 |
| reflens colled | 16083 | 3370 |
| indpndt reflens | 5309 | 3370 |
| $R_{int}$ | 0.0206 | - |
| $\theta_{max}$ (deg) | 25.96 | 25.38 |
| Data/ restraints/ parameters | 5309/ 0/ 283 | 3370/ 1/ 126 |
| GoF[b] | 1.036 | 1.114 |
| R1(all data)[c] | 0.0360 | 0.0394 |
| wR2 (all data)[d] | 0.0811 | 0.1100 |
| largest diff peak and hole (e $Å^{-3}$) | 0.559 and -0.322 | 0.481 and -0.358 |

[a] The crystal was twinned and the orientation matrixes for two components were determined. The data were reduced and corrected for absorption. The $GeMe_2Cl$ group was disordered with two of the methyl groups occupying identical positions as chlorine. The site occupancies were determined using an anisotropic model with equal thermal and positional parameters

[b] $GOF = [\sum w(|F_o| - |F_c|)^2/(n-p)]^{1/2}$, where n = number of reflections, and p = number of parameters.

[c] $R1 = \sum ||F_o| - |F_c|| / \sum |F_o|$

[d] $wR2 = (\sum[w(F_o^2-F_c^2)^2]/\sum[wF_o^4])^{1/2}$, $w = [\sigma^2(F_o^2) + (0.0329P)^2 + (0.2239\ P)]^{-1}$, where $P = (\max(F_o^2, 0) + 2[F_c^2])/3$

Table 8.9.4 Selected crystallographic data and collection parameters for compounds in chapter 3.

| | **$[dmpe(Et_3Ge)_2][OTf]_2$** | **$[(dmpe)Me_2Ge][OTf]_2$**[a] |
|---|---|---|
| Empirical formula | $C_{20}H_{46}F_6Ge_2O_6P_2S_2$ | $C_{10}H_{22}F_6GeO_6P_2S_2$ |
| Fw (g/mol) | 767.81 | 550.93 |
| T (K) | 198(1) | 173(1) |
| λ( Mo Kα) (Å) | 0.71073 | 0.7173 |
| color and habit | Colorless, parallelepiped | Colorless, plate |
| cryst syst | Triclinic | Monoclinic |
| space group | $P_1$ | $C_2/c$ |
| a (Å) | 8.0773(2) | 39.533(3) |
| b (Å) | 8.5118(2) | 8.1862(7) |
| c (Å) | 12.5957(4) | 13.4920(11) |
| α (deg) | 102.357(2) | 90 |
| β (deg) | 92.889(2) | 104.289(2) |
| γ (deg) | 101.5730(10) | 90 |
| V ($Å^3$) | 824.77(4) | 4231.3(6) |
| Z | 1 | 8 |
| cryst size ($mm^3$) | 0.40 x 0.30 x 0.20 | 0.35 x 0.30 x 0.10 |
| abs coeff ($mm^{-1}$) | 2.110 | 1.871 |
| reflens colled | 9463 | 13973 |
| indpndt reflens | 6827 | 4725 |
| $R_{int}$ | 0.0152 | 0.0231 |
| $\theta_{max}$ (deg) | 25.85 | 26.44 |
| GoF[b] | 1.093 | 1.037 |
| Data/ restraints/ parameters | 6827/ 3/ 354 | 4725/ 28/ 320 |
| R1(all data)[c] | 0.0311 | 0.0460 |
| wR2 (all data)[d] | 0.0733 | 0.1002 |
| largest diff peak and hole (e $Å^{-3}$) | 1.021 and -0.368 | 0.890 and -0.847 |

[a] The diphosphine ligand and one of the OTf anions were disordered. The site occupancies were determined using an isotropic model and fixed in subsequent refinement cycles. The triflate ion was further disordered but modeling proved impossible. To insure convergence of the refinement, equivalent distances in the two components of the disordered diphosphine moiety were constrained and thermal parameters of atoms in close proximity were set equal. The absorption coefficient is very large due to the heavy atom nature of the compound. Face indexing is required for absorption correction; however, this is impossible with plates as thin as the ones submitted.

[b] $GOF = [\sum w(|F_o| - |F_c|)^2/(n-p)]^{1/2}$, where n = number of reflections, and p = number of parameters.

[c] $R1 = \sum ||F_o| - |F_c|| / \sum |F_o|$

[d] $wR2 = (\sum[w(F_o^2-F_c^2)^2]/\sum[wF_o^4])^{1/2}$, $w = [\sigma^2(F_o^2) + (0.0329P)^2 + (0.2239\ P)]^{-1}$, where $P = (\max(F_o^2, 0) + 2[F_c^2])/3$

Table 8.9.5 Selected crystallographic data and collection parameters for compounds in chapter 3.

| | **$[dmpe(Ph_3Ge)_2][OTf]_2 \cdot 2CH_2Cl_2 \cdot 0.5C_6H_6$**[a] |
|---|---|
| Empirical formula | $C_{49}H_{53}Cl_4F_6Ge_2O_6P_2S_2$ |
| Fw (g/mol) | 1264.95 |
| T (K) | 173(1) |
| λ( Mo Kα) (Å) | 0.71073 |
| color and habit | Colorless, rod |
| cryst syst | Triclinic |
| space group | P-1 |
| a (Å) | 13.102(3) |
| b (Å) | 14.569(4) |
| c (Å) | 16.593(4) |
| α (deg) | 77.041(4) |
| β (deg) | 72.606(4) |
| γ (deg) | 68.421(4) |
| V ($Å^3$) | 2787.1(12) |
| Z | 2 |
| cryst size ($mm^3$) | 0.65 x 0.20 x 0.20 |
| abs coeff ($mm^{-1}$) | 1.468 |
| reflens colled | 19423 |
| indpndt reflens | 12084 |
| $R_{int}$ | 0.0264 |
| $\theta_{max}$ (deg) | 26.20 |
| GoF[b] | 1.085 |
| Data/ restraints/ parameters | 12084/ 0/ 617 |
| R1(all data)[c] | 0.0743 |
| wR2 (all data)[d] | 0.1393 |
| largest diff peak and hole (e $Å^{-3}$) | 2.094 and -1.197 |

[a] One benzene molecule was found in the lattice. It was badly disordered and could not be modelled properly. Its contribution to the scattering was modelled using disordered electron density (SQUEEZE)[102]. The formulae, FW, F(000), d and μ were changed accordingly

[b] $GOF = [\sum w(|F_o| - |F_c|)^2/(n-p)]^{1/2}$, where n = number of reflections, and p = number of parameters.

[c] $R1 = \sum ||F_o| - |F_c|| / \sum |F_o|$

[d] $wR2 = (\sum[w(F_o^2-F_c^2)^2]/\sum[wF_o^4])^{1/2}$, $w = [\sigma^2(F_o^2) + (0.0329P)^2 + (0.2239\ P)]^{-1}$, where $P = (\max(F_o^2, 0) + 2[F_c^2])/3$

Table 8.9.6 Selected crystallographic data and collection parameters for compounds in chapter 4.

| | $SnCl_4(PMe_3)_2$[a] | $SnCl_4(PMe_3)_2$ | $[SnCl_3(PMe_3)_2][AlCl_4]$ |
|---|---|---|---|
| Empirical formula | $C_6H_{18}Cl_4P_2Sn$ | $C_6H_{18}Cl_4P_2Sn$ | $C_6H_{18}AlCl_7P_2Sn$ |
| Fw (g/mol) | 412.63 | 412.63 | 545.96 |
| T (K) | 198(1) | 188(1) | 198(1) |
| λ( Mo Kα) (Å) | 0.71073 | 0.71073 | 0.71073 |
| color and habit | Colorless, irregular | Colorless, irregular | Colorless, irregular |
| cryst syst | Monoclinic | Monoclinic | Monoclinic |
| space group | C2/m | $P2_1/c$ | $P2_1/c$ |
| a (Å) | 13.397(3) | 6.6923(14) | 9.164(3) |
| b (Å) | 8.419(3) | 8.4333(17) | 10.897(3) |
| c (Å) | 6.6910(18) | 13.376(3) | 10.684(3) |
| α (deg) | 90 | 90 | 90 |
| β (deg) | 100.165(5) | 100.204(2) | 105.708(3) |
| γ (deg) | 90 | 90 | 90 |
| V ($Å^3$) | 742.8(4) | 743.0(3) | 1027.1(5) |
| Z | 2 | 2 | 2 |
| cryst size ($mm^3$) | 0.20 x 0.08 x 0.05 | 0.25 x 0.10 x 0.10 | 0.35 x 0.35 x 0.15 |
| abs coeff ($mm^{-1}$) | 2.618 | 2.617 | 2.334 |
| reflens colled | 2591 | 3093 | 7106 |
| indpndt reflens | 890 | 1656 | 2430 |
| $R_{int}$ | 0.0247 | 0.0315 | 0.0248 |
| $\theta_{max}$ (deg) | 24.59 | 24.63 | 25.52 |
| GoF[b] | 1.107 | 1.033 | 1.069 |
| Data/ restraints/ parameters | 890/ 0/ 47 | 1656/ 0/ 64 | 2430/ 12/ 110 |
| R1(all data)[c] | 0.0230 | 0.0311 | 0.0262 |
| wR2 (all data)[d] | 0.0535 | 0.0573 | 0.0674 |
| largest diff peak and hole (e $Å^{-3}$) | 0.702 and -0.272 | 0.551 and -0.474 | 0.871 and -0.701 |

[a] The phosphine and chlorine groups were disordered such that the position for Cl(1) is fully occupied with chlorine but the position for Cl(2)/P(1) is 50 % chlorine and 50% phosphine. These two atoms were refined using identical positional and thermal parameters resulting in averaged Sn-E bond length. All non-hydrogen atoms were refined using anisotropic displacement parameters.

[b] $GOF = [\sum w(|F_o| - |F_c|)^2/(n-p)]^{1/2}$, where n = number of reflections, and p = number of parameters.

[c] $R1 = \sum ||F_o| - |F_c|| / \sum |F_o|$

[d] $wR2 = (\sum[w(F_o^2-F_c^2)^2]/\sum[wF_o^4])^{1/2}$, $w = [\sigma^2(F_o^2) + (0.0329P)^2 + (0.2239\ P)]^{-1}$, where $P = (\max(F_o^2, 0) + 2[F_c^2])/3$

Table 8.9.7 Selected crystallographic data and collection parameters for compounds in chapter 4.

| | $[SnCl_3(PMe_3)_2][GaCl_4]$[a] | $[SnCl_2(PMe_3)_2][AlCl_4]_2$ |
|---|---|---|
| Empirical formula | $C_6H_{18}Cl_7GaP_2Sn$ | $C_6H_{18}Al_2Cl_{10}P_2Sn$ |
| Fw (g/mol) | 588.70 | 679.29 |
| T (K) | 188(1) | 173(1) |
| λ( Mo Kα) (Å) | 0.71073 | 0.71073 |
| color and habit | Colorless, irregular | Colorless, parallelepiped |
| cryst syst | Monoclinic | Monoclinic |
| space group | $P2_1$ | $P2_1/n$ |
| a (Å) | 9.1752(11) | 7.2557(10) |
| b (Å) | 10.9062(13) | 13.2556(18) |
| c (Å) | 10.6926(13) | 25.966(4) |
| α (deg) | 90 | 90 |
| β (deg) | 105.684(2) | 95.068(2) |
| γ (deg) | 90 | 90 |
| V ($Å^3$) | 1030.2(2) | 2487.6(6) |
| Z | 2 | 4 |
| cryst size ($mm^3$) | 0.45 x 0.30 x 0.20 | 0.40 x 0.25 x 0.22 |
| abs coeff ($mm^{-1}$) | 3.564 | 2.291 |
| reflens colled | 5153 | 16786 |
| indpndt reflens | 3905 | 5573 |
| $R_{int}$ | 0.0276 | 0.0247 |
| $\theta_{max}$ (deg) | 25.51 | 25.93 |
| GoF[b] | 1.313 | 1.056 |
| Data/ restraints/ parameters | 3905/ 41/ 173 | 5573/ 0/ 196 |
| R1(all data)[c] | 0.0361 | 0.0247 |
| wR2 (all data)[d] | 0.0891 | 0.0569 |
| largest diff peak and hole (e $Å^{-3}$) | 1.118 and -0.905 | 0.867 and -0.581 |

[a] The gallate was made for the purpose of Raman studies, no further characterization data collected on the compound.

[b] $GOF = [\sum w(|F_o| - |F_c|)^2/(n-p)]^{1/2}$, where n = number of reflections, and p = number of parameters.

[c] $R1 = \sum ||F_o| - |F_c|| / \sum |F_o|$

[d] $wR2 = (\sum[w(F_o^2-F_c^2)^2]/\sum[wF_o^4])^{1/2}$, $w = [\sigma^2(F_o^2) + (0.0329P)^2 + (0.2239P)]^{-1}$, where $P = (\max(F_o^2, 0) + 2[F_c^2])/3$

Table 8.9.8 Selected crystallographic data and collection parameters for compounds in chapter 5.

| | **$[Me_3PMe_3Sn][AlCl_4]$** | **$[Me_3PMe_3Sn][OTf]$** |
|---|---|---|
| Empirical formula | $C_6H_{18}AlCl_4PSn$ | $C_7H_{18}F_3O_3PSSn$ |
| Fw (g/mol) | 408.64 | 388.93 |
| T (K) | 213(1) K | 173(2) |
| λ( Mo Kα) (Å) | 0.71073 | 0.71073 |
| color and habit | Colorless, parallelepiped | Colorless, prism |
| cryst syst | Orthorhombic | Monoclinic |
| space group | Pnma | $P2_1/c$ |
| a (Å) | 17.813(2) | 9.4562(7) |
| b (Å) | 10.7242(12) | 11.5716(8) |
| c (Å) | 8.699(1) | 26.3115(19) |
| α (deg) | 90 | 90 |
| β (deg) | 90 | 92.1142(9) |
| γ (deg) | 90 | 90 |
| V ($Å^3$) | 1661.8(3) | 2877.1(4) |
| Z | 4 | 8 |
| cryst size ($mm^3$) | 0.40 x 0.30 x 0.25 | 0.30 x 0.21 x 0.17 |
| abs coeff ($mm^{-1}$) | 2.297 | 2.056 |
| reflens colled | 6116 | 6607 |
| indpndt reflens | 1932 | 6325 |
| $R_{int}$ | 0.0283 | 0.0151 |
| $\theta_{max}$ (deg) | 25.21 | 55.1 |
| GoF[a] | 1.126 | 1.175 |
| Data/ restraints/ parameters | 1932/ 0/ 72 | 6325/ 0/ 302 |
| R1(all data)[b] | 0.0243 | 0.0458 |
| wR2 (all data)[c] | 0.0677 | 0.1243 |
| largest diff peak and hole (e $Å^{-3}$) | 0.475 and -0.421 | 0.170 and -0.899 |

[a] $GOF = [\sum w(|F_o| - |F_c|)^2/(n-p)]^{1/2}$, where n = number of reflections, and p = number of parameters.

[b] $R1 = \sum ||F_o| - |F_c|| / \sum |F_o|$

[c] $wR2 = (\sum[w(F_o^2-F_c^2)^2]/\sum[wF_o^4])^{1/2}$, $w = [\sigma^2(F_o^2) + (0.0329P)^2 + (0.2239P)]^{-1}$, where $P = (\max(F_o^2, 0) + 2[F_c^2])/3$

Table 8.9.9 Selected crystallographic data and collection parameters for compounds in chapter 5.

| | **$[Cy_3PMe_3Sn][AlCl_4]$** | **$[iPr_3PMe_3Sn][AlCl_4]$** |
|---|---|---|
| Empirical formula | $C_{21}H_{42}AlC_{l4}PSn$ | $C_{12}H_{30}AlCl_4PSn$ |
| Fw (g/mol) | 612.99 | 492.80 |
| T (K) | 213(1) | 198(1) |
| λ( Mo Kα) (Å) | 0.71073 | 0.71073 |
| color and habit | Colorless, block | Colorless, irregular |
| cryst syst | Orthorhombic | Monoclinic |
| space group | $Pca2_1$ | $P2_1/n$ |
| a (Å) | 17.066(3) | 12.9637(17) |
| b (Å) | 9.3044(19) | 13.1094(17) |
| c (Å) | 18.081(4) | 13.0112(17) |
| α (deg) | 90 | 90 |
| β (deg) | 90 | 90.843(2) |
| γ (deg) | 90 | 90 |
| V ($Å^3$) | 2871.0(10) | 2211.1(5) |
| Z | 4 | 4 |
| cryst size ($mm^3$) | 0.50 x 0.40 x 0.25 | 0.40 x 0.30 x 0.10 |
| abs coeff ($mm^{-1}$) | 1.355 | 1.740 |
| reflens colled | 18948 | 14086 |
| indpndt reflens | 6247 | 4807 |
| $R_{int}$ | 0.0251 | 0.0261 |
| $\theta_{max}$ (deg) | 25.31 | 25.30 |
| GoF[a] | 1.058 | 1.081 |
| Data/ restraints/ parameters | 6247/ 1/ 256 | 4807/ 0/ 181 |
| R1(all data)[b] | 0.0406 | 0.0425 |
| wR2 (all data)[c] | 0.1178 | 0.0627 |
| largest diff peak and hole (e $Å^{-3}$) | 1.045 and -0.805 | 0.611 and -0.267 |

[b] GOF = $[\sum w(|F_o| - |F_c|)^2/(n-p)]^{1/2}$, where n = number of reflections, and p = number of parameters.

[a] $R1 = \sum ||F_o| - |F_c|| / \sum |F_o|$

[b] $wR2 = (\sum[w(F_o^2-F_c^2)^2]/\sum[wF_o^4])^{1/2}$, $w = [\sigma^2(F_o^2) + (0.0329P)^2 + (0.2239P)]^{-1}$, where $P = (\max(F_o^2, 0) + 2[F_c^2])/3$

Table 8.9.10 Selected crystallographic data and collection parameters for compounds in chapter 5.

| | **$[tBu_3PMe_3Sn][AlCl_4]$**[a] | **$[(dmpe)SnMe_3][AlCl_4]$** |
|---|---|---|
| Empirical formula | $C_{15}H_{36}AlCl_4PSn$ | $C_9H_{25}AlCl_4P_2Sn$ |
| Fw (g/mol) | 534.88 | 482.70 |
| T (K) | 293(2) | 213(1) |
| λ( Mo Kα) (Å) | 0.71073 | 0.71073 |
| color and habit | Colorless | Colorless, block |
| cryst syst | Orthorhombic | Monoclinic |
| space group | $Pca2_1$ | Cc |
| a (Å) | 24.174(4) | 9.3162(13) |
| b (Å) | 11.894(2) | 16.286(3) |
| c (Å) | 16.999(3) | 14.0784(19) |
| α (deg) | 90 | 90 |
| β (deg) | 90 | 106.382(2) |
| γ (deg) | 90 | 90 |
| V ($Å^3$) | 4887.6(14) | 2049.3(5) |
| Z | 8 | 4 |
| cryst size ($mm^3$) | - | 0.12 x 0.08 x 0.08 |
| abs coeff ($mm^{-1}$) | 1.580 | 1.950 |
| reflens colled | 10121 | 7065 |
| indpndt reflens | 7507 | 4274 |
| $R_{int}$ | 0.0591 | 0.0399 |
| $\theta_{max}$ (deg) | 25.82 | |
| GoF[b] | 1.185 | 1.004 |
| Data/ restraints/ parameters | 7507/ 1/ 332 | 4274/ 2/ 161 |
| R1(all data)[c] | 0.1077 | 0.0673 |
| wR2 (all data)[d] | 0.1802 | 0.0767 |
| largest diff peak and hole (e $Å^{-3}$) | - | 0.802 and -0.460 |

[a] Preliminary structure, data is not of a high enough quality for publication.

[b] $GOF = [\sum w(|F_o| - |F_c|)^2/(n-p)]^{1/2}$, where n = number of reflections, and p = number of parameters.

[c] $R1 = \sum ||F_o| - |F_c|| / \sum |F_o|$

[d] $wR2 = (\sum[w(F_o^2-F_c^2)^2]/\sum[wF_o^4])^{1/2}$, $w = [\sigma^2(F_o^2) + (0.0329P)^2 + (0.2239P)]^{-1}$, where $P = (\max(F_o^2, 0) + 2[F_c^2])/3$

Table 8.9.11 Selected crystallographic data and collection parameters for compounds in chapter 5.

| | **[dmpe(SnMe$_3$)$_2$][OTf]$_2$** | **[(dmpm)Me$_3$Sn][AlCl$_4$]** |
|---|---|---|
| Empirical formula | $C_{14}H_{34}F_6O_6P_2S_2Sn_2$ | $C_8H_{23}AlCl_4P_2Sn$ |
| Fw (g/mol) | 775.85 | 468.67 |
| T (K) | 173(1) | 198(1) |
| λ( Mo Kα) (Å) | 0.71073 | 0.71073 |
| color and habit | Colorless, rod | Colorless, irregular |
| cryst syst | Monoclinic | Monoclinic |
| space group | $P2_1/c$ | Cm |
| a (Å) | 13.348(4) | 12.4132(18) |
| b (Å) | 15.848(5) | 10.1466(18) |
| c (Å) | 13.795(4) | 9.2676(16) |
| α (deg) | 90 | 90 |
| β (deg) | 96.132(4) | 122.121(3) |
| γ (deg) | 90 | 90 |
| V (Å$^3$) | 2901.5(16) | 988.6(3) |
| Z | 4 | 2 |
| cryst size (mm$^3$) | 0.55 x 0.10 x 0.10 | 0.60 x 0.40 x 0.20 |
| abs coeff (mm$^{-1}$) | 2.039 | 2.018 |
| reflens colled | 18550 | 3340 |
| indpndt reflens | 6439 | 2121 |
| $R_{int}$ | 0.0454 | 0.0254 |
| $\theta_{max}$ (deg) | 25.97 | 24.91 |
| GoF[a] | 1.085 | 1.068 |
| Data/ restraints/ parameters | 6439/ 0/ 299 | 2121/ 2/ 89 |
| R1(all data)[b] | 0.0343 | 0.0240 |
| wR2 (all data)[c] | 0.0868 | 0.0584 |
| largest diff peak and hole (e Å$^{-3}$) | 0.788 and -0.633 | 1.017 and -0.417 |

[a] GOF = $[\sum w(|F_o| - |F_c|)^2/(n-p)]^{1/2}$, where n = number of reflections, and p = number of parameters.

[b] $R1 = \sum ||Fo| - |Fc|| / \sum |Fo|$

[c] wR2 = $(\sum[w(Fo2-Fc2)2]/\sum[wFo4])1/2$, $w = [\sigma 2(Fo2) + (0.0329P)2 + (0.2239P)]-1$, where P = (max (Fo2, 0) +2[Fc2])/3

Table 8.9.12 Selected crystallographic data and collection parameters for compounds in chapter 5.

| | **[dmpm(Me$_3$Sn)$_2$][AlCl$_4$]$_2$** | **[(dmpe)Bu$_2$Sn][AlCl$_4$]$_2$** |
|---|---|---|
| Empirical formula | $C_{11}H_{32}Al_2Cl_8P_2Sn_2$ | $C_{14}H_{34}Al_2C_{l8}P_2Sn$ |
| Fw (g/mol) | 801.25 | 720.60 |
| T (K) | 188(1) | 173(1) |
| λ( Mo Kα) (Å) | 0.71073 | 0.71073 |
| color and habit | Colorless, rod | Colorless, irregular |
| cryst syst | Monoclinic | Monoclinic |
| space group | $P2_1/n$ | $P2_1/n$ |
| a (Å) | 12.496(4) | 11.629(3) |
| b (Å) | 11.058(3) | 11.765(3) |
| c (Å) | 21.727(6) | 23.499(6) |
| α (deg) | 90 | 90 |
| β (deg) | 94.612(4) | 102.874(4) |
| γ (deg) | 90 | 90 |
| V (Å$^3$) | 2992.7(15) | 3134.3(15) |
| Z | 4 | 4 |
| cryst size (mm$^3$) | 0.40 x 0.10 x 0.05 | 0.40 x 0.30 x 0.25 |
| abs coeff (mm$^{-1}$) | 2.549 | 1.658 |
| reflens colled | 6737 | 21287 |
| indpndt reflens | 6737 | 7013 |
| $R_{int}$ | - | 0.0235 |
| $\theta_{max}$ (deg) | 25.68 | 25.74 |
| GoF[a] | 0.997 | 1.056 |
| Data/ restraints/ parameters | 6737/ 0/ 236 | 7013/ 2/ 254 |
| R1(all data)[b] | 0.0592 | 0.0286 |
| wR2 (all data)[c] | 0.0.0721 | 0.0767 |
| largest diff peak and hole (e Å$^{-3}$) | 0.819 and -0.533 | 0.0822 and -0.533 |

[a] GOF = $[\sum w(|F_o| - |F_c|)^2/(n-p)]^{1/2}$, where n = number of reflections, and p = number of parameters.
[b] $R1 = \sum ||F_o| - |F_c|| / \sum |F_o|$
[c] $wR2 = (\sum[w(F_o^2-F_c^2)^2]/\sum[wF_o^4])^{1/2}$, $w = [\sigma^2(F_o^2) + (0.0329P)^2 + (0.2239P)]^{-1}$, where $P = (\max(F_o^2, 0) + 2[F_c^2])/3$

Table 8.9.13 Selected crystallographic data and collection parameters for compounds in chapter 5.

| | **[(dmpe)$Bu_2$Sn][OTf]$_2$**[a] | **[(dmpe)$Bu_2$Sn][OTf]$_2$**[b] |
|---|---|---|
| Empirical formula | $C_{16}H_{34}F_6O_6P_2S_2Sn$ | $C_{16}H_{34}F_6O_6P_2S_2Sn$ |
| Fw (g/mol) | 681.18 | 681.18 |
| T (K) | 173(2) | 198(2) |
| λ( Mo Kα) (Å) | 0.71073 | 0.71073 |
| color and habit | Colorless, parallelepiped | Colorless, parallelepiped |
| cryst syst | Orthorhombic | Orthorhombic |
| space group | $P2_12_12_1$ | $Pna2_1$ |
| a (Å) | 12.608(4) | 27.091(6) |
| b (Å) | 12.973(4) | 8.5435(18) |
| c (Å) | 34.280(11) | 11.979(3) |
| α (deg) | 90 | 90 |
| β (deg) | 90 | 90 |
| γ (deg) | 90 | 90 |
| V (Å$^3$) | 5607(3) | 2772.6(10) |
| Z | 8 | 4 |
| cryst size (mm$^3$) | 0.45 x 0.35 x 0.25 | 0.30 x 0.05 x 0.05 |
| abs coeff (mm$^{-1}$) | - | 1.256 |
| reflens colled | 26129 | 5592 |
| indpndt reflens | 9431 | 3306 |
| $R_{int}$ | 0.0511 | 0.1023 |
| $\theta_{max}$ (deg) | 23.93 | 25.99 |
| GoF[b] | 1.223 | 1.103 |
| Data/ restraints/ parameters | 9431/ 29/ 624 | 5592/ 1/5592/ 305 |
| R1(all data)[c] | 0.2026 | 0.1320 |
| wR2 (all data)[d] | 0.2066 | 0.1659 |
| largest diff peak and hole (e Å$^{-3}$) | 1.314 and -1.826 | 0.140 and -1.051 |

[a] The crystal is a multiple twin and split as well. Data had to be collected at 6 cm to facilitate integration. One of the butyl groups and one of the bridging $C_2H_2$ were disordered and the site occupancies fixed at 0.5 in subsequent refinement cycles.

[b] The crystal is a multiple twin and split as well. Data had to be collected at 6 cm to facilitate integration albeit the same quality as the first with a different space group/unit cell.

[c] $R1 = \sum | |F_o| - |F_c| | / \sum |F_o|$

[d] $wR2 = (\sum[w(F_o^2-F_c^2)^2]/\sum[wF_o^4])^{1/2}$, $w = [\sigma^2(F_o^2) + (0.0329P)^2 + (0.2239P)]^{-1}$, where $P = (\max(F_o^2, 0) + 2[F_c^2])/3$

Table 8.9.14 Selected crystallographic data and collection parameters for compounds in chapter 5.

| | **$[(dmpm)Bu_2Sn][AlCl_4]_2$** | **$[(dmpm)Me_2Sn][OTf]_2$[a]** |
|---|---|---|
| Empirical formula | $C_{13}H_{32}Al_2Cl_8P_2Sn$ | $C_9H_{20}F_6O_6P_2S_2Sn$ |
| Fw (g/mol) | 706.58 | 583.00 |
| T (K) | 188(1) | 199(1) |
| λ( Mo Kα) (Å) | 0.71073 | 0.71073 |
| color and habit | Colorless, rod | Colorless, irregular |
| cryst syst | Monoclinic | Monoclinic |
| space group | $P2_1/n$ | $C_2/c$ |
| a (Å) | 12.496(4) | 21.900(8) |
| b (Å) | 11.058(3) | 8.681(3) |
| c (Å) | 21.727(6) | 13.250(6) |
| α (deg) | 90 | 90 |
| β (deg) | 94.612(4) | 123.943(9) |
| γ (deg) | 90 | 90 |
| V ($Å^3$) | 2992.7(15) | 2089.7(13) |
| Z | 4 | 4 |
| cryst size ($mm^3$) | 0.40 x 0.10 x 0.05 | 0.60 x 0.40 x 0.20 |
| abs coeff ($mm^{-1}$) | 2.549 | 1.649 |
| reflens colled | 6737 | 6495 |
| indpndt reflens | 6737 | 2298 |
| $R_{int}$ | - | 0.0196 |
| $\theta_{max}$ (deg) | 25.68 | 25.26 |
| GoF[c] | 0.997 | 1.098 |
| Data/ restraints/ parameters | 6742/ 15/ 269 | 2298/ 0/ 128 |
| R1(all data)[d] | 0.0592 | 0.0388 |
| wR2 (all data)[e] | 0.0721 | 0.0783 |
| largest diff peak and hole (e $Å^{-3}$) | 0.819 and -0.533 | 0.630 and -0.943 |

[a] One of the butyl groups was disordered and the site occupancy ws determined using an anisotropic model as 0.6 [C(1)-C(4)] and 0.4 [C(1a)-C(4a)] and fixed in subsequent refinement cycles.

[b] The crystal was twinned and the orientation matrix for the major component was determined. The data were reduced and corrected for absorption. C(4) was disordered over two positions that are symmetry related and refined with a site occupancy of 0.5. The disorder in the methyl groups could not be modeled properly due to the close proximity of the carbon atoms.

[c] $GOF = [\sum w(|F_o| - |F_c|)^2/(n-p)]^{1/2}$, where n = number of reflections, and p = number of parameters.

[d] $R1 = \sum ||F_o| - |F_c|| / \sum |F_o|$

[e] $wR2 = (\sum[w(F_o^2-F_c^2)^2]/\sum[wF_o^4])^{1/2}$, $w = [\sigma^2(F_o^2) + (0.0329P)^2 + (0.2239P)]^{-1}$, where $P = (\max(F_o^2, 0) + 2[F_c^2])/3$

Table 8.9.15 Selected crystallographic data and collection parameters for compounds in chapter 6.

| | **$[Me_3P(Me_2SnCl)][AlCl_4]$** | **$dmpe(Me_2SnCl_2)_2$** |
|---|---|---|
| Empirical formula | $C_5H_{15}AlCl_5PSn$ | $C_{10}H_{28}Cl_4P_2Sn_2$ |
| Fw (g/mol) | 429.06 | 589.44 |
| T (K) | 173(1) | 173(1) |
| λ( Mo Kα) (Å) | 0.71073 | 0.71073 |
| color and habit | Colorless, rod | Colorless, plate |
| cryst syst | Monoclinic | Monoclinic |
| space group | $P2_1/c$ | $P2_1/n$ |
| a (Å) | 7.1687(10) | 12.335(3) |
| b (Å) | 16.457(2) | 6.7593(17) |
| c (Å) | 13.3079(18) | 13.389(3) |
| α (deg) | 90 | 90 |
| β (deg) | 91.616(2) | 108.414(3) |
| γ (deg) | 90 | 90 |
| V ($Å^3$) | 1569.4(4) | 1059.2(5) |
| Z | 4 | 4 |
| cryst size ($mm^3$) | 0.55 x 0.15 x 0.12 | 0.45 x 0.30 x 0.05 |
| abs coeff ($mm^{-1}$) | 2.601 | 2.999 |
| reflens colled | 10755 | 7002 |
| indpndt reflens | 3521 | 2380 |
| $R_{int}$ | 0.0292 | 0.0413 |
| $\theta_{max}$ (deg) | 25.53 | 25.51 |
| GoF[a] | 1.080 | 1.051 |
| Data/ restraints/ parameters | 3521/ 0/ 123 | 2380/ 0/ 86 |
| R1(all data)[b] | 0.0201 | 0.0226 |
| wR2 (all data)[c] | 0.0457 | 0.0554 |
| largest diff peak and hole (e $Å^{-3}$) | 0.576 and -0.252 | 0.796 and -0.680 |

[a] GOF = $[\sum w(|F_o| - |F_c|)^2/(n-p)]^{1/2}$, where n = number of reflections, and p = number of parameters.

[b] $R1 = \sum ||F_o| - |F_c|| / \sum |F_o|$

[c] $wR2 = (\sum[w(F_o^2-F_c^2)^2]/\sum[wF_o^4])^{1/2}$, $w = [\sigma^2(F_o^2) + (0.0329P)^2 + (0.2239P)]^{-1}$, where $P = (\max(F_o^2, 0) + 2[F_c^2])/3$

Table 8.9.16 Selected crystallographic data and collection parameters for compounds in chapter 6.

| | **[(dmpe)$Bu_2$SnCl][$AlCl_4$]** | **[(dmpm)$Me_2$SnCl][$AlCl_4$]** |
|---|---|---|
| Empirical formula | $C_{14}H_{34}AlCl_5P_2Sn$ | $C_7H_{20}AlCl_5P_2Sn$ |
| Fw (g/mol) | 587.27 | 489.09 |
| T (K) | 173(1) | 173(1) |
| λ( Mo Kα) (Å) | 0.71073 | 0.71073 |
| color and habit | Colorless, plate | Colorless, irregular |
| cryst syst | Orthorhombic | Monoclinic |
| space group | Pbca | $P2_1/c$ |
| a (Å) | 20.697(3) | 8.842(3) |
| b (Å) | 12.2475(17) | 13.400(5) |
| c (Å) | 20.815(3) | 16.335(6) |
| α (deg) | 90 | 90 |
| β (deg) | 90 | 99.305(5) |
| γ (deg) | 90 | 90 |
| V ($Å^3$) | 5276.5(12) | 1910.0(13) |
| Z | 8 | 4 |
| cryst size ($mm^3$) | 0.55 x 0.40 x 0.10 | 0.45 x 0.40 x 0.30 |
| abs coeff ($mm^{-1}$) | 1.627 | 2.229 |
| reflens colled | 33731 | 12914 |
| indpndt reflens | 5818 | 4271 |
| $R_{int}$ | 0.0410 | 0.0324 |
| $\theta_{max}$ (deg) | 25.54 | 25.51 |
| GoF[a] | 1.155 | 1.086 |
| Data/ restraints/ parameters | 5818/ 0/ 214 | 4271/ 0/ 151 |
| R1(all data)[b] | 0.0264 | 0.0210 |
| wR2 (all data)[c] | 0.675 | 0.0516 |
| largest diff peak and hole (e $Å^{-3}$) | 0.711 and -0.478 | 0.479 and -0.627 |

[a] $GOF = [\sum w(|F_o| - |F_c|)^2/(n-p)]^{1/2}$, where n = number of reflections, and p = number of parameters.

[b] $R1 = \sum ||F_o| - |F_c|| / \sum |F_o|$

[c] $wR2 = (\sum[w(F_o^2-F_c^2)^2]/\sum[wF_o^4])^{1/2}$, $w = [\sigma^2(F_o^2) + (0.0329P)^2 + (0.2239P)]^{-1}$, where $P = (\max(F_o^2, 0) + 2[F_c^2])/3$

Table 8.9.17 Selected crystallographic data and collection parameters for compounds in chapter 7.

| | **dmpe(iPr$_3$SnOTf)$_2$** | **[SnCl$_4$][CoCp$_2$]·CH$_2$Cl$_2$**[a] |
|---|---|---|
| Empirical formula | $C_{26}H_{58}F_6O_6P_2S_2Sn_2$ | $C_{21}H_{22}Cl_6CoSn$ |
| Fw (g/mol) | 944.16 | 723.64 |
| T (K) | 188(1) | 188(1) |
| λ( Mo Kα) (Å) | 0.71073 | 0.71073 |
| color and habit | Colorless, irregular | Yellow, irregular |
| cryst syst | Monoclinic | Monoclinic |
| space group | $P2_1/n$ | $P2_1$ |
| a (Å) | 8.9771(11) | 7.266(2) |
| b (Å) | 15.8771(19) | 16.735(5) |
| c (Å) | 13.9947(16) | 10.361(3) |
| α (deg) | 90 | 90 |
| β (deg) | 95.247(2) | 90.235(4) |
| γ (deg) | 90 | 90 |
| V (Å$^3$) | 1986.3(3) | 1259.9(7) |
| Z | 2 | 2 |
| cryst size (mm$^3$) | 0.40 x 0.20 x 0.10 | 0.35 x 0.20 x 0.15 |
| abs coeff (mm$^{-1}$) | 1.505 | 2.929 |
| reflens colled | 13180 | 8488 |
| indpndt reflens | 4414 | 4759 |
| $R_{int}$ | 0.0341 | 0.0268 |
| $\theta_{max}$ (deg) | 25.56 | 26.27 |
| GoF[b] | 1.145 | 1.101 |
| Data/ restraints/ parameters | 4414/ 0/ 207 | 4759/ 1/ 272 |
| R1(all data)[c] | 0.0323 | 0.0260 |
| wR2 (all data)[d] | 0.0668 | 0.0583 |
| largest diff peak and hole (e Å$^{-3}$) | 0.960 and -0.339 | 0.649 and -0.642 |

[a] This monoclinic system has a beta angle of approximately 90 degrees and emulates orthorhombic.
[b] GOF = $[\sum w(|F_o| - |F_c|)^2/(n-p)]^{1/2}$, where n = number of reflections, and p = number of parameters.
[c] $R1 = \sum ||F_o| - |F_c|| / \sum |F_o|$
[d] $wR2 = (\sum[w(F_o^2-F_c^2)^2]/\sum[wF_o^4])^{1/2}$, $w = [\sigma^2(F_o^2) + (0.0329P)^2 + (0.2239P)]^{-1}$, where $P = (\max(F_o^2, 0) + 2[F_c^2])/3$

Table 8.9.18 Selected crystallographic data and collection parameters for compounds in chapter 7.

| | **$Me_3P(Me_3SnCl)_2$[a]** | **$[(PMe_3)_2Ge][OTf]_2$** |
|---|---|---|
| Empirical formula | $C_9H_{27}Cl_2PSn_2$ | $C_8H_{18}F_6GeO_6P_2S_2$ |
| Fw (g/mol) | 474.56 | 522.87 |
| T (K) | 188(1) | 173(1) |
| λ( Mo Kα) (Å) | 0.71073 | 0.7173 |
| color and habit | Colorless, plate | Colorless, irregular |
| cryst syst | Orthorhombic | Monoclinic |
| space group | $Pna2_1$ | $P2_1/n$ |
| a (Å) | 13.426(3) | 18.235(4) |
| b (Å) | 7.3206(15) | 11.937(3) |
| c (Å) | 19.027(4) | 18.956(4) |
| α (deg) | 90 | 90 |
| β (deg) | 90 | 93.407(3) |
| γ (deg) | 90 | 90 |
| V ($Å^3$) | 1870.1(7) | 4119.0(16) |
| Z | 4 | 8 |
| cryst size ($mm^3$) | 0.45 x 0.40 x 0.10 | 0.60 x 0.20 x 0.05 |
| abs coeff ($mm^{-1}$) | 3.017 | 1.917 |
| reflens colled | 4163 | 27675 |
| indpndt reflens | 4163 | 9187 |
| $R_{int}$ | - | 0.0553 |
| $\theta_{max}$ (deg) | 25.36 | 25.90 |
| GoF[b] | 1.064 | 1.019 |
| Data/ restraints/ parameters | 4163/ 1/ 136 | 9187/ 0/ 463 |
| R1(all data)[c] | 0.0186 | 0.0692 |
| wR2 (all data)[d] | 0.0432 | 0.1349 |
| largest diff peak and hole (e $Å^{-3}$) | 0.575 and -0.232 | 1.339 and -0.714 |

[a] The crystal was twinned and the orientation matrixes for two components were determined. The data were reduced and corrected for absorption.

[b] $GOF = [\sum w(|F_o| - |F_c|)^2/(n-p)]^{1/2}$, where n = number of reflections, and p = number of parameters.

[c] $R1 = \sum ||F_o| - |F_c|| / \sum |F_o|$

[d] $wR2 = (\sum[w(F_o^2-F_c^2)^2]/\sum[wF_o^4])^{1/2}$, $w = [\sigma^2(F_o^2) + (0.0329P)^2 + (0.2239P)]^{-1}$, where $P = (\max(F_o^2, 0) + 2[F_c^2])/3$

Table 8.9.19 Selected crystallographic data and collection parameters for compounds in chapter 7.

| | **[(dmpe)GeCl][OTf]** | **[$Me_3PCl$][$GeCl_3$]** |
|---|---|---|
| Empirical formula | $C_7H_{16}ClF_3GeO_3P_2S$ | $C_3H_9Cl_4GeP$ |
| Fw (g/mol) | 407.24 | 290.46 |
| T (K) | 173(1) | 173(1) |
| λ( Mo Kα) (Å) | 0.71073 | 0.71073 |
| color and habit | Colorless, Plate | Colorless, irregular |
| cryst syst | Orthorhombic | Rhombohedral |
| space group | $Pna2_1$ | R3 |
| a (Å) | 20.789(3) | 9.379(5) |
| b (Å) | 19.918(3) | 9.379(5) |
| c (Å) | 7.4243(10) | 10.623(5) |
| α (deg) | 90 | 90 |
| β (deg) | 90 | 90 |
| γ (deg) | 90 | 120 |
| V ($Å^3$) | 3074.3(7) | 809.3(7) |
| Z | 8 | 3 |
| cryst size ($mm^3$) | 0.65 x 0.25 x 0.03 | 0.30 x 0.30 x 0.20 |
| abs coeff ($mm^{-1}$) | 2.538 | 3.908 |
| reflens colled | 20692 | 1805 |
| indpndt reflens | 6090 | 773 |
| $R_{int}$ | 0.0509 | 0.0436 |
| $\theta_{max}$ (deg) | 26.07 | 24.33 |
| GoF[a] | 1.039 | 0.991 |
| Data/ restraints/ parameters | 6090/ 1/ 334 | 773/ 1/ 30 |
| R1(all data)[b] | 0.0398 | 0.0269 |
| wR2 (all data)[c] | 0.0888 | 0.0570 |
| largest diff peak and hole (e $Å^{-3}$) | 1.437 and -0.463 | 0.643 and -0.271 |

[a] GOF = $[\sum w(|F_o| - |F_c|)^2/(n-p)]^{1/2}$, where n = number of reflections, and p = number of parameters.
[b] $R1 = \sum ||F_o| - |F_c|| / \sum |F_o|$
[c] $wR2 = (\sum[w(F_o^2-F_c^2)^2]/\sum[wF_o^4])^{1/2}$, $w = [\sigma^2(F_o^2) + (0.0329P)^2 + (0.2239P)]^{-1}$, where $P = (\max(F_o^2, 0) + 2[F_c^2])/3$

Table 8.9.20 Selected crystallographic data and collection darameters for $[(dmpe)_2AlCl_2][AlCl_4]$, a byproduct from reactions involving dmpe and $AlCl_3$.

| | **$[(dmpe)_2AlCl_2][AlCl_4]$** |
|---|---|
| Empirical formula | $C_{12}H_{32}Al_2Cl_6P_4$ |
| Fw (g/mol) | 566.92 |
| T (K) | 188(1) |
| λ( Mo Kα) (Å) | 0.71073 |
| color and habit | Colourless, cube |
| cryst syst | Orthorhombic |
| space group | Pbca |
| a (Å) | 19.664(3) |
| b (Å) | 16.141(3) |
| c (Å) | 34.853(6) |
| α (deg) | 90 |
| β (deg) | 90 |
| γ (deg) | 90 |
| V ($Å^3$) | 11062(3) |
| Z | 16 |
| cryst size ($mm^3$) | 0.40 x 0.40 x 0.35 $mm^3$ |
| abs coeff ($mm^{-1}$) | 0.915 |
| reflens colled | 70548 |
| indpndt reflens | 12584 |
| $R_{int}$ | 0.0998 |
| $\theta_{max}$ (deg) | 25.71 |
| GoF[a] | 1.100 |
| Data/restraints/ parameters | 12584/ 7/ 455 |
| R1(all data)[b] | 0.1307 |
| wR2 (all data)[c] | 0.1763 |
| largest diff peak and hole (e $Å^{-3}$) | 0.982 and -0.581 |

[a] GOF = $[\sum w(|F_o| - |F_c|)^2/(n-p)]^{1/2}$, where n = number of reflections, and p = number of parameters.
[b] R1 = $\sum ||F_o| - |F_c|| / \sum |F_o|$
[c] wR2 = $(\sum[w(F_o^2-F_c^2)^2]/\sum[wF_o^4])^{1/2}$, w = $[\sigma^2(F_o^2) + (0.0329P)^2 + (0.2239P)]^{-1}$, where P = (max $(F_o^2, 0)$ $+2[F_c^2])/3$

## APPENDIX A1. NOMENCLATURE

IUPAC nomenclature is most appropriate for naming compounds but can sometimes be inefficient for the identification of molecular species within a discussion. Therefore, the common names presented below are used throughout the thesis to describe tin and germanium centers with varying coordination numbers, charges, and oxidation states.

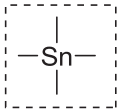


Stannane
Tin(IV)

Germane
Germanium(IV)

Stannylene
Tin(II)

Germylene
Germanium(II)

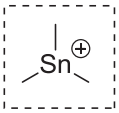


Stannylium
$Tin(IV)^{+}$

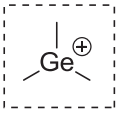


Germylium
$Germanium(IV)^{+}$

Stannyliumylidene
$Tin(II)^{+}$

Germyliumylidene
$Germanium(II)^{+}$

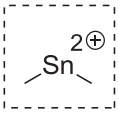


Stannyldiylium
$Tin(IV)^{2+}$

Germyldiylium
$Germanium(IV)^{2+}$

Stannyliumdiylidene
$Tin(II)^{2+}$

Germyliumdiylidene
$Germanium(II)^{2+}$

= Moieties that have been isolated in this thesis

## REFERENCES


1. Dyker C. A.; Burford, N., *Chem. Asian J.* **2008**, *3*, 28–36.

2. Burford, N.; Ragogna, P. J., *J. Chem. Soc., Dalton Trans.* **2002**, *23*, 4307-4315.

3. Burford, N.; Ragogna, P. J.; Robertson, K. N.; Cameron, T. S.; Hardman N. J.; Power, P. P., *J. Am. Chem. Soc.* **2002**, *124*, 382-383.

4. Burford, N.; Losier, P.; Phillips, A. D.; Ragogna, P. J.; Cameron, T. S., *Inorg. Chem.* **2003**, *42*, 1087-1091.

5. Burford, N.; Herbert, D. E.; Ragogna, P. J.; McDonald, R.; Ferguson, M. J., *J. Am. Chem. Soc.* **2004**, *126*, 17067-17073.

6. Burford, N.; Dyker C. A.; Decken, A., *Angew. Chem.* **2005**, *117*, 2416-2419; *Angew. Chem. Int. Ed.* **2005**, *44*, 2364-2367.

7. Krossing, I., *J. Chem. Soc., Dalton Trans.* **2002**, *4*, 500-512.

8. Burford, N.; Ragogna, P. J.; McDonald, R.; Ferguson, M. J., *J. Am. Chem. Soc.* **2003**, *125*, 14404-14410.

9. Lynam, J. M.; Copsey, M. C.; Green, M.; Jeffery, J. C.; McGrady, J. E.; Russell, C. A.; Slattery, J. M.; Swain, A. C., *Angew. Chem.* **2003**, *115*, 2884-2888; *Angew. Chem. Int. Ed.* **2003**, *42*, 2778-2782.

10. Althaus, H.; Breunig, H. J.; Lork, E., *Chem. Commun.* **1999**, *19*, 1971-1972.

11. Conrad, E.; Burford, N.; McDonald, R.; Ferguson, M. J., *Inorg. Chem.* **2008**, *47*, 2952-2954.

12. Conrad, E.; Burford, N.; McDonald, R.; Ferguson, M. J., *J. Am. Chem. Soc.* **2009**, *131*, 17000-17008.

13. Conrad, E.; Burford, N.; McDonald, R.; Ferguson, M. J., *J. Am. Chem. Soc.* **2009**, *131*, 5066-5067.

14. Conrad, E.; Burford, N.; Werner-Zwanziger, U.; McDonald, R.; Ferguson, M. J., *Chem. Commun.* **2010**, *46*, 2465-2467.

15. Chitnis, S. S.; Burford, N.; Ferguson, M. J., *Angew. Chem. Int. Ed.* **2013**, *52*, 2042-2045.

16. Chitnis, S. S.; Carpenter, Y.-Y.; Burford, N.; McDonald, R.; Ferguson, M. J., *Angew Chem Int. Ed.* **2013**, *52*, 4863-4866.

17. Kárpáti, T.; Veszprémi, T.; Thirupathi, N.; Liu, X.; Wang, Z.; Ellen, A.; Nyulászi, L.; Verkade, J. G., *J. Am. Chem. Soc.* **2006**, *128*, 1500-1512.

18. Hill, N. J.; Levason, W.; Reid, G., *J. Chem. Soc., Dalton Trans.* **2002**, 1188-1192.

19. Coote, M. L.; Krenske, E. H.; Porter, K. A.; Weir, M. L.; Willis, A. C.; Zhou, X.; Wild, S. B., *Organometallics* **2008**, *27*, 5099-5107.

20. Clegg, W.; Elsegood, M. R. J.; Graham, V.; Norman, N. C.; Pickett, N. L.; Tavakkoli, K., *J. Chem. Soc., Dalton Trans.* **1994**, *12*, 1743-1751.

21. Genge, A. R. J.; Hill, N. J.; Levason, W.; Reid, G., *J. Chem. Soc., Dalton Trans.* **2001**, 1007-1012.

22. Breunig, H. J.; Denker, M.; Ebert, K. H., *Chem. Commun.* **1994**, *7*, 875-876.

23. Schmidpeter, A.; Lochschmidt, S.; Sheldrick, W. S., *Angew. Chem. Int. Ed.* **1985**, *24*, 226–227.

24. Donath, M.; Conrad, E.; Jerabek, P.; Frenking, G.; Frölich, R.; Burford, N.; Weigand, J. J., *Angew. Chem. Int. Ed.* **2012**, *51*, 2964-2967.

25. Wharf, I.; Onyszchuk, M., *Can J. Chem.* **1970**, *48*, 2250-2256.

26. Kraus, F.; Baer, S. A., *Z. Anorg. Allg. Chem.* **2010**, *636*, 414.

27. Ault, B. S. J., *Mol. Struct.* **1985**, *129*, 287.

28. Ault, B. S. J., *Mol. Struct.* **1985**, *130*, 215.

29. Cheng, F.; Davis, M. F.; Hector, A. L.; Levanson, W.; Reid, G.; Webster, M.; Zhang, W., *Eur. J. Inorg. Chem.* **2007**, *2007*, 4897-4905.

30. Davis, M. F., Levason, W.; Reid, G.; Webster, M., *Dalton Trans.* **2008**, 2261-2269.

31. Beattie, I. R.; Ozin, G. A., *J. Chem. Soc. (A)* **1970**, 370-377.

32. Frieson, D. K.; Ozin, G. A., *Can. J. Chem.* **1973**, *51*, 2685-2696.

33. Izod, K., *Coord. Chem. Rev.* **2012**, *256*, 2972-2993.

34. Schfer, A.; Saak, W.; Haase, D.; Muller, T., *Chem. Eur. J.* **2009**, *15*, 3945-3950.

35. Krummenacher, I.; Fernandez, I.; Ruegger, H.; Weigand, F.; Breher, F., *Dalton Trans.* **2009**, 5335-5347.

36. Jutzi, P.; Mix, A.; Rummel, B.; Schoeller, W. W.; Neumann, B., *Science* **2004**, *305*, 849-851.

37. Rupar, P. A.; Staroverov, V. N.; Baines, K. M. *Science* **2008**, *322*, 1360-1362.

38. Jutzi, P.; Kohl, F.; Hofmann, P.; Kruger, C.; Tsay, Y., *Chem. Ber.* **1980**, *113*, 757-769.

39. Jutzi, P.; Dickbreder R.; Noth, H., *Chem. Ber.* **1989**, *122*, 865-870.

40. Schmidbaur, H.; Schier, A., *Organometallics* **2008**, *27*, 2361-2395.

41. Driess, M.; Yao, S.; Brym, M.; van Wullen, C., *Angew. Chem. Int. Ed.* **2006**, *45*, 4349-4352.

42. Rupar, P. A.; Bandyopadhyay, R.; Cooper, B. F. T.; Stinchcombe, M. R.; Ragogna, P. J.; Macdonald, C. L. B.; Baines, K. M., *Angew. Chem. Int. Ed.* **2009**, *48*, 5155-5158.

43. Cheng, F.; Hector, A. L.; Levason, W.; Reid, G. Webster, M.; Zhang, W., *Angew Chem. Int. Ed.* **2009**, *48*, 5152-5154

44. Cheng, F.; Hector, A. L.; Levason, W.; Reid, G.; Webster, M.; Zhang, W., *Inorg. Chem.* **2010**, *49*, 752-760.

45. Genge, A. R. J.; Levason, W.; Reid, G., *Inorg. Chem. Acta.* **1999**, *288*, 142-149.

46. Adley, A. D.; Bird, P. H.; Fraser, A. R.; Onyszchuk, M., *Inorg. Chem.* **1972**, *11*, 1402-1409.

47. Levason, W.;McAuliffe, C. A., *Coord. Chem. Rev.* **1976**, *19*, 173-185.

48. Lin, T-P; Gualco, P.; Laderia, S.; Amgoune, A.; Bourissou, D.; Gabbaï, F. P., *C. R. Chimie*, **2010**, *13*, 1168-1172.

49. Mather, G. G.; McLaughlin, G. M.; Pidcock, A., *J. Chem. Soc., Dalton Trans.*, **1973**, 1823-1827.

50. Davis, M. F.; Clarke, M.; Levason, W.; Reid, G.; Webster, M., *Eur. J. Inorg. Chem.* **2006**, 2773-2782.

51. Hoppe, S.; Weichmann, H.; Jurkschat, K.; Schneider-Koglin, C.; Drager, M., *J. Organomet. Chem.* **1995**, *505*, 63-72.

52. Mahon, M. F.; Moldovan, N. L.; Molloy, K. C.; Muresan, A.; Silaghi-Dumitrescu, I.; Silaghi-Dumitrescu, L., *Dalton Trans.* **2004**, 4017-4021.

53. Sarazin, Y.; Coles, S. J.; Hughes, D. L.; Hursthouse, M. B.; Bochmann, M., *Eur. J. Inorg. Chem.* **2006**, 3211.

54. Nechaev, M. S.; hernov, O. V.; Portnyagin, I. A.; Khrustalev, V. N.; Aysin, R. R.; Lunin, V. V., *J. Organomet. Chem.* **2010**, *695*, 365-369.

55. Annunziata, L.; Pappalardo, D.; Tedesco, C.; Pellecchia, C., *Organometallics* **2005**, *24*, 1947-1952.

56. Annunziata, L.; Pappalardo, D.; Tedesco, C.; Pellecchia, C., *Eur. J. Inorg. Chem.* **2007**, 5752-5779.

57. Sakamoto, K.; Hamada, Y.; Akashi, H.; Orita, A.; Otera, J., *Organometallics* **1999**, *18*, 3555-3557.

58. Durand S.; Sakamoto, K.; Fukuyama, T.; Orita, A.; Otera, J.; Duthie, A.; Dakternieks, D.; Schulte, M.; Jurkschat, K., *Organometallics* **2000**, *19*, 3220-3223.

59. Johannsen, M.; Jorgensen, K. A.; Helmchen, G., *J. Am. Chem. Soc.* **1998**, *120*, 7637-7638.

60. Olah G. A.; Rasul, G.; Prakash, G. K. S., *J. Am. Chem. Soc.* **1999**, *121*, 9615-9617.

61. Sekiguchi, A.; Fukawa, T.; Lee, V. Y.; Nakamoto, M., *J. Am. Chem. Soc.* **2003**, *125*, 9250-9251.

62. Pettinari, C.; Marchetti, F.; Pellei, M.; Cingolani, A.; Barba, L.; Cassetta, A., *J. Organomet. Chem.* **1996**, *515*, 119-130.

63. Turek, J.; Z. Padělkova, Z.; Cernošek, Z. C.; Erben, M.; Lycka, A.; Nechaev, M. S.; Cisarova, I.; Ruzicka, A., *J. Organomet. Chem.* **2009**, *694*, 3000-3007.

64. Mehring, M.; Löw, C.; Schürmann, M.; Uhlig, F.; Jurkschat, K.; Mahieu, B., *Organometallics* **2000**, *19*, 4613-4623.

65. Driess, M.; Merz, K.; Monse, C.; Wullen, C., *Angew. Chem. Int. Ed.* **2000**, *39*, 3684-3686.

66. Driess, M.; Merz, K.; Monse, C., *Chem. Commun.* **2003**, 2608-2609.

67. Pi, C.; Elguero, J.; Wan, L.; Alkorta, I.; Zheng, W.; Weng, L.; Chen, Z.; Wu, L., *Chem. Eur. J.* **2009**, *15*, 6581-6585.

68. Zharov, I.; King, B. T.; Havlas, Z.; Pardi, A.; Michl, J., *J. Am. Chem. Soc.* **2000**, *122*, 10253-10254.

69. Lambert, J. B.; Lin, L.; Keinan, S.; Müller, T., *J. Am. Chem. Soc.* **2003**, *125*, 6022-6023.

70. Davies, A. G. *Organotin Chemistry, 2nd edition*, Wiley-VCH, Weinheim, Germany, 2004.

71. Newmann, W. P.; Schick, R.; Köster, R., *Angew. Chem.* **1964**, *76*, 380.

72. Norman, N. C.; Pickett, N. L., *Coord. Chem. Rev.* **1995**, *145*, 27-54.

73. Norman, N. C.; Pickett, N. L., *Coord. Chem. Rev.* **1995**, *145*, 27-54.

74. Mather, G. G.; McLaughlin, G. M.; Pidcock, A., *J. Chem. Soc., Dalton Trans* **1973**, 1823-1827.

75. Davis, M. F.; Clarke, M.; Levason, W.; Reid, G.; Webster, M., *Eur. J. Inorg. Chem.* **2006**, 2773–2782.

76. Bricklebank, N.; Godfrey, S. M.; McAuliffe, C. A.; Pritchard, R. G., *J. Chem. Soc., Chem. Commun.* **1994**, 695-696.

77. Genge, A. R. J.; Levason, W.; Reid, G., *Inorg. Chem. Acta.*, **1999**, *288*, 142-149.

78. Beattie, I. R.; McQuillan, G. P.; Rule, L.; Webster, M., *J. Chem. Soc.* **1963**, 1514.

79. Calculations completed by Saurabh S. Chitnis, University of Victoria, Canada.

80. MacDonald, E.; Doyle, L.; Chitnis, S. C.; Burford, N.; Werner-Zwanziger, U.; Decken, A., *Chem. Commun.*, **2012**, *48*, 7922-7924.

81. Frenking, G.; Fau, S.; Marchand, C. M.; Grützmacher, H., *J. Am. Chem. Soc.* **1997**, *119*, 6648-6655.

82. MacDonald, E.; Doyle, L.; Burford, N.; Werner-Zwanziger, U.; Decken, A., *Angew. Chem. Int. Ed.* **2011**, *50*, 11474-11477.

83. Miessler, G. L.; Tarr, D. A. *Inorganic Chemistry, 3rd edition*, Pearson Prentice hall, New Jersey, USA, 2004.

84. Martens, R.; du Mont, W.-W.; Jeske, J.; Jones, P. G.; Saak, W.; Pohl, S., *J. Organomet. Chem.* **1995**, *501*, 251-261.

85. Sokol, V. I.; Vasilenko, T. G.; Porai-Koshits, M. A.; Molodkin, A. K.; Vasnin, S. V.; Russ. J., *Inorg. Chem.* **1990**, *35*, 2017-2024.

86. Chong, C.; Sasaki, T.; Jimbo-Kobayashi, A.; Tada, M.; Iwasawa, Y., *Bull. Chem. Soc. Jpn.* **2007**, *80*, 2365-2374.

87. Angenault, J.; Couturier, J.-C.; Reculeau, E., *Rev. Chim. Miner.* **1979**, *16*, 157-164.

88. Davis, M. F.; Levason, W.; Ratnani, R.; Reid, G.; Rose, T.; Webster, M., *Eur. J. Inorg. Chem.* **2007**, 306-313.

89. Apostolico, L.; Mahon, M. F.; Molloy, K. C.; Binions, R.; Blackman, C. S.; Carmalt, C. J.; Parkin, I. P., *Dalton Trans.* **2004**, 470-475.

90. Weigand, J. J.; Burford, N.; Riegel, S. D.; Decken, A., *J. Am. Chem. Soc.* **2007**, *129*, 7969-7976.

91. Beattie, I. R.; Jones, P. J.; Reid, G.; Webster, M., *Inorg. Chem.* **1998**, *37*, 6032-6034.

92. Dyker, C. A.; Burford, N.; Menard, G.; Lumsden, M. D.; Decken, A., *Inorg. Chem.* **2007**, *46*, 4277-4285.

93. Baudler, M.; Glinka, K., *Inorg. Synth.* **1989**, *25*, 1-5.

94. Henderson, W. A.; Epstein, M.; Seichter, F. S., *J. Am. Chem. Soc.* **1993**, *85*, 2462-2466.

95. Breen, T. L.; Stephan, D. W., *Organometallics* **1997**, *16*, 365-369

96. Baudler, M.; Hellmann, J., *Z. Anorg. Allg. Chem.* **1981**, *480*, 129-141.

97. SAINT 7.23A, 2006, Bruker AXS, Inc., Madison, Wisconsin, USA.

98. SADABS 2008, George Sheldrick, 2008, Bruker AXS, Inc., Madison, Wisconsin, USA.

99. Sheldrick, G.M. SHELXTL. *Acta Cryst.* **2008**, *A64*, 112-122.

100. CELL_NOW, V. 2008/2, George Sheldrick, Bruker AXS, Inc., Madison, Wisconsin, USA.

101. TWINABS 1.05, George Sheldrick, 2004, Bruker Nonius, Inc., Madison, Wisconsin, USA.

102. Platon, Spek, A.L. *J.Appl.Cryst.* **2003**, *36*, 7-13